

Process and media development of an MR fluid-based finishing for high efficiency material removal

Kum, Chun Wai

2016

Kum, C. W. (2016). Process and media development of an MR fluid-based finishing for high efficiency material removal. Doctoral thesis, Nanyang Technological University, Singapore.

<https://hdl.handle.net/10356/69007>

<https://doi.org/10.32657/10356/69007>



**PROCESS AND MEDIA DEVELOPMENT
OF AN MR FLUID-BASED FINISHING
FOR HIGH EFFICIENCY MATERIAL REMOVAL**

KUM CHUN WAI

SCHOOL OF MECHANICAL AND AEROSPACE ENGINEERING

2016

**Process and Media Development of an MR Fluid-based Finishing for
High Efficiency Material Removal**

Kum Chun Wai, BEng (Mechanical Engineering)

School of Mechanical and Aerospace Engineering

A thesis submitted to the Nanyang Technological University
in partial fulfillment to the requirement for the degree of
Doctor of Philosophy (Mechanical and Aerospace Engineering)

2016

Curriculum Vitae

Kum Chun Wai was born in Kuala Lumpur, Malaysia on 25 February 1987. He was awarded the ASEAN Pre-University scholarship for A-level studies in National Junior College in Singapore from 2004 to 2005. Upon graduation, he was awarded the ASEAN Undergraduate scholarship to attend the Faculty of Engineering in National University of Singapore, where he graduated with a Bachelor of Engineering in mechanical engineering with Second Upper Class Honours in 2010. After a two-year stint as Research Engineer in the Singapore Institute of Manufacturing Technologies (SIMTech), he was awarded the A*STAR Graduate Scholarship for Ph.D. research in magnetic field-assisted finishing in Nanyang Technological University and SIMTech under the guidance of Associate Professor David Butler, with co-supervision initially from Dr. Sato Takashi, and later from Dr. Liu Kui.

Acknowledgements

Firstly, I would like to begin by expressing my deepest appreciation to Dr. Sato Takashi, who has set me to on this journey to pursue my Ph.D. research. He is a brilliant researcher, an inspiring mentor, an excellent teacher, and an even better friend. Despite moving to another research institute two and half years into my research, he continued to show concern and give sound advice. I look forward to potential collaborations on exciting projects in the future. どうもありがとうございます。

Deepest gratitude must also be expressed to two other equally important and inspiring people to have graced my Ph.D. journey. Firstly, thank you to David (first-name basis at his insistence), my ever-affable professor and undoubtedly the top metrologist in Singapore. It has been honour to have you as a mentor, a wise teacher, and a loquacious (in a fun way) friend. Next is Dr. Liu Kui, who has been my co-supervisor for the final third of my Ph.D. research. Despite the relatively short time of working together, there has never been a dearth of wise words and helpful advice. Thank you very much and I look forward to be (very likely) working with you again in the near future as colleagues.

I have also been very fortunate to be given the opportunity to work in the Machining Technology Group in SIMTech with a wonderful group of people. Special mention must be given to Shaw Kah Chuan and Ng Seow Tong, who have been very helpful with engineering problems, machine operations and administrative matters, and without whom the lab would have been much less lively place to be in. Next, thank you to Candice Au Ka Hing and Ang Yu Jing for the countless times both of you have helped me with various technical and administrative issues. Also, thank you to all other colleagues in MTG who have been making the lab a very pleasant place to work in.

I am also very thankful and blessed to have met Gerald Fong Weng Seng and Mark Tan, who were MTG colleagues and ‘buddies’ during my early days in SIMTech. Both of them have since left SIMTech to explore other avenues in life. To this day, I am extremely grateful that both of you have faith and confidence in my ability to complete my Ph.D. research by agreeing to be my guarantors for the scholarship, despite our relatively short acquiescence. It is a touching gesture that will never be forgotten.

Lastly, but definitely not the least, the deepest gratitude is reserved for my other significant half, who is the most important person in my life. Thank you for being the co-pilot during my most emotional journey in my life so far, for the endless emotional support, for the loving care and for the wonderful companionship. I look forward to writing many more chapters with you in the future, together. This thesis is dedicated to you.

Abstract

Magnetic field-assisted finishing (MFAF) is a class of non-conventional polishing processes that utilize ferromagnetic smart fluids. As the final stage in a chain of manufacturing processes, these processes are used for surface texture reduction, removal of sub-surface damage layer, or for form correction. Recently, the aerospace industry has identified MFAF processes as a potential solution for polishing of freeform external surfaces of aerospace components made of titanium alloy (Ti-6Al-4V). Two of the most pressing issues are the process efficiency in terms of material removal rate, and the ability to predict material removal based on process conditions, with the ultimate goal of process automation.

The two main focus of this project reflect the two aforementioned issues. For the first focus pertaining to increasing the process efficiency, a new MFAF process is developed. The double-magnet configuration of the polishing unit used in the process, which is a novel concept, is developed to achieve high material removal rate. Two factors contributing to the increased material removal rate are identified and established. The first factor is the high magnetic flux density in the polishing zone, which is verified by magnetostatic analysis and measurement on physical setups with a magnetometer. The second factor is the *in situ* reformation of finishing media during the process, which allows the finishing media to exert sustainable pressure on the workpiece surface. The mechanism responsible for the *in situ* reformation of finishing media is also identified, described and established.

Following that, the effect of the tool parameters on the process outcome is studied. Specifically, the parameters studied are the magnet-to-magnet gap, magnet-to-

workpiece gap, and the thickness of magnet. Using magnetostatic analysis, the relationships between these parameters and the magnetic flux density are established. Additionally, the use of magnetic cap to augment the magnetic flux density is also assessed. Based on the findings from these studies, a set of dimensions is recommended for the polishing unit.

The capabilities of the new MFAF process are demonstrated. Surface texture reduction is confirmed for both stainless steel (SUS316) and titanium workpieces, where a final surface texture of 0.016 $\mu\text{m Ra}$ and 0.073 $\mu\text{m Ra}$ are achieved respectively, from an initial surface texture of approximately 1 to 2 $\mu\text{m Ra}$. The removal rate of the new MFAF process is also compared against similar processes, and its material removal rate of 11.8 $\mu\text{m/min}$ is among the highest. Finally, the feasibility of the process for surface finishing of structured surfaces is also assessed. 2.5-D V-shaped channels with depth of 0.1 mm and width of 0.2 mm are polished. Surface texture of both the peaks and valleys is reduced, but the removal rates are different. As a result, the peak-to-valley height of the channels is reduced from 100 μm to 14 μm . Non-uniformity of removal rate is a weakness of the new MFAF process that needs to be considered in future work.

For the second focus pertaining to prediction of material removal rate, a material removal model based on contact mechanics is proposed to better represent the complexity of the finishing media in the MFAF process. The proposed model consists of a base model and two extensions for conditions where assumptions made for the base model are not fulfilled. The complete derivation of the base model and both extensions is presented in this thesis. Then, experiments are conducted to verify the proposed model. The theoretical trends given by the proposed model are found to be in good agreement with the experimental trends.

Table of contents

Table of contents	viii
List of tables	xiv
List of figures	xv
List of abbreviations and symbols	xxii
Chapter 1: Introduction	1
1.1 Mechanical surface finishing in precision engineering	1
1.2 Precision surface removal techniques	2
1.3 Magnetic field-assisted finishing (MFAF)	4
1.4 Motivations	6
1.5 Scopes and objectives	8
1.6 Report Structure	9
1.7 Contributions of the Candidate	10
References	12
Chapter 2: Review of magnetic field-assisted finishing (MFAF) processes	14
2.1 Introduction	14
2.1.1 Four classes of finishing media for MFAF	14
2.1.2 Comparisons of the finishing media	16
2.1.3 Review structure	18
2.2 Ferrofluid	19
2.2.1 MFAF processes based on ferrofluid	19
2.2.1.1 MFAF with sealed ferrofluid	19
2.2.1.2 Magnetic fluid grinding	20
2.2.1.3 MFAF of micropore X-ray optics	24

2.2.2	Reported studies on ferrofluid	25
2.3	Magnetic compound fluid (MCF)	28
2.3.1	MFAF processes based on MCF	28
2.3.1.1	MCF pad polishing	28
2.3.1.2	MCF wheel polishing	30
2.3.2	Reported studies on MCF	31
2.4	MR fluid	32
2.4.1	MFAF processes based on MR fluid	32
2.4.1.1	Magnetorheological finishing (MRF)	32
2.4.1.2	Magnetorheological jet (MR jet) finishing	35
2.4.1.3	Magnetorheological abrasive flow finishing (MRAFF)	37
2.4.1.4	Ball end magnetorheological finishing (BEMRF)	38
2.4.1.6	MFAF of wafers	40
2.4.2	Reported studies on MR fluid	41
2.5	Magnetic abrasives	47
2.5.1	MFAF processes based on magnetic abrasives	47
2.5.1.1	Magnetic abrasive finishing (MAF)	47
2.5.1.2	Flexible magnetic abrasive brush (FMAB) finishing	49
2.5.2	Reported studies on magnetic abrasives	50
2.6	Chapter summary	56
2.6.1	Cited contents of reviewed literature	56
2.6.2	Process development	58
2.6.3	Finishing media development	60
	References	61

Chapter 3: Development of a new magnetic field-assisted finishing (MFAF) process 67

3.1	Introduction	67
3.2	Goals of new MFAF process	68
3.3	Principles of new MFAF process	69
3.3.1	High magnetic flux density in the polishing zone	71

3.3.2	<i>In situ</i> media reformation	74
3.3.3	Finishing forces comparison	80
3.4	Effect of tool parameters on magnetic flux density in the finishing zone	81
3.4.1	Methodology	83
3.4.2	Effect of gap between magnets, w_{gap} , and the gap between magnet and workpiece, z	84
3.4.3	Effect of thickness of magnet, t_{magnet}	88
3.4.4	Effect of magnetic caps and their thickness, t_{cap}	89
3.4.5	Permanent magnets versus electromagnet.....	91
3.5	Finishing characteristics.....	92
3.5.1	Surface texture.....	94
3.5.2	Removal rate	98
3.5.3	Polishing of 2.5D structured surface	99
3.6	Chapter summary	103
	References	105

Chapter 4: Material removal rate model..... 107

4.1	Introduction	107
4.2	Review of existing models	108
4.3	Motivation	110
4.4	Material removal rate model	111
4.4.1	Assumptions	111
4.4.2	General expression	113
4.4.3	Total MRR as sum of two MRR components	116
4.5	Number of active particles	117
4.5.1	Existing approaches.....	118
4.5.2	Proposed approach	121
4.5.3	Maximum allowable abrasive size	122
4.5.4	Maximum allowable volumetric ratio of abrasives to carbonyl iron particles.....	124
4.5.5	Number of active carbonyl iron particles	126

4.5.6	Number of active abrasives	128
4.6	Force per particle	131
4.6.1	Existing approaches.....	132
4.6.2	Proposed approach	133
4.6.3	Force per carbonyl iron particle	134
4.6.4	Force per abrasive particle	136
4.7	Summary	137
4.7.1	Assumptions and scope of model.....	137
4.7.2	General material removal expression	138
4.7.3	Number of active particles	139
4.7.4	Force per particle.....	139
	References	141

Chapter 5: Extensions to material removal rate model 142

5.1	Introduction	142
5.2	Model extension for abrasive size criterion	143
5.2.1	Proposed approach	143
5.2.2	Number of active particles	146
5.2.3	Force per particle.....	149
5.3	Model extension for abrasive volume criterion	150
5.3.1	Proposed approach	150
5.3.2	Number of active particles	152
5.3.3	Force per particle.....	154
5.4	Summary	154
5.4.1	Material removal rate expression	155
5.4.2	Number of active particles	155
5.4.3	Force per particle.....	156

Chapter 6: Experimental verification of material removal rate model	157
6.1 Introduction	157
6.2 Setup of experiment	158
6.2.1 Workpiece	158
6.2.2 Finishing media	159
6.2.3 Machine setup	159
6.2.4 Material removal rate measurement	161
6.2.5 Experimental conditions.....	161
6.3 Experimental results and discussions.....	165
6.3.1 Abrasive size – Experimental results	165
6.3.2 Abrasive size – Theoretical model	166
6.3.3 Abrasive size – further discussion.....	170
6.3.4 Abrasive concentration – Experimental results.....	175
6.3.5 Abrasive concentration – Theoretical model	176
6.3.6 Abrasive concentration – further discussion	178
6.5 Comments on robustness of model	182
6.6 Comments on effect of workpiece material	182
6.7 Summary	183
References	184
 Chapter 7: Summary	 185
7.1 Development of new MFAF process	185
7.1.1 Principles and advantages of new MFAF process	185
7.1.2 Magnetostatic analysis of tool parameters	186
7.1.3 Capabilities of new MFAF process	188
7.2 Material removal rate model	189

Chapter 8: Future work	191
8.1 Goals of surface finishing development.....	191
8.2 Process development.....	191
8.3 Material removal rate model	195
 Appendix A: Magnetostatic analysis with ANSYS	 197
A.1 Introduction	197
A.2 Theory	197
A.3 Preprocessing	198
A.3.1 Model generation.....	198
A.3.2 Element properties.....	199
A.3.3 Material properties	199
A.4 Solving and postprocessing.....	204
A.5 Validation of magnetostatic analysis	206
A.5.1 Validation for single-magnet configuration	207
A.5.2 Validation for double-magnet configuration	207
References	210
 Appendix B: Measurement of material removal rate.....	 211

List of tables

Table 1.1:	Precision surface removal processes.	3
Table 2.1:	Reported results for MFG or MFP of Si_3N_4 balls.	22
Table 2.2:	Reported results for MFG of Si_3N_4 rollers.	23
Table 2.3:	Cited contents of reviewed literature.	56
Table 3.1:	Comparison of magnetic flux density at the centre of polishing zone and at edge of magnet for different values of w_{gap} , when $z = 0.5$ mm.	87
Table 3.2:	Experimental conditions for polishing of SUS316 flat workpiece.	94
Table 4.1:	Volumetric ratio of carbonyl iron particles, abrasives and interstitial spaces in FCC unit cube at critical point, where interstitial spaces are fully occupied by abrasives.	125
Table 6.1:	Experimental conditions for first set of experiments, where abrasive size varies between $0.6 \mu\text{m}$ and $15 \mu\text{m}$	162
Table 6.2:	Experimental conditions where abrasive concentration varies.	163
Table 6.3:	Values of constants for theoretical model.	167
Figure A.1:	An image capture in the ANSYS environment of the plane selected for magnetostatic analysis.	198
Table A.1:	Material properties for the five material types.	200
Table A.2:	Data input for B-H curve of Grade N35 neodymium permanent magnet.	202
Table A.3:	Data input for B-H curve of Grade N35 neodymium permanent magnet [4].	202

List of figures

Figure 1.1:	Schematic diagram to illustrate the conformable nature of magnetic particles.	5
Figure 1.2:	Schematic diagram to illustrate that the motion of magnetic particles can be influenced even when not in direct contact with a magnetic pole.	6
Figure 2.1:	Comparison of finishing media used for MFAF processes.	17
Figure 2.2:	Flowchart of the literature review chapter.	18
Figure 2.3:	Schematic diagram of MFAF with sealed ferrofluid [7].	19
Figure 2.4:	Schematic diagram of the MFG apparatus for the finishing of ceramic ball [11].	21
Figure 2.5:	Schematic diagram of the magnetic fluid grinding apparatus for the finishing of ceramic rollers [12].	23
Figure 2.6:	Schematic diagram of apparatus for MFAF of micropore X-ray optics [13].	24
Figure 2.7:	Surface texture after 60 minutes of polishing with diamond abrasives of different sizes [13].	25
Figure 2.8:	Effects of abrasive sizes on the (a) wear coefficient and (b) Ra [10].	26
Figure 2.9:	Effects of abrasive type on (a) removal rate and (b) surface texture [12].	28
Figure 2.10:	Schematic diagram pad polishing using MCF [3].	29
Figure 2.11:	Schematic diagram of MCF wheel polishing [21].	30
Figure 2.12:	Schematic diagram of MRF [23].	32
Figure 2.13:	Schematic of an in-house MRF platform [31].	35
Figure 2.14:	Jet snapshot images at 30 m/s and nozzle diameter 2 mm [33].	36
Figure 2.15:	Schematic of MRAFF experimental setup [34].	37

Figure 2.16:	Schematic of the BEMRF process [37].	39
Figure 2.19:	Schematic diagram of an MFAF process for polishing of wafers [41].	40
Figure 2.20:	Relationships between (a) viscosity of MF fluid and water content (vol %), and (b) peak removal rate and viscosity of MR fluid. Workpiece is fused silica [43].	42
Figure 2.21:	Effect of water content in MR fluid composition on (a) removal rate, and (b) surface texture [45]. The remaining 40 % of the MR fluid composition is carbonyl iron powder.	43
Figure 2.22:	Effect of type of abrasives on the removal rate of fused silica [45].	44
Figure 2.23:	Effect of abrasive concentration for different types of abrasive on the removal rate of fused silica: ● diamond, ▲ CeO ₂ , ■ Al ₂ O ₃ [45].	45
Figure 2.24:	Effect of abrasive concentration on the tangential and normal forces [29].	45
Figure 2.25:	Schematic diagram of MAF apparatus for Si ₃ N ₄ rollers [5].	48
Figure 2.26:	Schematic diagram of the MAF of the internal surface of a tube [55].	49
Figure 2.27:	Schematic diagram of FMAB finishing of cutting tool faces (a) with non-magnetic jigs and (b) with magnetic jig [57].	50
Figure 2.28:	Effect of the diamond particle size on the (a) stock removal and (b) surface texture profiles [5].	51
Figure 2.29:	Effect of the magnetic abrasive size on the (a) stock removal and (b) surface texture profiles [5].	51
Figure 2.30:	Comparison of removal rate and surface texture for bonded and unbonded abrasives [53].	52
Figure 2.31:	Surface texture and removal rate for steel grit of different sizes and SiC of 5.5 μm [59].	53

Figure 2.32:	Surface texture and removal rate for different SiC sizes and constant steel grit size [59].	54
Figure 2.33:	Percentage change in surface texture against wt. % of SiC abrasives for different abrasive sizes [58].	55
Figure 3.1:	Schematic diagram of the polishing tool and the polishing zone.	70
Figure 3.2:	Magnetic flux lines for (a) single-magnet configuration, and (b) double-magnet configuration.	72
Figure 3.3:	Contour plots of magnetic flux density for (a) single-magnet configuration, and (b) double-magnet configuration.	73
Figure 3.4:	Shape of the finishing media during the polishing process using the single-magnet configuration (a) before polishing, (b) after initial contact with the workpiece, (c) after losing contact with the workpiece, and (d) after coming into contact with the workpiece again.	74
Figure 3.5:	Shape of the finishing media during the polishing process using the double-magnet configuration (a) before polishing, (b) after initial contact with the workpiece, (c) after losing contact with the workpiece, and (d) after coming into contact with the workpiece again.	75
Figure 3.6:	The magnetic flux density profile of moving points <i>X</i> and <i>Y</i> for (a) single-magnet configuration, and (b) double-magnet configuration.	77
Figure 3.7:	Shape of finishing media when (a) the two magnets are separated from each other, and (b) when a small air gap is maintained between the two magnets. Finishing media on the two magnets interfere and are physically squeezed. Contact forces arising from it is accountable for the observed <i>in situ</i> reformation of the finishing media.....	79

Figure 3.8:	(a) Shear forces and (b) normal forces during polishing for single-magnet (S) and double-magnet (D) configurations, with different supplied amount of finishing media.	80
Figure 3.9:	Polishing tool in the ANSYS environment. Magnet thickness, t_{magnet} , and gap between magnets, w_{gap} , are variables.	82
Figure 3.10:	Magnetic flux density profiles at different z values when w_{gap} is a variable.	84
Figure 3.11:	Magnetic flux density at $x = 0$ mm against thickness of magnet, t_{magnet} , for different values of z	88
Figure 3.12:	Polishing tool in the ANSYS environment, with magnetic caps.	89
Figure 3.13:	Magnetic flux lines of double-magnet configuration (a) without magnetic cap, and (b) with magnetic caps of 5 mm thickness.	90
Figure 3.14:	Magnetic flux density at $x = 0$ mm against thickness of magnetic cap, t_{cap} at different z values.	91
Figure 3.15:	Prototype of the polishing unit mounted on a desktop milling machine.	93
Figure 3.16:	Surface texture (Ra) of SUS316 workpiece versus polishing time for three different abrasive sizes.	95
Figure 3.17:	Micrographs of the SUS316 workpiece surface before and after polishing with three different abrasive sizes.	96
Figure 3.18:	Surface texture (Ra) of Ti-6Al-4V workpiece versus polishing time for three different values of z	98
Figure 3.19:	Peak removal rates of selected MFAF and non-MFAF processes.	99
Figure 3.20:	Schematic diagram of the V-grooves geometry on the workpiece.	100
Figure 3.21:	Optical images of the V-grooves before and after polishing with the new MFAF process.	101

Figure 3.22:	2D profile scans of the V-grooves before and after polishing with the new MFAF process.....	102
Figure 4.1:	Scanning electron micrograph of (a) CI particles and (b) alumina abrasive particles.....	112
Figure 4.2:	Schematic diagram of the projected area of indentation, A , and depth of indentation, h	114
Figure 4.3:	Schematic diagram of the typical approach in modeling the number of active abrasives [8].	119
Figure 4.4:	Configuration of active and inactive particles in the model proposed by Sidpara and Jain [10].	120
Figure 4.5:	Model of particle configuration in the finishing media. Carbonyl iron particles are arranged in FCC configuration and abrasives are dispersed uniformly in the interstitial spaces.....	122
Figure 4.6:	Calculation of maximum allowable diameter for abrasives in the model.	123
Figure 4.7:	Interface of carbonyl iron particles and the workpiece surface. Abrasives are not shown.	126
Figure 4.8:	Unit triangle on the CI plane.....	127
Figure 4.9:	Interface of carbonyl iron particles, abrasives, and the workpiece surface. ...	129
Figure 4.10:	Force per particle in the model proposed by Luo and Dornfeld [6] for the CMP process, for (a) hard polishing pad and (b) soft polishing pad.	132
Figure 5.1:	Distance between carbonyl iron particles is increased in an orderly manner when abrasive size exceeds critical value given by abrasive size criterion.	144
Figure 5.2:	Unit triangle when abrasive size exceeds the critical value. Abrasives are not shown.	145

Figure 5.3:	When abrasive volume exceeds critical value, an orderly arrangement of larger abrasives with equivalent abrasive size is considered.	151
Figure 6.1:	SUS316 workpieces after wire EDM (left) and after sandpapering to remove oxide layer (right).	158
Figure 6.2:	Schematic diagram of the polishing unit with a double-tool configuration....	160
Figure 6.3:	Experimental results of material removal depth against abrasive size.	165
Figure 6.4:	Multiplicative relationships (black lines) and relative relationships (red arrows) between the four constants in the proposed model and extensions.....	168
Figure 6.5:	Experimental results and theoretical curves of material removal depth against abrasive size.....	169
Figure 6.6:	(a) Number of active carbonyl iron particles (black) and (b) number of active abrasives (red) against abrasive size, according to theoretical model.....	171
Figure 6.7:	(a) Force per carbonyl iron particle (black) and (b) force per abrasive particle (red) against abrasive size, according to theoretical model.	173
Figure 6.8:	Experimental results of material removal depth against abrasive-to-carbonyl-iron volumetric ratio.	175
Figure 6.9:	Experimental results and theoretical curves of material removal depth against abrasive-to-carbonyl-iron volumetric ratio.....	177
Figure 6.10:	(a) Number of active carbonyl iron particles (black) and (b) number of active abrasives (red) against abrasive-to-carbonyl-iron volumetric ratio, according to theoretical model.....	179
Figure 6.11:	Force per carbonyl iron particle (solid line) and force per abrasive particle (dashed line), according to theoretical model.	180

Figure 8.1:	Tilted polishing unit as described in patent awarded for the new MFAF process.....	193
Figure A.2:	Selected element type options for PLANE53.	199
Figure A.3:	B-H and demagnetization curves for Grade N35 neodymium permanent magnet supplied by HKCM Engineering [3].	201
Figure A.4:	B-H curve for SUS430 by Carpenter [4]. Annealed (75.5 HRB), 788 °C H ₂ dried for 2 hours.....	203
Figure A.5:	Selected options for magnetostatics solver.	204
Figure A.6:	Magnetic flux lines for (a) single-magnet configuration, and (b) double-magnet configuration. Magnets are highlighted for clarity.	205
Figure A.7:	Contour plots of magnetic flux density for (a) single-magnet configuration, and (b) double-magnet configuration. Magnets are highlighted for clarity.	206
Figure A.8:	Measurement of magnetic flux density components in the (a) x direction and (b) z direction, using a vector magnetometer.	208
Figure A.9:	Comparison between calculated and measured values of magnetic flux density, for (a) x component, and (b) z component.....	209
Figure B.1:	(a) Schematic diagram of the two-dimensional line scans on a flat workpiece, and (b) an example of the profile obtained.	212

List of abbreviations and symbols

Δ MRR	Material removal rate per particle
a	Radius of projected circle of contact – for particle indentation
A	Projected area of indentation – for particle indentation
AC	Alternating current
$A_{\text{available, abr plane}}$	Area available for abrasives on abrasive plane
a_{CI}	Ratio of area in unit triangle occupied by carbonyl iron particles
A_{CI}	Area occupied by carbonyl iron particles in unit triangle
$A_{\text{CI, abr plane}}$	Area occupied by carbonyl iron particles on abrasive plane
A_{contact}	Contact area between finishing media and workpiece
A_{unit}	Area of a unit triangle
AFM	Abrasive flow machining
B	Magnetic flux density
BEMRF	Ball-end magnetorheological finishing
CBN	Cubic boron nitride
CC Grade	Carbonyl iron particles with mean diameter of 3.8 μm -5.3 μm
CI	Carbonyl iron
CIP	Carbonyl iron particle or powder
CM Grade	Carbonyl iron particles with mean diameter of 7.0 μm – 9.5 μm
CMP	Chemical-mechanical polishing
CNC	Computer numerical control
CS Grade	Carbonyl iron particles with mean diameter of 6.0 μm – 7.0 μm
CVD	Chemical vapour deposition

D	Diameter of particle
D_{abr}	Diameter of abrasive particle
$D_{abr, crit}$	Critical diameter of abrasive particle for occupation of interstitial space in carbonyl iron matrix
$D_{abr, eqv}$	Equivalent abrasive diameter – used in extension for abrasive volume criterion
D_{CI}	Diameter of carbonyl iron particle
DAE	Dicarboxylic acid ester
DoE	Design of experiment
E	Young's modulus
EDM	Electro-discharge machining
FMAB	Flexible magnetic abrasive brush
F	Force per particle
F_{abr}	Force per abrasive particle
FCC	Face-centred cubic
F_{CI}	Force per carbonyl iron particle
F_n	Normal force
F_s	Shear force
h	Indentation depth of particle
H	Magnetic field strength vector
HCP	Hexagonal close packed
IR	Infrared
k_{abr}	MRR factor constant for abrasives
k_{CI}	MRR factor constant for carbonyl iron particles
$k_{F, abr}$	Force factor constant for abrasives

$k_{F, CI}$	Force factor constant for carbonyl iron particles
m_{abr}	Mass of abrasives
$m_{abr, max}$	Mass of abrasives corresponding to saturation level
MAF	Magnetic abrasive finishing
MCF	Magnetic compound fluid
MFAF	Magnetic field-assisted finishing
MFG	Magnetic fluid grinding
MFP	Magnetic float polishing
MR	Magnetorheological
MRAFF	Magnetorheological abrasive flow finishing
MRD	Material removal depth
MRF	Magnetorheological finishing
MRR	Material removal rate
MRR_{peak}	Peak material removal rate
N	Number of active particles
N_{abr}	Number of active abrasives
$N_{abr, max}$	Maximum number of active abrasives – at saturation level
N_{CI}	Number of active carbonyl iron particles
NdFeB magnet	Neodymium magnet
P	Polishing pressure
Ra	Arithmetical mean roughness
Rt or Ry	Maximum roughness height
Rz	Ten-point mean roughness
SUS304	Stainless steel grade 304 (non-ferrous)
SUS316	Stainless steel grade 316 (non-ferrous)

SUS430	Stainless steel grade 430 (Ferrous)
t_{cap}	Thickness of magnetic cap in polishing unit
t_{magnet}	Thickness of magnet in polishing unit
v	Relative velocity between abrasive and workpiece
v_{abr}	Volumetric ratio of abrasives in FCC unit cell
v_{CI}	Volumetric ratio of carbonyl iron particles in FCC unit cell
$v_{\text{interstitial}}$	Volumetric ratio of interstitial spaces in FCC unit cell
V	Volume of magnetic particle
w_{gap}	Magnet-to-magnet gap of polishing unit
χ	Susceptibility of magnetic particle
z	Magnet-to-workpiece gap of polishing unit

Chapter 1

Introduction

1.1 MECHANICAL SURFACE FINISHING IN PRECISION ENGINEERING

Surface finishing is typically the final step in a chain of manufacturing processes for high precision components. There are numerous surface finishing techniques available which can be broadly classified as mechanical, chemical, chemically-assisted or vibration-assisted. This thesis mainly considers mechanical processes in both assisted and non-assisted forms.

Surface finishing processes have several purposes. Firstly, they are used to achieve fine surface finish that high efficiency manufacturing processes such as conventional machining (which includes processes such as milling, turning, drilling and grinding) and forming (which includes processes such as forging and molding) cannot produce. In such applications, surface finishing processes are also referred to as polishing processes. A fine surface finish is important either for functional or aesthetic purposes or both. There is currently no strict definition for a fine surface finish, though a surface texture below $0.1 \mu\text{m Ra}$ is typically classified as fine finish for metal surfaces [1]. For example, the joint of a hip implant and the turbine blades of an aircraft engine require fine surface finish for friction reduction and reduced drag force respectively. On the other hand, cranks of high performance bicycles and the cylindrical chassis of the Apple Mac Pro (2015 version) require a fine surface finish to give a clean and reflective surface for aesthetic appeal. An emerging application at time of writing is the surface finishing of

parts produced by additive manufacturing or 3-D printing, which are complex in shape but typically have surface textures exceeding 20 $\mu\text{m Ra}$.

Secondly, surface finishing may be used to correct dimensional inaccuracies introduced by machining or forming processes. For instance, chemical mechanical polishing is used to improve the flatness of silicon wafers sliced by a sawing process, while magnetorheological finishing can be used for form correction of optical surfaces produced by single point diamond turning. In some applications, surface finishing processes may be used to achieve a fine surface finish, as well as for correcting dimensional inaccuracy.

There are at least two key areas of interest in the development of surface finishing techniques. The first is in developing new solutions for the processing of freeform and structured surfaces. These surfaces are difficult to process and typically require specialized process or tooling that are not transferrable from one component to another. An emerging demand is for the finishing of complex internal surface, which is driven by the meteoric rise in interests of additive manufacturing. Additively manufactured parts may include complex internal passages not reachable by conventional tools, and they require post-processing for surface texture improvement. Therefore, there are substantial academic and commercial interests in developing new techniques that are more generally applicable.

Another key area of interest is in the automation of these processes. Currently, many surface finishing jobs of complex components are carried out manually by skilled workers. In addition to the high overhead involved, this may result in inconsistent part quality, which leads to lower yield. Process automation typically requires an understanding of the process, and process modeling is crucial to that end.

1.2 PRECISION SURFACE REMOVAL TECHNIQUES

There are many precision surface removal techniques, and a thorough review and treatment of all the processes is beyond the scope of this work. Instead, a brief overview is given, with the intention of providing a context for the selection of magnetic field-assisted finishing as the approach. A list of precision surface removal techniques is presented below in Table 1.1.

Table 1.1: Precision surface removal techniques.

	Freeform	Structured	Internal	Remarks
Manual polishing	O	O	Δ	Skill-dependent, high cost, inconsistent outcome.
Classical lapping	X	X	X	Very good for flat surface.
VIBE polishing [2]	O	X	X	Typically for aspheric surface of optics component.
Fluid jet	O	Δ	Δ	Structured and internal capabilities limited by jet size and reachability.
Precessions bonnet polishing [3]	O	X	X	Capable of achieving superfinish at high removal rate.
Shape adaptive grinding [4]	O	X	X	Uses a conformable tool.
Reactive atom plasma [5]	O	O	X	In developmental phase.
MRF [6]	O	X	X	Developed for processing of optics
AFM [7]	Δ	X	O	Mainly for internal surfaces. External surfaces require fixturing.
ECM [8]	O	O	Δ	Requires specially shaped tooling.

It can be seen that there are many solutions targeting freeform surfaces, but not many for structured surfaces. Processes that depend on the rotation of a rigid tool for material removal are not suitable, while processes with a linear motion or stationary tooling (ECM) will require specially shaped tools. For internal surfaces, the key challenge for existing processes is reachability of the internal surfaces by tools.

With an understanding of the challenges facing conventional processes, magnetic field-assisted finishing processes have been identified as a unique, potential solution.

1.3 MAGNETIC FIELD-ASSISTED FINISHING (MFAF)

Magnetic field-assisted finishing (MFAF) is a broad category of non-conventional finishing processes that harnesses the unique properties of ferromagnetic smart fluids for surface finishing. Since its early development in the United States in the 1930's, many different techniques and embodiments of MFAF such as magnetic fluid grinding [9], magnetic abrasive finishing (MAF) [10] and magnetorheological finishing (MRF) [6] have been reported in the literature. Generally, these approaches manipulate magnetic fields to drive magnetic media onto a target surface to remove material or to assist in removing material. Material removal from the target surface is typically gentle enough to achieve reduction in asperity heights and therefore improves the surface texture.

The cornerstone of MFAF is the unique behaviour of ferrous particles under the influence of a magnetic field generated by permanent magnets or electromagnets. Under the magnetic field's influence, ferrous particles link together along the magnetic field lines, forming flexible chains suspended by the magnetic force. Seen as a bulk, the layer of ferrous particles behaves like a Bingham plastic - solid-like at rest but yields when subjected to a critical level of shear stress. When in contact with an external surface, the

layer of ferrous particles conforms to the geometry of the external surface, as shown in Figure 1.1. By mixing abrasives into the layer of ferrous particles and introducing relative motion between the layer and the external surface (by rotation, vibration, or any other form of actuation), material may be removed from the workpiece surface. The ability to remove material from an external surface with freeform features and complex geometry is a distinct advantage of MFAF.

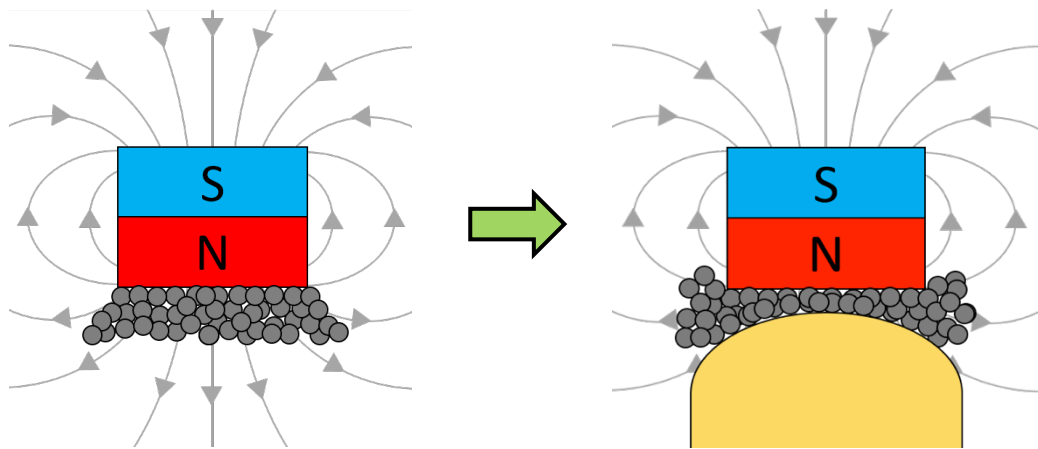


Figure 1.1: Schematic diagram to illustrate the conformable nature of magnetic particles.

In addition, magnetic flux flows unimpeded and unperturbed through any non-ferrous and non-magnetic workpiece. As such, the motion of ferrous particles can be influenced and controlled even when they are not in direct contact with a magnetic pole. Thus, MFAF can also be used as a finishing operation on hard-to-reach areas such as internal surfaces, as shown in Figure 1.2. This constitutes another distinct advantage of MFAF.

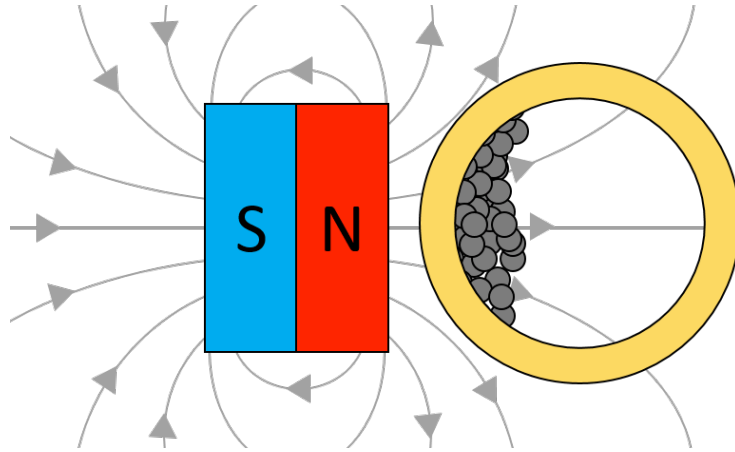


Figure 1.2: Schematic diagram to illustrate that the motion of magnetic particles can be influenced even when not in direct contact with a magnetic pole.

1.4 MOTIVATIONS

There have been recent demands from the aerospace industry for an automated surface finishing technology capable of polishing complex geometry and hard-to-reach internal surfaces. Traditionally, mass finishing operations such as vibratory finishing and drag finishing were used to polish external freeform surfaces when a fine surface finish is not required. Components requiring fine surface finish below $0.01 \mu\text{m Ra}$ are manually polished by skilled craftsmen with traditional polishing tools. As a result, the quality of components produced may vary from part to part and is dependent on the skill level of the craftsmen. Attempts to automate conventional surface finishing operations have thus far achieved limited success. The main challenge of automating finishing processes based on conventional tools is arguably the compensation for changes in tool geometry due to tool wear. Huang et al. [11] have demonstrated methods to empirically compensate for the tool wear, but such methods may be cumbersome, inflexible and unreliable. Compensation by force control is more promising, but any such solution must consider

the fluctuation of contact forces arising from a dynamic contact area during the polishing process.

MFAF processes, which use conformable finishing media, may therefore be a viable substitute for the conventional tools and thus eliminate the need for compensation. However, certain technological hurdles prevent wide adoption of the technology for commercial applications. Firstly, formulation of finishing media for MFAF processes is dependent on the target material, and there is a paucity of knowledge for the MFAF of materials other than optical glasses. Therefore, commercial applications of MFAF are thus far limited to the polishing of high value-added optics. Secondly, finishing media of MFAF processes are known to deteriorate over time due to debris from material removal, oxidation of magnetic particles, and carrier fluid degradation. These translate into stability issues that must be addressed before an MFAF process can be viably applied for commercial purposes. Lastly, the removal rate of MFAF processes is low compared to conventional abrasive processes, while commercial applications usually require high efficiency material removal. As such, MFAF processes are currently used only for commercial applications of small volume.

Fortunately, the technological hurdles mentioned above are not insurmountable. The capability for MFAF to polish exotic materials such as titanium alloys, nickel alloys and tungsten carbide can be investigated and better understood through theoretical analyses, or empirically by conducting appropriate process studies to test different finishing media formulations and process parameters. In terms of process stability, some solutions have already been proposed to improve the stability of the finishing media [12, 13]. Lastly, the material removal rate may be improved by optimizing the process conditions. In addition, the process efficiency may see significant improvements through

innovations on the finishing media and innovative manipulation of magnetic properties to develop new MFAF processes with high efficiency.

The combination of commercial interests and technical challenges make the development of MFAF processes a meaningful topic to both the scientific community and the manufacturing industry. As a bonus, positive outcomes may lead to lucrative rewards commercially.

1.5 SCOPES AND OBJECTIVES

The overarching goal of this thesis is to initiate the development of a new MFAF process that is capable of achieving high material removal rate, feasible for polishing structured surfaces, and is suitable for automation. In a preliminary study, a new process capable of achieving high material removal rate has been proposed.

The first objective of this thesis is to establish the principles of the new process that contribute to the increased material removal rate. Theoretical magnetostatic analyses and empirical observations are both employed to that end. The second objective, which is related to the first, is to establish the capability of the new process to improve surface texture on both flat surfaces and freeform surfaces. Experiments will be conducted and the capability will be verified by inspection of the polished surfaces through microscopic observations and two-dimensional profilometry. For experimentation, the workpiece material chosen is stainless steel (SUS 316), which is a common material to allow comparison with other processes, and aerospace grade titanium alloys, such as Ti-6Al-4V. For freeform surface, the selected surface is micro-scale V-grooves array (0.2 mm wide and 0.1 mm deep) on a flat surface, which is extremely challenging to polish with currently available techniques. Note that the selected surface geometry is in fact

classified as a structured surface rather than a freeform surface. The reason for choosing structured surface is that it is arguably a bigger challenge compared to freeform surface.

The third objective is to establish a method to predict the material removal rate of the process when the polishing conditions are varied. The ability to predict the material removal rate is critical for process automation. To that end, a material removal rate model is proposed to describe the relationship between material removal rate and the polishing parameters. Many material removal rate models that pertain to common polishing parameters such as revolution speed, polishing time, and material properties of workpiece have already been reported in the literature. For the new material removal rate model, the focus is on the relationship between material removal rate and some properties related to the finishing media.

The last and final objective is to validate the proposed model experimentally for a selected range of values of parameters in the proposed model.

1.6 REPORT STRUCTURE

A background on the role of surface finishing and MFAF as manufacturing technologies has been presented at the beginning of this chapter. Thereafter, the motivations, objectives and scopes of this thesis have been outlined. Following this introductory chapter, there are six more chapters.

Chapter 2 covers the literature review conducted on the current state of MFAF processes. The review will be structured according to the four classes of finishing media currently used in MFAF processes – ferrofluid, magnetic compound fluid, magnetorheological fluid and magnetic abrasive. Chapter 2 will be concluded with a summary on research opportunities in the field of MFAF.

Chapter 3 pertains to the early developmental work of the new MFAF process. The process principles of the new process are established by both theoretical analyses and empirical observations. Parameters of the proposed polishing tool are also studied theoretically with magnetostatic analyses. Based on the simulation results, a set of parameters is suggested for the first prototype. Finally, the capability of the process for improving surface texture and polishing freeform surfaces is validated with the prototype.

Chapter 4 and 5 embody the theoretical work on proposing a material removal rate model for the new MFAF process. The complete derivation of the base model is presented in chapter 4, while two extensions for the base model to include conditions that are invalid for the base model are presented in chapter 5.

Chapter 6 is the experimental verification of the base model and its two extensions presented in the previous two chapters. The trends between the properties of the finishing media, such as the abrasive particle concentration and abrasive particle size, and the material removal rate are verified experimentally.

Chapter 7 summarizes the work done in this thesis and provides suggestions on direction for future research work for this topic.

1.7 CONTRIBUTIONS OF THE CANDIDATE

The development of the new MFAF process was a joint effort between the candidate and his supervisor. In the awarded patent, the candidate is listed as a one of the two co-inventors, with equal weightage. Most of the experiments up to Chapter 3 was conducted by the candidate, while some results were drawn from experiments conducted jointly with co-workers in the institute.

The proposed model was the candidate's original work. The candidate was responsible for all the work conducted and reported from Chapter 4 onwards.

REFERENCES

- [1] All Seals Inc. Surface finish cross reference chart. Retrieved on 31 December 2015 from http://www.allsealsinc.com/surface_finish_chart.pdf
- [2] Klinger C, *Vibe: A new process for high speed polishing of optical elements*. Optifab: Technical Digest, SPIE Technical Digest TD04, 2007.
- [3] Beaucamp A, Namba Y and Charlton P. *Corrective finishing of extreme ultraviolet photomask blanks by precessed bonnet polisher*. Applied Optics, 2014. **53**(14): p. 3075-3080.
- [4] Beaucamp A, Namba Y, Combrinck H, Charlton P and Freeman R, *Shape adaptive grinding of CVD silicon carbide*. CIRP Annals - Manufacturing Technology, 2014. **63**(1): p.317-320.
- [5] Fanara C, Shore P, Nicholls JR, Lyford N, Kelley J, Carr J and Sommer P. *A new reactive atom plasma technology (RAPT) for precision machining: the etching of ULE® surfaces*. Advanced Engineering Materials, 2006. **8**(10): p.933-9.
- [6] Kordonski WI. *Adaptive structures based on magnetorheological fluids*. In *Third International Conference on Adaptive Structures*. 1993.
- [7] Loveless TR, Williams RE, Rajurkar KP. *A study of the effects of abrasive-flow finishing on various machined surfaces*. Journal of Materials Processing Technology, 1994. **47**(1): p. 133-51.
- [8] McGeough JA. Principles of electrochemical machining. CRC Press; 1974.
- [9] Umehara N and Kato K, *Principles of magnetic fluid grinding of ceramic balls*. Journal of Applied Electromagnetic Materials, 1990. **1**: p. 37-43.
- [10] Shinmura T, Takazawa K, Hatano E, Matsunaga M and Matsuo T, *Study on magnetic abrasive finishing*. CIRP Annals-Manufacturing Technology, 1990. **39**(1): p. 325-328.
- [11] Huang H, Gong Z, Chen X and Zhou L, *Robotic grinding and polishing for turbine-vane overhaul*. Journal of Materials Processing Technology, 2002. **127**(2): p. 140-145.
- [12] Shafrir SN, Romanofsky HJ, Skarlinski M, Wang M, Miao C, Salzman S, Chartier T, Mici J, Lambropoulos JC and Shen R, *Zirconia-coated carbonyl-iron-particle-based magnetorheological fluid for polishing optical glasses and ceramics*. Applied Optics, 2009. **48**(35): p. 6797-6810.

- [13] Hanada K, Yamaguchi H and Zhou H, *New spherical magnetic abrasives with carried diamond particles for internal finishing of capillary tubes*. Diamond and Related Materials, 2008. **17**(7): p. 1434-1437.

Chapter 2

Review of magnetic field-assisted finishing (MFAF) processes

2.1 INTRODUCTION

In this chapter, relevant literatures published on MFAF processes are reviewed and presented. Jain [1] has previously summarized some developments in MFAF by describing four MFAF processes, namely magnetic float polishing, magnetic abrasive finishing, magnetorheological finishing and magnetorheological abrasive flow finishing. Jain's review is focused on the process principles and capabilities of the MFAF processes. The review presented in this chapter will take a different approach, emphasizing instead on the finishing media used in MFAF processes.

2.1.1 Four classes of finishing media for MFAF

The four classes of finishing media used for MFAF processes are ferrofluid (also known as magnetic fluid), magnetorheological fluid (also known as MR fluid), magnetic compound fluid (MCF) and magnetic abrasives. The key characteristic that distinguishes these four classes of finishing media is the size of the magnetic particles used.

Ferrofluid contains the smallest magnetic particles, which typically have an average diameter smaller than 1 μm , but more commonly between 10 nm - 100 nm. Magnetic particles in ferrofluid are typically magnetite (Fe_3O_4). In addition to magnetic particles, ferrofluid used for MFAF processes also contains non-magnetic abrasives. Both the magnetic particles and non-magnetic abrasives are suspended in a carrier fluid with chemical additives to promote better particle dispersion.

MR fluid contains larger magnetic particles, which typically have an average diameter of between 1 μm - 10 μm . Magnetic particles in MR fluid are usually carbonyl iron particles of high purity (greater than 99 %) produced by the thermal decomposition of iron pentacarbonyl ($\text{Fe}(\text{CO})_5$) [2]. In addition to magnetic particles, MR fluid used for MFAF processes also contains non-magnetic abrasives. Both the magnetic particles and non-magnetic abrasives are also suspended in a carrier fluid with chemical additives to promote better particle dispersion.

MCF, essentially a mixture of ferrofluid and MR fluid, contains magnetic particles that are both micro-sized (1 μm - 10 μm) and nano-sized (10 nm - 100 nm). Physical properties of MCFs typically fall in-between ferrofluid and MR fluid. In addition to magnetic particles, MCF used for MFAF processes also contains non-magnetic abrasives and α -cellulose fibers suspended in a carrier fluid with chemical additives [3].

Lastly, magnetic abrasives have the largest magnetic particles, which typically have an average diameter exceeding 10 μm , but more commonly between 100 μm - 1000 μm . In the literature, the term ‘magnetic abrasives’ have been used to describe both unbonded magnetic abrasives, where magnetic particles and non-magnetic abrasives are mixed mechanically [4] and bonded magnetic abrasives, where non-magnetic abrasives are embedded onto the magnetic particles [5]. Magnetic abrasives are also used together with a carrier fluid for lubrication purposes. Magnetic abrasives typically do not suspend well in a carrier fluid due to their large particle size.

2.1.2 Comparisons of the finishing media

The size of magnetic particles critically affects both the physical characteristics and behavior of the finishing media, regardless of the presence of a magnetic field. When not under the influence of a magnetic field, finishing media with smaller magnetic particles are less viscous than finishing media with larger magnetic particles, as smaller magnetic particles are better suspended in a carrier fluid. This is true when mass of particles per unit volume in the finishing media is constant. Hence, ferrofluid, MR fluid and MCF are typically fluidic and flow easily. For these fluidic finishing media, the viscosity increases with the size of magnetic particles, *ceteris paribus*. On the other hand, magnetic abrasives in a carrier fluid usually appear as visible grains that settle at the bottom of the container quickly. The fluid dynamics of finishing media is an important engineering consideration for media circulation in MFAF processes.

Under the influence of a magnetic field, finishing media of different magnetic particle sizes also behave differently. Firstly, the magnetic force exerted on a magnetic particle is directly proportional to its volume. Larger magnetic particles therefore form stronger chains along the magnetic field lines. As a result, the increase in viscosity of finishing media rank in the following order: ferrofluid, MCF, MR fluid, magnetic abrasives. Viscosity is an important characteristic of the finishing media that affects both the process efficiency and the process outcome. Generally, a higher viscosity means a higher removal rate, but also a rougher surface finish. Secondly, as larger magnetic particles do not suspend well in the carrier fluid, there is a propensity for the carrier fluid and non-magnetic abrasives to separate from them. In the example of a magnetic abrasives media on a rotating permanent magnet tool, the magnetic particles may be held in place by the strong magnetic force while the carrier fluid and non-magnetic particles are scattered due to centrifugal force from the tool rotation.

Lastly, from an academic viewpoint, the physics required to analyze the behavior of finishing media with different sizes of magnetic particles, regardless of whether a magnetic field is present, may be substantially different. When the magnetic particles are large, solid behaviour dominates and solid mechanics may be sufficient for analysis of the material removal mechanism. However, as the magnetic particles decrease in size, the influence of the carrier fluid becomes significant and may not be negligible. A complex combination of fluid mechanics and solid mechanics may be required for proper analyses of MFAF finishing media with small magnetic particles.

Figure 2.1 summarizes the aforementioned comparisons.

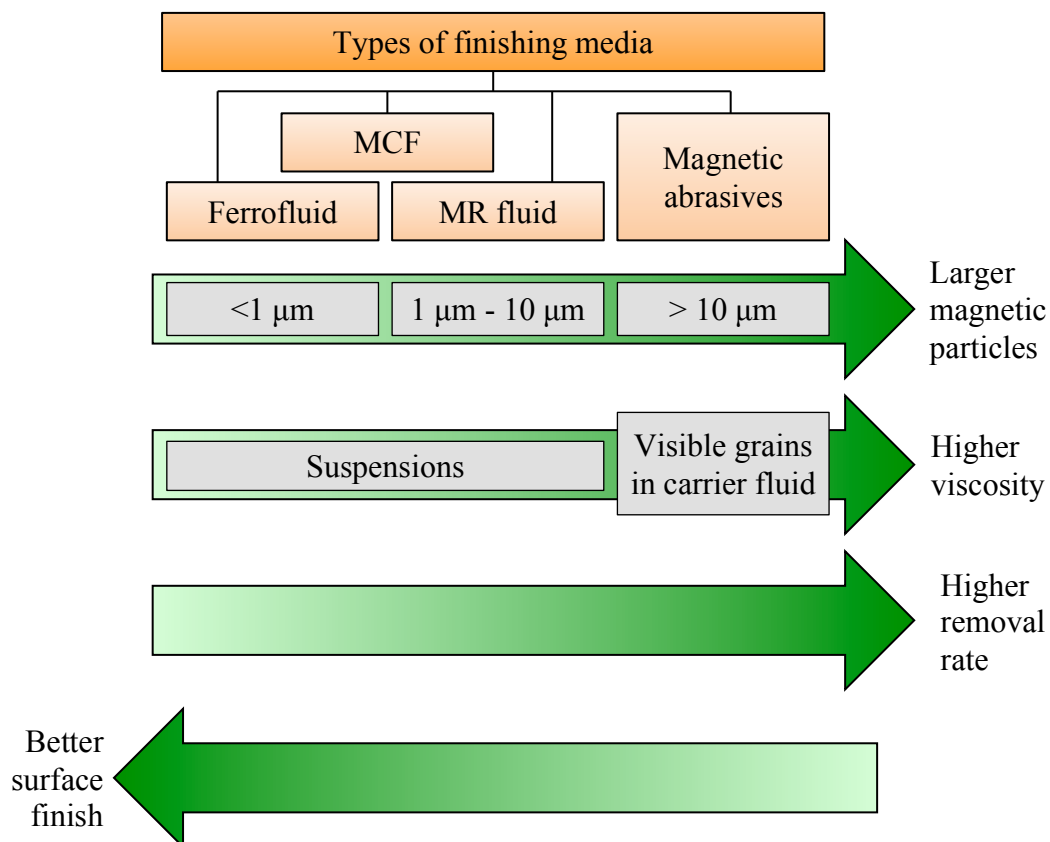


Figure 2.1: Comparison of finishing media used for MFAF processes.

2.1.3 Review structure

This literature review is organized into four major parts, one for each of the four classes of finishing media, in the following order: ferrofluid, MCF, MR fluid and magnetic abrasives. Within each major part, related processes will first be briefly described, followed by a review of the media studies reported in literature. Focus will be given mainly to MR fluid, which is the class of finishing media used in a new MFAF process to be proposed in a latter chapter.

Following that, a summary of the review will be presented. Research opportunities for process and media development for MFAF are then proposed. Figure 2.2 shows a flowchart that summarizes the content and structure of this chapter.

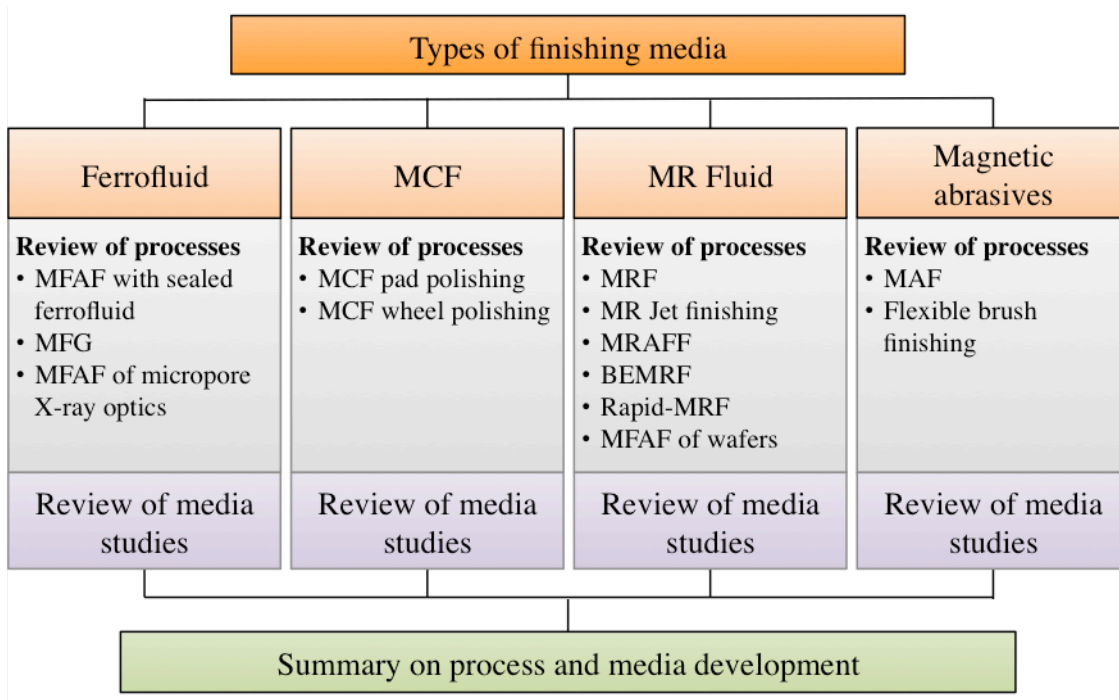


Figure 2.2: Flowchart of the literature review chapter.

2.2 FERROFLUID

2.2.1 MFAF processes based on ferrofluid

2.2.1.1 MFAF with sealed ferrofluid

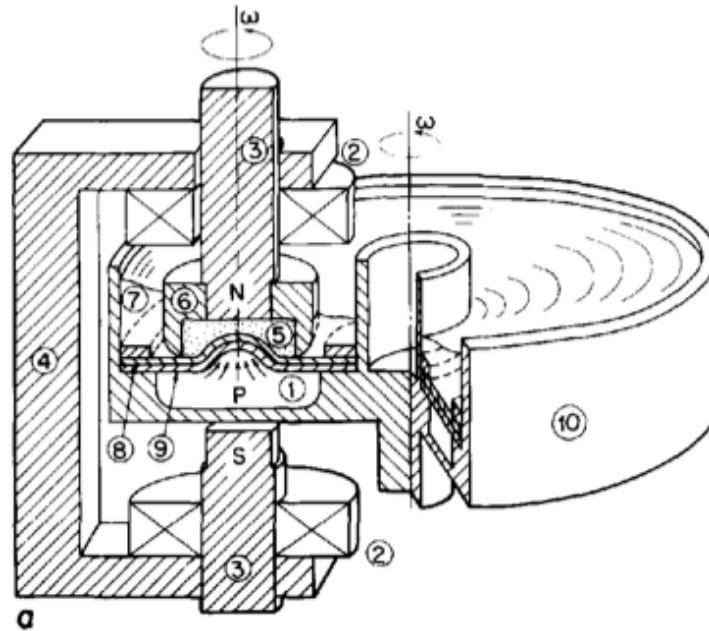


Figure 2.3: Schematic diagram of MFAF with sealed ferrofluid [7].

One of the earliest applications of ferrofluid for an MFAF process is the MFAF with sealed ferrofluid developed by Kurobe and Imanaka [7]. Figure 2.3 shows the schematic diagram of the process. In the process, magnetic force on ferrofluid is used to deform an elastic on a polishing sheet, which then applies pressure on the workpiece. Detailed descriptions of the process can be found elsewhere [6, 7]. In this process, the ferrofluid is sealed and only used to provide pressure to a polishing sheet made of rubber. The finishing media (silicon carbide abrasives suspended in water) responsible for material removal is separate from the ferrofluid. Since the ferrofluid does not come into

direct contact with the workpiece, the composition of the ferrofluid is not critical, with fluid stability and saturation magnetization instead being the primary concerns.

2.2.1.2 Magnetic fluid grinding

Ferrofluid is used in a process known as magnetic fluid grinding (MFG), which was originally introduced by Umehara and Kato [8] as a finishing process for silicon nitride (Si_3N_4) ceramic balls used for advanced ball bearings applications. It was proposed as a competing technology to the lapping process, which was then the state-of-the-art finishing operation for ball bearings. The apparatus of MFG for ceramic balls is illustrated in Figure 2.4. In MFG, workpieces (typically spherical or cylindrical) are submerged a ferrofluid reservoir and is sandwiched between a rotating shaft and a float, which applies pressure on the workpieces. The float presses the workpiece towards the shaft as a result of magnetic levitation force. A detailed exposition of the principles of MFG is available in the original article [8]. In later years, MFG has also been referred to as magnetic float polishing (MFP), in reference to the float, which is a key hardware in MFG.

For MFG of Si_3N_4 balls, Umehara and Kalpakjian [9] utilized a finishing media with SiC abrasives (median size $17.3\text{ }\mu\text{m}$) suspended in a water-based ferrofluid. A minimum surface texture and sphericity of $0.1\text{ }\mu\text{m Rz}$ and $0.14\text{ }\mu\text{m}$ respectively were reported. Sphericity was defined as the difference between the largest and smallest diameters of a ball arising from repeated measurements (a smaller sphericity is therefore more desirable). A maximum removal rate of $12.4\text{ }\mu\text{m/min}$ was also quoted, and the initially rough surface was described to have turned shiny after three hours of MFG. Childs *et al.* [10] also performed MFG experiments on Si_3N_4 balls using diamond

abrasives (20 μm - 40 μm) and reported an average surface texture and average sphericity of 0.2 μm Ra and 1.4 μm respectively. Using smaller diamond abrasives (1 μm - 2 μm), an average surface texture and average sphericity of 0.05 μm Ra and 0.6 μm respectively were also obtained, albeit at about one-tenth of the removal rate. About a decade later, Umehara *et al.* [11] reported on a new apparatus for finishing large batches of Si_3N_4 balls, together with some process refinements. A multistep approach with decreasing abrasive sizes was also used to achieve the best possible surface finish. A surface finish of 0.0082 μm Ra and an average sphericity of 0.27 μm were reported. Table 2.1 summarizes the aforesaid, although direct comparison must be done with caution as the reported values were based on different apparatus, different finishing media formulations and different experimental conditions.

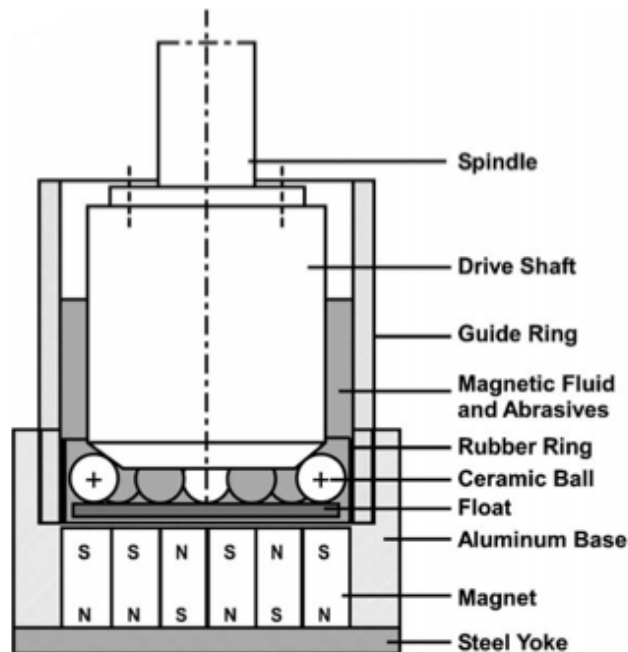


Figure 2.4: Schematic diagram of the MFG apparatus for the finishing of ceramic ball [11].

Table 2.2: Reported results for MFG or MFP of Si_3N_4 balls.

	Umehara and Kalpakjian [9]	Childs <i>et al.</i> [10]		Umehara <i>et al.</i> [11]
Workpiece	Si ₃ N ₄ balls			
Abrasive type and size	SiC #400 (17.3 μm, median)	Diamond (20 μm - 40 μm)	Diamond (1 μm - 2 μm)	B ₄ C #500 (12 μm, median)
Ra (μm)	-	0.2 ± 0.1	0.05	0.0082
Rz (μm)	0.1 (min)	-	-	-
Removal rate (μm/min)	12.4 (max)	5	0.5	1 to 1.5
Sphericity (μm)	0.14 (min)	1.4 ± 0.6	0.6	0.27

While polishing Si_3N_4 balls is the main objective of MFG, MFG has also been used for polishing of other workpieces such as Si_3N_4 rollers and flat alumina plates. In addition to results for polishing of Si_3N_4 balls, Umehara and Kalpakjian [9] also reported works on to the MFG of as-sintered Si_3N_4 rollers using the apparatus shown in Figure 2.5. The finishing media utilized for their experiments was similar to that for MFG of Si_3N_4 balls, except that SiC abrasives were substituted by cubic boron nitride (CBN) abrasives (median size 29.2 μm). The straightness and roundness of Si_3N_4 rollers were improved to 22 μm and 3.18 μm respectively, although a surface texture of 2.0 μm Rz meant that they were not well polished. A removal rate of 0.76 $\mu\text{m}/\text{min}$ was also quoted, which is significantly lower than the removal rate achieved for Si_3N_4 balls. In a separate study, Umehara and Komanduri [12] experimented on the MFG of hot isostatically pressed (HIP) Si_3N_4 rollers, but with different abrasives compared to their earlier study. With

chromium oxide (Cr_2O_3) abrasives (median size $3\text{ }\mu\text{m}$), the straightness and roundness of Si_3N_4 rollers were improved to $10\text{ }\mu\text{m}$ and $4.25\text{ }\mu\text{m}$ respectively, and a surface texture of $0.091\text{ }\mu\text{m Rz}$ and $0.029\text{ }\mu\text{m Ra}$ were achieved.

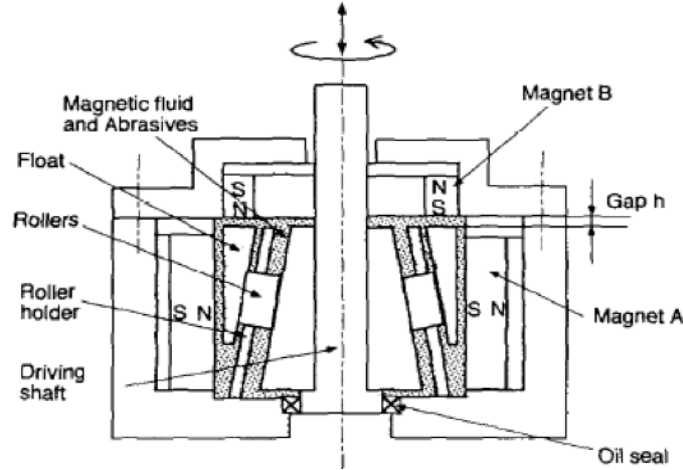


Figure 2.5: Schematic diagram of the magnetic fluid grinding apparatus for the finishing of ceramic rollers [12].

Table 3.2: Reported results for MFG of Si_3N_4 rollers.

	Umehara and Kalpakjian [9]	Umehara and Komanduri [12]
Workpiece	As-sintered Si_3N_4 rollers	HIP- Si_3N_4 rollers
Abrasive type and size	CBN #320 ($29.2\text{ }\mu\text{m}$, median)	Cr_2O_3 ($3\text{ }\mu\text{m}$, median)
Ra (μm)	-	0.029
Rz (μm)	2.0	0.091
Removal rate ($\mu\text{m}/\text{min}$)	0.76	1.11
Straightness (μm)	22	10
Roundness (μm)	3.18	4.25

2.2.1.3 MFAF of micropore X-ray optics

Ferrofluid was utilized in an MFAF process developed by Yamaguchi *et al.* [13] for the polishing of high aspect ratio sidewalls of micropore structures found in X-ray optics. Figure 2.6 illustrates the apparatus used for the polishing work, where the two electromagnets on either side of the container were switched on and off alternately by an AC current supply. That created a dynamic magnetic field that caused the magnetic particles in the ferrofluid to oscillate in the finishing media and remove material by mechanical actions. A more complete description of the process principles can be found in the original article [13]. The finishing media used for the process consisted of diamond abrasives of different sizes ($< 0.05 \mu\text{m}$, $< 0.2 \mu\text{m}$ and $< 0.5 \mu\text{m}$) suspended within a water-based ferrofluid.

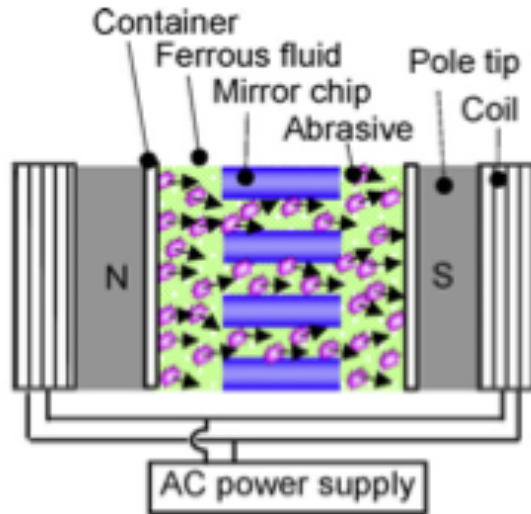


Figure 2.6: Schematic diagram of apparatus for MFAF of micropore X-ray optics [13].

Figure 2.7 shows the reported surface texture of the micropore sidewalls after 60 minutes of processing. The reduction in surface texture demonstrates the capability of the process.

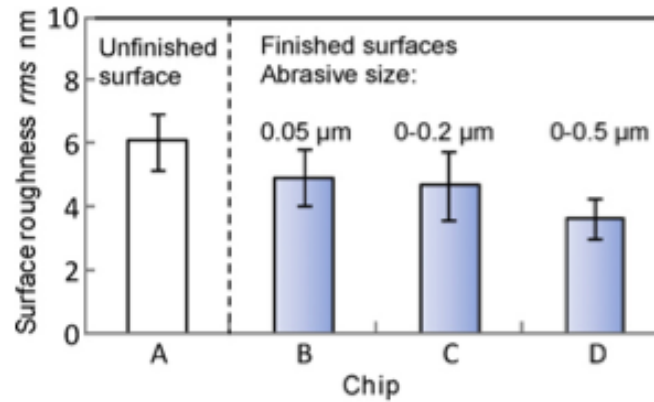


Figure 2.7: Surface texture after 60 minutes of polishing with diamond abrasives of different sizes [13].

2.2.2 Reported studies on ferrofluid

The importance of the formulation of ferrofluid-based finishing media in determining the success of an MFAF process has been intuitive to researchers from the beginning. This is apparent from the frequency of which research groups focusing on different MFAF processes carried out studies related to the properties of finishing media. For example, Childs *et al.* [10] conducted MFG on Si_3N_4 balls with different abrasive sizes ranging from 1 μm to 80 μm to study its effect on the removal rate and the achievable surface texture. Figure 2.8 shows the results reproduced from the original article. The removal rate was found to peak when the abrasive size is in the 10 μm - 20 μm range, while the surface texture increased with the abrasive size. The fact that increasing abrasive size can cause a reduction in removal rate may be a strange notion to some, and these are examined later in this thesis (Section 6.3.3). These results partially agree with the general observation in abrasive processes such as lapping, which is that both the removal rate and the surface texture increase with the abrasive size.

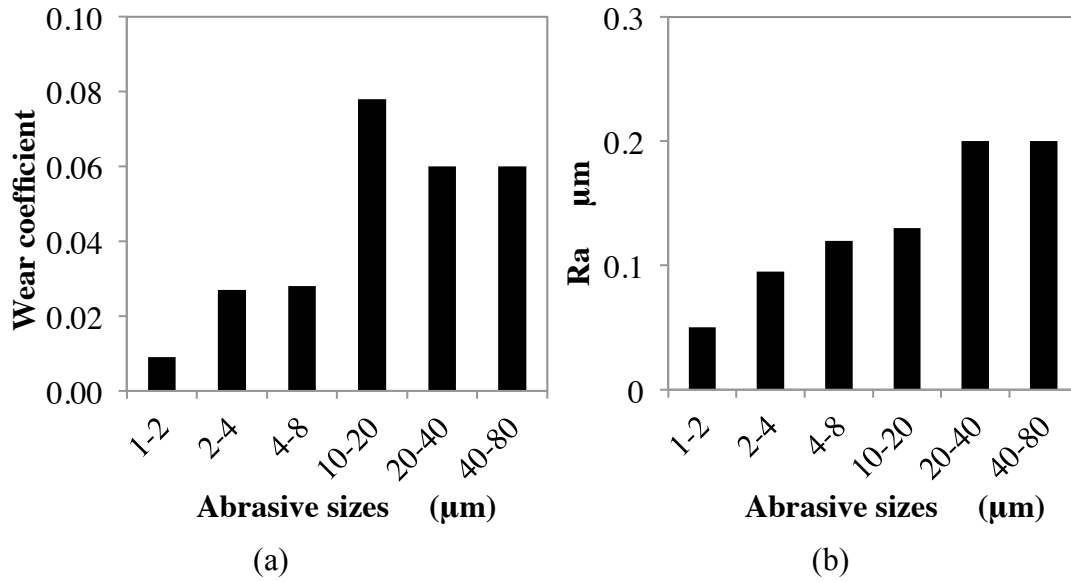


Figure 2.8: Effects of abrasive sizes on the (a) wear coefficient and (b) Ra [10].

A similar trend was also observed by Umehara and Komanduri [12] for the polishing of Si_3N_4 rollers with three different sizes of Cr_2O_3 abrasives, although results obtained by Yamaguchi *et al.* [13] during the polishing of micropore sidewalls, where abrasive sizes were also varied, show contradiction to results reported by Childs *et al.* [10] and Umehara and Komanduri [12]. From Figure 2.7 shown earlier, it can be seen that the final surface texture decreased when the diamond abrasive sizes were increased. Yamaguchi *et al.* reasoned that larger diamond abrasives left deeper cuts, removed more materials and hence achieved a lower surface texture. Common understanding of abrasive processes however tends to suggest the contrary, that larger abrasive sizes will result in a rougher surface. However, the MFAF process reported by Yamaguchi *et al.* is unconventional and its mechanism may therefore be different compared to conventional abrasive processes.

In addition to the study of abrasive sizes, Childs *et al.* [10] also tested five different ferrofluid formulations composed of either water-based or oil-based carrier fluid with different viscosity. It was found that an ideal carrier fluid viscosity to obtain the optimum removal rate exists. Childs *et al.* hypothesized that too low a fluid viscosity did not cause skidding of the ceramic balls while too high a viscosity of the carrier fluid caused skidding but also induced the formation of a lubrication film that retarded the abrasive actions of the abrasives. The explanation provided by Childs *et al.* is in good agreement to the modern elasto-hydrodynamic lubrication theory, which is often quoted to explain similar observations made in chemo-mechanical polishing [14].

In the report by Umehara and Komanduri [12] on MFG of Si_3N_4 rollers that has been mentioned earlier, the authors also conducted studies to investigate the effect of the abrasive type. Three different abrasive types – boron carbide (B_4C) (hardest), SiC and Cr_2O_3 (softest) were tested. In agreement with conventional knowledge, it was found that the removal rate increased with the abrasive hardness. Despite the low removal rate, Cr_2O_3 gave the best surface finish. The original results reported by Umehara and Komanduri are shown in Figure 2.9. It may be difficult to draw a clear conclusion on the effect of abrasive type on the surface texture as Cr_2O_3 also reacts chemically with Si_3N_4 favourably to improve the surface finish [15].

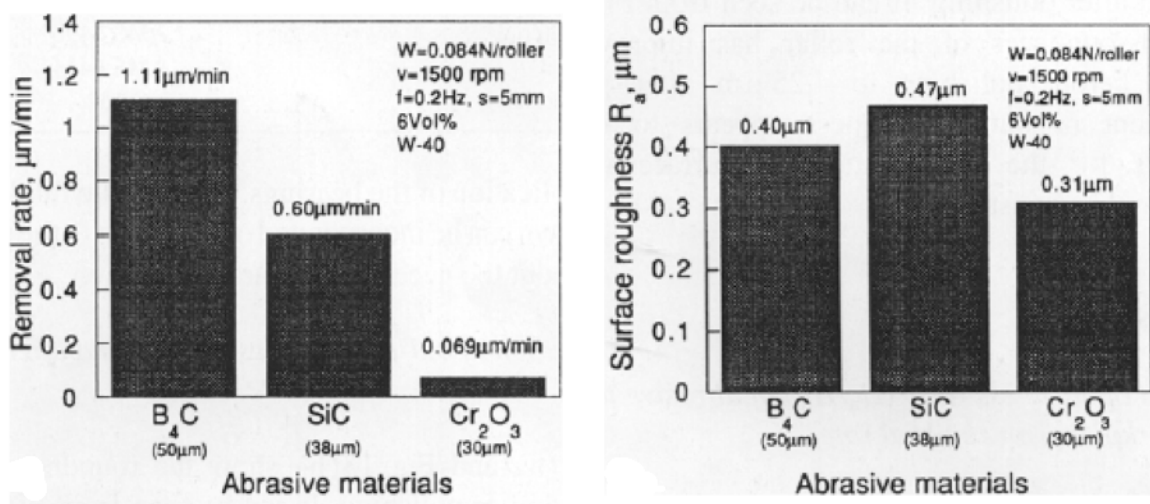


Figure 2.9: Effects of abrasive type on (a) removal rate and (b) surface texture [12].

Other media-related observations for ferrofluid-based finishing media include findings reported by Jiang and Komanduri [16], where their design of experiment (DoE) study indicated that a 5 vol. % concentration of abrasives was more favourable than 10 or 20 vol. % to achieve a smooth surface finish during the MFG of Si₃N₄ balls. The authors did not provide any explanation for this observation. In a separate study, Umehara and Komanduri [12] attempted to correlate the removal rate and surface texture to the abrasive-to-workpiece hardness ratio. Although the hardness ratio is regularly used in wear study for conventional abrasive processes, the authors obtained no clear correlation.

2.3 MAGNETIC COMPOUND FLUID (MCF)

2.3.1 MFAF processes based on MCF

2.3.1.1 MCF pad polishing

MCF, which was introduced by Shimada *et al.* [3], is the newest class of polishing fluid used for MFAF processes. In the beginning, MCF was a blend of magnetite (10 nm)

coated with oleic acid, carbonyl iron particles ($1.2\ \mu\text{m} - 1.6\ \mu\text{m}$), Al_2O_3 abrasives ($3\ \mu\text{m}$) and kerosene. MCF was initially studied for the polishing of pure titanium using a pad polishing process as shown in Figure 2.10. The principles of MCF are similar to that of lapping, except that magnetic force acts on the slurry (MCF fluid) to augment the pressure on the workpiece. A detailed description of the processing principle has been reported elsewhere [17].

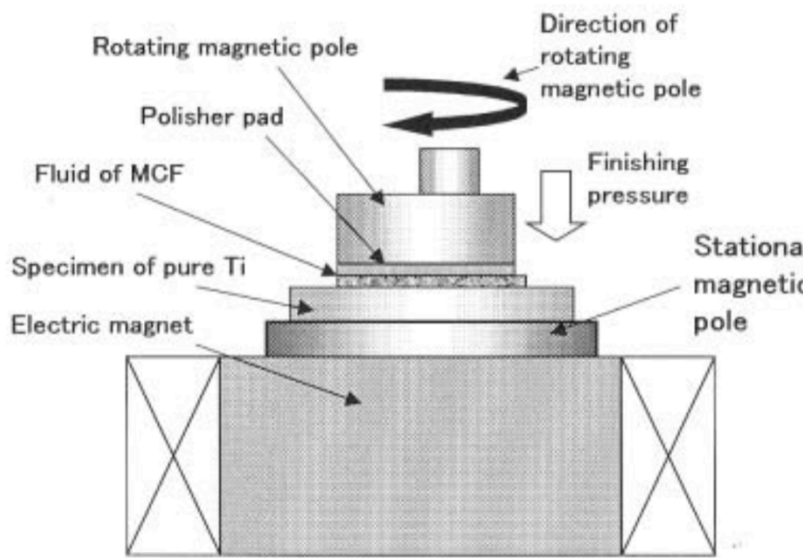


Figure 2.10: Schematic diagram pad polishing using MCF [3].

The capability of the process was demonstrated with the titanium workpiece polished from $0.367\ \mu\text{m Ra}$ initially to $0.132\ \mu\text{m Ra}$. It was also reported that a fluctuating magnetic field gave better surface finish than a steady magnetic field and an optimum value for the magnetic field strength exists. Shimada *et al.* [18] later showed that this optimal value is approximately $0.15\ \text{T}$ for their apparatus, regardless of the workpiece material.

In their subsequent work, Shimada *et al.* [19] incorporated α -cellulose fibers into the MCF to replace the physical polishing pad. The results were positive, and the latest embodiment of MCF now includes α -cellulose fibers in the finishing media.

2.3.1.2 MCF wheel polishing

A wheel consisting of an outer layer of MCF has also been proposed for the use of polishing [20]. The principles of the process are akin to grinding, whereby bonded materials are replaced by an MCF layer held together by magnetic forces. Figure 2.11 shows the schematic diagram of the most recently reported design of an MCF wheel [21].

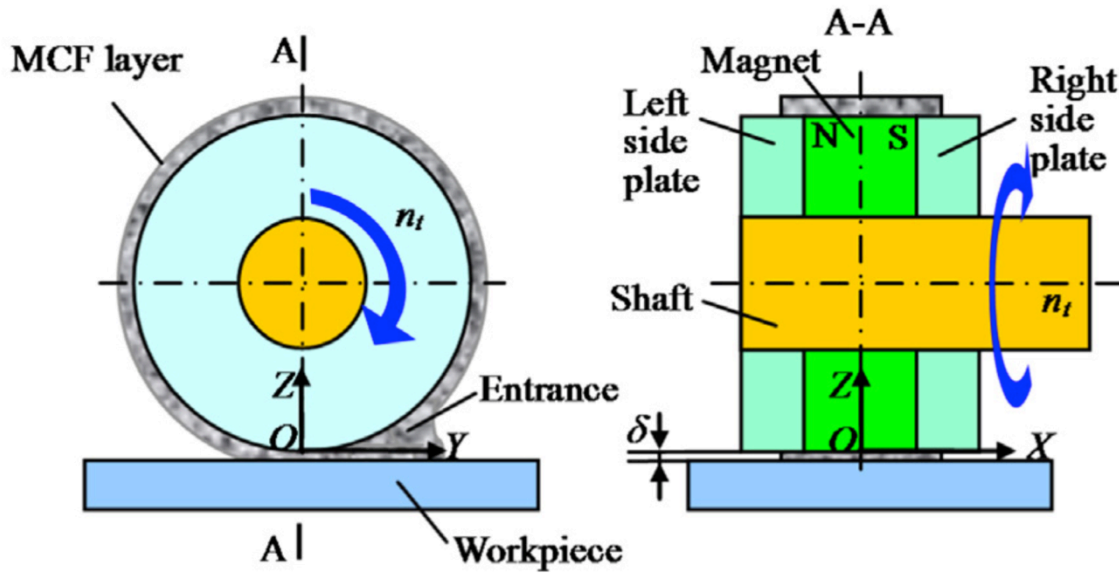


Figure 2.11: Schematic diagram of MCF wheel polishing [21].

Using the MCF wheel, Jiao *et al.* reported that fused silica was successfully polished from 200 nm Ra to 5.26 nm Ra in only one minute. The MCF used was a composition of water-based ferrofluid (10 nm), carbonyl iron particles (7.5 μm), cerium oxide (CeO_2) abrasives (1.5 μm) and α -cellulose fibers.

2.3.2 Reported studies on MCF

MCF, being the newest class of finishing media for MFAF, is a niche research area. While Shimada *et al.* [18] have made significant contributions in explaining the behaviour of MCF under the influence of a magnetic field, not many studies that investigate the effects of MCF properties on the finishing performance have been published. Still, Furuya *et al.* [22] performed extensive work in investigating the effects of the abrasive sizes and the MCF composition on the surface texture and removal rate. Comparing 0.3 μm , 1 μm and 3 μm Al_2O_3 abrasives, Furuya *et al.* showed that larger abrasives resulted in better surface texture and highest material removal. In addition, Furuya *et al.* also reported that there is an optimum weight composition for the carbonyl iron particles and abrasives. They reasoned that too small an amount of abrasives would result in low availability of active abrasives, while too large an amount of abrasives would retard the formation of magnetic clusters.

2.4 MR FLUID

2.4.1 MFAF processes based on MR fluid

2.4.1.1 Magnetorheological finishing (MRF)

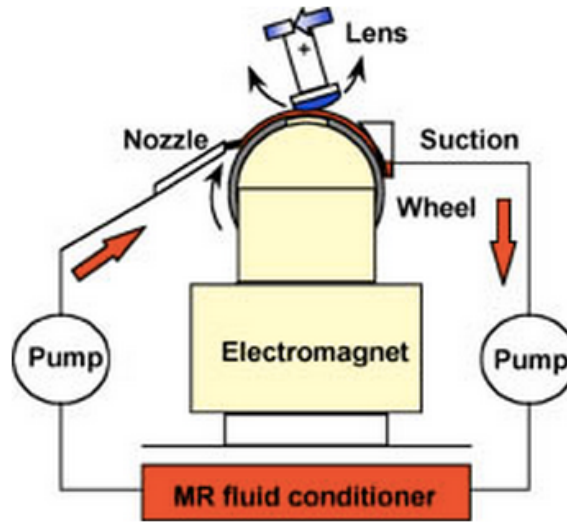


Figure 2.12: Schematic diagram of MRF [23].

MR fluid is predominantly used for magnetorheological finishing (MRF). Figure 2.12 shows the principles of MRF. The key principles of MRF are the delivery of the MR-fluid based slurry in a fluid form, followed by hardening of the fluid by a magnetic field at the polishing spot. A workpiece is brought into contact with the continuous stream of slurry, and the resultant shear stress is responsible for the material removal from the workpiece. The slurry conditions and polishing outcome are all tightly controlled in the MRF process, allowing deterministic material removal to be achieved following a spotting run to obtain removal data. Detailed descriptions of the process can be found elsewhere [24]. One of the main strengths of MRF is its well-defined polishing spot. Together with on-site interferometry and numerical control, MRF is able to

deterministically remove material from a target surface. Thus, MRF is excellent for figure correction. Material removal by MRF also simultaneously reduces surface texture to sub-nanometer level. For example, it had been reported that a three-step MRF of convex fused silica parts (40 mm diameter, 58 mm radius of curvature) reduced the surface texture from 4 nm Ra to 0.8 nm Ra [25]. The peak-to-valley figure error also reduced from 0.31 μm to 0.09 μm after 80 minutes of polishing time. On another optical glass part (convex SK7 lens, 40 mm diameter, 58 mm radius of curvature), a similar three-step MRF reduced the surface texture significantly from 940 nm Ra to 1 nm Ra. The peak-to-valley figure error also reduced from 6.42 μm to 0.86 μm in 140 minutes. Extensive studies on the capabilities of MRF on many other optical glasses are available in the literature. Jacobs *et al.* [26] comprehensively compared the peak removal rate of MRF on fourteen different types of optical glasses available from major glass manufacturers at that time.

Aside from optical glasses, MRF have also been demonstrated for optical infrared (IR) materials such as LiF, ZnSe, CaF₂, ZnS, MgF₂, Al₂O₃ and CVD diamond [26]. Using appropriate conditions, plano-convex plugs (25 mm to 40 mm diameter, 70 mm radius of curvature) of LiF, CaF₂, ZnS and MgF₂ were smoothened from an initial surface texture of about 2000 nm Ra to 4 nm - 6 nm Ra. With the addition of nanodiamond abrasives, surface texture of CVD diamond plano-convex plug was also reduced from 400 nm Ra to 40 nm Ra, although the process took 80 hours. Peak-to-valley figure error was reduced from 9 μm to 1 μm .

There are also reports in existing literature that outlined the feasibility of MRF for optical polymers such as PMMA, PS, COP and CP [27]. A ZrO₂-based MR fluid was found to be effective for smoothening and figure correction of PMMA parts to 0.5 nm Ra and 0.4 μm peak-to-valley respectively. Polishing of PS, COP and CP were limited in

success, although Al_2O_3 -based MR fluid was reported to be the most promising for processing the said materials without roughening the surface or introducing artifacts on the surface.

From the examples above, it can be observed that MRF have mainly been used for non-magnetic convex optical glasses and ceramics, rather than metals or magnetic materials. Cost may be a reason that metal parts are preferably polished using other techniques, as MRF is a relatively expensive process. Large optical lenses and ceramics are generally high value-added components, hence justifying the use of expensive processes to achieve stringent requirements. For magnetic materials, MRF is not the preferred process, as they interfere with the magnetic field of the polishing wheel and potentially the polishing spot. The material removal may therefore be difficult to control and makes the process non-deterministic. Still, Shafrir *et al.* [28] demonstrated that MRF spots can be placed on cobalt-based magnetic WC materials and the damaged layer from previous machining processes was removed.

Besides the state-of-the-art MRF technology, other research teams have built platform similar to MRF for academic studies. For example, Sidpara and Jain [29] performed experimental investigations and a design of experiment (DoE) study of the forces during the MRF process on an in-house platform, which is shown in Figure 2.13. Principally it is the same as the commercial MRF system but without the sophisticated control of the process conditions. In their work, Sidpara and Jain used a finishing media of magnetic carbonyl iron particles (2 μm median diameter) and non-magnetic CeO_2 abrasives (1.1 μm - 1.8 μm median diameter) suspended in a carrier fluid consisting of water and glycerol. Polishing experiments were conducted on a single crystal silicon blank, demonstrating the capability of the platform in reducing the surface texture from 1.3 μm Ra to 0.008 μm Ra in 210 minutes. In a follow-up to their work, Sidpara and Jain

[30] investigated by a DoE study the effects of working gap, concentration of carbonyl iron particles and abrasives, and the wheel speed on the finishing forces.

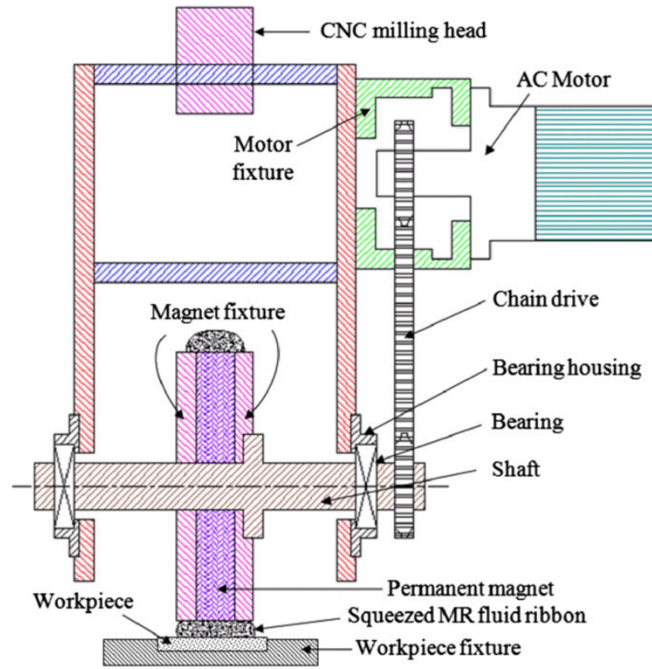


Figure 2.13: Schematic of an in-house MRF platform [31].

2.4.1.2 Magnetorheological jet (MR jet) finishing

Kordonski *et al.* [32] proposed a new process known as MR jet finishing, whereby a jet of MR fluid is stabilized by an axial magnetic field when it flowed out of the nozzle to achieve a highly collimated and coherent jet. Principally it is the same as conventional jet machining, except that the jet is more collimated due to the presence of magnetic field at the nozzle exit. For nozzle sizes of the order of 1 mm in diameter, coherent jets of 0.5 m in length were routinely achieved. Figure 2.14 shows snapshot images of the jet for water, MR fluid with magnetic field off, and MR fluid with magnetic

field on. The improved coherence of the MR fluid jet with magnetic field on can be verified visually.

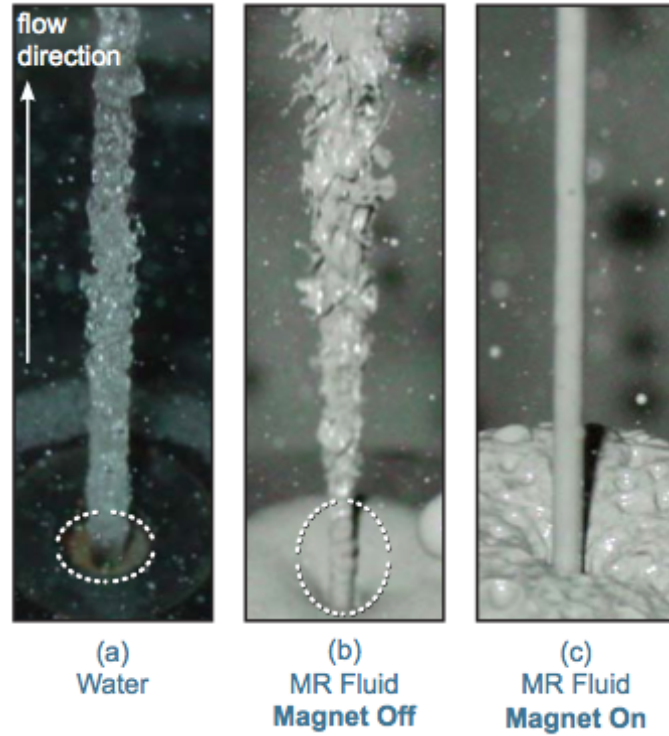


Figure 2.14: Jet snapshot images at 30 m/s and nozzle diameter 2 mm [33].

MR jet finishing is advantageous over conventional MRF process for surfaces inaccessible by a wheel. Concave surfaces of a mold cavity exemplify surfaces that are preferentially polished by an MR jet. Tricard *et al.* [33] demonstrated the ability of MR jet finishing by reducing the peak-to-valley figure error of a cavity from 304 nm to 47 nm while achieving a surface texture of less than 1 nm Ra simultaneously.

2.4.1.3 Magnetorheological abrasive flow finishing (MRAFF)

MR fluid was also used for the MRAFF process. MRAFF, which is a combination of abrasive flow machining (AFM) and MRF, was proposed by Jha and Jain [34] for the finishing of freeform internal surfaces. The basic principles of MRAFF is similar to conventional AFM, whereby finishing media is extruded back and forth under high pressure through a passage formed by the workpiece and fixture. For MRAFF, Jha and Jain used an electromagnet coil at the finishing area to generate a magnetic field that stiffened the finishing media, which comprised magnetic carbonyl iron particles ($6\text{ }\mu\text{m}$) and non-magnetic SiC abrasives ($17\text{ }\mu\text{m}$) suspended in a viscoplastic base medium. Figure 2.15 shows the schematic of the MRAFF experimental setup.

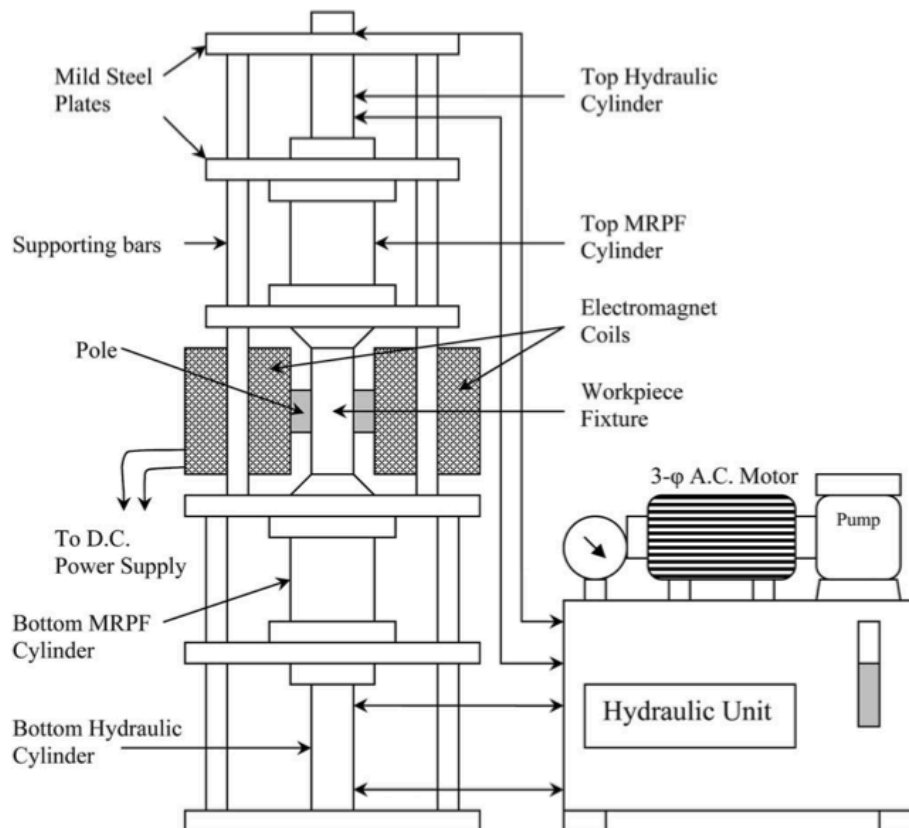


Figure 2.15: Schematic of MRAFF experimental setup [34].

Using the experimental setup shown in the previous figure, Jha and Jain demonstrated the ability of MRAFF to reduce the surface texture of a flat stainless steel workpiece from 0.47 $\mu\text{m Ra}$ to 0.34 $\mu\text{m Ra}$ after 200 extrusion cycles at 3.75 MPa extrusion pressure and 0.575 T magnetic field strength. The surface reduction can be attributed to the presence of a magnetic field, as no surface texture reduction was observed in the absence of a magnetic field. However, the surface texture reduction was not significant. Subsequent works in MFAFF pertained to theoretical modeling and simulation of the process [35, 36].

2.4.1.4 Ball end magnetorheological finishing (BEMRF)

Another embodiment of MFAF that utilized MR fluid is the BEMRF process, which was developed by Singh *et al.* [37]. Principally, this process works like a conventional polishing tool, except that the head consists of MR-fluid, which is held together by a magnetic field and is conformable to the workpiece surface. Compared to other processes reviewed so far, this process has a tool-to-part configuration, which allows independent module to be developed and attached to a conventional CNC machine or as end effector of a robotic arm. The schematic of BEMRF is shown in Figure 2.16. BEMRF used similar finishing media as MRAFF, which consisted of magnetic carbonyl iron particles (6 μm) and non-magnetic SiC abrasives (5 μm - 10 μm) suspended in a viscoplastic base medium. Singh *et al.* performed polishing experiments on both non-magnetic and magnetic workpieces and have successfully demonstrated the capability of BEMRF in reducing surface texture. The non-magnetic workpiece was polished from 0.414 $\mu\text{m Ra}$ to 0.070 $\mu\text{m Ra}$ in 100 minutes, while the magnetic workpiece was polished

from $0.337 \mu\text{m Ra}$ to $0.102 \mu\text{m Ra}$ in 60 minutes. The relative difficulty of polishing ferromagnetic workpiece is consistent with observations made by Shafrir *et al.* [28].

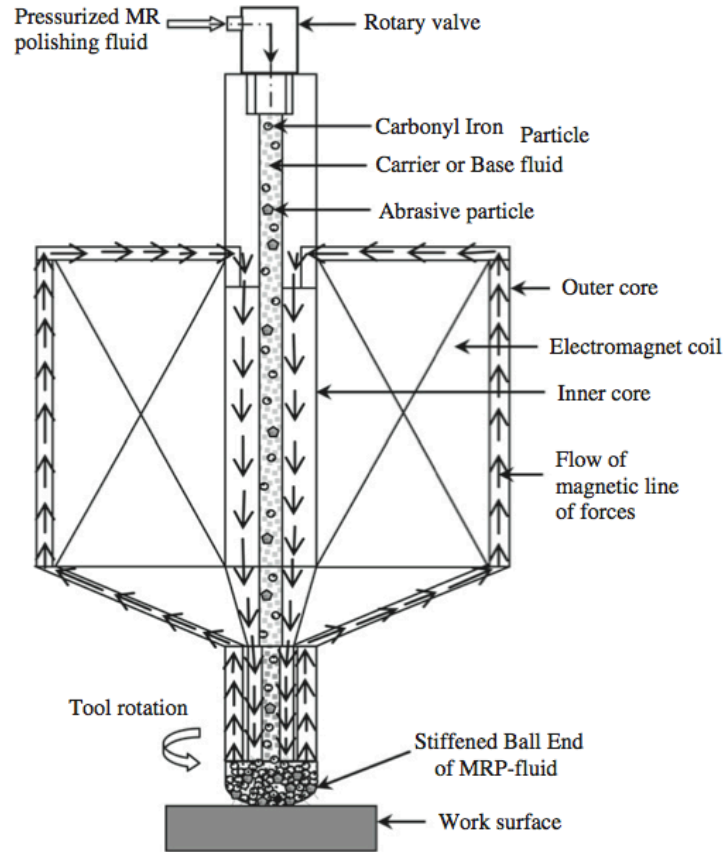


Figure 2.16: Schematic of the BEMRF process [37].

Later, Singh *et al.* [38] expanded upon their previous work and demonstrated the ability to polish the external surface of a freeform component. It was observed that the final roughness of the external surface was not uniform and dependent on the angle between the tool and the normal of the surface. The inability to obtain a uniform change in surface texture without tilting the tool to follow the workpiece surface is consistent with initial observations made for the new process to be developed in this thesis [39].

Subsequent work in BEMRF pertained to the theoretical analyses of forces during the finishing process and comparisons with experimental data [40].

2.4.1.6 MFAF of wafers

Yamaguchi *et al.* [41] utilized MR fluid for an MFAF process for the polishing of wafers. Figure 2.19 shows the schematic of the process. Principally, this process is similar to conventional lapping, except that the normal force is a result of the magnetic force. Using magnetic carbonyl iron particles ($7\text{ }\mu\text{m}$) and non-magnetic diamond abrasives ($< 0.25\text{ }\mu\text{m}$) suspended in silicone oil as finishing media, the surface texture of wafer was successfully reduced from 1.14 nm to 0.58 nm after 5 minutes of polishing. Using diamond abrasives of larger size ($< 0.5\text{ }\mu\text{m}$), the surface texture of the wafer instead deteriorated from 1.27 nm Ra to 2.04 nm Ra .

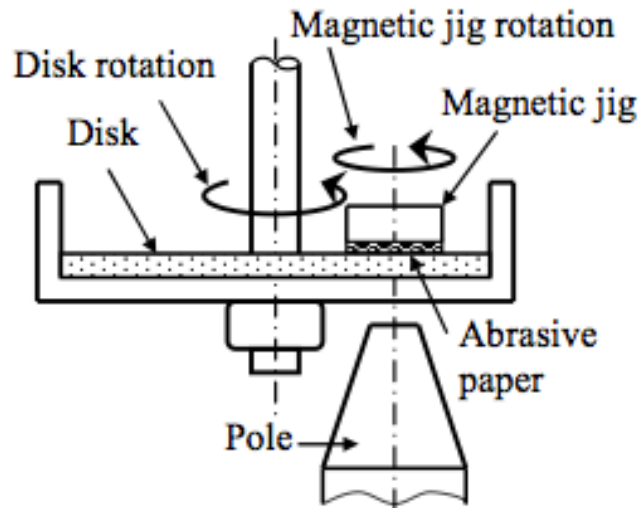


Figure 2.19: Schematic diagram of an MFAF process for polishing of wafers [41].

2.4.2 Reported studies on MR fluid

Being one of the key aspects to the MRF process, MR fluid has been extensively studied in the context of MRF. It is known that the conditions of MR fluid evolve with time due to particle sedimentation, evaporation of the water content in MR fluid, and breakdown of abrasive agglomerates. Changes in the conditions of MR fluid translate into a change in the processing capability of MRF. Thus, maintaining the MR fluid condition is crucial to achieve a well-defined finishing spot and a deterministic material removal. To that end, MRF has a persistent fluid circulation system with on-line viscosity control for fluid maintenance. Even then, the removal rate was found to drop with time and was halved after six weeks of non-continuous use due to fluid degradation [42].

Experiments have shown that removal rate in MRF is a strong function of the fluid viscosity, whereby an increase in the MR fluid viscosity translated into an increased peak removal rate [43, 44]. The MR fluid viscosity is strongly dependent of the water content in the MR fluid. A 2 % change in water content can lead to a 30 % change in MR fluid viscosity. The relationships between the water content, viscosity of MR fluid and peak removal rate for polishing of fused silica are shown in Figure 2.20.

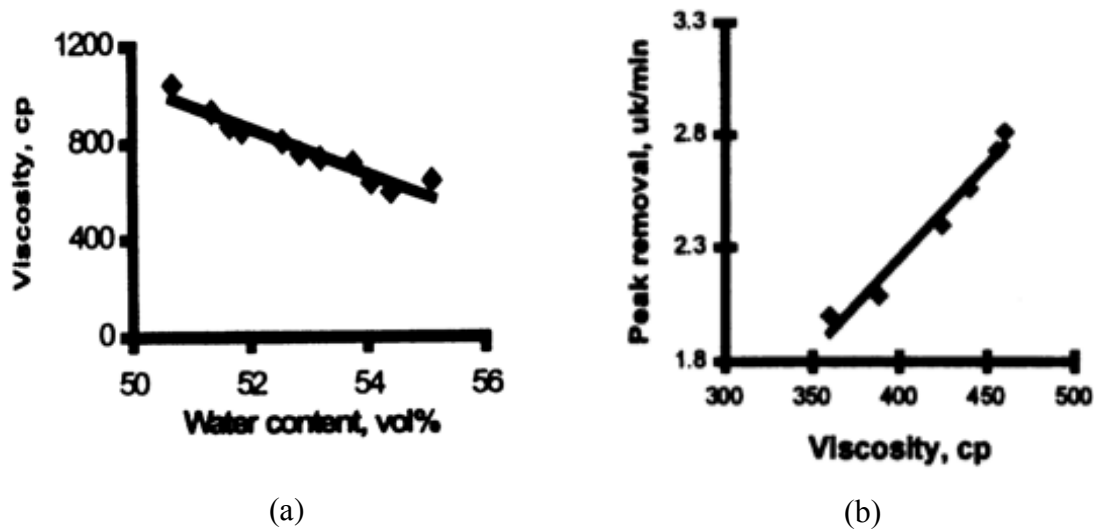


Figure 2.20: Relationships between (a) viscosity of MF fluid and water content (vol %), and (b) peak removal rate and viscosity of MR fluid. Workpiece is fused silica [43].

While the maintenance of MR fluid conditions is paramount for a deterministic MRF, the composition of the MR fluid is equally important in determining the outcome of MRF, especially on new materials. The ‘standard’ MR fluid developed by QED Technologies, which consisted of 36 vol. % magnetic carbonyl iron particles (4.5 μm), 6 vol. % non-magnetic CeO_2 abrasives (3.5 μm), 55 vol. % water and 3 vol. % sodium carbonate as stabilizers is extremely effective on optical glasses. Studies have found that substituting water with dicarboxylic acid ester (DAE), which is non-aqueous, drastically reduced the removal rate on optical glasses and introduced pits and streaks on the surface that compromised surface texture [45]. Substituting as little as 1 vol. % of DAE back to water resulted in a significant improvement in material removal and eliminated the pits and streaks from the surface. Figure 2.21 is a graphical representation of the results from the original source. The results reported by Shorey *et al.* is consistent with Cook’s [46] description of how CeO_2 abrasives bond more readily to the silica network of optical

glasses in an aqueous environment, which is a beneficial phenomenon for the material removal.

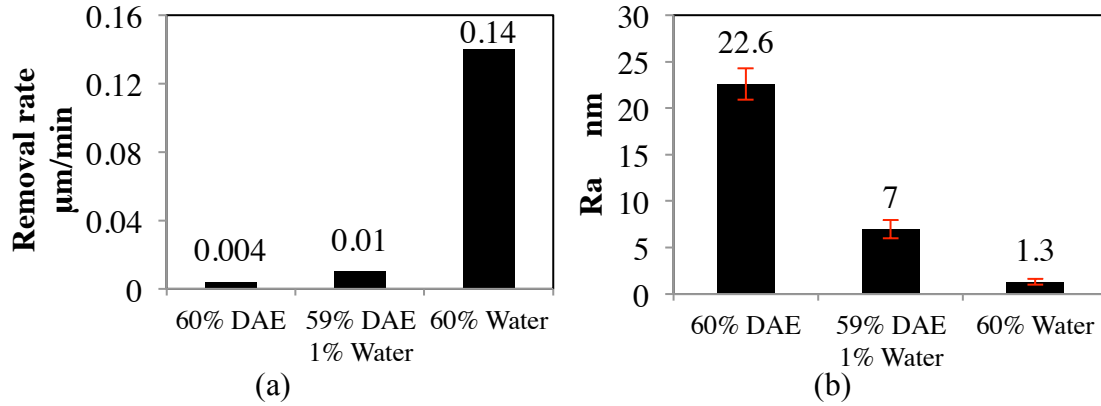


Figure 2.21: Effect of water content in MR fluid composition on (a) removal rate, and (b) surface texture [45]. The remaining 40 % of the MR fluid composition is carbonyl iron powder.

The type of abrasives used also play an important role for the MRF process. Shorey *et al.* [45] studied the removal rate using MR fluid with 40 vol. % to 45 vol. % carbonyl iron particles with three different types of non-magnetic abrasives – Al_2O_3 , CeO_2 and diamond – for the polishing of fused silica. In addition, the abrasives were added gradually to also investigate the effect of the abrasive concentration. Firstly, it was reported that diamond abrasives, being the hardest, resulted in the highest removal rate. This was followed by CeO_2 abrasives, which react favorably with glass, and lastly Al_2O_3 abrasives, which were reported to leave discontinuous grooves on the surface. The results reported, shown in Figure 2.22, are similar to observations reported by Schinhaerl *et al.* [47].

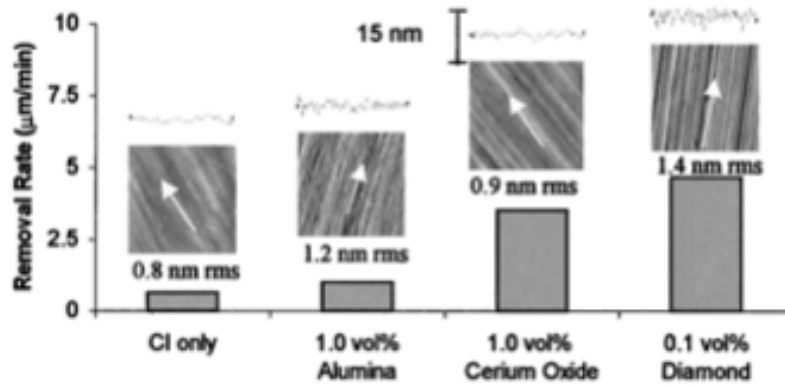


Figure 2.22: Effect of type of abrasives on the removal rate of fused silica [45].

Secondly, it was reported that a small amount of abrasives can have a large effect on the removal rate, and that the removal rate increases with the concentration of abrasives at a diminishing rate. Figure 2.23 is the results reported by Shorey *et al.* The onset of saturation occurred very early for diamond abrasives, at approximately 0.1 vol. %, and later for both CeO_2 and Al_2O_3 abrasives. The reason for this is not fully understood, although Miao *et al.* [48] reported similar observations of removal rate saturation at approximately 0.1 vol. % for diamond abrasives. In a separate report, tangential and normal forces measurements by Sidpara and Jain [29] on their in-house MRF platform showed that further addition of abrasives beyond the saturation point caused a drop in both the tangential and normal forces. This is illustrated in Figure 2.24.

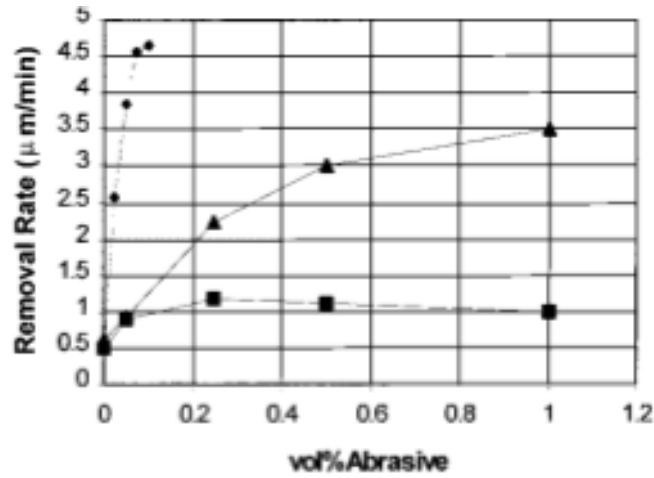


Figure 2.23: Effect of abrasive concentration for different types of abrasive on the removal rate of fused silica: ● diamond, ▲ CeO₂, ■ Al₂O₃ [45].

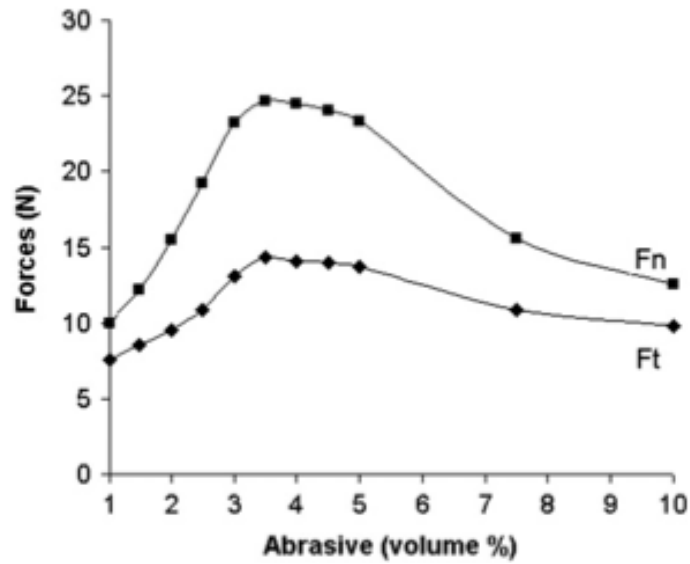


Figure 2.24: Effect of abrasive concentration on the tangential and normal forces [29].

While the combination of CeO₂ and water is favourable for material removal of most optical glasses, the standard MR fluid composition was reported to be unsuccessful for some materials. For example, Arrasmith *et al.* [49] found that CeO₂ abrasives have to be substituted by nanodiamond abrasives for the MRF of CaF₂. They explained that this

is to achieve a gentler material removal and prevent deep grooves on the CaF_2 surface, which compromised the surface finish. For KDP, which is highly soluble in water, DAE was found to be a promising candidate as carrier fluid for the MR fluid composition. Both CaF_2 and KDP are soft single crystal optical materials. A similar strategy was adopted by Jacobs *et al.* [26] for the MRF of various IR materials, whereby the experimental conditions were relaxed by substituting CeO_2 abrasives with smaller nanoalumina and nanodiamond abrasives. For the MRF of several optical polymers, deGroote *et al.* [27] investigated the use of different abrasives and found that only selected abrasives were suitable.

In summary, the formulation of MR fluid is largely based on conventional wisdom and informed estimates, which are then investigated and validated empirically. This is the most common approach taken by research groups in their studies of MR fluid formulation [26, 27, 45, 47, 49]. Miao *et al.* [48] and deGroote *et al.* [50] have both empirically correlated the removal rate to the $1/3$ power of the nanodiamond concentration in the MR fluid, although the correlation may not be universal, given that removal rate is dependent on many interacting factors.

Some of the recent studies aimed at improving the properties of MR fluid are innovative and exciting. Shafrir *et al.* [51] studied the coating of carbonyl iron particles with a 50 nm - 100 nm thick zirconia layer by sol-gel technique. The zirconia layer is to prevent oxidation of the carbonyl iron particles, hence improving the stability of the finishing media. Using the coated carbonyl iron particles for MRF, they reported that the removal rate remained stable for up to three weeks, with no drop in the removal rate.

In a separate study, Hanada *et al.* [52] embedded diamond abrasives (0.3 μm) on the surface of carbonyl iron particles (7.2 μm). Magnetic particles embedded with abrasives are common in magnetic abrasive finishing, where the magnetic particle size is

larger, but are uncommon for MR fluid where the magnetic particle size are much smaller. The particles were fabricated by plasma spraying at a plasma current of 100 A after mechanical mixing. The performance of the particles was demonstrated for the surface finishing of SUS304 flat plates, whereby a final surface texture of 77 nm Rt was achieved after 4 minutes of processing time. However, the authors reported that the diamond abrasives separated from the carbonyl iron particles during polishing.

2.5 MAGNETIC ABRASIVES

2.5.1 MFAF processes based on magnetic abrasives

2.5.1.1 Magnetic abrasive finishing (MAF)

MAF was initiated by Shinmura *et al.* [5] for the polishing of Si₃N₄ rollers. The magnetic abrasives used were of the bonded type, whereby diamond particles of different sizes (5 µm, 10 µm, 20 µm and 40 µm) were embedded onto either sintered (100 µm - 200 µm) or cast (50 µm - 500 µm) iron balls. Material removal is achieved by the relative motion between a magnetic ‘brush’ formed by chains of magnetic abrasives under the influence of a magnetic field, and a workpiece. Figure 2.25 shows a schematic diagram of MAF. A more complete description of the principles of MAF can be found in the original article. Shinmura *et al.* reported that the surface texture of the roller was reduced from 0.45 µm Ra to 0.04 µm Ra, while studies reported in later years have successfully achieved surface texture as low as 0.0076 µm Ra [53].

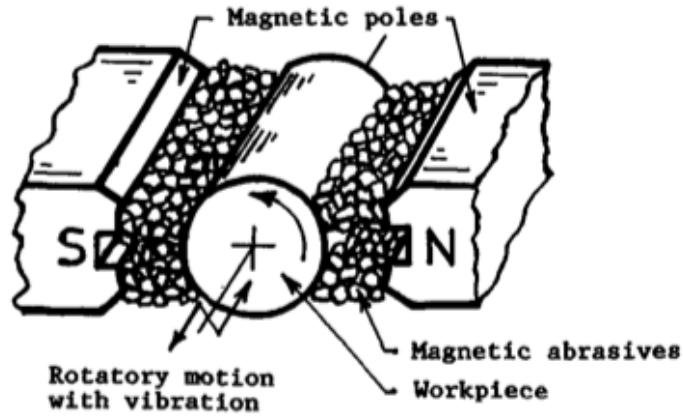


Figure 2.25: Schematic diagram of MAF apparatus for Si_3N_4 rollers [5].

While the MAF was initiated as a method for the surface finishing of the external surface of cylinders, the strength of the process is its ability to reduce surface texture of internal surfaces, such as that of cylindrical tubes [54]. Figure 2.26 shows the schematic of an MAF apparatus for the finishing of the internal surface of a tube. The magnetic abrasives apply pressure on the internal surface of the tube because they are attracted towards the magnetic poles. Simultaneously, the tube is rotated to cause a relative motion between the magnetic abrasives and the workpiece inner surface, resulting in material removal. Yamaguchi and Shinmura [54] reported that the internal surface of a stainless steel (Grade 304) tube was polished from $2.0\text{ }\mu\text{m Ry}$ to $0.2\text{ }\mu\text{m Ry}$.

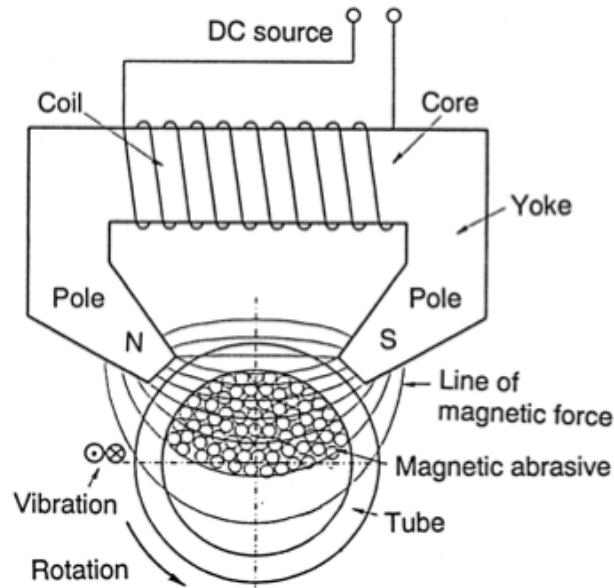


Figure 2.26: Schematic diagram of the MAF of the internal surface of a tube [55].

2.5.1.2 Flexible magnetic abrasive brush (FMAB) finishing

FMAB is a term coined by Singh *et al.* [56] to describe the magnetic abrasives brush at the open end of a magnetic pole. The processing principle of FMAB is similar to MAF, although FMAB is shaped like a milling tool and is therefore able to target an external surface locally, and can be attached to a conventional CNC machine or as the end effector of a robot arm. Figure 2.27 shows the apparatus for the polishing of a cutting tool by FMAB using a magnetic jig and a non-magnetic jig to target different faces of the cutting tool [57]. The flank and rake faces of the cutting tools were polished from 80 nm - 110 nm Ra to less than 25 nm Ra and less than 50 nm Ra respectively.

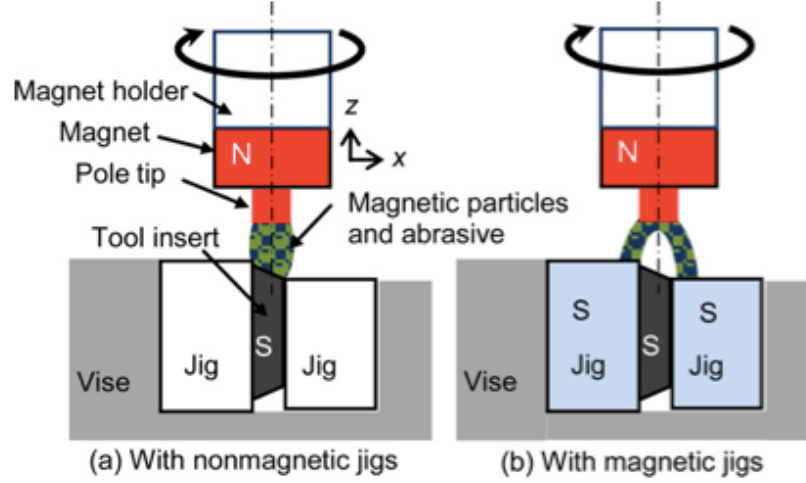


Figure 2.27: Schematic diagram of FMAB finishing of cutting tool faces (a) with non-magnetic jigs and (b) with magnetic jig [57].

2.5.2 Reported studies on magnetic abrasives

The characteristics and properties of magnetic abrasives are one of the main aspects of MAF that have been greatly researched. The significance of the finishing media in MAF is evident even to the pioneers, as Shinmura *et al.* [5] conducted studies to investigate the effect of the bonded magnetic abrasive size. Firstly, it was reported that increasing the diamond abrasive size while maintaining the magnetic abrasive size did not change the removal rate, but caused the surface texture to deteriorate. This is shown in Figure 2.28. Secondly, it was reported that the removal rate increased with the magnetic abrasive size while roughness deteriorated. This is shown in Figure 2.29.

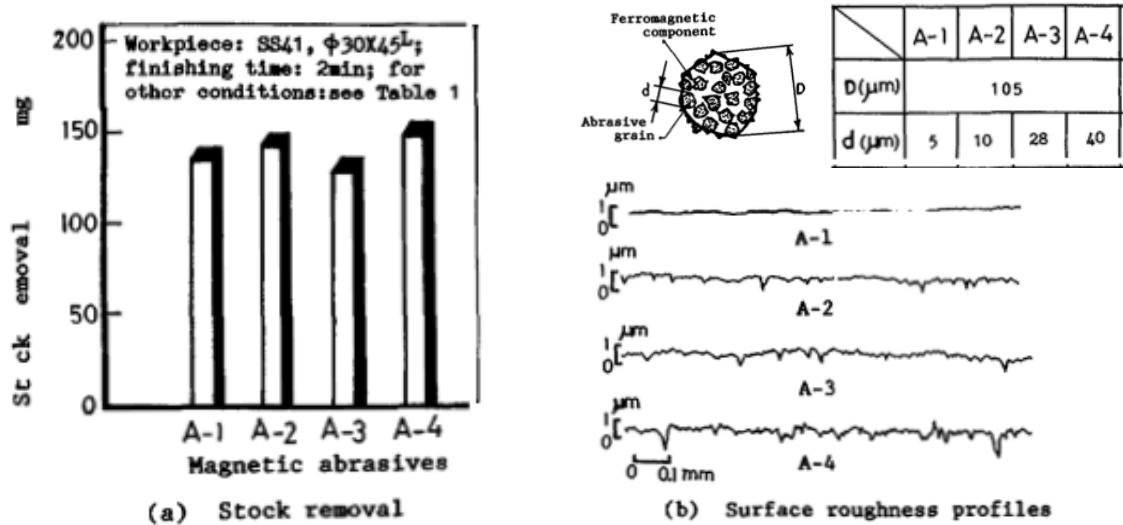


Figure 2.28: Effect of the diamond particle size on the (a) stock removal and (b) surface texture profiles [5].

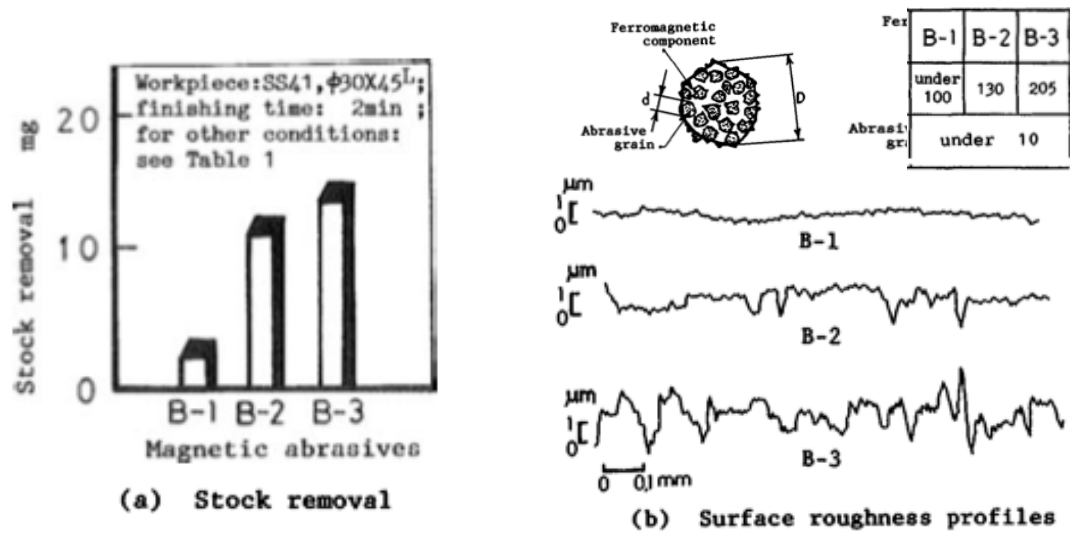


Figure 2.29: Effect of the magnetic abrasive size on the (a) stock removal and (b) surface texture profiles [5].

Fox *et al.* [53] performed MAF using unbonded abrasives, whereby the abrasives were simply mixed with the magnetic particles instead of being embedded. The use of unbonded abrasives bestows the benefits of not needing to prepare magnetic abrasives by

sintering and also allow better control of the choice of particle sizes. Fox *et al.* reported that unbonded abrasives gave approximately 15 to 20 times the removal rate compared to bonded abrasives, although the final surface texture was significantly inferior (300 nm Ra for unbonded abrasives versus 20 nm Ra for bonded abrasives). These are shown in Figure 2.30. Fox *et al.* attributed this effect to the better availability of abrasives when they were unbonded to the iron particles. A more recent work by Mulik and Pandey [58] obtained some contradicting observations, where the surface texture for unbonded magnetic abrasives improved faster than that of bonded abrasives, although the experimental conditions were sufficiently different and their process included the assistance of ultrasonic vibration, which removed the directional grinding tracks.

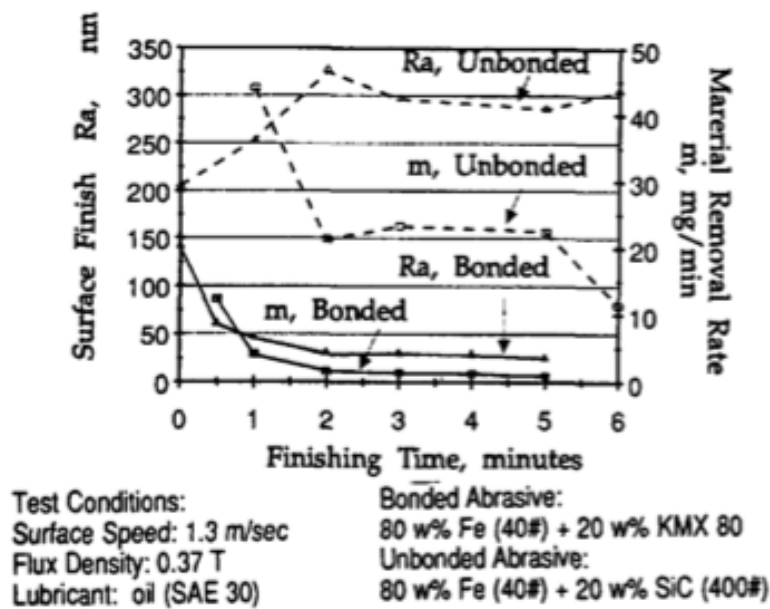


Figure 2.30: Comparison of removal rate and surface texture for bonded and unbonded abrasives [53].

Chang *et al.* [59] performed in-depth studies on unbonded magnetic abrasives by investigating the effects of the magnetic particle material (steel grit and iron grit),

magnetic particle size (80 μm , 130 μm and 180 μm) and abrasive size (1.2 μm and 5.5 μm) on removal rate and surface texture. Figure 2.31 shows the surface texture and removal rate versus the finishing time for steel grit of different sizes and SiC of 5.5 μm .

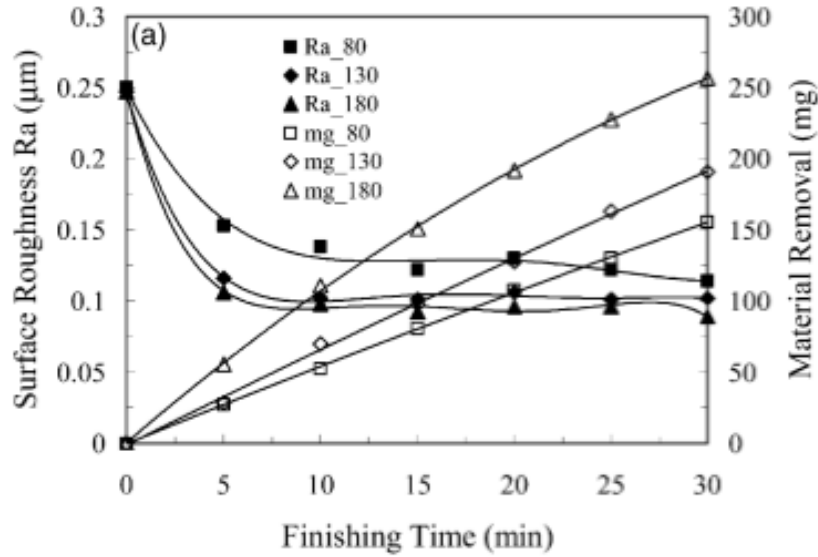


Figure 2.31: Surface texture and removal rate for steel grit of different sizes and SiC of 5.5 μm [59].

It can be observed that an increase in the magnetic particle size resulted in greater removal rate and better surface texture, contrary to results reported by Shinmura *et al.* [5] when bonded abrasives were used, where the removal rate increased but surface texture deteriorated. Disparity was also observed when the SiC abrasive size was changed while keeping the steel grit size constant, as shown in Figure 2.32. Chang *et al.* reported that an increase in the SiC abrasive size improved removal rate and caused minimal change in surface texture, while Shinmura *et al.* reported that the removal rates were similar and the surface texture deteriorated. These disparities may be attributed to differences in the material removal mechanism between bonded and unbonded magnetic abrasives.

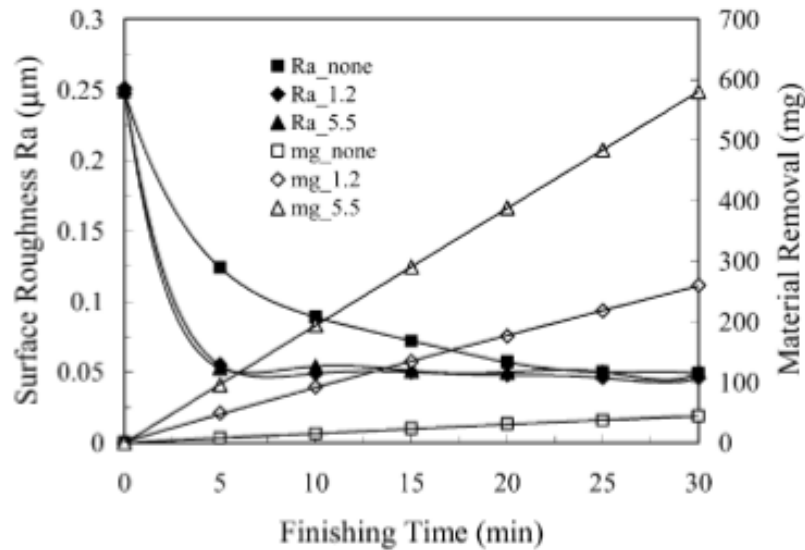


Figure 2.32: Surface texture and removal rate for different SiC sizes and constant steel grit size [59].

In addition to studies related to particle type and size, studies have also been undertaken on other media properties. For example, Mulik and Pandey [58] observed for their ultrasonic vibration-assisted process that an optimum amount of abrasives for the best improvement in surface texture exists, as shown in Figure 2.33. In a separate study, Wang and Hu [60] demonstrated the benefits of using a lubricant to increase removal rate and also showed that 4% stearic acid in oil is a significantly better lubricant than transformer oil. An older study by Fox *et al.* [53] also advocated the use of zinc stearate for lubricant and showed that the surface finish was optimized when the lubricant was a 5 wt. % zinc stearate.

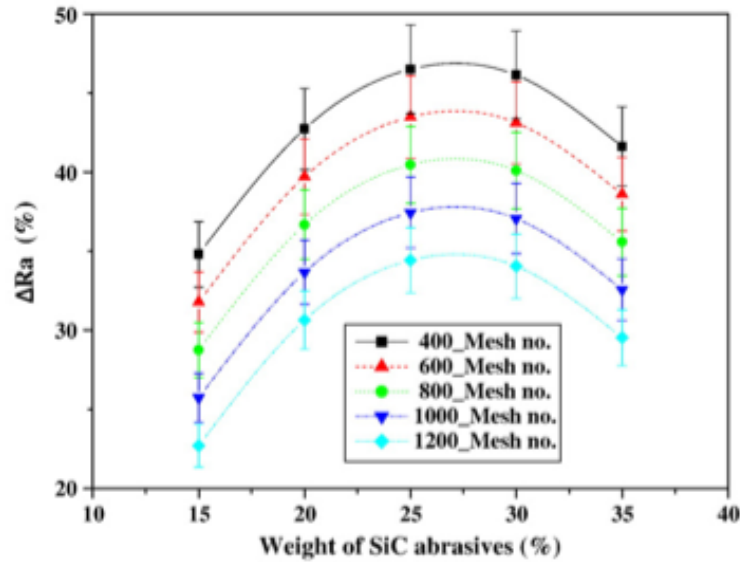


Figure 2.33: Percentage change in surface texture against wt. % of SiC abrasives for different abrasive sizes [58].

One of the major developments related to magnetic abrasives was the study by Yamaguchi and Shinmura [41] to include larger iron particles (510 μm) into the finishing media to allow the magnetic abrasives and larger iron particles to bind magnetically and form large magnetic clusters. This mixed type of finishing media was reported to be more efficient for surface finishing than finishing media consisting purely of magnetic abrasives. Subsequent research works by the same research group have since been using this mixed type of magnetic abrasives [61, 62, 63].

Another noteworthy development is the use of a silicone gel-based finishing media for the MAF for internal surface as reported by Wang and Lee [64]. The results reported were in line with results reported by other research groups for unbonded abrasives. This gel-based media may be perceived as another option in addition to bonded magnetic abrasives and unbonded magnetic abrasives.

2.6 CHAPTER SUMMARY

2.6.1 Cited contents of reviewed literature

Table 2.3 summarizes the publications quoted in this literature review section. From the literature review, it is evident that the development of MFAF processes is an active research topic. Despite that, new solutions and innovations are still needed to address many technological gaps. These are presented in the final two sections in this chapter after Table 2.3.

Table 2.3: Cited contents of reviewed literature.

Authors	Process	Cited contents of reviewed literature
Ferrofluid		
Suzuki <i>et al.</i> [6]	MFAF with sealed ferrofluid	Process study for polishing of curved surface.
Kurobe and Imanaka [7]		Study of abrasive size.
Umehara and Kalpakjian [9]	MFG	Process study for polishing of Si ₃ N ₄ balls and rollers.
Childs <i>et al.</i> [10]		Study of abrasive size. Study of media viscosity.
Umehara and Komanduri [12]		Study of abrasive size.
Jiang and Komanduri [16]		DOE study of abrasive concentration.
Umehara <i>et al.</i> [11]		Process study for polishing large batch size.
Yamaguchi <i>et al.</i> [13]	MFAF of micropore	Study of abrasive size.
MCF		
Shimada <i>et al.</i> [17]	-	Characteristics of MCF.
Shimada <i>et al.</i> [3]	MCF pad polishing	Process study for polishing of titanium.
Shimada <i>et al.</i> [18]		Optimization of magnetic field strength.
Shimada <i>et al.</i> [19]		Study on the use of alpha-cellulose in MCF.
Furuya <i>et al.</i> [22]		Study of abrasive size.
Sato <i>et al.</i> [20]	MCF wheel polishing	Process study for polishing of three-dimensional surface.
Jiao <i>et al.</i> [21]		Process study for polishing of optical glass.
MR fluid		
Cook <i>et al.</i> [46]	-	Chemical reactions between CeO ₂ and glass.

continued on the next page...

... continued from the previous page

Jacobs <i>et al.</i> [25]	MRF	Process study for polishing of optical glass
Jacobs <i>et al.</i> [26]		Study of abrasive type. Media formulation for IR materials.
Kordonski and Golini [43]		Study of stabilizer concentration. Study of water content in MR fluid.
Arrasmith <i>et al.</i> [49]		Process study for polishing of CaF ₂ and KDP. Study of nanodiamond concentration for polishing of CaF ₂ . Study of carrier fluid for polishing of KDP.
Shorey <i>et al.</i> [45]		Study of effects of abrasive concentration, abrasive type and carbonyl iron concentration on removal rate.
DeGroote <i>et al.</i> [27]		Process study for polishing of polymers. Study of abrasive type.
Schinhaerl <i>et al.</i> [42]		Study of media stability.
Schinhaerl <i>et al.</i> [44]		Study of media viscosity.
Schinhaerl <i>et al.</i> [47]		Study of commercial media. Study of media viscosity.
Shafrir <i>et al.</i> [28]		Process study for polishing of ferrous materials.
Shafrir <i>et al.</i> [51]		Zirconia coating of carbonyl iron particles.
Miao <i>et al.</i> [48]		Correlation between removal rate to 1/3 power of nanodiamond concentration.
Sidpara and Jain [29]		Study of carbonyl iron concentration. Study of abrasive concentration.
Sidpara and Jain [30]		Process modeling.
Sidpara and Jain [31]		Process study for polishing of silicon blank.
Kordonski <i>et al.</i> [32]	MR jet finishing	Patent for MR jet finishing
Tricard <i>et al.</i> [33]		Process study for polishing of concave optics.
Jha and Jain [34]	MRAFF	Process study.
Jha and Jain [36]		Modeling and simulation.
Das <i>et al.</i> [37]		Fluid flow analysis.
Singh <i>et al.</i> [37]	BEMRF	Process study.
Singh <i>et al.</i> [38]		Study of polishing of ferrous materials.
Sidpara and Jain [40]		Force analysis.
Yamaguchi <i>et al.</i> [41]	MFAF of wafer	Process study.
Hanada <i>et al.</i> [52]	Internal finishing	Carbonyl iron embedded with diamond.
Magnetic abrasives		
Shinmura <i>et al.</i> [5]	MAF	Process study for polishing of Si ₃ N ₄ rollers. Study of abrasive size.
Fox <i>et al.</i> [53]		Process study for polishing of Si ₃ N ₄ rollers.

continued on the next page...

... continued from the previous page

		Study of unbonded abrasives. Study of lubricant concentration.
Yamaguchi <i>et al.</i> [54]		Process study for internal polishing.
Yamaguchi and Shinmura [55]		Process study for internal polishing.
Yamaguchi <i>et al.</i> [61]		Removal mechanism.
Chang <i>et al.</i> [59]		Study of abrasive size. Study of unbonded abrasives.
Wang and Lee [60]		Study of silicone gel as carrier fluid. Study of abrasive size. Study of abrasive concentration.
Mulik and Pandey [58]		Study of unbonded abrasives. Study of abrasive concentration.
Kang <i>et al.</i> [62]		Process study.
Kang and Yamaguchi [63]		Process study for high-speed rotation.
Singh <i>et al.</i> [56]	FMAB finishing	Surface texture analysis.
Yamaguchi <i>et al.</i> [57]		Process study for polishing of cutting tools.

2.6.2 Process development

One of the key goals of process development is to develop capability to polish complex geometry that is currently difficult to assess with conventional techniques. This is evident from the literature review, where processes are developed to polish a variety of geometries such as the convex surface of an optical glass, internal surface of a small diameter tube, cutting edges of a tool insert, sidewalls of micropore X-ray optics, steep concave surfaces of a mold insert and freeform external. Even so, many technological gaps still exist, as there is a lack of capability or solution to polish structured surfaces (grooves, pins, holes and optical arrays), textured surfaces, blind holes, and complex internal surfaces or internal features. There are demands for these capabilities, but no viable solution is currently available.

Besides assessing difficult-to-reach surfaces described above, there is also demand for surface finishing processes capable of uniform material removal over a large surface. Processes covered in this literature review mostly have localized material

removal. For these processes, achieving uniform material removal across a large surface is challenging, as the removal profile must be known and the tool path has to be controlled precisely. The MRF process reviewed earlier features a combination of these, allowing deterministic material removal from a concave surface. New process principles capable of achieving ‘global’ material removal with simpler setups will be advantageous, especially for the surface finishing of internal surfaces.

From the literature review, it can be seen that there is also a significant emphasis on the removal rate of processes. High efficiency processes are highly desirable, and new processes capable of achieving high removal rate are constantly in demand. Novel and innovative applications of chemicals, magnetic field, vibration, or other principles may create new solutions to substantially improve efficiency of surface finishing. In addition to a high removal rate, another key point pertaining to removal rate is the determinism or predictability of removal rate, which is imperative for form correction or simply for the removal of a uniform layer of material.

Lastly, there is also significant interest in the ability to predict the process outcome of surface finishing processes. The process outcome of key interest typically consists of the material removal and the surface texture. Prediction of process outcome is the key to process automation, which is another area of high commercial interest. The mechanism of abrasive processes is generally not well understood. Achieving the required process outcome is typically done through experimentation and tapping on experience from similar jobs in the past. Therefore, process modeling capable of predicting process outcome is also in high demand and an area of key interest.

2.6.3 Finishing media development

The importance of finishing media development for MFAF processes is evident from the literature review. One of the key goals is to understand and establish the relationship between the finishing media properties and the process outcome. Many of the reviewed studies have investigated the effect of abrasive type, abrasive size, abrasive concentration and other properties on the process outcome. Despite that, the physics and chemistry involving the finishing media are complex and not currently completely understood. As a result, there is no clear understanding of how the removal rate and surface texture are influenced by the finishing media properties. Theoretical analyses and process modeling are therefore needed to help establish the relationship between finishing media properties and process outcome.

A second goal of media development is to improve the media stability. Finishing media used in current processes are known to degrade over time, causing changes in the finishing performance and characteristics over time. Efforts made in this area have been covered in the literature review. Examples include the coating of carbonyl iron particles with a layer of zirconia, and the bonding of abrasives onto carbonyl iron particles to engineer a new type of particles for surface finishing. New solutions and innovations in improving the media stability and in storing, circulating, recycling the finishing media are still needed.

REFERENCES

- [1] Jain VK, *Magnetic field assisted abrasive based micro-/nano-finishing*. Journal of Materials Processing Technology, 2009. **209**(20): p. 6022-6038.
- [2] BASF. *How is carbonyl iron powder manufactured?*, 2013. Retrieved 4 December 2013 from <http://www.monomers.basf.com/cm/internet/en/content/Produkte/Metallsysteme/CIP/Technology>.
- [3] Shimada K, Akagami T, Kamiyama S, Fujita T, Miyazaki T and Shibayama A, *New microscopic polishing with magnetic compound fluid (MCF)*. Journal of Intelligent Material Systems and Structures, 2002. **13**(7-8): p. 405-408.
- [4] Yamaguchi H and Shinmura T, *Study of the surface modification resulting from an internal magnetic abrasive finishing process*. Wear, 1999. **225**: p. 246-255.
- [5] Shinmura T, Takazawa K, Hatano E, Matsunaga M and Matsuo T, *Study on magnetic abrasive finishing*. CIRP Annals-Manufacturing Technology, 1990. **39**(1): p. 325-328.
- [6] Suzuki H, Koder S, Hara S, Matsunaga H and Kurobe T, *Magnetic field-assisted polishing—application to a curved surface*. Precision Engineering, 1989. **11**(4): p. 197-202.
- [7] Kurobe T and Imanaka O, *Magnetic field-assisted fine finishing*. Precision Engineering, 1984. **6**(3): p. 119-124.
- [8] Umehara N and Kato K, *Principles of magnetic fluid grinding of ceramic balls*. Journal of Applied Electromagnetic Materials, 1990. **1**: p. 37-43.
- [9] Umehara N and Kalpakjian S, *Magnetic fluid grinding – a new technique for finishing advanced ceramics*. CIRP Annals-Manufacturing Technology, 1994. **43**(1): p. 185-188.
- [10] Childs T, Mahmood S and Yoon H, *Magnetic fluid grinding of ceramic balls*. Tribology International, 1995. **28**(6): p. 341-348.
- [11] Umehara N, Kirtane T, Gerlick R, Jain VK and Komanduri R, *A new apparatus for finishing large size/large batch silicon nitride (Si_3N_4) balls for hybrid bearing applications by magnetic float polishing (MFP)*. International Journal of Machine Tools and Manufacture, 2006. **46**(2): p. 151-169.

- [12] Umehara N and Komanduri R, *Magnetic fluid grinding of HIP-Si₃N₄ rollers*. Wear, 1996. **192**(1): p. 85-93.
- [13] Yamaguchi H, Riveros R, Mitsuishi I, Takagi U, Ezoe Y, Yamasaki N, Mitsuda K and Hashimoto F, *Magnetic field-assisted finishing for micropore X-ray focusing mirrors fabricated by deep reactive ion etching*. CIRP Annals-Manufacturing Technology, 2010. **59**(1): p. 351-354.
- [14] Mullany B and Byrne G, *The effect of slurry viscosity on chemical–mechanical polishing of silicon wafers*. Journal of Materials Processing Technology, 2003. **132**(1): p. 28-34.
- [15] Komanduri R, Umehara N and Raghunandan M, *On the possibility of chemo-mechanical action in magnetic float polishing of silicon nitride*. Journal of Tribology, 1996. **118**(4): p. 721-727.
- [16] Jiang M and Komanduri R, *Application of Taguchi method for optimization of finishing conditions in magnetic float polishing (MFP)*. Wear, 1997. **213**(1): p. 59-71.
- [17] Shimada K, Akagami Y, Fujita T, Miyazaki T, Kamiyama S and Shibayama A, *Characteristics of magnetic compound fluid (MCF) in a rotating rheometer*. Journal of Magnetism and Magnetic Materials, 2002. **252**: p. 235-237.
- [18] Shimada K, Wu YB and Wong YC, *Effect of magnetic cluster and magnetic field on polishing using magnetic compound fluid (MCF)*. Journal of Magnetism and Magnetic Materials, 2003. **262**(2): p. 242-247.
- [19] Shimada K, Wu YB, Matsuo Y and Yamamoto K, *Float polishing technique using new tool consisting of micro magnetic clusters*. Journal of Materials Processing Technology, 2005. **162**: p. 690-695.
- [20] Sato T, Wu YB, Lin WM and Shimada K, *Study of three-dimensional polishing using magnetic compound fluid (MCF)*. Advanced Materials Research, 2009. **76**: p. 288-293.
- [21] Jiao L, Wu YB, Wang X, Guo H and Liang Z, *Fundamental performance of magnetic compound fluid (MCF) wheel in ultra-fine surface finishing of optical glass*. International Journal of Machine Tools and Manufacture, 2013. **75**: p. 109-118.
- [22] Furuya T, Wu YB, Nomura M, Shimada K and Yamamoto K, *Fundamental performance of magnetic compound fluid polishing liquid in contact-free*

- polishing of metal surface*. Journal of Materials Processing Technology, 2008. **201**(1): p. 536-541.
- [23] Jacobs SD, *Prof. Steve Jacobs' team website*. Retrieved on 7 October 2013 from http://www.opticsexcellence.org/SJ_TeamSite/
 - [24] Kordonski WI. *Adaptive structures based on magnetorheological fluids*. In *Third International Conference on Adaptive Structures*. 1993.
 - [25] Jacobs SD, Golini D, Hsu Y, Puchebner BE, Strafford D, Prokhorov IV, Fess EM, Pietrowski D and Kordonski WI. *Magnetorheological finishing: A deterministic process for optics manufacturing*. In *International Conferences on Optical Fabrication and Testing and Applications of Optical Holography*. 1995.
 - [26] Jacobs SD, Yang F, Fess EM, Feingold J, Gillman BE, Kordonski WI, Edwards H and Golini D, *Magnetorheological finishing of IR materials*. Optical Manufacturing and Testing II, 1997. **3134**: p. 258-269.
 - [27] deGroote JE, Romanofsky HJ, Kozhinova IA, Schoen JM and Jacobs SD. *Polishing PMMA and other optical polymers with magnetorheological finishing*. In *Optical Science and Technology, SPIE's 48th Annual Meeting*. 2004.
 - [28] Shafrir SN, Lambropoulos JC and Jacobs SD, *Toward magnetorheological finishing of magnetic materials*. Journal of Manufacturing Science and Engineering, 2007. **129**(DOE/SF/19460-781).
 - [29] Sidpara A and Jain VK, *Experimental investigations into forces during magnetorheological fluid based finishing process*. International Journal of Machine Tools and Manufacture, 2011. **51**(4): p. 358-362.
 - [30] Sidpara A and Jain VK, *Nano-level finishing of single crystal silicon blank using magnetorheological finishing process*. Tribology International, 2012. **47**: p. 159-166.
 - [31] Sidpara A and Jain VK, *Theoretical analysis of forces in magnetorheological fluid based finishing process*. International Journal of Mechanical Sciences, 2012. **56**(1): p. 50-59.
 - [32] Kordonski WI, Golini D, Hogan S and Sekeres A, *System for abrasive jet shaping and polishing of a surface using magnetorheological fluid*. U.S. Patent No. 5,971,835. 1999.

- [33] Tricard M, Kordonski WI, Shorey AB and Evans C, *Magnetorheological jet finishing of conformal, freeform and steep concave optics*. CIRP Annals-Manufacturing Technology, 2006. **55**(1): p. 309-312.
- [34] Jha S and Jain VK, *Design and development of the magnetorheological abrasive flow finishing (MRAFF) process*. International Journal of Machine Tools and Manufacture, 2004. **44**(10): p. 1019-1029.
- [35] Das M, Jain VK and Ghoshdastidar P, *Fluid flow analysis of magnetorheological abrasive flow finishing (MRAFF) process*. International Journal of Machine Tools and Manufacture, 2008. **48**(3): p. 415-426.
- [36] Jha S and Jain VK, *Modeling and simulation of surface texture in magnetorheological abrasive flow finishing (MRAFF) process*. Wear, 2006. **261**(7): p. 856-866.
- [37] Singh AK, Jha S and Pandey PM, *Design and development of nanofinishing process for 3D surfaces using ball end MR finishing tool*. International Journal of Machine Tools and Manufacture, 2011. **51**(2): p. 142-151.
- [38] Singh AK, Jha S and Pandey PM, *Nanofinishing of a typical 3D ferromagnetic workpiece using ball end magnetorheological finishing process*. International Journal of Machine Tools and Manufacture, 2012.
- [39] Sato T, Kum CW and Venkatesh V, *Rapid magnetorheological finishing of Ti-6Al-4V for aerospace components*. International Journal of Nanomanufacturing, 2013. **9**(5): p. 431-445.
- [40] Sidpara A and Jain VK, *Analysis of forces on the freeform surface in magnetorheological fluid based finishing process*. International Journal of Machine Tools and Manufacture, 2013.
- [41] Yamaguchi H, Yumoto K, Shinmura T and Okazaki T, *Study of finishing of wafers by magnetic field-assisted finishing*. Journal of Advanced Mechanical Design, Systems, and Manufacturing, 2009. **3**(1): p. 35-46.
- [42] Schinhaerl M, Pitschke EG, Rascher R, Sperber P, Stamp R, Smith LN and Smith G. *Temporal stability and performance of mr polishing fluid*. In *Optical Science and Technology, the SPIE 49th Annual Meeting*. 2004.
- [43] Kordonski WI and Golini D, *Fundamentals of magnetorheological fluid utilization in high precision finishing*. Journal of Intelligent Material Systems and Structures, 1999. **10**(9): p. 683-689.

- [44] Schinhaerl M, Pitschke EG, Geiss A, Rascher R, Sperber P, Stamp R, Smith LN and Smith G. *New viscosity measurement for magnetorheological polishing fluid*. In *Optics & Photonics 2005*. 2005.
- [45] Shorey AB, Jacobs SD, Kordonski WI and Gans RF, *Experiments and observations regarding the mechanisms of glass removal in magnetorheological finishing*. Applied Optics, 2001. **40**(1): p. 20-33.
- [46] Cook LM, *Chemical processes in glass polishing*. Journal of Non-Crystalline Solids, 1990. **120**(1): p. 152-171.
- [47] Schinhaerl M, Pitschke EG, Geiss A, Rascher R, Sperber P, Stamp R, Smith LN and Smith G. *Comparison of different magnetorheological polishing fluids*. In *Proc. SPIE*. 2005.
- [48] Miao C, Lambropoulos JC and Jacobs SD, *Process parameter effects on material removal in magnetorheological finishing of borosilicate glass*. Applied Optics, 2010. **49**(10): p. 1951-1963.
- [49] Arrasmith SR, Kozhinova IA, Gregg LL, Shorey AB, Romanofsky HJ, Jacobs SD, Golini D, Kordonski WI, Hogan SJ and Dumas P. *Details of the polishing spot in magnetorheological finishing (MRF)*. In *SPIE's International Symposium on Optical Science, Engineering, and Instrumentation*. 1999.
- [50] deGroote, JE, Marino AE, Wilson JP, Bishop AL, Lambropoulos JC and Jacobs SD, *Removal rate model for magnetorheological finishing of glass*. Applied Optics, 2007. **46**(32): p. 7927-7941.
- [51] Shafrir SN, Romanofsky HJ, Skarlinski M, Wang M, Miao C, Salzman S, Chartier T, Mici J, Lambropoulos JC and Shen R, *Zirconia-coated carbonyl-iron-particle-based magnetorheological fluid for polishing optical glasses and ceramics*. Applied Optics, 2009. **48**(35): p. 6797-6810.
- [52] Hanada K, Yamaguchi H and Zhou H, *New spherical magnetic abrasives with carried diamond particles for internal finishing of capillary tubes*. Diamond and Related Materials, 2008. **17**(7): p. 1434-1437.
- [53] Fox M, Agrawal K, Shinmura T and Komanduri R, *Magnetic abrasive finishing of rollers*. CIRP Annals-Manufacturing Technology, 1994. **43**(1): p. 181-184.
- [54] Yamaguchi H, Shinmura T and Kaneko T, *Development of a new internal finishing process applying magnetic abrasive finishing by use of pole rotation system*. International Journal of the Japan Society for Precision Engineering, 1996. **30**(4): p. 317-322.

- [55] Yamaguchi H and Shinmura T, *Study of an internal magnetic abrasive finishing using a pole rotation system: Discussion of the characteristic abrasive behavior*. Precision Engineering, 2000. **24**(3): p. 237-244.
- [56] Singh DK, Jain VK, Raghuram V and Komanduri R, *Analysis of surface texture generated by a flexible magnetic abrasive brush*. Wear, 2005. **259**(7): p. 1254-1261.
- [57] Yamaguchi H, Srivastava AK, Tan MA, Riveros RE and Hashimoto F, *Magnetic abrasive finishing of cutting tools for machining of titanium alloys*. CIRP Annals-Manufacturing Technology, 2012. **61**(1): p. 311-314.
- [58] Mulik RS and Pandey PM, *Ultrasonic assisted magnetic abrasive finishing of hardened AISI 52100 steel using unbonded SiC abrasives*. International Journal of Refractory Metals and Hard Materials, 2011. **29**(1): p. 68-77.
- [59] Chang GW, Yan BH and Hsu RT, *Study on cylindrical magnetic abrasive finishing using unbonded magnetic abrasives*. International Journal of Machine Tools and Manufacture, 2002. **42**(5): p. 575-583.
- [60] Wang Y and Hu D, *Study on the inner surface finishing of tubing by magnetic abrasive finishing*. International Journal of Machine Tools and Manufacture, 2005. **45**(1): p. 43-49.
- [61] Yamaguchi H, Kang J and Hashimoto F, *Metastable austenitic stainless steel tool for magnetic abrasive finishing*. CIRP Annals-Manufacturing Technology, 2011. **60**(1): p. 339-342.
- [62] Kang J, George A and Yamaguchi H, *High-speed internal finishing of capillary tubes by magnetic abrasive finishing*. Procedia CIRP, 2012. **1**: p. 414-418.
- [63] Kang J and Yamaguchi H, *Internal finishing of capillary tubes by magnetic abrasive finishing using a multiple pole-tip system*. Precision Engineering, 2012. **36**(3): p. 510-516.
- [64] Wang A and Lee S, *Study the characteristics of magnetic finishing with gel abrasive*. International Journal of Machine Tools and Manufacture, 2009. **49**(14): p. 1063-1069.

Chapter 3

Development of a new magnetic field-assisted finishing (MFAF) process

3.1 INTRODUCTION

Based on the literature review in the previous topic, the ability to polish complex geometry and high process efficiency has been identified as two of the key demands for surface finishing processes. In the aerospace industry specifically, there are existing and emerging applications requiring surface finishing processes capable of high efficiency material removal on freeform surfaces. Emerging applications may be various components in aero engines, such as next-generation blisks and more recently, additively manufactured parts of the same. For structured surfaces, one of the key potential applications is in processing of structured surfaces in mold for complex components.

To that end, the development of a new magnetic field-assisted finishing (MFAF) process targeted at high material removal on freeform surfaces has been initiated. The process uses novel principles to increase the removal rate. A prototype has been designed, fabricated, and incrementally improved to demonstrate the capability of the process. The work reported in this thesis forms the initial phase of a longer-term project in the research institute to develop a commercially viable MFAF process.

In this chapter, the development of the new MFAF process is reported. First, the requirements, goals, and visions of the new process are outlined. Following that, the principles of the process are established theoretically with magnetostatic analyses and empirically verified with experiments. Next, the parameters of the polishing tool are

theoretically analysed to understand their effects on the process outcome. Based on that, a set of parameters is suggested for the prototype of the polishing tool. Lastly, the prototype is used to validate and evaluate the capability of the polishing tool in achieving surface texture reduction and to polish selected freeform surfaces.

The work and results presented in this chapter have been published in one journal paper [1] and two conference papers [2, 3]. An international patent [4] has also been awarded for the new MFAF process.

3.2 GOALS OF NEW MFAF PROCESS

For surface finishing processes, no one-size-fit-all solution currently exists. The best surface finishing process is application-specific, and is dependent on many factors such as the target geometry, target material, required surface finish, production rate and production cost. New solutions and innovations are required when the combination of requirements cannot be met with any existing technique. The new MFAF process that has been developed seeks to address one such combination of requirements.

The new process is intended to be an automated process capable of polishing freeform surfaces to obtain surface texture around 0.1 to 0.01 $\mu\text{m Ra}$ from initial values of approximately 1 to 2 $\mu\text{m Ra}$. These were the guideline values proposed by industrial partners of the research institute at the inception of this work. The target freeform surfaces are either concave, convex, or a combination of both. As mentioned in Chapter 1, these freeform surfaces are typically polished manually with traditional polishing tools. The wear of these tools pose a significant challenge in automating the process. Microstructured surfaces for emerging applications [5] in functional surfaces are also of

keen interest, as no viable solution currently exists for the surface finishing of these surfaces.

High removal rate is another key requirement for the new process, as the process may be used for the surface finishing of large aerospace components, or for the surface finishing of surface with high initial roughness. In this instance, no specific value has been provided but a minimum removal rate of 10 $\mu\text{m}/\text{min}$ is desirable.

At this phase of development, there is no specific target material for the new process, although advanced materials such as aerospace superalloys are of keen interest.

3.3 PRINCIPLES OF NEW MFAF PROCESS

In this section, the processing principles of the new MFAF process are introduced. A link between these principles and an increased removal rate is established theoretically and validated empirically. Figure 3.1 is a schematic diagram of the polishing tool, with a magnified view of the polishing zone. Particle sizes are exaggerated.

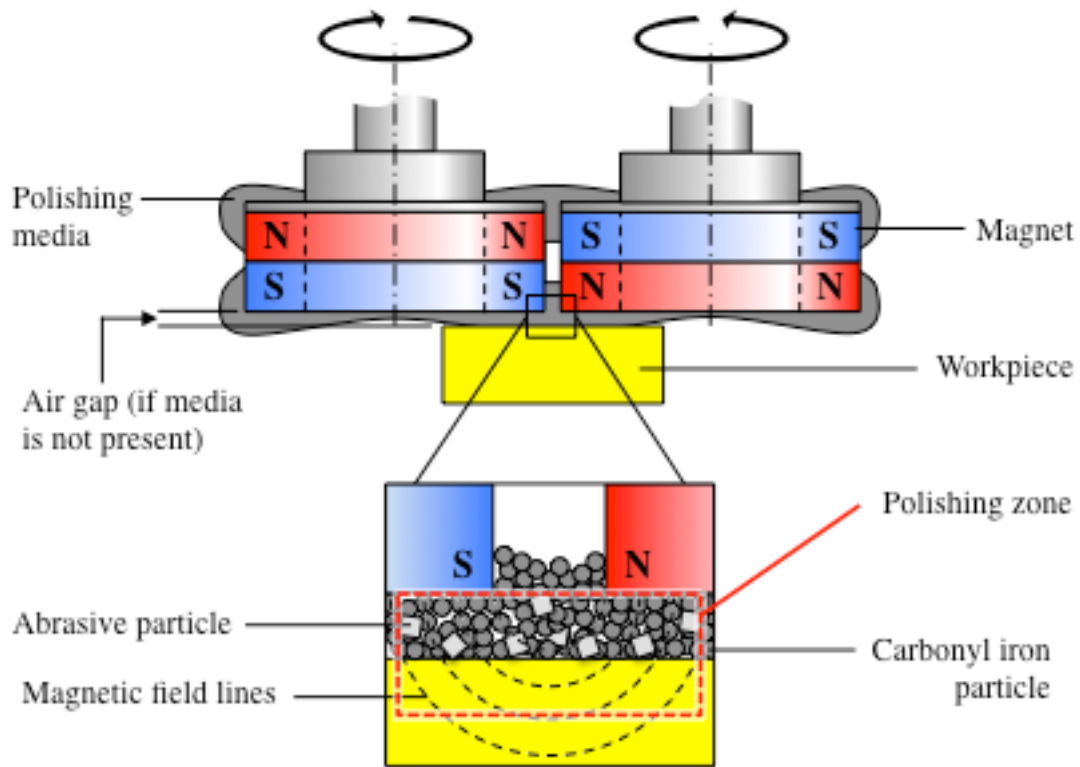


Figure 3.1: Schematic diagram of the polishing tool and the polishing zone.

The new MFAF process uses an MR fluid-based finishing media, with non-magnetic abrasives suspended within. The MR fluid is prepared by mixing dry carbonyl iron particles and water, which acts as the carrier fluid. Under the influence of a magnetic field, the carbonyl iron particles form chain-like structures, resulting in an exponential increase in the viscosity of the finishing media. The viscosity profile is similar to that of a Bingham plastic. In this semi-solid form, the finishing media is utilised as a conformable polishing lap that is adaptable to the geometry of the workpiece. This is advantageous for the polishing of freeform surfaces.

The polishing tool consists of two ring magnets positioned next to each other with their axes parallel and their magnetic poles opposite of each other. An air gap is

maintained between the two magnets. Another air gap is also maintained between the planar end of the two magnets and the workpiece. During polishing, the second air gap is occupied by finishing media, which interfaces the magnets and the workpiece surface. The two magnets are rotated in opposite directions by a gear mechanism, but can also be driven independently. A relative velocity between the finishing media and the workpiece surface is created by the rotation of the magnets. As a result, the abrasives in the finishing media abrade and remove materials from the workpiece surface.

The relatively high removal rate of the new MFAF process can be attributed to two key principles, which are discussed in the following sections.

3.3.1 High magnetic flux density in the polishing zone

The new MFAF process employs a unique double-magnet configuration, which creates a magnetic circuit passing through both magnets to reduce the magnetic flux leakage from the system. This is illustrated by an image capture from the magnetostatic analysis shown in Figure 3.2. Magnetostatic analyses in this chapter are performed using the ANSYS software package and have been verified against actual values measured by a vector magnetometer. Complete technical details of the simulation are available in Appendix A.

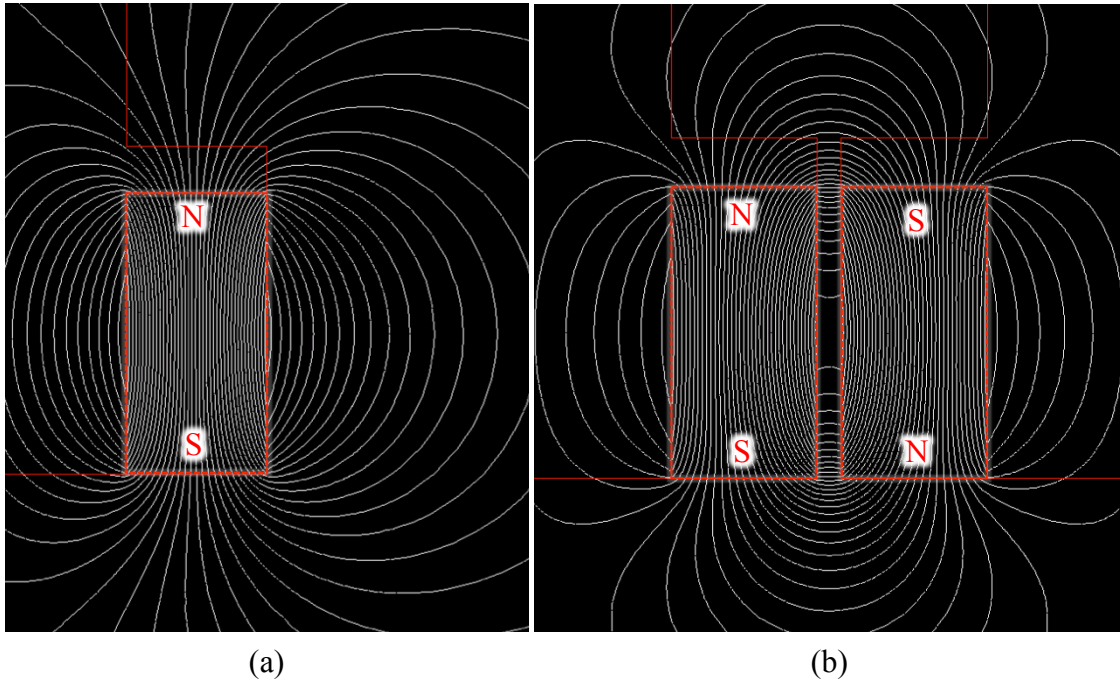


Figure 3.2: Magnetic flux lines for (a) single-magnet configuration, and (b) double-magnet configuration.

The reduced magnetic flux leakage for the double-magnet configuration creates a region of high magnetic flux density in the air space on the planar end of both magnets. This region is the designated polishing zone of the polishing tool. The contour plots of the magnetic flux density for the single-magnet and double-magnet configurations, also obtained with magnetostatic simulations, are shown in Figure 3.3. Both contour plots share a common colour scale.

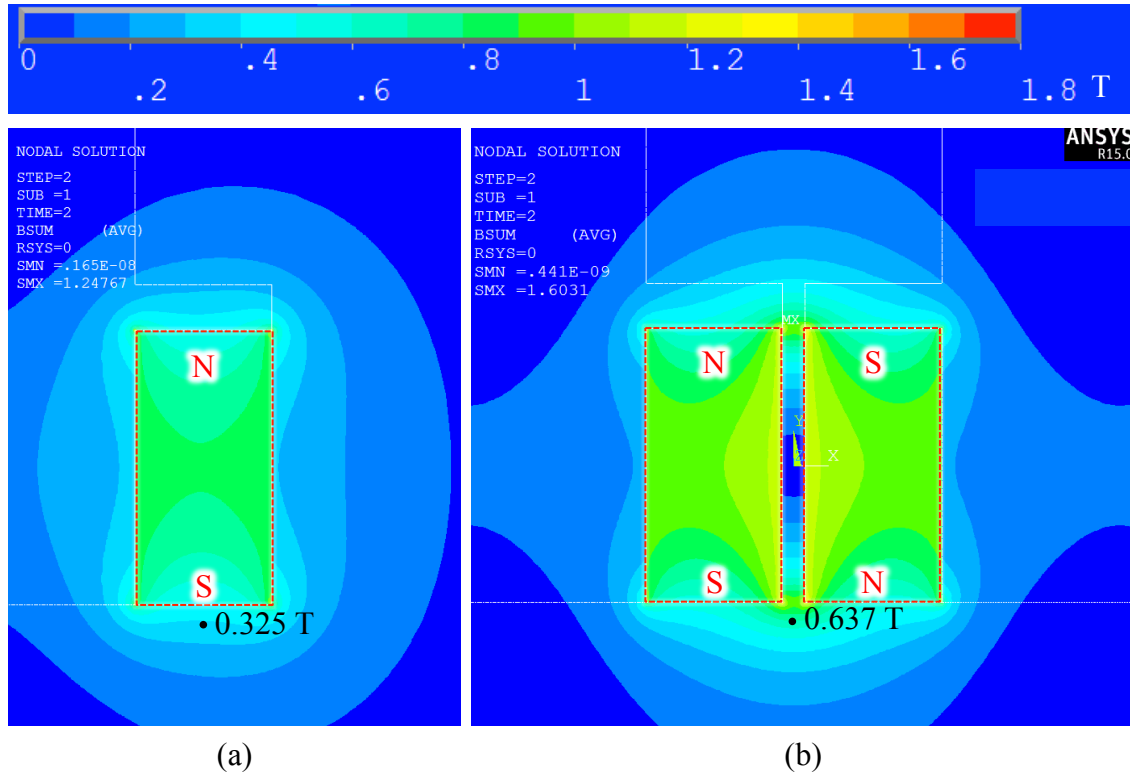


Figure 3.3: Contour plots of magnetic flux density for (a) single-magnet configuration, and (b) double-magnet configuration.

At a distance of 1 mm away from the planar end of the magnets, the calculated magnetic flux density for the double-magnet configuration is 0.637 T. This is approximately double the magnetic flux density of 0.325 T obtained for the single-magnet configuration. A high magnetic flux density is advantageous because it increases the viscosity of the finishing media, which typically translates into a higher removal rate. Therefore, the advantage of the double-magnet configuration is evident from the theoretical results presented above.

3.3.2 *In situ* media reformation

The second key feature of the double-magnet configuration is the ability of the finishing media to reform its shape *in situ* during the process. This is not possible for the single-magnet configuration. The photographs of the shape of the finishing media during different stages of the polishing process using the single-magnet configuration are shown in Figure 3.4.

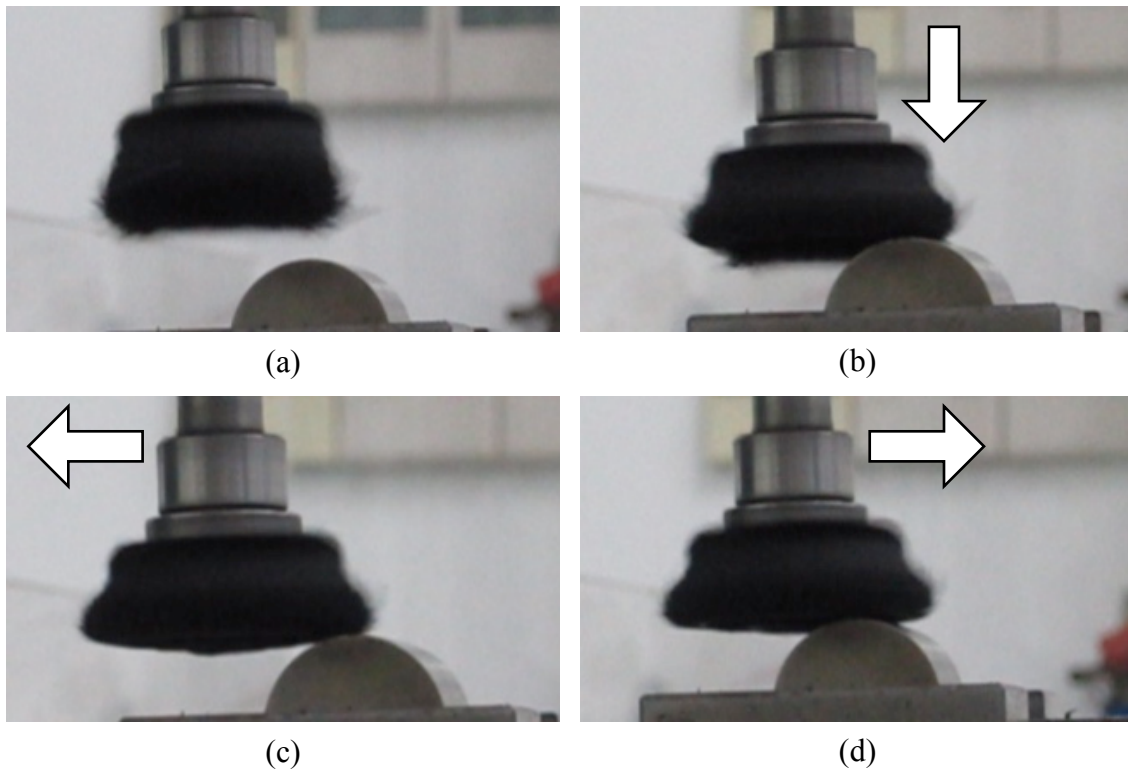


Figure 3.4: Shape of the finishing media during the polishing process using the single-magnet configuration (a) before polishing, (b) after initial contact with the workpiece, (c) after losing contact with the workpiece, and (d) after coming into contact with the workpiece again.

Figure 3.4(a) shows the shape of the finishing media after it has been supplied to the tool and before polishing begin. Magnet is rotated at this stage. When the finishing

media is brought into initial contact with the workpiece in (b), the shape of the finishing media changes to conform to the geometry of the workpiece. In (c), the polishing tool is deliberately moved away from the workpiece so that contact is lost between the finishing media and the workpiece. It can be observed that the shape of the finishing media remains deformed, and is different compared to the initial shape in (a). When the polishing tool is brought into contact with the workpiece again in (d), the deformed finishing media is no longer able to exert a sustained pressure on the workpiece. As a result, the removal rate will be reduced.

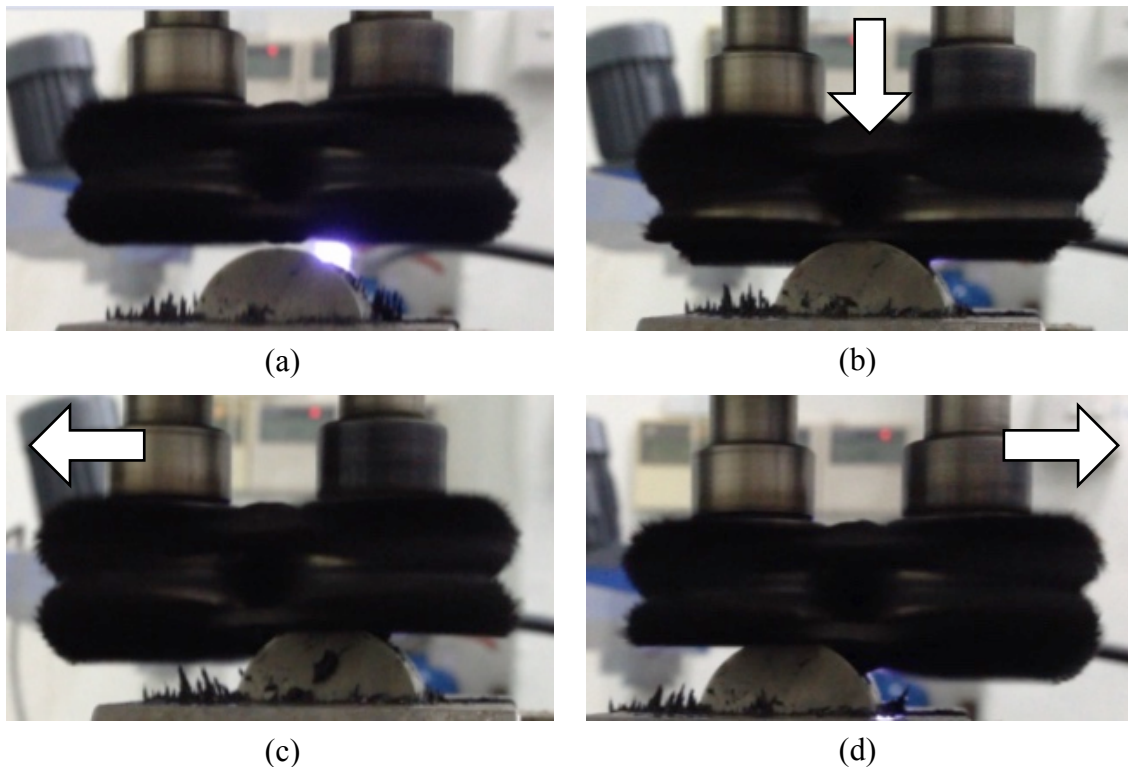


Figure 3.5: Shape of the finishing media during the polishing process using the double-magnet configuration (a) before polishing, (b) after initial contact with the workpiece, (c) after losing contact with the workpiece, and (d) after coming into contact with the workpiece again.

Figure 3.5(a) shows the shape of the finishing media for the double-magnet configuration after it has been supplied to the tool and before polishing begin. In (b), the finishing media is brought into initial contact with the workpiece and its shape changes to adapt to the geometry of the workpiece. When the polishing tool is deliberately moved away from the workpiece in (c), contact is lost between the finishing media on the left magnet and the workpiece. Unlike the single-magnet configuration, the shape of the finishing media is reformed to its initial shape. This occurs *in situ* without any form of external input or assistance. The same can be observed in (d) when contact is lost between the finishing media on the right magnet and the workpiece.

The ability of the finishing media in the double-magnet configuration to reform to its initial shape *in situ* is advantageous, as it allows the finishing media to exert a sustained pressure on the workpiece. As a result, the removal rate will be higher compared to the single-magnet configuration. This advantage is also in addition to the increased magnetic flux density attributed to the double-magnet configuration described in the previous section.

The observed *in situ* reformation of finishing media in the double-magnet configuration occurs via two different mechanisms. The first mechanism is the dynamic magnetic field experienced by the magnetic particles in the double-magnet configuration. Likewise, no *in situ* reformation is observed for the single-magnet configuration because the magnetic particles experience a static magnetic field. To illustrate the magnetic field in the single-magnet configuration, a moving point X on the planar surface of the magnet is considered, as shown in Figure 3.6(a). The moving point X is at a constant distance r from the centre of the magnet. When the magnet rotates, the locus of moving point X is therefore a circle concentric with the magnet, with a radius of r . As θ changes during the magnet rotation, the moving point X experiences no change in magnetic flux density

because the magnetic field is axisymmetric. This is illustrated in the plot of magnetic flux density at moving point X against the angle θ , shown to the right of Figure 3.6(a).

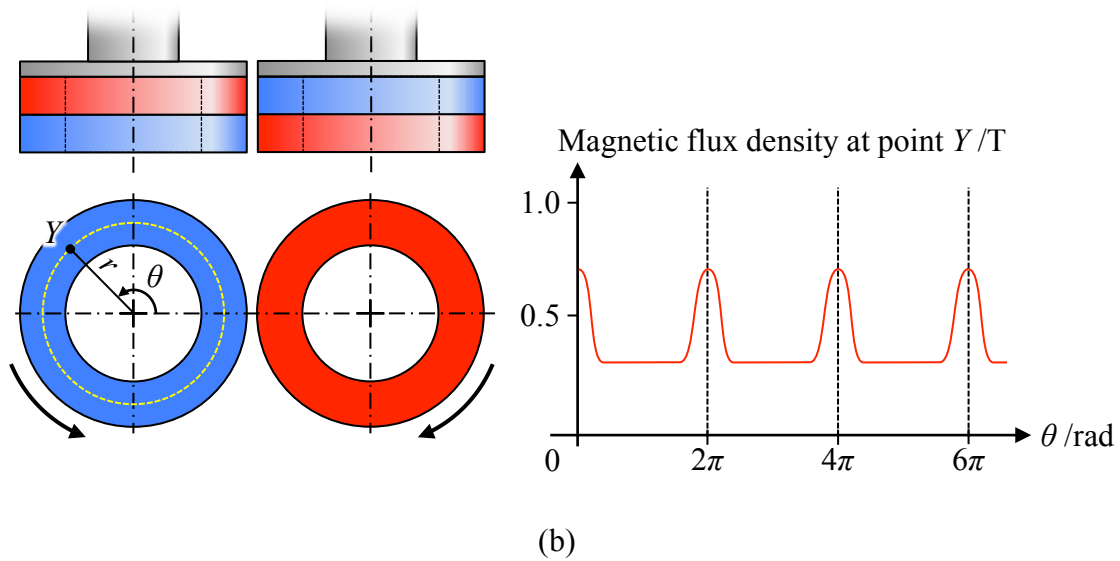
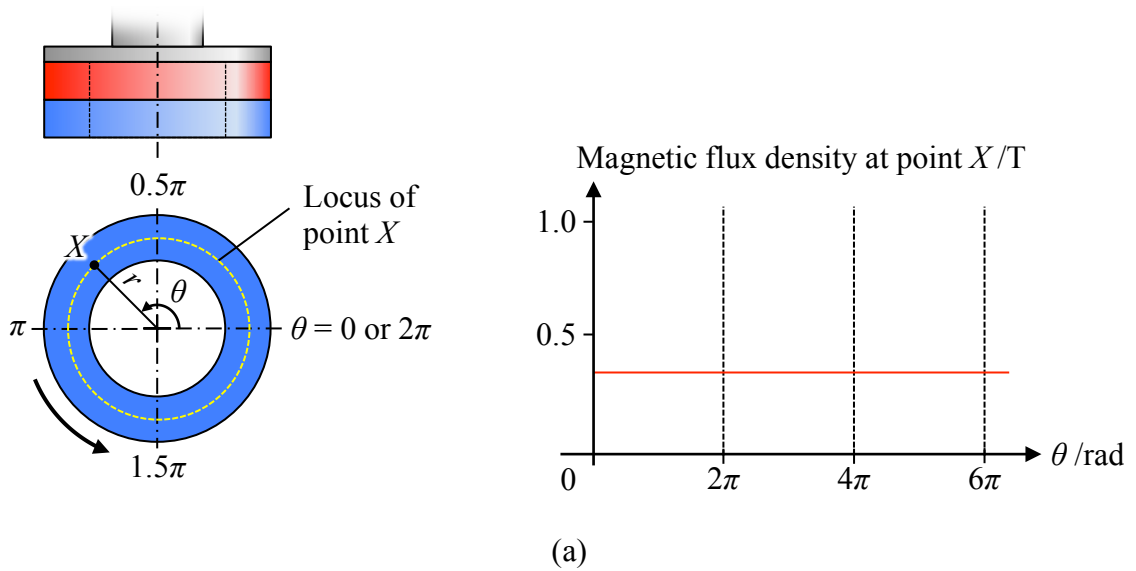


Figure 3.6: The magnetic flux density profile of moving points X and Y for (a) single-magnet configuration, and (b) double-magnet configuration.

Similarly, a moving point Y is considered on the planar surface of the left magnet in the double-magnet configuration, as shown in Figure 3.6(b). The locus of moving point Y is a circle concentric with the left magnet, with a radius of r . The key difference is that the moving point Y passes through the region of high magnetic flux density in the polishing zone for every complete revolution of the magnets. Specifically, the moving point Y experiences maximum magnetic flux density when its angle θ is a multiple of 2π . The moving point Y therefore experiences a dynamic magnetic field when the magnets rotate. This is illustrated in the plot of magnetic flux density at moving point Y against the angle θ , shown to the right of Figure 3.6(b). A dynamic magnetic field introduces as a non-zero magnetic field gradient, exerting a magnetic pressure force on the magnetic particles in the finishing media, which is given by the following expression [6]:

$$F = V\chi\mathbf{H} \cdot \nabla\mathbf{H} \quad (3.1)$$

where F is the magnetic pressure force on one magnetic particle, V is the volume of the magnetic particle, χ is the susceptibility of the magnetic particle, and \mathbf{H} is the magnetic field strength vector at the centre of the magnetic particle. This magnetic pressure force provides the impetus for rearrangement of the magnetic particles in the finishing media, which is manifested as the observed *in situ* reformation of the finishing media.

The second mechanism of the *in situ* reformation is the physical squeezing of the finishing media in the polishing zone. The finishing media is physically squeezed due to geometrical interference of the finishing media on each magnet as they enter the polishing zone. This is illustrated in Figure 3.7. The observed *in situ* reformation can be attributed to the contact forces resulting from the physical squeezing of the finishing media.

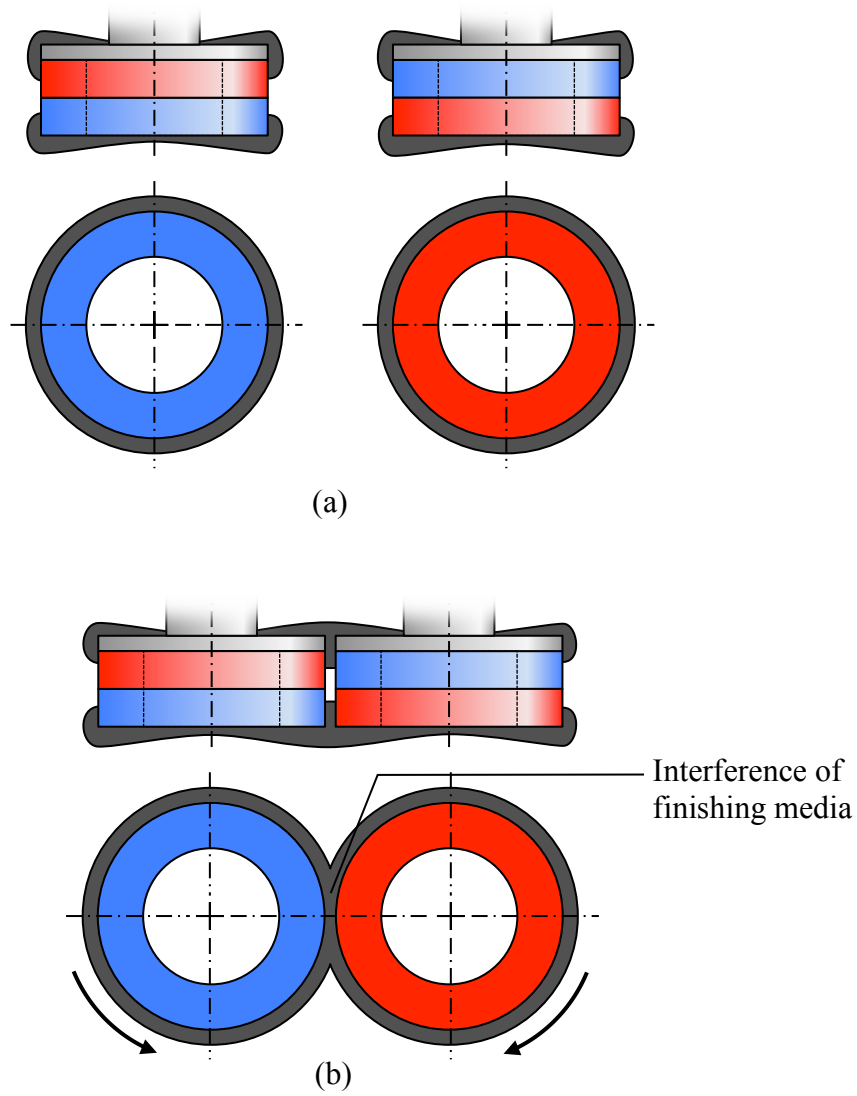


Figure 3.7: Shape of finishing media when (a) the two magnets are separated from each other, and (b) when a small air gap is maintained between the two magnets. Finishing media on the two magnets interfere and are physically squeezed. Contact forces arising from it is accountable for the observed *in situ* reformation of the finishing media.

3.3.3 Finishing forces comparison

The effect of the high magnetic flux density in the polishing zone and the *in situ* reformation of finishing media will be validated and evaluated by comparing the shear and normal forces on the workpiece during polishing for the single-magnet and double-magnet configurations. Force measurements are conducted by mounting the workpiece on a three-component dynamometer (Kistler, Type 9265B+9443B). Figure 3.8 shows the relationship between shearing and normal forces, F_s and F_n , and the gap between magnet and workpiece, z , for the single-magnet (S) and double-magnet (D) configurations. The supplied amount of finishing media is also varied.

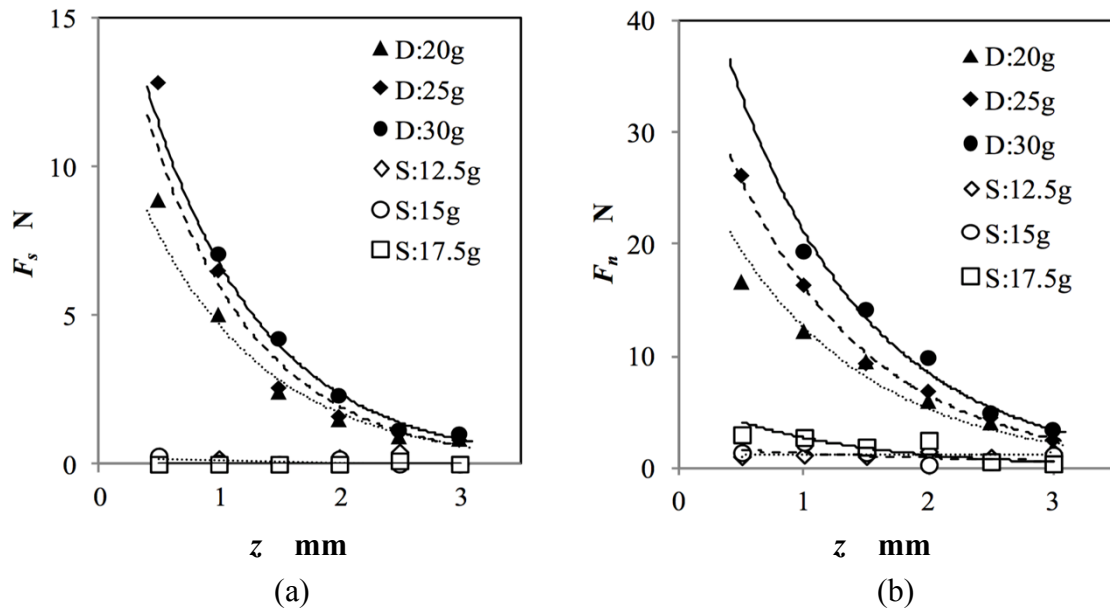


Figure 3.8: (a) Shear forces and (b) normal forces during polishing for single-magnet (S) and double-magnet (D) configurations, with different supplied amount of finishing media.

It can be observed that both the shear and normal forces for double-magnet configuration are about one order of magnitude higher than that for the single-magnet

configuration. The significant difference of finishing forces between the single-magnet and double-magnet configurations can be attributed to the high magnetic flux density and the *in situ* reformation as discussed earlier. Comparison of the finishing forces have thus established and validated the two principles of the new MFAF process.

In addition, the finishing forces decrease with an increasing z , and increase with an increasing supplied amount of finishing media. These factors are addressed in the next section.

3.4 EFFECT OF TOOL PARAMETERS ON MAGNETIC FLUX DENSITY IN THE FINISHING ZONE

In the previous section, the two principles of the novel MFAF process have been established and photographic evidence together with magnetostatic analyses have been presented for validation. Measurements of finishing forces have also been used as a proxy to establish the advantage of a high magnetic flux density in the polishing zone for achieving a high removal rate.

In this section, the relationships between selected tool parameters and the magnetic flux density in the finishing zone are established and evaluated. Specifically, the effects of the gap between magnets, w_{gap} , the gap between magnets and workpiece, z , and the thickness of the magnets, t_{magnet} , on the magnetic flux density in the finishing zone are evaluated. These variables are illustrated in an image capture of the polishing tool in the ANSYS environment, shown in Figure 3.9. Additionally, the merit of including magnetic caps in the polishing tool to augment the magnetic flux density in the polishing zone is studied. The relationship between the thickness of the magnetic caps, t_{cap} , and the increase in magnetic flux density is also evaluated.

Finally, a brief discussion on the differences between selecting permanent magnets and electromagnet for the polishing tool is presented.

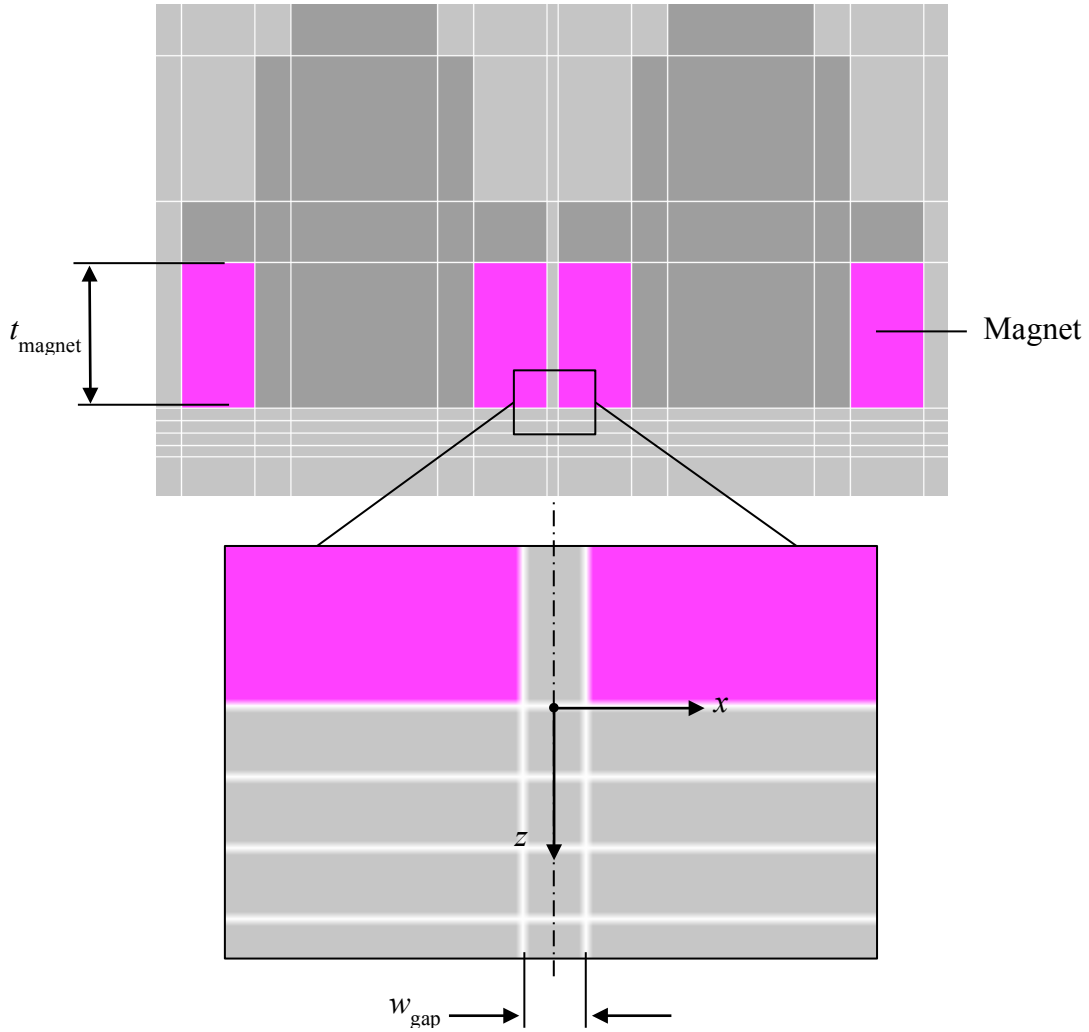


Figure 3.9: Polishing tool in the ANSYS environment. Magnet thickness, t_{magnet} , and gap between magnets, w_{gap} , are variables.

3.4.1 Methodology

Magnetic flux density is obtained from magnetostatic analyses conducted with the ANSYS software package, similar to results presented earlier in this chapter. Simulations in this section are based on permanent ring magnets (neodymium, Grade N35) with 30 mm outer diameter, 18 mm inner diameter, and thickness of 12 mm. These dimensions are based on stock magnets available for experiments. Simulations are also categorized into three different batches.

For the first batch, the gap between magnets, w_{gap} , is a variable with values of 1 mm, 2 mm and 3 mm. For each value of w_{gap} , magnetic flux density is recorded at selected nodes in the finishing zone. The nodes are spaced apart evenly in the x -axis and almost evenly in the z -axis. In the x -axis, the nodes are positioned between $x = 0$ mm and up to $x = 2.5$ mm, with a uniform spacing of 0.1 mm between each node. In the z -axis, the nodes are positioned between $z = 0.1$ mm and $z = 3.0$ mm, with uniform spacing of 0.5 mm for nodes between $z = 0.5$ mm and $z = 3.0$ mm. The value of z is equivalent to the distance between the magnets and the workpiece. Collectively, the nodes form a rectangular grid. The thickness of the magnet, t_{magnet} , is set to 12 mm.

For the second batch, the thickness of magnet, t_{magnet} , is a variable with values of 3 mm, 6 mm, 12 mm, 24 mm, 48 mm and 96 mm. Magnetic flux density is compared for the nodes at $x = 0$ mm and $z = 1$ mm, 1.5 mm and 2.0 mm. The gap between magnets, w_{gap} , is set to 1 mm.

For the last batch of simulation, magnetic caps with material properties corresponding to stainless steel (Grade 430) are added on top of the existing magnets. The thickness of the magnetic caps, t_{cap} , is a variable with values between 0 mm (no magnetic cap) and 20 mm. The thickness of the magnets, t_{magnet} , is set to 12 mm and the

gap between magnets, w_{gap} , is set to 1 mm. Magnetic flux density is compared for the nodes at $x = 0$ mm and $z = 1$ mm, 1.5 mm and 2.0 mm.

3.4.2 Effect of gap between magnets, w_{gap} , and the gap between magnet and workpiece, z

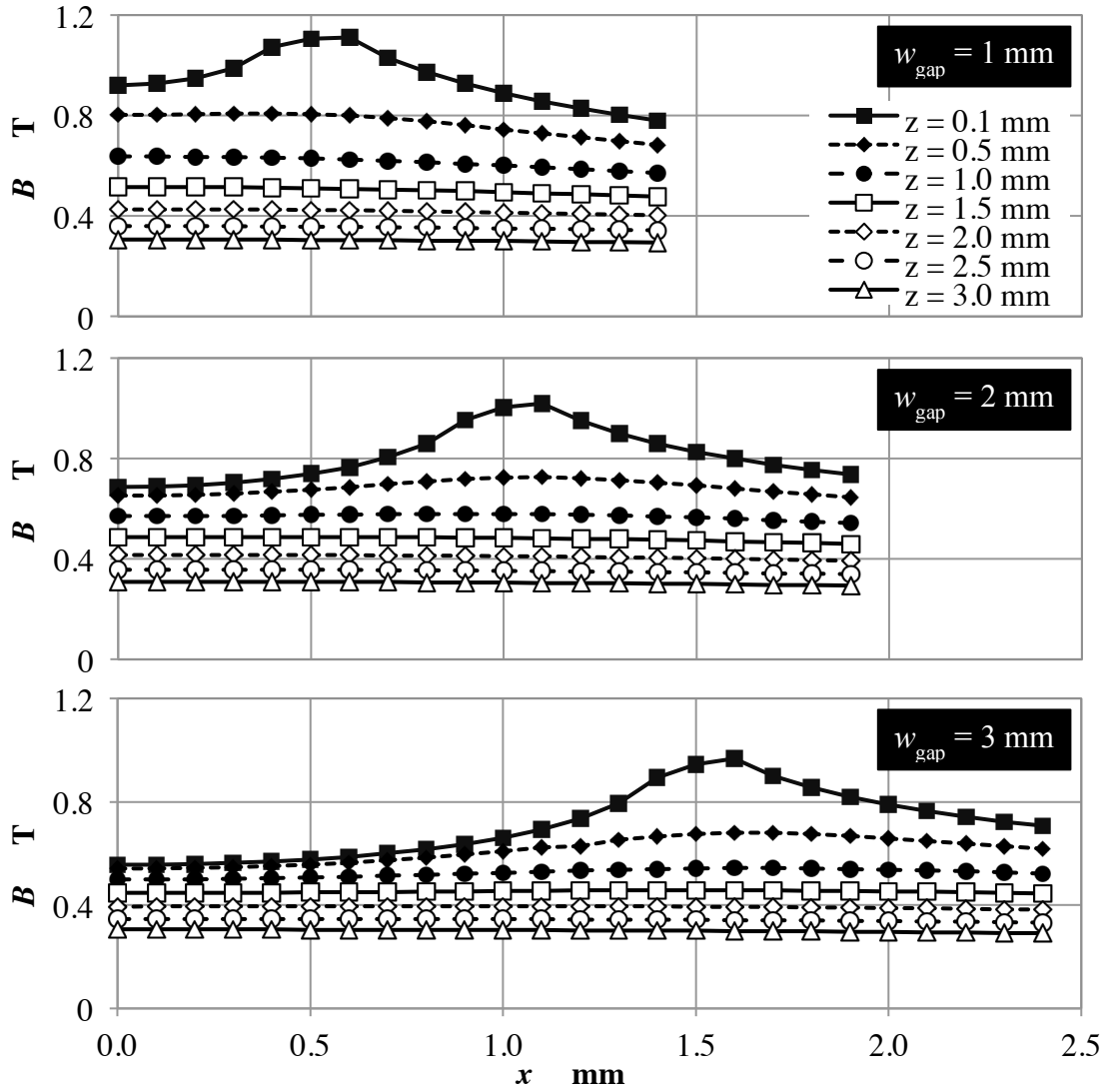


Figure 3.10: Magnetic flux density profiles at different z values when w_{gap} is a variable.

The three graphs in Figure 3.10 show the values of magnetic flux density at selected nodes when the gap between magnets, w_{gap} , is varied. Firstly, it can be observed that the magnetic flux density decreases with an increasing value of z for all three sets of curves. This is expected as magnetic flux density is inversely related to z . Using the magnitude of the magnetic flux density as the criterion, selecting small values of z is advantageous.

However, small values of z present a different issue. Consider the curves of $z = 0.1$ mm for all three values of w_{gap} . The three curves exhibit distinct maximum points at $x = 0.5$ mm, $x = 1.0$ mm and $x = 1.5$ mm respectively. The x -coordinates of these maximum points correspond to the edge of the magnet. These maximum points are attributable to the well-documented edge effect of magnet [7], where magnetic flux density is significantly higher along the edge or at the corner of a magnet. The variation of magnetic flux density along the x -axis resulting from these maximum points is significant and will cause uneven removal rate along the x -axis. However, the spike in magnetic flux density is less prominent with a decreasing z . To achieve better uniformity of the magnetic flux density profile, selecting large values of z is advantageous.

With two conflicting criteria for the selection of value for z , the ideal value for z is therefore neither too small, such that the non-uniformity of the magnetic flux density profile along the x -axis is too significant, nor too large, such that the magnetic flux density is too low. Based on these criteria and the curves in Figure 3.10, the recommended range of values of z is between 0.5 mm and 1.0 mm. Selecting a value of z smaller than 0.5 mm will result in an uneven removal rate in the x -axis, while selecting a value larger than 1.0 mm will result in low removal rate. For the experimental trials in this thesis, a value of $z = 0.5$ mm or 1.0 mm is selected.

In addition, it is to be noted that the magnetic flux density is sensitive to changes in the values of z . As such, it is critical to tightly control the dimensional tolerance of the gap between magnet and workpiece during the polishing process to achieve a repeatable removal rate. No quantification of the required tolerance is carried out in this thesis, but a speculative value for the tolerance of z based on experience with setting up the apparatus is 100 μm .

Next, the effect of the gap between magnets, w_{gap} , is also evaluated by comparing the three plots in Figure 3.10. When w_{gap} is increased from 1 mm to 2 mm and to 3 mm, the magnetic flux density at $x = 0$ mm decreases (when comparing at the same z). The reduction of magnetic flux density is especially significant when values of z are between 0.1 mm and 1.5 mm, while magnetic flux density for z values between 1.5 mm and 3.0 mm decreases marginally. The reduction in the magnetic flux density when increasing w_{gap} is caused by a greater flux leakage through the air gap, which nullifies the advantage of using the double-magnet configuration. The effect of flux leakage is quantified from the results presented in Table 3.1.

Table 3.1: Comparison of magnetic flux density values at the centre of polishing zone and at edge of magnet for different values of w_{gap} , when $z = 0.5$ mm.

w_{gap}	Magnetic flux density (T)		Change
	At edge of magnet; $x = (0.5 \times w_{\text{gap}})$ mm	At centre of polishing zone; $x = 0$ mm	
1.0	0.806	0.802	-0.5 %
2.0	0.724	0.652	-9.9 %
3.0	0.675	0.542	-19.7 %

Table 3.1 compares the magnetic flux density at the centre of the polishing zone at $x = 0$ mm and at the edge of the magnet for the three values of w_{gap} . As discussed earlier, the magnetic flux density at the edge of the magnet is the maximum. The drop in magnetic flux density at $x = 0$ mm is therefore attributable to the leakage of magnetic flux. Therefore, the percentage reduction in magnetic flux density is used as a proxy to quantify the magnetic flux leakage. From the table, the percentage reduction increases substantially when the w_{gap} is increased from 1 mm to 3 mm. Based on the criterion of minimizing the flux leakage and maximizing the magnitude of magnetic flux density, selecting small values of w_{gap} is advantageous.

However, small values of w_{gap} result in a smaller area of the polishing zone. The width of the polishing area is approximately w_{gap} . While small values of w_{gap} increases the magnetic flux density at $x = 0$ and consequently the peak removal rate at that point, it may not result in the maximum volumetric removal rate, which is calculated based on the magnetic flux density profile and the polishing area. Optimization of w_{gap} to achieve

maximum volumetric removal rate is not in the scope of this thesis. Therefore, a value of $w_{\text{gap}} = 1.0$ mm is selected for future experimental trials in this thesis.

3.4.3 Effect of thickness of magnet, t_{magnet}

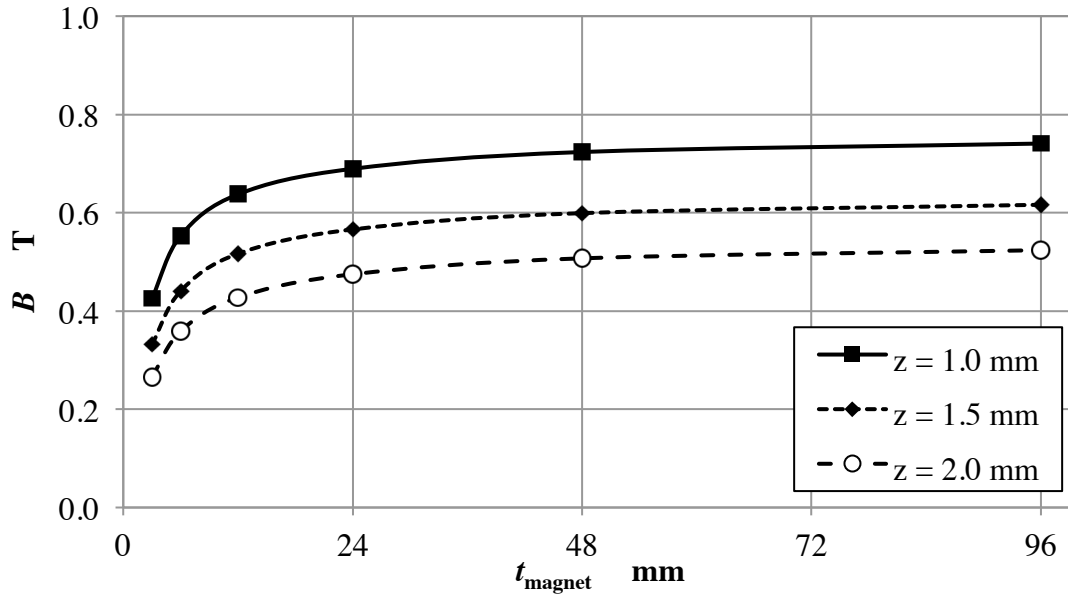


Figure 3.11: Magnetic flux density at $x = 0$ mm against thickness of magnet, t_{magnet} , for different values of z .

Figure 3.11 shows the relationship between magnetic flux density at $x = 0$ mm against the thickness of magnet, t_{magnet} , for three different values of z between 1.0 mm and 2.0 mm. Generally, the magnetic flux density increases with t_{magnet} and approaches an asymptote. When $z = 1.0$ mm, the asymptote is at 0.75 T. When $z = 1.0$ mm, a magnet thickness of 12 mm and 24 mm can achieve approximately 85 % and 92 % of the asymptotic value respectively. Therefore, increasing t_{magnet} beyond 12 mm does not result in a substantial increment of the magnetic flux density. For convenience, magnets with $t_{\text{magnet}} = 12$ mm are selected for experimental trials in this thesis. For industrial

applications, the optimal t_{magnet} will be dependent on economics and engineering factors, which are not considered in this thesis.

3.4.4 Effect of magnetic caps and their thickness, t_{cap}

To augment the magnetic flux density in the polishing zone, the use of magnetic caps has been considered. Magnetic caps are components made of magnetic materials, such as ferritic stainless steel (400 series), positioned on top of the magnets to close the magnetic circuit and reduce magnetic flux leakage. Reduction in the magnetic flux leakage translates to an increased magnetic flux density in the polishing zone. An image capture of the double-magnet configuration with magnetic caps in the ANSYS environment are shown in Figure 3.12. The magnetic properties of the magnetic caps are based on magnetic properties of SUS430.

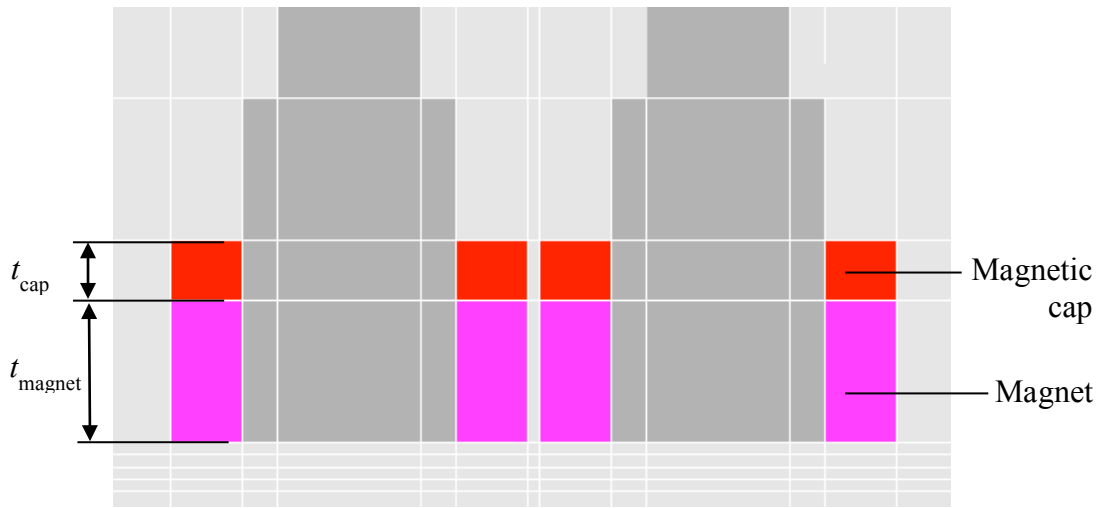


Figure 3.12: Polishing tool in the ANSYS environment, with magnetic caps.

Figure 3.13(a) shows the magnetic flux lines in the double-tool configuration when no magnetic cap is present, and (b) is the magnetic flux lines when magnetic caps

are present. The magnetic flux lines are concentrated at the air gap between the magnetic caps. The function of the magnetic caps in closing the magnetic circuit and reducing flux leakage have thus been validated.

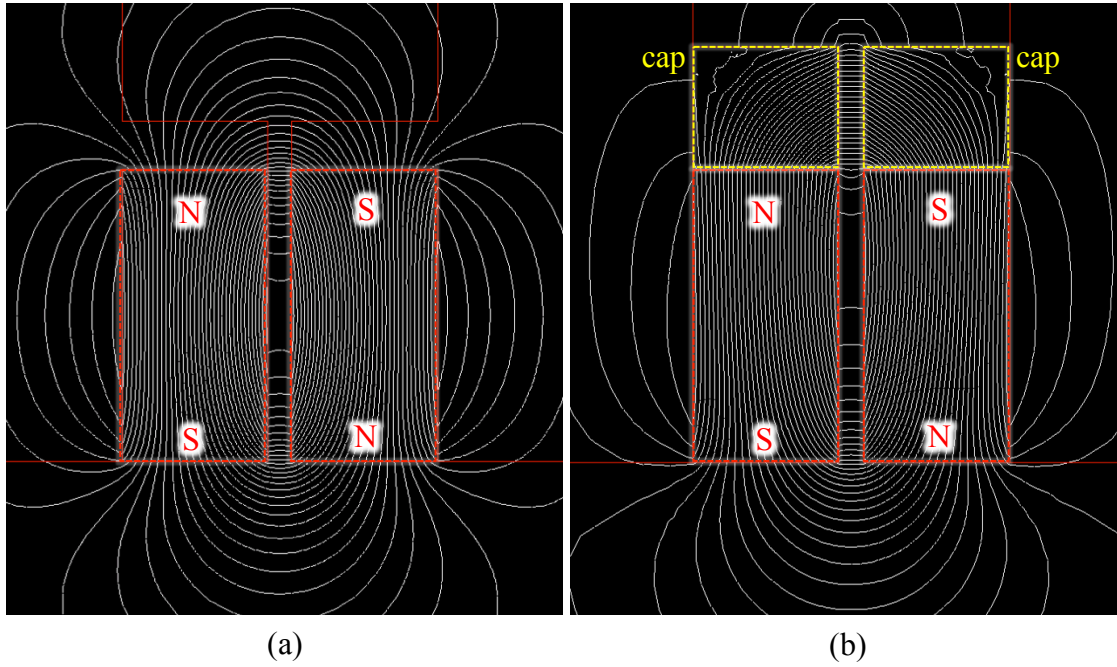


Figure 3.13: Magnetic flux lines of double-magnet configuration (a) without magnetic cap, and (b) with magnetic caps of 5 mm thickness.

The effectiveness of the magnetic caps in increasing the magnetic flux density in the polishing zone is dependent on the magnetic properties of the magnetic caps, and also the thickness of the magnetic caps, t_{cap} . Simulations have been carried out to quantify the effect of varying t_{cap} on the magnetic flux density at $x = 0$ mm for $z = 1.0$ mm, 1.5 mm and 2.0 mm. Figure 3.14 shows the relationship between magnetic flux density and t_{cap} for the z values aforementioned.

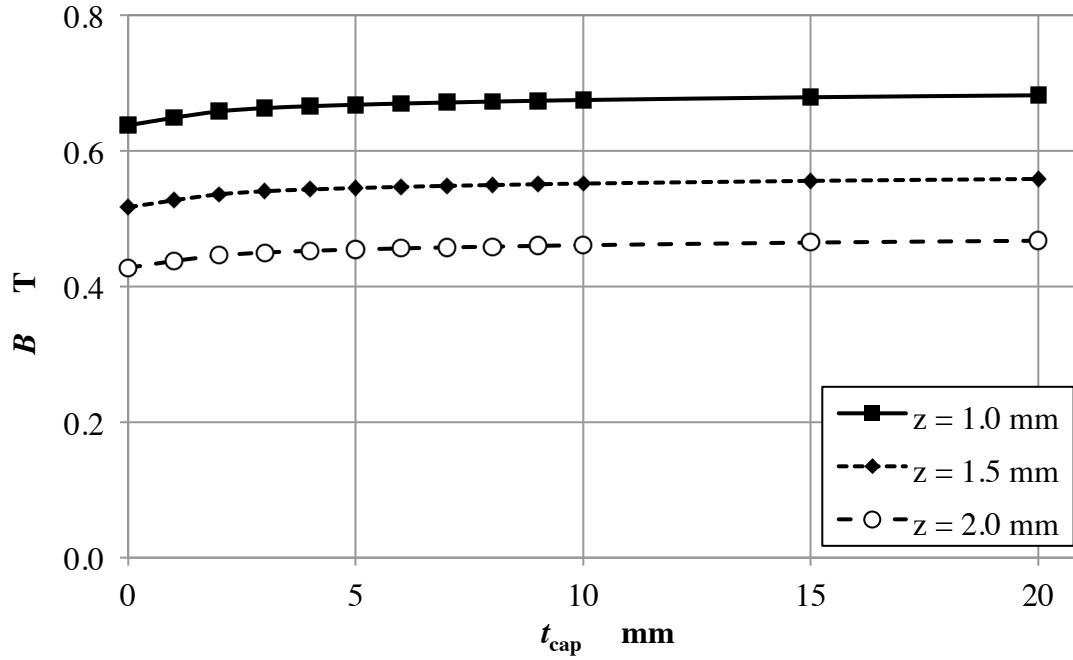


Figure 3.14: Magnetic flux density at $x = 0$ mm against thickness of magnetic cap, t_{cap} at different z values.

Note that $t_{\text{cap}} = 0$ mm is equivalent to no magnetic cap. For all three values of z , the inclusion of magnetic caps augments the magnetic flux density. However, the increase in the magnetic flux density is not significant. For example, magnetic caps with thickness of 5 mm augment the magnetic flux density by approximately 5 %. In actual applications where optimization of polishing tool is required, the inclusion of magnetic caps is advantageous. For convenience, no magnetic cap will be used for experimental trials in this thesis because the increase in magnetic flux density is insignificant.

3.4.5 Permanent magnets versus electromagnet

The magnetic field for the polishing tool can be created either by permanent magnets or electromagnet. For permanent magnets, neodymium (NdFeB) magnets, which are currently the strongest commercially available magnets, are the preferred type.

On a per-volume basis, neodymium magnets are typically stronger than an electromagnet. In addition, an electromagnet system requires wiring and power supply, and also complex electrical coupling for the rotating magnetic poles in the double-magnet configuration. On the other hand, with neodymium magnets, a high magnetic flux density can be obtained in the finishing zone with minimal setup. For convenience and ease of prototyping, the setup used for experimental trials in this thesis is based on neodymium magnets instead of electromagnet.

However, a polishing tool based on electromagnet is recommended for industrial applications as the ability to configure the magnetic field strength brings several key advantages. Firstly, the magnetic field can be turned off to drastically improve the change or removal of finishing media from the magnetic poles. This will significantly reduce the downtime in a process cycle. Secondly, the magnetic field strength can be varied during process, which may be advantageous for control of process outcome. While desirable, the ability to configure magnetic field strength is not required for experimental trials in this thesis. As such, the use of permanent magnets is sufficient.

3.5 FINISHING CHARACTERISTICS

In the previous section, the tool parameters have been analysed theoretically to understand their effects on the magnetic flux density in the polishing zone, which is a proxy for the removal rate of the new MFAF process. From the analyses, a set of values for the tool parameters has been suggested for the prototype.

In this section, experimental trials are conducted with the prototype to study the finishing characteristics of the double-magnet configuration. Firstly, the ability of the new MFAF process to achieve surface texture reduction is validated experimentally. The

achievable surface texture is quantified for stainless steel (SUS 316) and titanium alloy (Ti-6Al-4V) workpieces. Then, the peak removal rate of the process is measured and benchmarked against other processes to validate the ability of the process for high removal rate. Lastly, the capability of the process in polishing freeform surfaces is demonstrated through the polishing of a 2.5D microtextured surface.

Experimental trials are conducted using a prototype of the polishing unit, as shown in Figure 3.15.

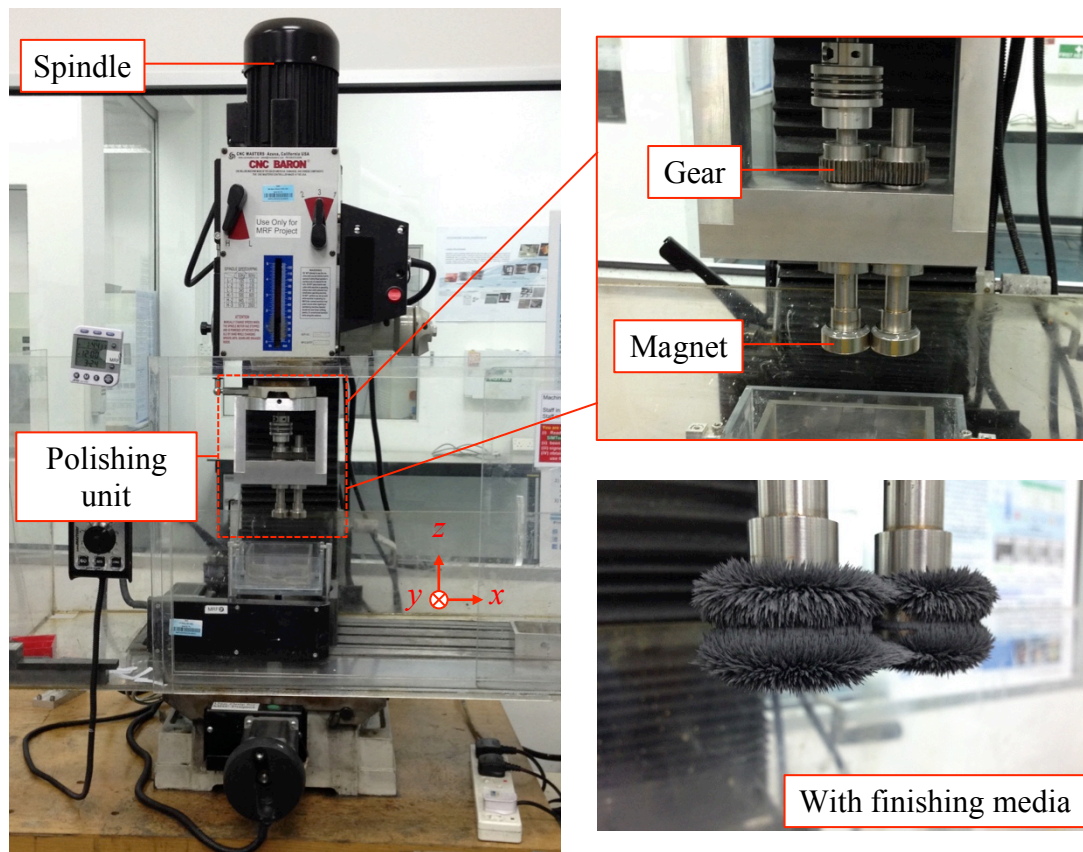


Figure 3.15: Prototype of the polishing unit mounted on a desktop milling machine.

3.5.1 Surface texture

Table 3.2: Experimental conditions for polishing of SUS316 flat workpiece.

Machine	CNC Baron desktop milling machine
Workpiece	Stainless steel (SUS316) <i>Dimension: 25 mm × 25 mm × 3 mm</i> <i>Ground with sandpaper (#320)</i>
Polishing unit	
Magnets	Neodymium ring magnets (Grade N35) <i>OD Ø30 mm, ID Ø18 mm, $t_{magnet} = 12\text{ mm}$</i>
w_{gap}	1 mm
z	1 mm
Spindle revolutions	300 /min
Finishing media	
Carbonyl iron particles	BASF CM Grade <i>Supplied mass: 20 g</i> <i>Mean particle size: 7.0 μm – 9.5 μm</i>
Abrasives	Alumina (Universal Photonics) <i>Supplied mass: 2.0 g</i> <i>Mean particle size: 0.6 μm</i> Alumina (Kemet) <i>Supplied mass: 2.0 g</i> <i>Mean particle size: 3 μm, 15 μm</i>
Carrier fluid	Distilled water <i>Initial supplied mass: 8.0 g</i>
Polishing method	Areal raster <i>Scan area: 100 mm²</i> <i>Tool feed rate: 200 mm/min</i>

Preliminary trials have been conducted to polish stainless steel (SUS 316) workpieces using the new MFAF process to study the achievable surface texture in Ra.

Three different abrasive sizes were tested. The experimental conditions are shown in Table 3.2. Surface texture is measured with a laser profilometer (Taylor Hobson, Form Talysurf 2, vertical resolution 10 nm) with measurement conditions in accordance to the DIN EN ISO 4288:1988 standards.

Figure 3.16 shows the relationship between surface texture (Ra) and polishing time for the three different abrasive sizes. Note that the error bar caps correspond to the minimum and the maximum values recorded. With the 0.6 μm abrasives, the surface texture was reduced from an initial value of 0.431 μm Ra to 0.033 μm Ra after 10 minutes, and eventually reached a value of 0.016 μm Ra after 30 minutes. The surface texture reduction is not as sharp for the 3 μm and 9 μm abrasives, with surface texture of 0.127 μm Ra and 0.121 μm Ra achieved respectively after 30 minutes.

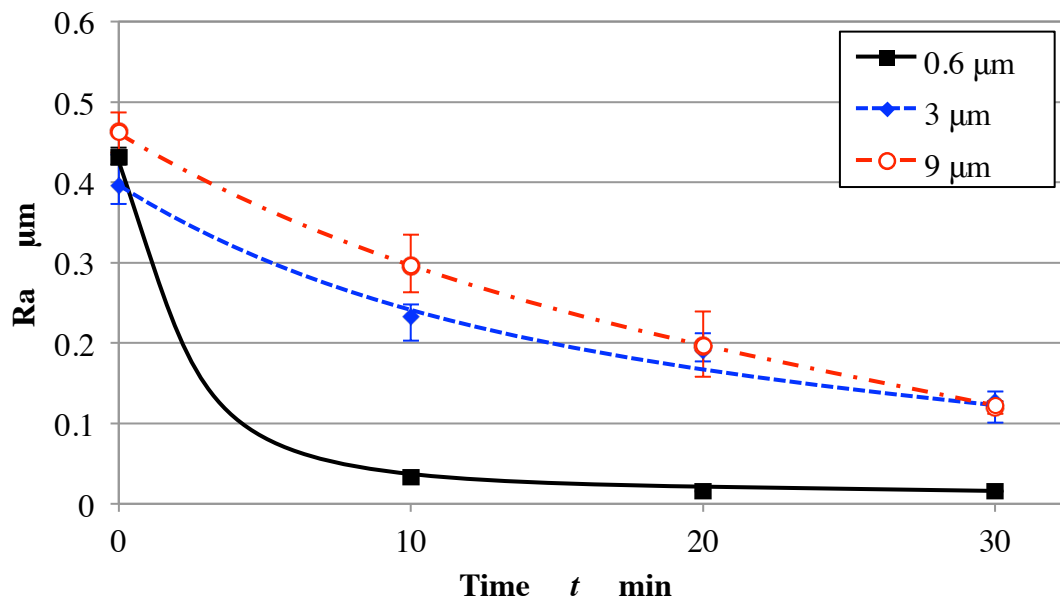


Figure 3.16: Surface texture (Ra) of SUS316 workpiece versus polishing time for three different abrasive sizes.

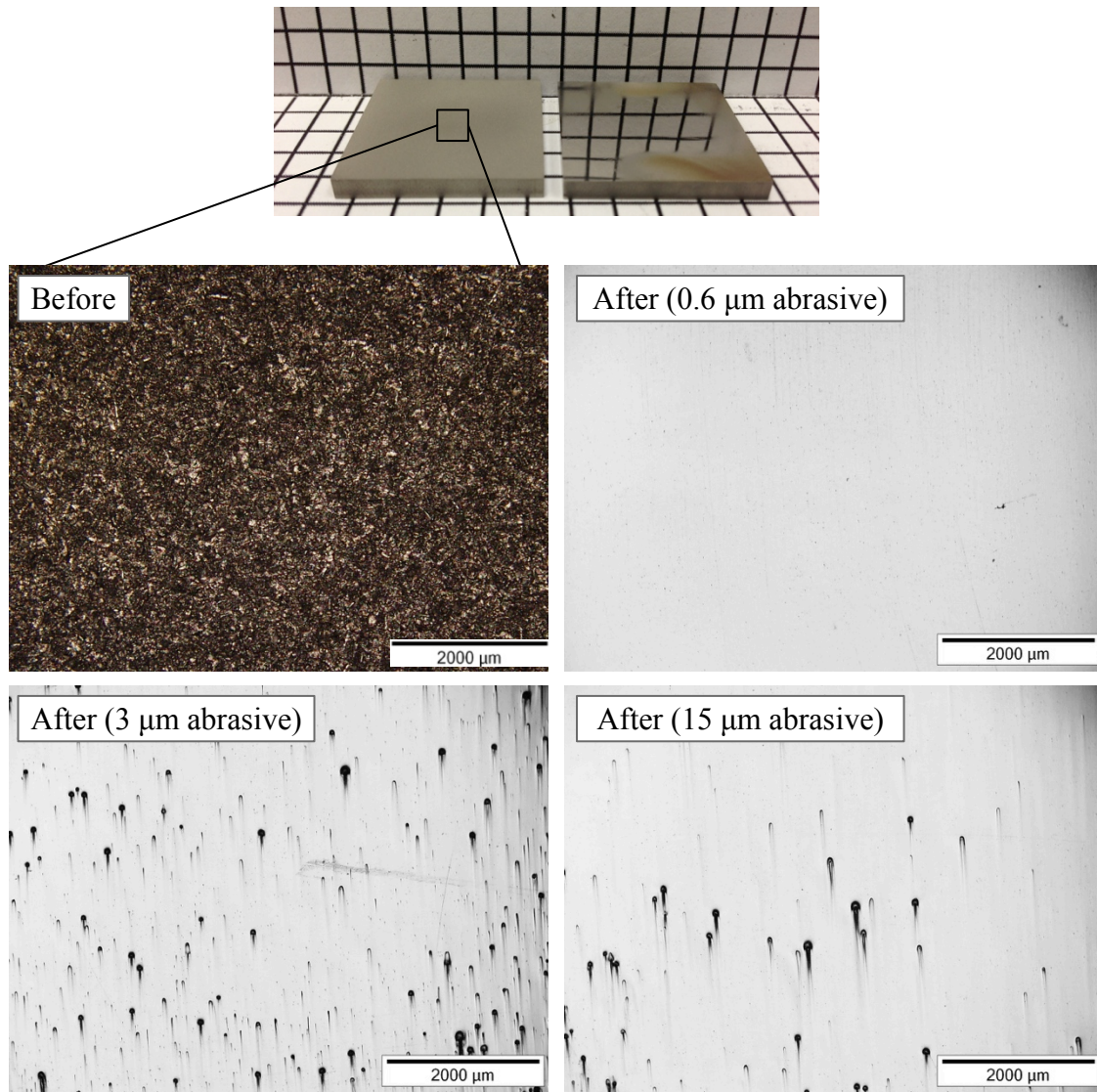


Figure 3.17: Micrographs of the SUS316 workpiece surface before and after polishing with three different abrasive sizes.

Figure 3.17 shows the micrographs of the workpiece surface before and after polishing with the three different abrasive sizes. The workpiece polished with 0.6 μm abrasives is mirror-finished and its micrograph shows minimal observable artifacts on the surface. The two workpieces polished with 3 μm and 9 μm abrasives are reflective, but the micrographs show defects on the surface that resemble comet tails. The mechanism

causing these defects is not known, although it may be due to overly aggressive material removal by larger abrasives.

Preliminary trials have also been conducted to polish titanium alloy (Ti-6Al-4V) workpieces with the new MFAF process. Titanium alloy is a difficult-to-machine material due to its low thermal conductivity and the high reactivity of a freshly machined surface. Removing material and achieving mirror finish is therefore not easily achieved with conventional processes [8].

The experimental conditions are similar to the earlier conditions for the polishing of stainless steel workpiece, except that alumina abrasives are substituted with diamond abrasives. The gap between magnets and workpiece, z , is also a variable with values of 0.5 mm, 1.0 mm and 1.5 mm. Figure 3.18 shows the graph of surface texture (R_a) against polishing time, reproduced from the original article [1]. After 20 minutes of polishing at the $z = 0.5$ mm condition, the surface texture of the titanium alloy workpiece is reduced from an initial value of $0.480 \mu\text{m } R_a$ to $0.073 \mu\text{m } R_a$. The final surface texture is higher than that achieved for SUS316 workpiece, due to the difficulty in polishing titanium alloy as discussed earlier. Also, the final surface texture increases when z is increased to 1.0 mm and 1.5 mm. While the reduction in surface texture validates the capability of the new MFAF process for surface finishing of titanium alloy workpiece, refinement to the process and formulation of finishing media is needed to improve the achievable surface texture.

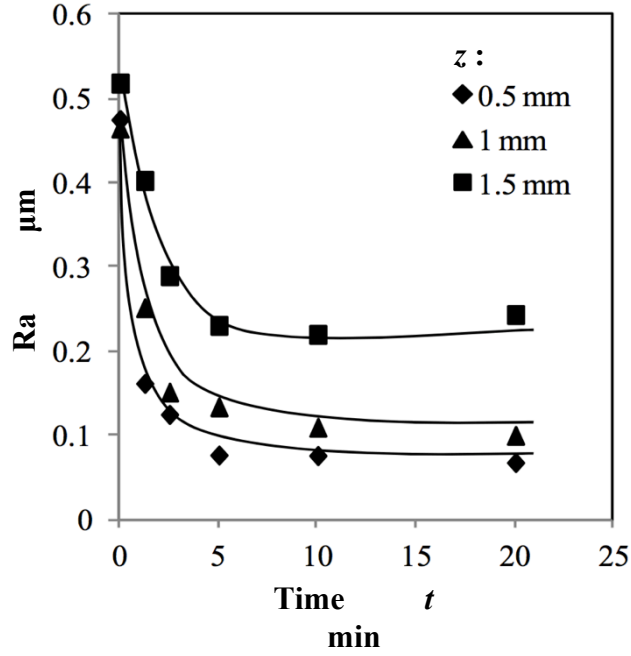


Figure 3.18: Surface texture (Ra) of Ti-6Al-4V workpiece versus polishing time for three different values of z .

3.5.2 Removal rate

A key requirement of the new MFAF process is high process efficiency as measured by the removal rate. Therefore, the peak removal rate of the new MFAF process is measured and compared with other MFAF processes. Polishing conditions are similar to the conditions in Table 3.2, except that the gap between magnets and workpiece, z , is changed to 0.5 mm to increase the removal rate. The peak removal rate is measured from 2D profile scans of the polished area obtained by a laser profilometer. Complete details on removal rate measurement are available in Appendix B. Figure 3.19 shows the removal rate of the new MFAF process in comparison with the reported removal rates of other MFAF processes in the literature.

Among the surveyed processes, the peak removal rate of the new MFAF process at 11.8 $\mu\text{m}/\text{min}$ is the highest and can be up to one order of magnitude higher than some other processes[9 – 13]. However, caution must be exercised in judging the capability of the cited processes based on the reported values, as the removal rate for a particular process is highly dependent on the target material and polishing conditions. In addition, comparison between different processes should be taken as a rough gauge only as the reported values are not optimized for removal rate. Notwithstanding that, the removal rates shown in Figure 3.19 validate the capability of the new MFAF process in achieving a high removal rate.

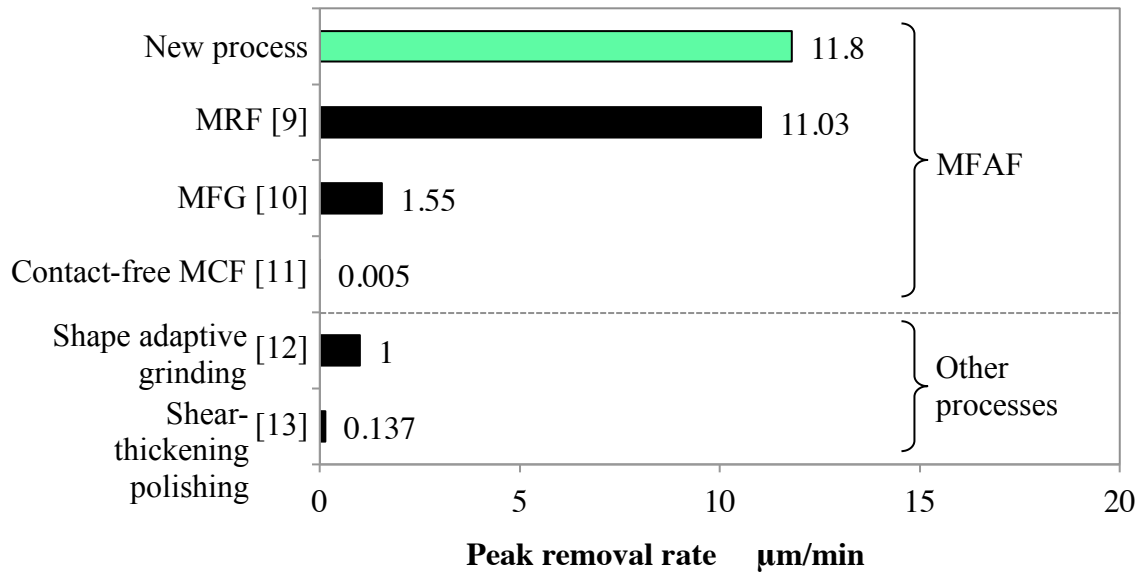


Figure 3.19: Peak removal rates of selected MFAF and non-MFAF processes.

3.5.3 Polishing of 2.5D structured surface

The conformable nature of the finishing media in MFAF processes is advantageous for the surface finishing of freeform surfaces compared to traditional polishing tools. To demonstrate the capability of the new MFAF process for freeform

surfaces, polishing trials have been conducted on 2.5D structured surfaces. Specifically, the 2.5D structures are V-grooves on a flat SUS316 workpiece. Figure 3.20 is a schematic diagram of the geometry of the V-grooves, which are created with the wire-EDM process. With traditional processes that use rigid polishing tools, the valleys of the V-grooves cannot be reached during the polishing process. Instead, the workpiece surface will be flattened, destroying the surface features in the process. No viable process is currently available for polishing of such structured surface.

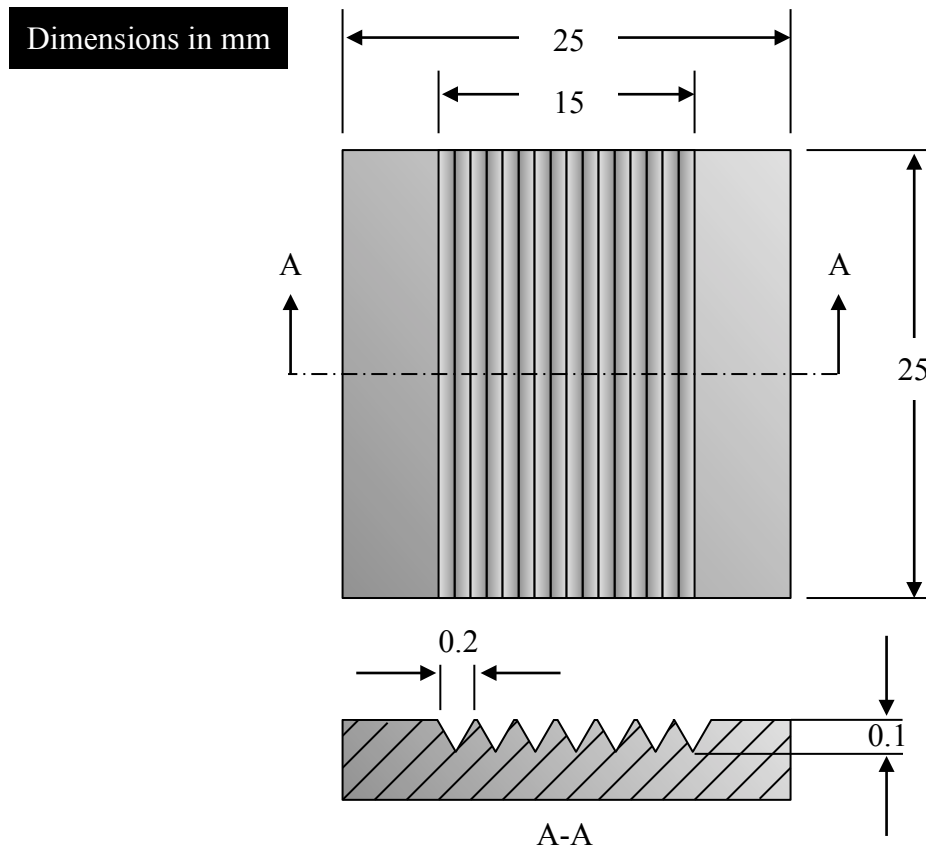


Figure 3.20: Schematic diagram of the V-grooves geometry on the workpiece.

The workpiece is polished with conditions similar to that in Table 3.2, using 0.6 μm alumina abrasives and with 30 minutes of polishing time. Figure 3.21 shows photographs of the V-grooves before and after polishing, with their corresponding micrographs.

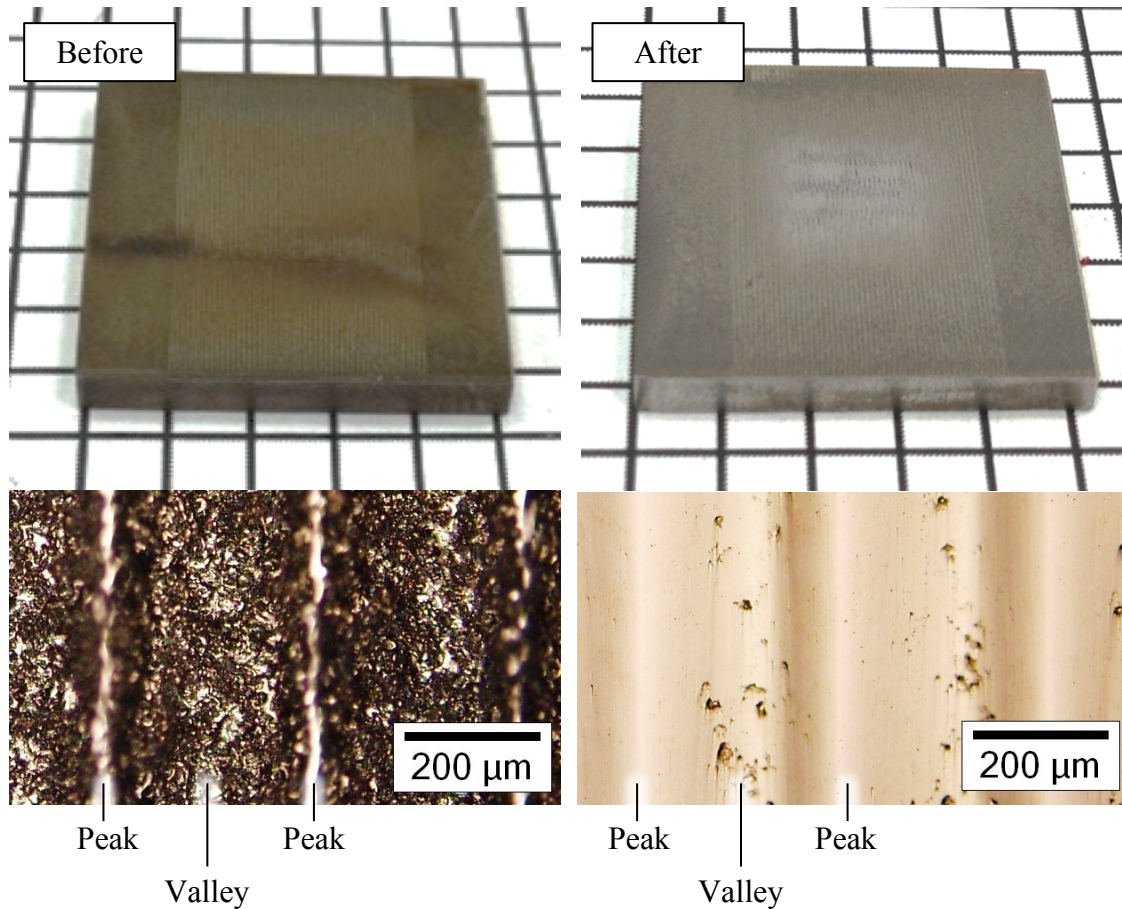


Figure 3.21: Optical images of the V-grooves before and after polishing with the new MFAF process.

From the photographs, it can be observed that the surface has become slightly reflective after polishing. The oxide layer covering the surface after the wire-EDM process has also been removed, which is apparent from the change in color of the sample.

The micrographs confirm that the V-grooves have been polished, without flattening the surface. The peaks are well polished, but some artifacts are still present in the valleys. However, the removal rate across the V-grooves is not uniform, as shown by the 2D profile scans in Figure 3.22.

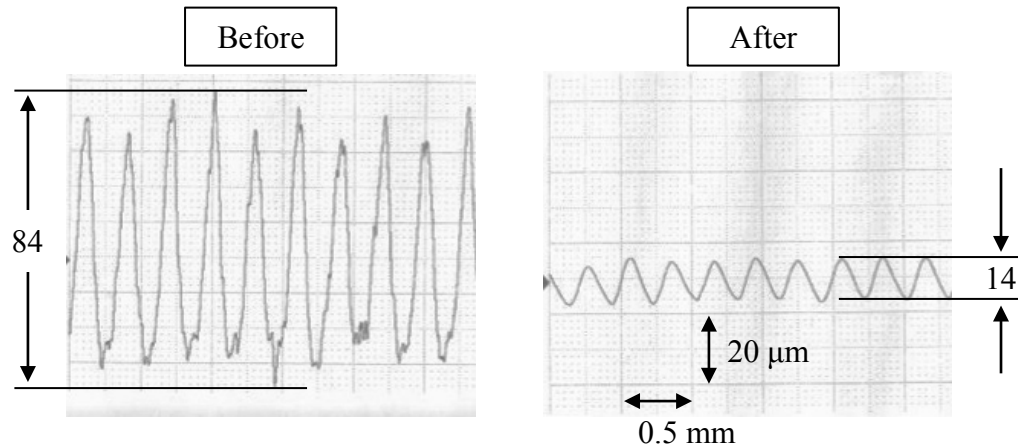


Figure 3.22: 2D profile scans of the V-grooves before and after polishing with the new MFAF process.

The non-uniform removal rate across the V-grooves is due to the directional effect of the motion of the finishing media, which is the nature of motion generated by spindle rotation, during the polishing process. As a result of the directional motion of the finishing media, the valleys are shielded by the peaks during polishing, resulting in higher removal rate from the peaks and lower removal rate from the valleys. Similar observations have been made during the polishing of cylindrical titanium alloy workpiece [1]. This occurs despite the conformable nature of the finishing media. However, as shown in the micrographs in Figure 3.21 previously, material removal still occurs at both the peaks and valleys of the V-grooves, albeit at different removal rates. Therefore, the

new MFAF process is advantageous for the polishing of 2.5D structured surface, which is not possible with traditional polishing tool.

Based on the results presented, the capability of the new MFAF process to remove material from selected freeform surfaces have been validated, although the removal rate is non-uniform and is dependent on the surface features and geometry.

3.6 CHAPTER SUMMARY

In this chapter, the principles of the newly developed MFAF process have been established. The two key principles of the new process are the high magnetic flux density in the polishing zone, and the ability of the finishing media to be reformed *in situ* during polishing. The novelty of the new MFAF process is ascertained by the award of an international patent [4].

Theoretical analyses have been conducted to understand the effect of the gap between magnets, w_{gap} , the gap between magnet and workpiece, z , and the thickness of magnet, t_{magnet} , on the magnetic flux density in the polishing zone. Firstly, small values of w_{gap} result in larger magnetic flux density and are ideal for increasing the peak removal rate. However, small values of w_{gap} mean a small polishing area, which may reduce the volumetric removal rate. Secondly, small values of z increase the magnetic flux density, but result in an uneven profile of the magnetic flux density. Lastly, increasing the thickness of the magnet, t_{magnet} , results in an increased magnetic flux density, although at a diminishing rate. From these analyses, the values of $w_{\text{gap}} = 1 \text{ mm}$, $z = 0.5 \text{ mm}$ to $z = 1.0 \text{ mm}$, and $t_{\text{magnet}} = 12 \text{ mm}$ were selected for experimental trials.

Inclusion of magnetic caps has been found to increase the magnetic flux density, although the augmentation is only approximately 5 %. Increasing the thickness of

magnetic caps, t_{cap} , increases the degree of augmentation, although only marginally and at a diminishing rate. In light of the marginal improvement and for convenience, no magnetic cap will be included for experimental trials in this thesis.

The finishing characteristics have been studied by conducting polishing trials with a prototype of the polishing tool. Firstly, surface texture reduction is demonstrated on both stainless steel (SUS 316) and titanium alloy (Ti-6Al-4V) flat workpieces. For the SUS316 workpiece, a surface texture of 0.016 Ra μm is achieved after 30 minutes of polishing. For the Ti-6Al-4V workpiece, a surface texture of 0.073 Ra μm is achieved after 20 minutes of polishing. While these validate the capability of the new MFAF process for surface texture reduction, the achievable surface texture needs further improvement.

Secondly, the removal rate of the new MFAF process is compared against selected MFAF and non-MFAF processes based on values reported in the literature. The removal rate of 11.8 $\mu\text{m}/\text{min}$ for the new MFAF process is among the highest, and is one magnitude higher compared to some other processes. The capability of the new MFAF process in achieving a relatively high removal rate is therefore validated.

Lastly, polishing trials have been conducted for 2.5D structures on a flat SUS316 workpiece. The 2.5D structures are V-grooves with 0.2 mm width and 0.1 mm depth. After 30 minutes of polishing, the V-grooves have been successfully polished, although the peaks and valleys have different removal rates. The shielding effect has been proposed to explain the different removal rates of peaks and valleys. Despite that, the capability of the new MFAF process for polishing of 2.5D structures, which has no viable solution currently, has been validated.

REFERENCES

- [1] Sato T, Kum CW and Venkatesh V, *Rapid magnetorheological finishing of Ti–6Al–4V for aerospace components*. International Journal of Nanomanufacturing, 2013. **9**(5): p. 431-445.
- [2] Kum CW, Sato T and Butler DL, *Development of magnetic field-assisted finishing (MFAF) for exotic materials using abrasive slurry circulation system – Effects of media properties on the finishing characteristics*. In *Proceedings of the 14th euspen International Conference, Dubrovnik*. 2014. **2**: p. 295-298.
- [3] Kum CW, Sato T and Butler DL, *Magnetostatic simulation of the double-tool configuration in Rapid-MRF of miniature components*. In *Proceedings of ICOMM, Singapore*. 2014, CD-format.
- [4] Sato T and Kum CW, *Surface polishing apparatus*. International Patent No. WO 2013/172785 A1. 21 November 2013.
- [5] Neo WK, Kumar AS and Rahman M, *Novel micro-grooving technique for machining of novel chevron sharkskin riblets on flat surface*. In *Proceedings of the 14th euspen International Conference, Dubrovnik*. 2014. **1**: p. 120-123.
- [6] Shinmura T, Takazawa K, Hatano E, Matsunaga M and Matsuo T, *Study on magnetic abrasive finishing*. CIRP Annals-Manufacturing Technology, 1990. **39**(1): p. 325-328.
- [7] Ruggiero, AG, *Sharp edge effects of the magnets of a FFAG accelerator*. Brookhaven National Laboratory, 2004.
- [8] Lütjering G and Williams JC. *Titanium*. Vol. 2: p.85-86. Berlin: Springer, 2003.
- [9] DeGroote, JE, *Surface interactions between nanodiamonds and glass in magnetorheological finishing (MRF)*. Doctoral thesis dissertation, 2007.
- [10] Umehara N, Kirtane T, Gerlick R, Jain VK and Komanduri R, *A new apparatus for finishing large size/large batch silicon nitride (Si_3N_4) balls for hybrid bearing applications by magnetic float polishing (MFP)*. International Journal of Machine Tools and Manufacture, 2006. **46**(2): p. 151-169.
- [11] Furuya T, Wu YB, Nomura M, Shimada K and Yamamoto K, *Fundamental performance of magnetic compound fluid polishing liquid in contact-free polishing of metal surface*. Journal of Materials Processing Technology, 2008. **201**(1): p. 536-541.

- [12] Beaucamp A, Namba Y, Combrinck H, Charlton P and Freeman R, *Shape adaptive grinding of CVD silicon carbide*. CIRP Annals - Manufacturing Technology, 2014. **63**(1): p.317-320.
- [13] Li M, Lyu B, Yuan J, Dong C and Dai W, *Shear-thickening polishing method*. International Journal of Machine Tools and Manufacture, 2015. **94**: p.88-95.

Chapter 4

Material removal rate model

4.1 INTRODUCTION

For abrasive processes, prediction of the material removal rate based on a given set of process parameters is an area of keen interest to both the research community and manufacturing industry. There are two key reasons for this. Firstly, when initiating a new polishing operation, it reduces the time spent on establishing the process conditions to achieve the required outcome. Secondly, the knowledge of material removal rate is important for process automation, specifically for the generation of tool path for CNC machining.

To that end, numerous removal rate models for different abrasive processes have been proposed and reported in the literature. As the material removal mechanism of abrasive processes has not been completely understood or universally agreed upon [1], currently there is no removal rate model that is generally applicable across all abrasive processes. Instead, models are derived with different approaches, and may be based on varying assumptions. Despite that, many of the existing models provide valuable insights and help to develop the understanding of the particular process.

In this chapter, a theoretical model for the new MFAF process is proposed to establish the relationship between the material removal rate and selected process parameters. The process parameters of interest are related to the properties of the finishing media, which include the size and concentration of abrasives, size of carbonyl iron particles, and the magnetic flux density at the polishing zone. Firstly, the assumptions and constraints of the proposed model are defined. Then, the components of

the model are fully derived across several sections of this chapter. Finally, these components are assembled together to form the complete model, which is presented at the end of this chapter.

4.2 REVIEW OF EXISTING MODELS

In this section, important material removal models that are deemed the most relevant to the new MFAF process are reviewed.

One of the earliest material removal rate models was proposed by Preston [2] to model the material removal for lapping of glass plates with a felt lap. Preston proposed that the material removal rate is independently proportional to the normal pressure P , the relative velocity v between the glass plate and the felt lap, and the polishing time t . It can be expressed as

$$\text{MRR} = k \cdot P \cdot v \quad (4.1)$$

where, k is a constant of proportionality that encapsulates other process parameters. This equation was then expanded by Buijs and Korpel-van Houten [3] to include variables related to the mechanical properties of the workpiece surface and some properties of the abrasives.

The MRF research team at the University of Rochester and QED Technologies has also presented several material removal rate models over the past two decades. Shorey proposed a model [4] to correlate the material removal rate of the MRF process to the drag force. The model was adapted and elaborated by DeGroote [5] to for the peak material removal rate of the MRF process for polishing of glass. In the proposed model,

the peak material removal rate is proportional to five different terms as shown in Equation 4.2:

$$\begin{aligned} \text{MRR}_{\text{peak}} \propto & \underbrace{\left[\frac{E_s}{K_c H_s^2} \right]}_{\text{Term 1}} \times \underbrace{\left[\frac{F_d}{A} v \right]}_{\text{Term 2}} \times \underbrace{\left[B_{\text{nd}} \phi_{\text{nd}}^{-1/3} C_{\text{nd}}^{1/3} + B_{\text{ci}} \phi_{\text{ci}}^{4/3} C_{\text{ci}} \right]}_{\text{Term 3}} \\ & \times \underbrace{\left[D_s (\text{pH}_{\text{MRF}})^{3/10} \right]}_{\text{Term 4}} \times \underbrace{\left[e^{-\text{sbs}/bRT} \right]}_{\text{Term 5}} \end{aligned} \quad (4.2)$$

Nomenclature is provided in the original article and not reproduced here. In summary, Term 1 embodies the ‘near surface’ mechanical properties, Term 2 is an equation modified from Preston’s, Term 3 considers the particle sizes and concentrations, Term 4 accounts for the glass chemical durability, and Term 5 relates to the average single bond strength of the glass. The model was verified against experimental data from 650 trials on six different types of glasses using six types of finishing media with nanodiamond concentrations between 0 to 0.01 vol. %. The proposed model fitted the experimental data points with a linear product moment correlation coefficient of 0.78.

Some material removal models for chemical-mechanical polishing (CMP) are also relevant to the new MFAF process. Contact mechanics, which considers the indentation of abrasives into the workpiece surface, is a typical approach for CMP process models. Examples include models by Luo and Dornfeld [6], Brown et al. [7], and Jeng and Huang [8]. All three models consider the material removal rate to be the product of the number of active abrasives and the removal rate per particle. In addition, the aforementioned

CMP models also consider the effects of abrasive sizes and concentration on the removal rate. These are variables of interest in the removal rate model for the new MFAF process.

A research team at the Indian Institute of Technology has also reported extensive work on the theory and modeling of MFAF processes [9, 10]. The proposed models are intended for several MFAF processes developed by the team. They are either based on contact mechanics, which takes a similar approach to the CMP models, or obtained by multi-linear regression using experimental data. Both the effect of magnetic field and the polishing forces have also been extensively studied.

4.3 MOTIVATION

For the new MFAF process, a model to predict the material removal rate is advantageous for the same two reasons mentioned at the beginning of this chapter. In addition, a quantifiable relationship between the process parameters and the material removal rate is of academic importance, as it enhances the theoretical understanding of the new MFAF process.

In this thesis, a new model is developed for the new MFAF process because the models reviewed in the previous section are not applicable, for several reasons. Firstly, the models proposed are intended for specific processes or applications. For example, the model proposed by Luo and Dornfeld is intended for the CMP process and is therefore not directly applicable for the new MFAF process, which is based on novel principles not found in CMP. The model by DeGroote is intended for the MRF process, which although is more similar to the new MFAF process, it is still based on slightly different principles. In addition, the model is intended only for polishing of glasses. The new model proposed

in this thesis is tailored for the new MFAF process, with some concepts that are applicable generally to most MFAF processes.

Secondly, the physics of the reviewed models do not sufficiently address the complexity of the finishing media in MFAF processes, which consists of magnetic particles and non-magnetic abrasives. Instead, the finishing media is often treated as a traditional polishing lap with bulk behavior. To understand the effect of the finishing media properties on the material removal rate, the interaction of particles in the finishing media should not be neglected. The model proposed in this thesis considers the physical interactions of the particles in the finishing media. This new approach allows for deeper insight about the process to be drawn, especially regarding properties of the finishing media, and establishes a framework for future theoretical studies.

4.4 MATERIAL REMOVAL RATE MODEL

In this section, the material removal rate expression is derived. The material removal rate considered in the model is the volumetric material removal rate, measured in volume per unit time, as opposed to the peak material removal rate, which is measured in depth per unit time. Additionally, the material removal in this process is considered to be due to plastic deformation of the workpiece material by abrasive particles, which has been established and verified by several studies for the CMP process [6, 11].

4.4.1 Assumptions

In the multistep derivation of the material removal rate model in this chapter, several assumptions are required. The key assumptions are summarized here, and they will be individually referred to again respectively when invoked.

The first assumption is the spherical shape of both CI and abrasive particles. As seen in the scanning electron micrograph in Figure 4.1, actual particles show some deviations from the spherical shape, but the assumption is reasonable as the shapes are close to spherical.

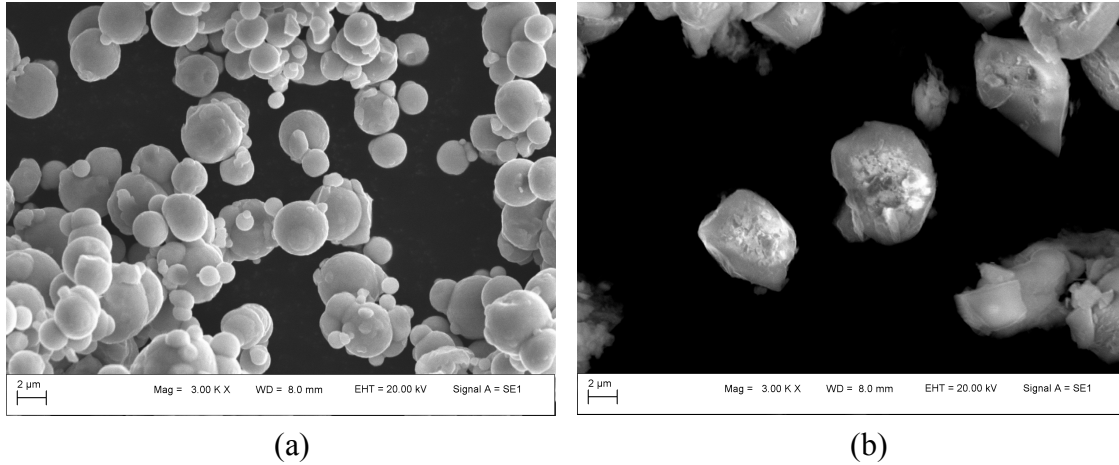


Figure 4.1: Scanning electron micrograph of (a) CI particles and (b) alumina abrasive particles.

The second assumption is the uniform size distribution of both CI and abrasive particles. Actual particle sizes are distributed. However, this is necessary for the analytical approach of the particle packing proposed in this model. A model considering the size distribution is much more challenging and can be one of the future works.

The third assumption is the face-centred cubic (FCC) configuration of the CI particles when they are densely packed when under the influence of a magnetic field. This assumption is deemed reasonable as the attractive magnetic forces tend to cause the particles to pack closely, and FCC has the highest atomic packing factor of 0.74. Verification with scanning electron microscope was not possible because a magnet cannot be admitted into the chamber.

The fourth assumption is that the workpiece surface is planar, such that particles that have penetrated the surface can move parallel to the workpiece surface without obstruction. In reality, there are asperities on the workpiece surface due to surface texture, which causes the particle not to travel parallel to the workpiece surface. As a result, the material removal per particle given by this model may differ from the actual material removal per particle, and the difference is more significant when surface texture is greater.

4.4.2 General expression

The material removal rate is taken as the sum of material removal rate of each active particle in the finishing media. In addition, the particles are assumed to be spherical in shape and of a uniform distribution. Therefore, the material removal rate becomes the product of the number of active particles and the material removal rate per active particle, as given in Equation 4.3:

$$\text{MRR} = N \cdot \Delta\text{MRR} \quad (4.3)$$

where N is the number of active particles and ΔMRR is the material removal rate per active particle.

To calculate ΔMRR , the product of the projected area of indentation, A , and the relative linear velocity between the particle and the polished surface, v , is considered. The projected area of indentation, A , is related geometrically to the depth of particle penetration, h . An illustration of these variables is shown in Figure 4.2. Indentation of the particle is exaggerated. Note that the asperities attributed to surface texture are not

considered. Instead, the workpiece is considered as an ideal planar surface. The model is therefore expected to be more representative for a low surface texture surface than a high surface texture surface.

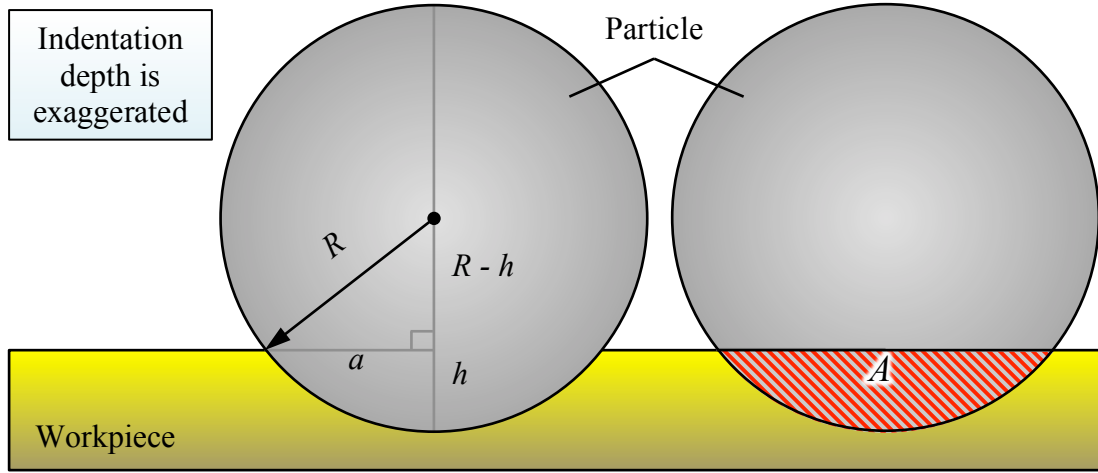


Figure 4.2: Schematic diagram of the projected area of indentation, A , and depth of indentation, h .

Using the geometrical approximation $A = h\sqrt{hD}$ where D is the particle diameter, the expression for material removal rate per particle, ΔMRR is given by:

$$\Delta\text{MRR} = h\sqrt{hD} \cdot v \quad (4.4)$$

Equation 4.4 is substituted into Equation 4.3 to obtain an expression relating the total material removal rate to the number of active particles, N , and the geometrical terms h and D , as given in Equation 4.5:

$$\text{MRR} = N \cdot h\sqrt{hD} \cdot v \quad (4.5)$$

Next, Hertz's equation for shallow spherical indentation of a half space [7] is used to obtain an expression for h . The Hertz's equation is given below:

$$a^3(t) = \frac{3DF}{8} \left(\frac{1}{E} + \frac{t}{\mu} \right) \quad (4.6)$$

where a is the radius of projected circle of contact (see Figure 4.2), D is the sphere diameter, F is the force per particle, E is the Young's modulus, t is the time and μ is the viscosity. By neglecting the time-dependent component of the equation and applying the geometrical approximation $a^2 = hD$, the expression for the depth of indentation, h , is obtained and given by:

$$h = \left(\frac{3F}{8E} \right)^{2/3} \cdot \frac{1}{D^{1/3}} \quad (4.7)$$

Substituting Equation 4.7 into Equation 4.5, the final expression for the total material removal rate is obtained and given by:

$$\text{MRR} = N \cdot \left(\frac{3F}{8E} \right) \cdot v \quad (4.8)$$

The material removal rate is thus a function of the number of active particles, N , the force per particle, F , the Young's modulus, E , and the relative linear velocity between particles and the polished surface, v .

4.4.3 Total MRR as sum of two MRR components

For the new MFAF process, the material removal rate can be attributed to both the carbonyl iron particles and the abrasives in the finishing media. Generally, material removal by abrasives is significantly higher, sometimes by up to several orders of magnitude. The efficacy of abrasives in material removal has conventionally been attributed to its hardness, although one theory suggests that the Young's modulus may also be a factor [7].

In the new MFAF process, the material removal rate is attributed to two sources – carbonyl iron particles and abrasives. Therefore, it is proposed that the total material removal rate be written as the sum of two components, one for the carbonyl iron particles and another for the abrasives. It is expected that the magnitude of the component representing the abrasives is significantly greater than the component representing the carbonyl iron particles.

However, the material removal rate expression in Equation 4.8 does not distinguish the different efficacies of the two particles in material removal. Therefore, it is proposed that a dimensionless constant is assigned to each component to account for the particle efficacy. As a result, the expression for the total material removal rate is given by Equation 4.9:

$$\text{MRR} = \underbrace{k_{\text{CI}} \cdot N_{\text{CI}} \cdot \left(\frac{3F_{\text{CI}}}{8E} \right) \cdot v}_{\text{MRR component for carbonyl iron particles}} + \underbrace{k_{\text{abr}} \cdot N_{\text{abr}} \cdot \left(\frac{3F_{\text{abr}}}{8E} \right) \cdot v}_{\text{MRR component for abrasives}} \quad (4.9)$$

where k_{CI} and k_{abr} are dimensionless constants that encapsulate the material properties of the carbonyl iron particles and abrasives respectively; N_{CI} and N_{abr} are the numbers of

active carbonyl iron particles and active abrasives respectively; F_{CI} and F_{abr} the forces per particle acting on carbonyl iron particles and abrasives respectively. As previously mentioned, it is anticipated that k_{abr} is up to several orders of magnitude greater than k_{CI} .

Equation 4.9 is generalized and applicable to all MFAF processes where the finishing media consists of two different particles. However, the expressions for number of active particles, force per particle and the dimensionless constants are process-specific. In the following sections, expressions for N_{CI} , N_{abr} , F_{CI} , and F_{abr} specific to the new MFAF process are derived.

4.5 NUMBER OF ACTIVE PARTICLES

In abrasive processes, not all particles are involved in material removal at the same time. Typically, particles that directly remove materials from the workpiece are considered active. Particles that do not are considered inactive. For the proposed model, a particle is defined as active if the particle is in contact with the target surface of the workpiece where material removal is intended. In addition, the finishing media in the new MFAF process consists of two types of particles that are both involved in material removal. Therefore, it is necessary to consider both the number of active carbonyl iron particle, N_{CI} , and the number of active abrasives, N_{abr} .

Expressions of both N_{CI} and N_{abr} form part of Equation 4.9 and are therefore required for the complete material removal model. In this thesis, new expressions are developed because existing approaches reported in the literature do not consider the interactions of the two types of particles in the finishing media. The existing approaches and why they are inappropriate for the new MFAF process are outlined in the next section. Following that, complete derivation for N_{CI} and N_{abr} are presented.

4.5.1 Existing approaches

The approach taken in modeling number of active particles is specific to a particular process. For the CMP process, the method used by Jeng and Huang [8] is representative of the typical approach to model the number of active abrasives. In essence, this approach comprises of two steps. In the first step, the number of abrasives in the fluid body between the polishing pad and the workpiece is calculated based on the dimensions of the fluid body and the abrasive concentration. In the second step when the polishing pad is brought into contact with the workpiece, certain criteria are applied to calculate the fraction of the number of abrasives in the first step that will directly contact the workpiece. The different CMP models that have been reported typically differ in terms of the applied criteria. Examples of the criteria include the asperity properties and the abrasive size distribution.

Finally, the fraction of particles in direct contact with the workpiece allows calculation of the number of active abrasives. Figure 4.3 illustrates the aforesaid steps.

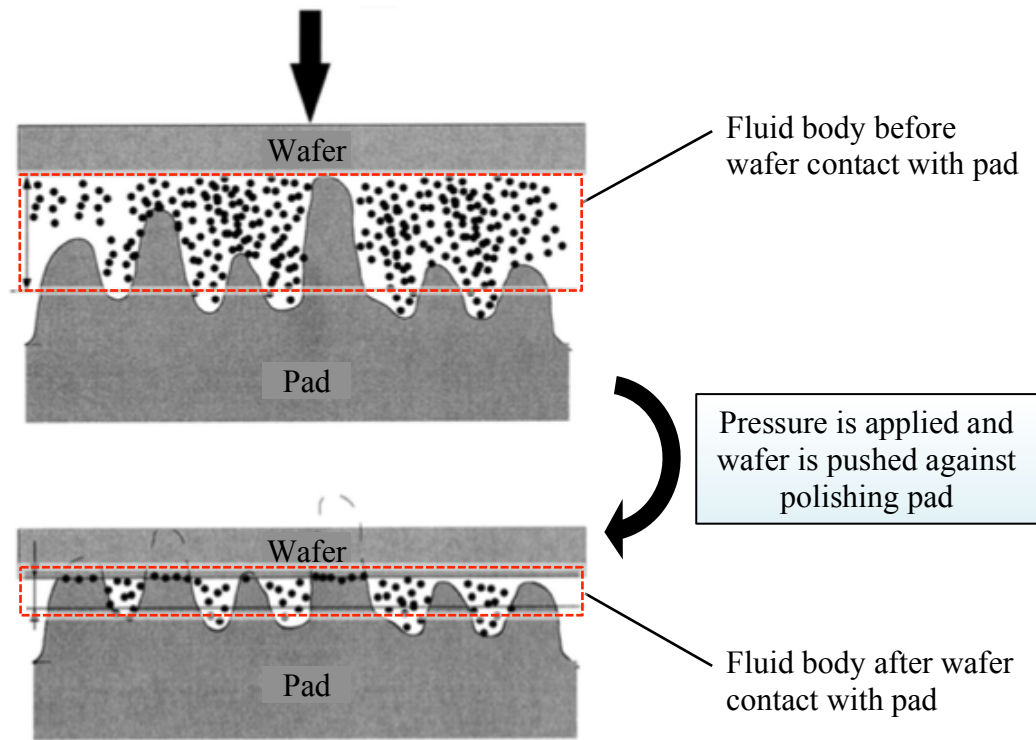


Figure 4.3: Schematic diagram of the typical approach in modeling the number of active abrasives [8].

The approach taken is reasonable for the CMP process, but does not sufficiently reflect the physics of the finishing media in the new MFAF process. One method to adopt the CMP model for the new MFAF process is to treat the carbonyl iron particles in the finishing media as a bulk material equivalent to the polishing pad in CMP. However, this does not mirror the actual MFAF process, as abrasives in the finishing media can in fact permeate into the carbonyl iron matrix. In CMP, abrasives do not permeate into the polishing pad, which is a solid material. As a result, the number of active abrasives given by the CMP model will be a gross overestimation for the new MFAF process. In addition, the CMP model is not compatible for the calculation of number of active carbonyl iron particles.

A different approach is considered by Sidpara and Jain [10] to calculate the number of active abrasives for their MFAF process, which is similar to the new MFAF process developed in this thesis. Figure 4.4 from the original article illustrates the configuration of the active and inactive particles according to their model.

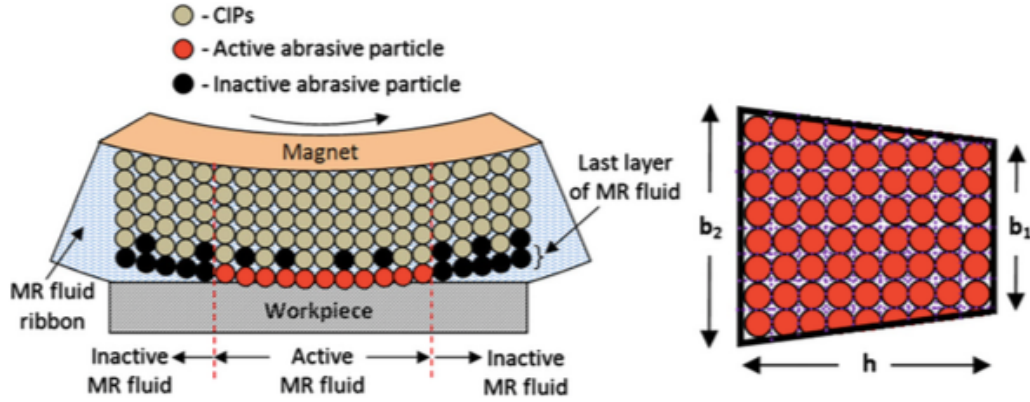


Figure 4.4: Configuration of active and inactive particles in the model proposed by Sidpara and Jain [10].

There are three reasons why the model proposed by Sidpara and Jain is not compatible for new MFAF process. Firstly, the model proposed by Sidpara and Jain requires the carbonyl iron particles and the abrasives to be of the same size. This restricts the model to very narrow applications because it is atypical for finishing media to consist of carbonyl iron particles and abrasives of equal sizes. More commonly, the abrasives are smaller than the carbonyl iron particles, allowing them to permeate into the interstitial spaces of the carbonyl iron matrix.

Secondly, their model assumes that the abrasives are pushed onto the outer layer of the finishing media during the process. This phenomenon has been claimed to be attributed to the magnetic forces exerted on the carbonyl iron particles, which pulls them towards the magnetic pole and simultaneously pushes the non-magnetic abrasives

outward. This explanation is satisfactory for some processes such as MRF, where validation of this principle has been done [4]. However, the same is not true for the new MFAF process. In the new MFAF process, *in situ* reformation of the finishing media causes the particles to be continuously mixed during the process. Therefore, the abrasives are distributed in the carbonyl iron matrix, instead of being concentrated on the outer layer of the finishing media.

Lastly, the model assumes that the particles are arranged in a simple cubic configuration. With strong magnetic forces acting on the carbonyl iron particles, the particles tend to be as close-packed as possible. Therefore, the assumption of face-centred cubic (FCC) or hexagonal close-pack (HCP) for the carbonyl iron particles is more reasonable.

4.5.2 Proposed approach

In the previous section, existing approaches have been argued to be insufficient in reflecting the physics of the particles in the finishing media for the new MFAF process. A new approach that considers the particle interactions is therefore needed to model the numbers of active carbonyl iron particles and active abrasives.

First, it is assumed that the carbonyl iron particles are arranged in an ideal FCC configuration to form the carbonyl iron matrix. Also, all the carbonyl iron particles are spherical and have the same size. The assumption of an FCC configuration is reasonable because the carbonyl iron particles are subjected to strong magnetic forces and will therefore assume configurations with the highest packing ratio. For spheres of equal size, FCC and HCP both have the highest packing ratio of 0.74.

Secondly, the abrasives are assumed to reside in the interstitial spaces in the carbonyl iron matrix. In addition, it is taken that the abrasives are dispersed uniformly within the interstitial spaces. Also, the presence of abrasives in the interstitial spaces is assumed not to affect the FCC configuration of the carbonyl iron particles since they are held strongly by magnetic forces. Figure 4.5 illustrates a unit cube of the particle configuration in the finishing media.

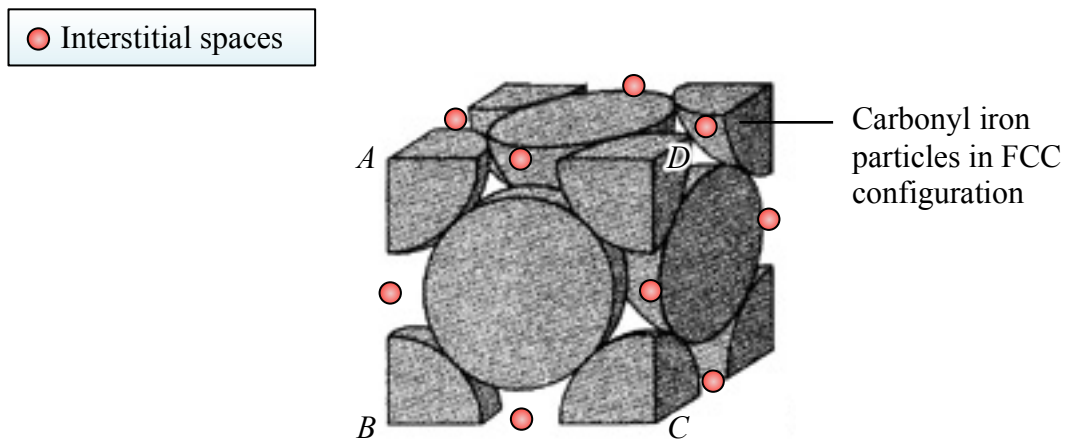


Figure 4.5: Model of particle configuration in the finishing media. Carbonyl iron particles are arranged in FCC configuration and abrasives are dispersed uniformly in the interstitial spaces.

The presented model of the particle configuration in the finishing imposes certain constraints on the particle properties in the finishing media. The following two sections address these constraints.

4.5.3 Maximum allowable abrasive size

The first constraint imposed by the assumptions described in the previous part pertains to the size of abrasives. The proposed model requires the FCC configuration of

the carbonyl iron particles to be intact. An abrasive particle that is too large will be unable to fit into the interstitial space. To accommodate the large abrasive particle, some carbonyl iron particles need to be displaced to create additional room for this large particle. The FCC configuration of the carbonyl iron particles is thus compromised. Therefore, there is a critical diameter that the abrasives must not exceed. Figure 4.6 illustrates the calculation of this critical diameter.

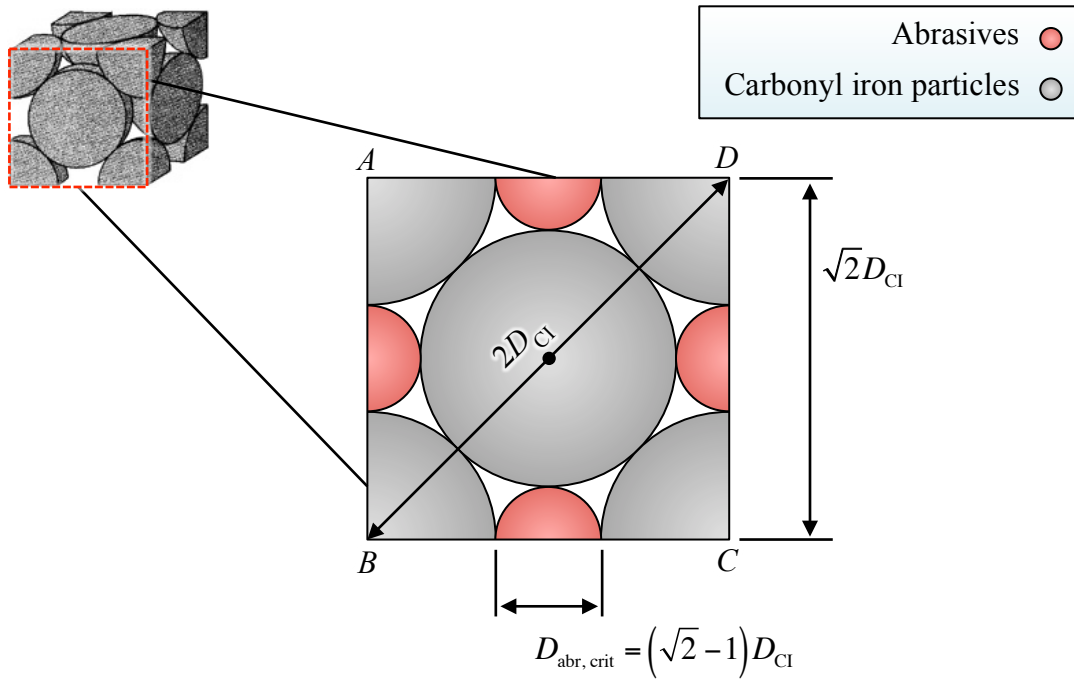


Figure 4.6: Calculation of maximum allowable diameter for abrasives in the model.

To calculate the critical diameter, $D_{abr, crit}$, one face of the FCC unit cube is considered. The critical diameter for abrasives is given by:

$$D_{abr, crit} = (\sqrt{2} - 1)D_{CI} \quad (4.10)$$

where D_{CI} is the diameter of a carbonyl iron particle. Therefore, the abrasive size criterion for the proposed model is given by:

$$D_{\text{abr}} \leq (\sqrt{2} - 1) D_{\text{CI}} \quad (4.11)$$

4.5.4 Maximum allowable volumetric ratio of abrasives to carbonyl iron particles

Another constraint imposed by the assumptions of the proposed approach pertains to the volume of abrasives in the finishing media. The interstitial spaces in the carbonyl iron matrix are finite and cannot accommodate an infinite amount of abrasives. At a critical volume of abrasives, the interstitial spaces will be fully occupied. Increasing the volume of abrasives beyond this critical volume will require the FCC configuration of the carbonyl iron particles to be compromised to create additional room for the abrasives.

Calculation of the critical volume is non-trivial due to the complex geometry of the interstitial spaces. In addition, the packing of abrasives in the interstitial spaces is dependent on the abrasive size. Therefore, the critical volume is not a constant, but rather a function of the abrasive size. In this thesis, the actual expression of the critical volume is not derived. Instead, a method to calculate the upper bound of the critical abrasive volume is proposed.

The critical abrasive volume is calculated in terms of volumetric ratio of abrasive in the FCC unit cube. First, it is noted that the volumetric ratio of the carbonyl iron particles in the FCC unit cube, v_{CI} , is 0.740. Therefore, the volumetric ratio of interstitial spaces in the FCC unit cube, $v_{\text{interstitial}}$, is 0.260. To calculate the volumetric ratio of the abrasives in the FCC unit cube, v_{abr} , the discontinuous interstitial spaces are considered as a single combined body, and that the abrasives are closed packed in this combined body.

By considering a combined body, the packing factor of 0.740 can thus be multiplied to $v_{\text{interstitial}}$ to obtain a value of 0.192 for v_{abr} . This is the upper bound of v_{abr} because the abrasives in fact cannot occupy some of the interstitial spaces in the actual FCC configuration due to geometrical constraints.

With abrasives in the FCC unit cube, $v_{\text{interstitial}}$ is reduced to 0.068, which is in fact its lower bound. Table 4.1 shows the volumetric ratios of the three entities in the FCC unit cube at the critical point.

Table 4.1: Volumetric ratio of carbonyl iron particles, abrasives and interstitial spaces in FCC unit cube at critical point, where interstitial spaces are fully occupied by abrasives.

v_{CI}	0.740
v_{abr} (upper bound)	0.192
$v_{\text{interstitial}}$ (lower bound)	0.068

For the purpose for finishing media preparation, it is convenient to calculate the ratio of v_{abr} to v_{CI} . The abrasive volume criterion for the proposed model is then given by:

$$\frac{v_{\text{abr}}}{v_{\text{CI}}} \leq 0.259 \quad (4.12)$$

As an example, consider a finishing media composed of carbonyl iron particles with density of 7.87 g/cm³, and Al₂O₃ abrasives with density of 4.1 g/cm³. Based on the criterion in Equation 4.12, it can be calculated that 100 g of carbonyl iron particles can

accommodate at most 13.5 g of Al_2O_3 abrasives. If the abrasives exceed this weight, the proposed model is not valid.

4.5.5 Number of active carbonyl iron particles

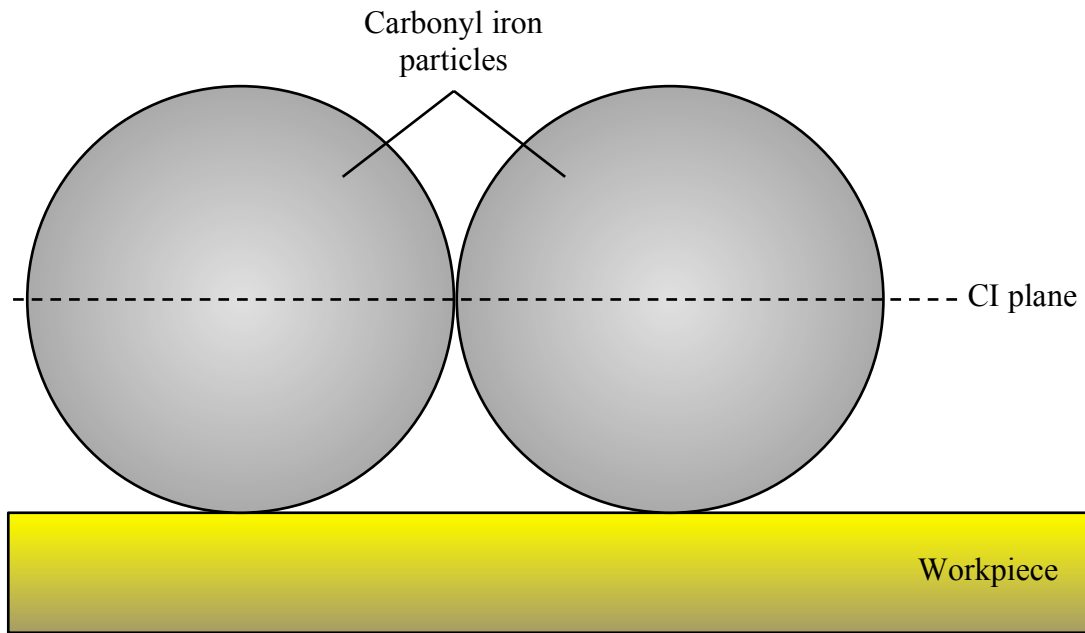


Figure 4.7: Interface of carbonyl iron particles and the workpiece surface. Abrasives are not shown.

To calculate the number of active carbonyl iron particles, N_{CI} , it is further assumed that the densest (111)-plane of the carbonyl iron matrix is parallel to the workpiece surface, as shown in Figure 4.7. A CI plane parallel to the workpiece surface, with an offset equal to the radius of the carbonyl iron particle, is considered. On the CI plane, a unit triangle as shown in Figure 4.8 is considered.

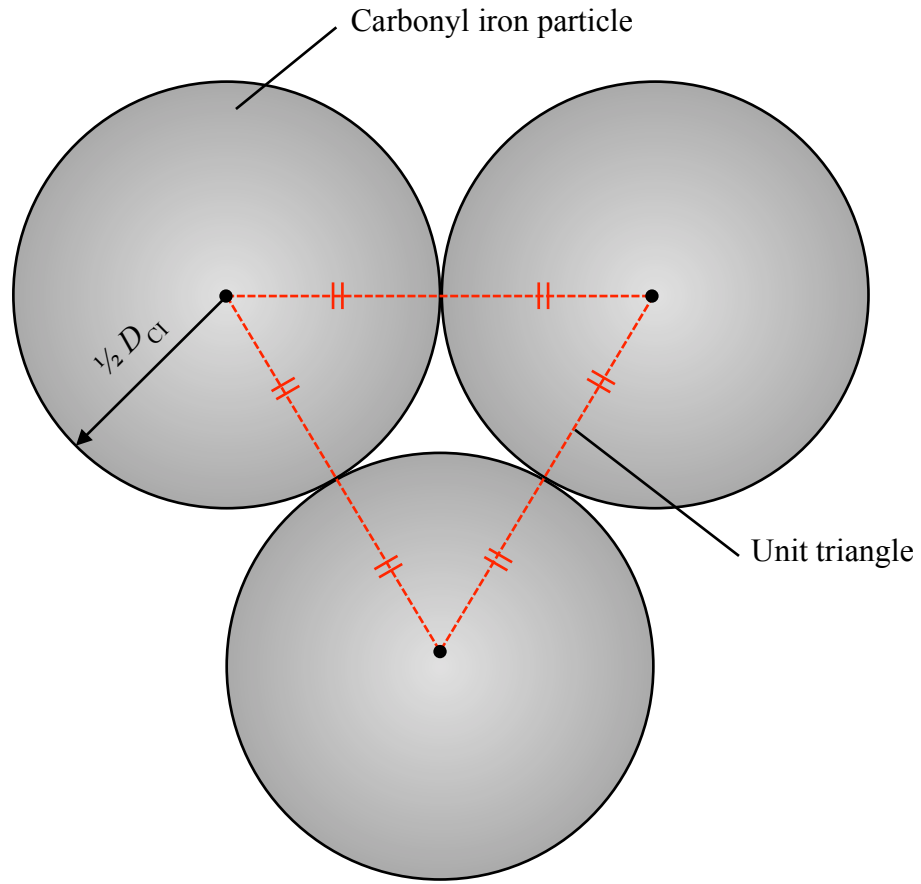


Figure 4.8: Unit triangle on the CI plane.

Area of unit triangle is given by:

$$A_{\text{unit}} = \frac{\sqrt{3}}{4} D_{\text{CI}}^2 \quad (4.13)$$

Area occupied by carbonyl iron particles is given by:

$$A_{\text{CI}} = \frac{\pi}{8} D_{\text{CI}}^2 \quad (4.14)$$

Therefore, the ratio of area in the unit triangle occupied by carbonyl iron particles, a_{CI} , is given by:

$$a_{CI} = \frac{A_{CI}}{A_{unit}} = \frac{1}{2\sqrt{3}}\pi \approx 0.9069 \quad (4.15)$$

Then, N_{CI} can be calculated by considering the ratio a_{CI} of the full contact area between finishing media and workpiece, $A_{contact}$, and dividing it by the projected area of one carbonyl iron particle. This is expressed as:

$$N_{CI} = \frac{(\text{contact area}) \times (\text{areal ratio of carbonyl iron particles})}{(\text{projected area of 1 carbonyl iron particle})} \quad (4.16)$$

$$N_{CI} = \frac{A_{contact} \times a_{CI}}{\frac{1}{4}\pi D_{CI}^2} \quad (4.17)$$

$$N_{CI} = \frac{2}{\sqrt{3}} A_{contact} \cdot \frac{1}{D_{CI}^2} \quad (4.18)$$

Equation 4.18 is the proposed expression for number of active carbonyl iron particles, N_{CI} , to be used in the proposed model for the new MFAF process.

4.5.6 Number of active abrasives

To calculate the number of active abrasives, N_{abr} , an abrasive plane parallel to the workpiece surface, with an offset equal to the radius of the abrasives, is considered. In accordance to the abrasive size criterion in Equation 4.11, the abrasive plane will be closer to the workpiece surface than the CI plane. Figure 4.9 illustrates the abrasive plane and the CI plane in the same schematic diagram.

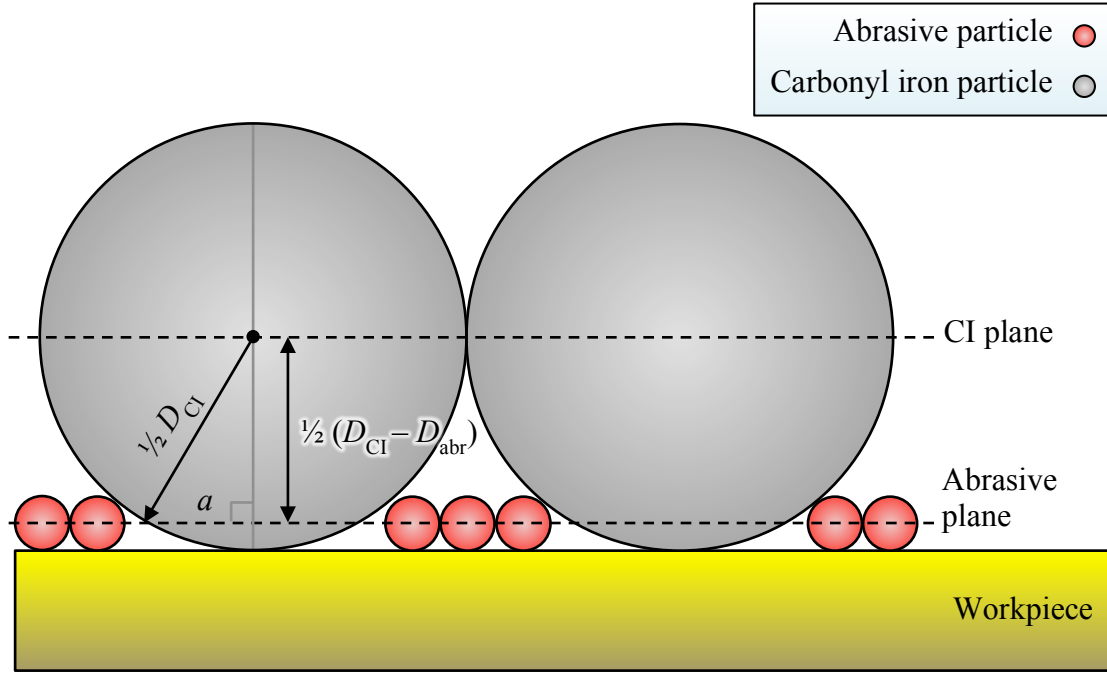


Figure 4.9: Interface of carbonyl iron particles, abrasives, and the workpiece surface.

Consider the abrasive plane across the full area of contact between the finishing media and the workpiece surface. Area already occupied by carbonyl iron particles on the abrasive plane, $A_{CI, \text{abr plane}}$, is given by:

$$A_{CI, \text{abr plane}} = N_{CI} \cdot \pi a^2 \quad (4.19)$$

To obtain the area on the abrasive plane that is available for abrasives, the area calculated above is subtracted from the full area of contact, A_{contact} . This available area however cannot be fully filled by abrasives because the existing carbonyl iron particles impose geometrical constraints, and the abrasives themselves will leave behind interstitial spaces. An upper bound of this available area can be calculated by applying the

maximum possible areal ratio, which is $\frac{1}{2\sqrt{3}}\pi$ or 0.9069, as given in Equation 4.15.

The area available for abrasives on the abrasive plane is therefore given by:

$$A_{\text{available, abr plane}} = \frac{1}{2\sqrt{3}}\pi \cdot (A_{\text{contact}} - N_{\text{CI}} \cdot \pi a^2) \quad (4.20)$$

Using the geometrical relationship $a^2 = \frac{1}{4}D_{\text{abr}}(2D_{\text{CI}} - D_{\text{abr}})$ and substituting the geometrical expression for number of active carbonyl iron particles, N_{CI} , the expression above becomes:

$$A_{\text{available, abr plane}} = \frac{1}{2\sqrt{3}}\pi \cdot A_{\text{contact}} \cdot \left(1 - \frac{1}{2\sqrt{3}}\pi \cdot \frac{D_{\text{abr}}}{D_{\text{CI}}} \cdot \frac{2D_{\text{CI}} - D_{\text{abr}}}{D_{\text{CI}}} \right) \quad (4.21)$$

To obtain the maximum number of active abrasives, $N_{\text{abr, max}}$, the expression above is simply divided by the projected area of one abrasive particle. The resulting expression is given below:

$$N_{\text{abr, max}} = \frac{A_{\text{available, abr plane}}}{(\text{projected area of 1 abrasive particle})} \quad (4.22)$$

$$N_{\text{abr, max}} = \frac{2}{\sqrt{3}} \cdot A_{\text{contact}} \cdot \left(1 - \frac{1}{2\sqrt{3}}\pi \cdot \frac{D_{\text{abr}}}{D_{\text{CI}}} \cdot \frac{2D_{\text{CI}} - D_{\text{abr}}}{D_{\text{CI}}} \right) \cdot \frac{1}{D_{\text{abr}}^2} \quad (4.23)$$

The number of abrasives given by the expression above coincides with the maximum value given by the abrasive volume criterion in Equation 4.12. When the abrasive volume is below this maximum value, the following proportionality between number of active abrasives and abrasive volume is considered:

$$\frac{N_{abr}}{N_{abr, \max}} = \frac{v_{abr}}{v_{abr, \max}} \quad (4.24)$$

The linear relationship above is following the assumption that abrasives are dispersed evenly in the carbonyl iron matrix. As a result, the expression for the number of active abrasives, N_{abr} , is given by:

$$N_{abr} = \frac{2}{\sqrt{3}} \cdot A_{\text{contact}} \cdot \left(1 - \frac{1}{2\sqrt{3}} \pi \cdot \frac{D_{abr}}{D_{CI}} \cdot \frac{2D_{CI} - D_{abr}}{D_{CI}} \right) \cdot \frac{1}{D_{abr}^2} \cdot \frac{v_{abr}}{v_{abr, \max}} \quad (4.25)$$

Equation 4.25 is the proposed expression for number of active abrasives, N_{abr} , to be used in the proposed model for the new MFAF process.

4.6 FORCE PER PARTICLE

In MFAF processes where the finishing media consists of a mixture of magnetic particles and non-magnetic abrasives suspended in a carrier fluid, calculating the force per particle is a difficult and unique problem. The new MFAF process proposed in this thesis is one such process.

Firstly, the forces acting on the magnetic particles and non-magnetic abrasives are different, and they must therefore be considered separately. For the magnetic particles, the magnetic force, the contact forces due to neighbouring particles, and the contact force due to workpiece must be considered. For the non-magnetic particles, the magnetic force is negligible, but the same contact forces must be considered. Secondly, more sophisticated models may also consider the hydrodynamics forces due to the carrier fluid. In existing approaches reported in the literature, none has considered the aforementioned

contact forces arising from interactions between the particles in the finishing media. In this thesis, a new approach that considers these interactions is thus proposed.

4.6.1 Existing approaches

There is no definitive approach or method to calculate the forces on particles in abrasive processes. Two methods that are most relevant to the new MFAF process are highlighted in this section. First, the modeling of forces done by Luo and Dornfeld [6] for the CMP process is considered. In their work, it is proposed that the calculations be based on whether the polishing pad is soft or hard, as illustrated in Figure 4.10.

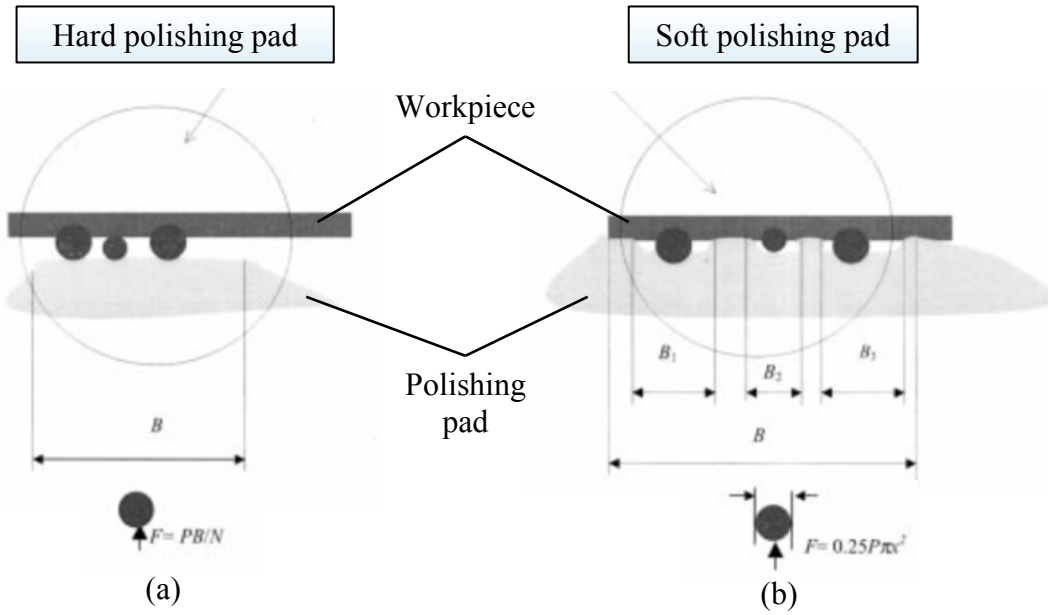


Figure 4.10: Force per particle in the model proposed by Luo and Dornfeld [6] for the CMP process, for (a) hard polishing pad and (b) soft polishing pad.

The mechanism in the new MFAF process is similar to the case of a soft polishing pad, with the carbonyl iron particles being approximated as the pad. However, the

approach by Luo and Dornfeld on its own is inadequate for the new MFAF process and has to be modified to consider the interaction of particles in the finishing media and the effect of magnetic forces onto the magnetic particles.

Secondly, the work done by Sidpara and Jain [10] in modeling the forces for their MFAF process is considered. In their work, it is proposed that the force on an abrasive be the sum of the ‘magnetic levitation force’, F_m , the gravitational force, F_g , and the centrifugal force, F_{cf} . In the original article, the equation is given by:

$$F_{n_abr} = (F_m \text{ or } F_{mg}) + F_g + F_{cf} \quad (4.26)$$

Of the three force components, the magnetic force is typically greater than the gravitational force and the centrifugal force. Also, the force vector is in the direction towards the magnet, acting away from the workpiece. There are insufficient details or explanation given as to how the resultant force, which acts away from the workpiece, is attributed to material removal. As such, this approach is deemed inadequate for modeling the forces for the new MFAF process.

4.6.2 Proposed approach

In the previous section, it has been argued that existing approaches are inadequate for modeling the forces in the new MFAF process. In this thesis, a new framework that considers the interaction of particles in the finishing media is proposed to obtain expressions for the forces acting on both the magnetic carbonyl iron particles and the non-magnetic abrasives.

It is proposed that force per particle be modeled as proportional to the product of two terms. The first term is the particle properties term, which encapsulates the properties of the particle itself. The second term is the neighbouring particles term, which takes into account the contact forces attributed to the neighbouring particles. This can be written as:

$$F \propto (\text{particle properties term}) \times (\text{neighbouring particles term}) \quad (4.27)$$

Based on this general expression, the force per particle expression is developed for both the carbonyl iron particles and the abrasives in the following sections.

4.6.3 Force per carbonyl iron particle

It is proposed that the particle properties term is BD_{CI}^3 , where B is the magnetic flux density at the centre of the carbonyl iron particle and D_{CI} is the diameter of the carbonyl iron particle. The term is proposed as such because magnetic force is dominant, and magnetic force is a function of the volume of the body as well as the magnetic flux density. Equation 4.27 therefore becomes:

$$F_{\text{CI}} \propto BD_{\text{CI}}^3 \times (\text{neighbouring particles term}) \quad (4.28)$$

Obtaining an expression for the neighbouring particles term is more complex. In the finishing media, the number of configurations in which the carbonyl iron particles and abrasives can be arranged is effectively infinite. Therefore, it is proposed that the expression be derived based on the average of the bulk, and in accordance to several idealized assumptions. Firstly, the neighbouring particles term is to be expressed as the

sum of two components – one for the neighbouring carbonyl iron particles, and another for the neighbouring abrasives. Secondly, these two components are assigned different weightage. It is proposed that this weightage is based on the ratio of the total projected area of the particle type to the total projected area of all the active particles. Projected area is chosen as the basis of the weightage because the magnitude of contact force exerted by a particle is dependent on its projected area. Thirdly, each of the two components is also assigned a constant of proportionality to represent the magnitude of the contact force that the neighbouring particles can exert on the particle. These constants are denoted as $k_{F, \text{CI}}$ and $k_{F, \text{abr}}$ for the neighbouring carbonyl iron particles and neighbouring abrasives respectively. Lastly, for neighbouring carbonyl iron particles, an additional BD_{CI}^3 term is included to account for the influence of the magnetic flux density on the contact forces that they can exert.

Based on the above, the neighbouring particles term for a carbonyl iron particle is given by:

$$\begin{array}{ccc}
 \text{Term for neighbouring} & & \text{Term for neighbouring} \\
 \text{carbonyl iron particles} & & \text{abrasives} \\
 \\
 \underbrace{k_{F, \text{CI}} \cdot BD_{\text{CI}}^3 \cdot \frac{N_{\text{CI}} \cdot D_{\text{CI}}^2}{N_{\text{CI}} \cdot D_{\text{CI}}^2 + N_{\text{abr}} \cdot D_{\text{abr}}^2}}_{\text{Ratio of projected area, based on active particles}} + \underbrace{k_{F, \text{abr}} \cdot \frac{N_{\text{abr}} \cdot D_{\text{abr}}^2}{N_{\text{CI}} \cdot D_{\text{CI}}^2 + N_{\text{abr}} \cdot D_{\text{abr}}^2}}_{\text{Ratio of projected area, based on active particles}} & & (4.29)
 \end{array}$$

where N_{CI} and N_{abr} are the numbers of active carbonyl iron particles and active abrasives respectively, D_{CI} and D_{abr} are the diameters of the carbonyl iron particles and abrasives

respectively, and $k_{F, \text{Cl}}$ (unit: $\text{N T}^{-2} \text{m}^{-6}$) and $k_{F, \text{abr}}$ (unit: $\text{N T}^{-1} \text{m}^{-3}$) are the constants of proportionality to represent the magnitude of the contact force that the neighbouring particles can exert on the particle.

It is expected that the neighbouring carbonyl iron particles provide significantly greater contact forces, as they are strongly held by the magnetic force. As a result, $k_{F, \text{Cl}}$ is expected to be significantly greater than $k_{F, \text{abr}}$, potentially by several orders of magnitude. Substituting Expression 4.29 into Equation 4.28, the complete expression for F_{Cl} is given by:

$$F_{\text{Cl}} = BD_{\text{Cl}}^3 \cdot \left(k_{F, \text{Cl}} \cdot BD_{\text{Cl}}^3 \cdot \frac{N_{\text{Cl}} \cdot D_{\text{Cl}}^2}{N_{\text{Cl}} \cdot D_{\text{Cl}}^2 + N_{\text{abr}} \cdot D_{\text{abr}}^2} + k_{F, \text{abr}} \cdot \frac{N_{\text{abr}} \cdot D_{\text{abr}}^2}{N_{\text{Cl}} \cdot D_{\text{Cl}}^2 + N_{\text{abr}} \cdot D_{\text{abr}}^2} \right) \quad (4.30)$$

Equation 4.30 is the proposed expression for force per carbonyl iron particle, F_{Cl} , to be used in the proposed model for the new MFAF process.

4.6.4 Force per abrasive particle

The force per abrasive particle is modeled in a similar way to the modeling of force per carbonyl iron particle. Therefore, it is also the product of the particle properties term and the neighbouring particles term.

For the particle properties term, it is proposed that the expression is simply D_{abr}^2 . The term is proposed as such because abrasives are not affected by magnetic field, and the force that it exerts on the workpiece is therefore a function of its projected area. For the neighbouring particles term, the same assumptions made for carbonyl iron particles

are applied to abrasives. As the composition of neighbouring particles is not a function of the particle itself, there is no change to the expression shown in Expression 4.29.

The complete expression for F_{abr} is therefore given by:

$$F_{abr} = D_{abr}^2 \cdot \left(k_{F, Cl} \cdot BD_{Cl}^3 \cdot \frac{N_{Cl} \cdot D_{Cl}^2}{N_{Cl} \cdot D_{Cl}^2 + N_{abr} \cdot D_{abr}^2} + k_{F, abr} \cdot \frac{N_{abr} \cdot D_{abr}^2}{N_{Cl} \cdot D_{Cl}^2 + N_{abr} \cdot D_{abr}^2} \right) \quad (4.31)$$

Equation 4.31 is the proposed expression for force per abrasive particle, F_{abr} , to be used in the proposed model for the new MFAF process.

4.7 SUMMARY

The components for the material removal model have all been derived in the previous sections. In this section, the assumptions and scope of the model are reiterated, and the derived components (N_{Cl} , N_{abr} , F_{Cl} , F_{abr}) are then assembled together to form the complete material removal model.

4.7.1 Assumptions and scope of model

Firstly, it was assumed that all carbonyl iron particles are spherical in shape and have the same diameter. The same was assumed for abrasives. Secondly, the carbonyl iron particles in the finishing media were assumed to be in a face-centred cubic (FCC) configuration, which is the configuration with the highest atomic packing factor at 0.74. Abrasives were assumed to reside in the interstitial spaces in the carbonyl iron matrix and

are uniformly dispersed. Lastly, it was assumed that the densest (111)-plane of the carbonyl iron matrix is the plane in contact with the workpiece surface.

Based on the assumptions above, two criteria were required for the proposed model to be valid. The first criterion was the abrasive size criterion, whereby the abrasive may not exceed a critical value. The abrasive size criterion is given by:

$$D_{abr} \leq (\sqrt{2} - 1) D_{CI} \quad (4.11)$$

The second criterion required that the abrasive volume or concentration not to be too high such that the interstitials are fully occupied and further addition of abrasives compromise the carbonyl iron matrix. The abrasive volume criterion is given by:

$$\frac{v_{abr}}{v_{CI}} \leq 0.259 \quad (4.12)$$

4.7.2 General material removal expression

The material removal rate is the sum of two components:

$$\text{MRR} = \underbrace{k_{CI} \cdot N_{CI} \cdot \left(\frac{3F_{CI}}{8E} \right) \cdot v}_{\text{MRR component for carbonyl iron particles}} + \underbrace{k_{abr} \cdot N_{abr} \cdot \left(\frac{3F_{abr}}{8E} \right) \cdot v}_{\text{MRR component for abrasives}} \quad (4.9)$$

where k_{CI} and k_{abr} are dimensionless constants that encapsulate the efficacy of the particles at material removal, N_{CI} and N_{abr} are the numbers of active carbonyl iron

particles and active abrasives respectively, F_{CI} and F_{abr} are the forces per particle for carbonyl iron particles and abrasives respectively, E is the Young's modulus of workpiece, and v is the relative linear velocity between particles and the workpiece surface.

4.7.3 Number of active particles

The number of active carbonyl iron particles, N_{CI} , and the number of active abrasives, N_{abr} , are given by:

$$N_{\text{CI}} = \frac{2}{\sqrt{3}} A_{\text{contact}} \cdot \frac{1}{D_{\text{CI}}^2} \quad (4.18)$$

$$N_{\text{abr}} = \frac{2}{\sqrt{3}} \cdot A_{\text{contact}} \cdot \left(1 - \frac{1}{2\sqrt{3}} \pi \cdot \frac{D_{\text{abr}}}{D_{\text{CI}}} \cdot \frac{2D_{\text{CI}} - D_{\text{abr}}}{D_{\text{CI}}} \right) \cdot \frac{1}{D_{\text{abr}}^2} \cdot \frac{v_{\text{abr}}}{v_{\text{abr, max}}} \quad (4.25)$$

where A_{contact} is the area of contact between polishing media and workpiece surface, D_{CI} and D_{abr} are the diameters of carbonyl iron particles and abrasives respectively, v_{abr} is the volumetric ratio of abrasives in the finishing media, and $v_{\text{abr, max}}$ is the maximum allowable volumetric ratio of abrasive particles in the polishing media.

4.7.4 Force per particle

The force per particle for carbonyl iron particles, F_{CI} , and force per particle for abrasives, F_{abr} , is given by:

$$F_{\text{Cl}} = BD_{\text{Cl}}^3 \cdot \left(k_{F,\text{Cl}} \cdot BD_{\text{Cl}}^3 \cdot \frac{N_{\text{Cl}} \cdot D_{\text{Cl}}^2}{N_{\text{Cl}} \cdot D_{\text{Cl}}^2 + N_{\text{abr}} \cdot D_{\text{abr}}^2} + k_{F,\text{abr}} \cdot \frac{N_{\text{abr}} \cdot D_{\text{abr}}^2}{N_{\text{Cl}} \cdot D_{\text{Cl}}^2 + N_{\text{abr}} \cdot D_{\text{abr}}^2} \right) \quad (4.30)$$

$$F_{\text{abr}} = D_{\text{abr}}^2 \cdot \left(k_{F,\text{Cl}} \cdot BD_{\text{Cl}}^3 \cdot \frac{N_{\text{Cl}} \cdot D_{\text{Cl}}^2}{N_{\text{Cl}} \cdot D_{\text{Cl}}^2 + N_{\text{abr}} \cdot D_{\text{abr}}^2} + k_{F,\text{abr}} \cdot \frac{N_{\text{abr}} \cdot D_{\text{abr}}^2}{N_{\text{Cl}} \cdot D_{\text{Cl}}^2 + N_{\text{abr}} \cdot D_{\text{abr}}^2} \right) \quad (4.31)$$

where B is the magnetic field strength is the magnetic field strength at the centre of the particle, D_{Cl} and D_{abr} are the diameters of carbonyl iron particles and abrasives respectively, N_{Cl} and N_{abr} are the numbers of active carbonyl iron particles and active abrasives respectively, and $k_{F,\text{Cl}}$ (unit: $\text{N T}^{-2} \text{m}^{-6}$) and $k_{F,\text{abr}}$ (unit: $\text{N T}^{-1} \text{m}^{-3}$) are the constants of proportionality to represent the magnitude of the contact force that the neighbouring particles can exert on the particle, respectively.

REFERENCES

- [1] Brinksmeier E, Riemer O and Gessengarter A, *Finishing of structured surfaces by abrasive polishing*. Precision Engineering, 2006. **30**(3), p.325-336.
- [2] Preston FW, *The theory and design of plate glass polishing machines*. J. Soc. Glass Tech., 1927. **11**: p.214.
- [3] Buijs M and Korpel-van Houten K, *A model for lapping of glass*. Journal of Materials Science, 1993. **28**(11): p. 3014-3020.
- [4] Shorey AB, *Mechanism of material removal in magnetorheological finishing (MRF) of glass*, Doctoral thesis dissertation, University of Rochester, Rochester, NY, 2000.
- [5] DeGroote, JE, *Surface interactions between nanodiamonds and glass in magnetorheological finishing (MRF)*. Doctoral thesis dissertation, University of Rochester, Rochester, NY, 2007.
- [6] Luo J and Dornfeld DA, *Material removal mechanism in chemical mechanical polishing – theory and modeling*. IEEE Transactions on Semiconductor Manufacturing, 2001. **14**(2): p.112-133.
- [7] Brown NJ, Baker PC and Maney RT, *Optical polishing of metals*. SPIE Vol. 306 Contemporary Methods of Optical Fabrication, 1981. **306**: p.42-57.
- [8] Jeng YR and Huang PY, *A material removal rate model considering interfacial micro-contact wear behaviour for chemical mechanical polishing*. Journal of Tribology, Transactions of the ASME, 2005. **127**: p.190-197.
- [9] Jha S and Jain VK, *Modeling and simulation of surface texture in magnetorheological abrasive flow finishing (MRAFF) process*. Wear, 2006. **261**(7): p. 856-866
- [10] Sidpara A and Jain VK, *Analysis of forces on the freeform surface in magnetorheological fluid based finishing process*. International Journal of Machine Tools and Manufacture, 2013. **69**: p.1-10.
- [11] Zhao Y and Chang L, *A micro-contact and wear model for chemical-mechanical polishing of silicon wafers*. Wear, 2002. **252**: p.220-226.

Chapter 5

Extensions to material removal rate model

5.1 INTRODUCTION

In the previous chapter, a new material removal rate model was proposed for the new MFAF process. The proposed model is only valid when the FCC configuration of the carbonyl iron matrix in the finishing media is not compromised. To not compromise the carbonyl iron matrix, two criteria must be fulfilled. The first is the abrasive size criterion, whereby the abrasive size must not exceed a critical value as given by Equation 4.11. The second is the abrasive volume criterion, whereby the abrasive volume must not exceed a critical value in relation to the volume of carbonyl iron particles, as given by Equation 4.12.

These criteria are reasonable, and are typical conditions for the finishing media. However, it is not inconceivable for either or both of the criteria to not be fulfilled. For example, the finishing media may be composed of abrasives larger than the critical value given by the first criterion, or is prepared with an abrasive concentration exceeding the maximum allowable volume given by the second criterion. Under these conditions, the model proposed in the previous chapter will be invalid.

In this chapter, the model developed in the previous chapter will be considered as the base model, and this base model will be extended to take into consideration conditions where either or both of the two criteria are not fulfilled. The first extension to the base model considers conditions where the abrasive size criterion is not fulfilled. The second extension considers conditions when the abrasive volume criterion is not fulfilled. For each extension, the changes to the terms in the base model, if any, are presented.

5.2 MODEL EXTENSION FOR ABRASIVE SIZE CRITERION

According to the abrasive size criterion, an abrasive particle is too large if it exceeds $\sqrt{2}-1$ times the diameter of a carbonyl iron particle. For illustration, in a typical condition where the carbonyl iron particle size is 8 μm in diameter, the criterion specifies that the critical value for abrasive diameter is 3.3 μm .

This critical value of the abrasive diameter is calculated based on the geometry of the interstitial spaces in the carbonyl iron matrix. When abrasive diameter exceeds the critical value, the carbonyl iron matrix is then necessarily compromised to create additional room for the large abrasives.

In this section, an orderly and quantifiable change in the carbonyl iron matrix to create additional room for the large abrasives is proposed. Based on this orderly change, modified expressions for N_{CI} , N_{abr} , F_{CI} , and F_{abr} are obtained.

5.2.1 Proposed approach

In the base model, all the carbonyl iron particles in the matrix are in contact with each other. When the abrasive size exceeds the critical value, it is proposed that the distance between carbonyl iron particles is increased in an orderly manner to accommodate the larger abrasives. Figure 5.1 illustrates the change in the carbonyl iron matrix when the abrasive size exceeds the critical value given by the abrasive size criterion.

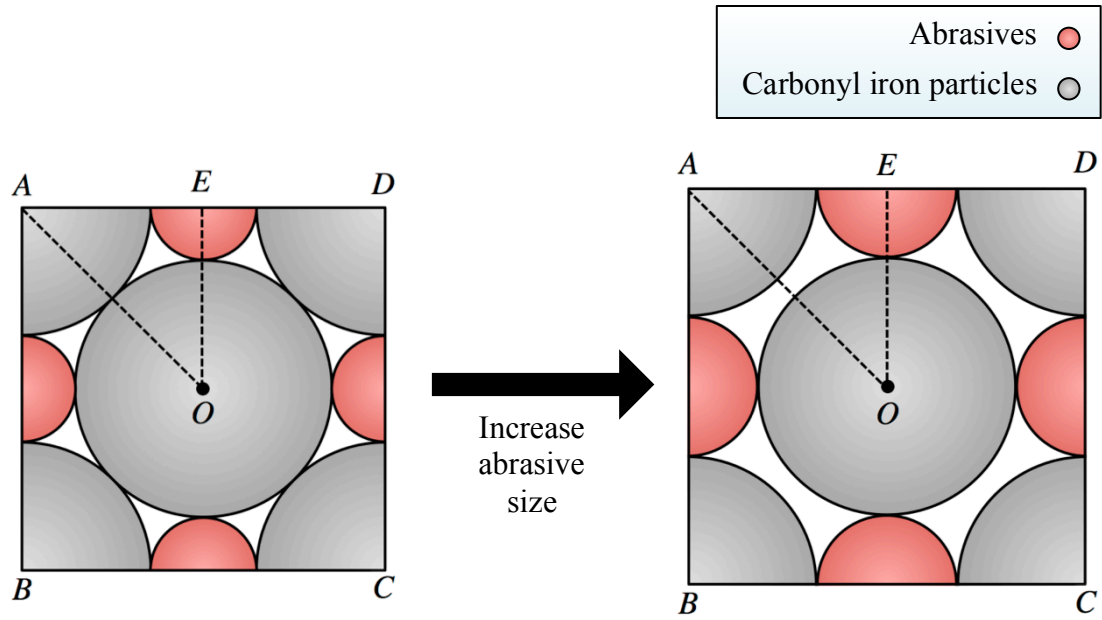


Figure 5.1: Distance between carbonyl iron particles is increased in an orderly manner when abrasive size exceeds critical value given by abrasive size criterion.

In Figure 5.1, OA is the distance between two carbonyl iron particles. When abrasive size is below the critical value, OA is simply the diameter of carbonyl iron particle. When abrasive size exceeds the critical value, OA can be calculated geometrically by:

$$OA^2 = OE^2 + EA^2 \quad (5.1)$$

$$OA^2 = \left(\frac{D_{Cl}}{2} + \frac{D_{abr}}{2} \right)^2 + \left(\frac{D_{Cl}}{2} + \frac{D_{abr}}{2} \right)^2 \quad (5.2)$$

$$OA = \frac{1}{\sqrt{2}} (D_{Cl} + D_{abr}) \quad (5.3)$$

As shown in Equation 5.3, the distance between two carbonyl iron particles is now also a function of the abrasive size. The change in OA is then visualized for the unit triangle on the CI plane, as shown in Figure 5.2.

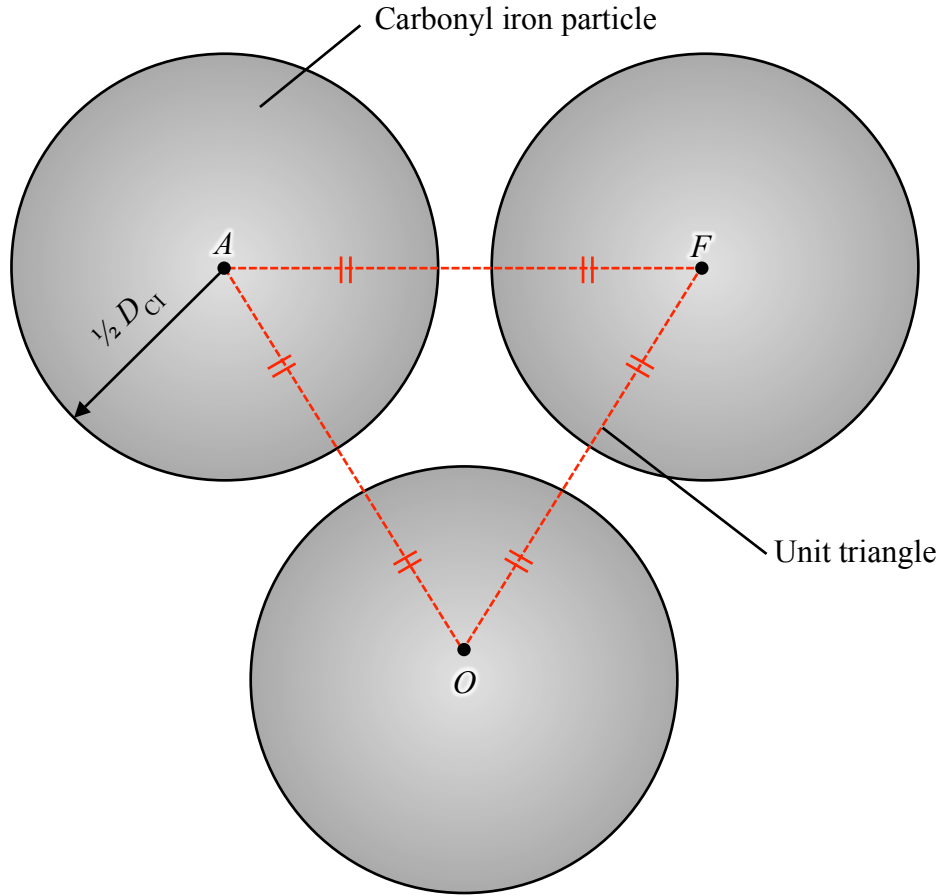


Figure 5.2: Unit triangle when abrasive size exceeds the critical value. Abrasives are not shown.

For the unit triangle, the edge length is OA , which is given by Equation 5.3. Therefore, area of unit triangle $\triangle OAF$ is given by:

$$A_{\text{unit}} = \frac{\sqrt{3}}{8} (D_{\text{CI}} + D_{\text{abr}})^2 \quad (5.4)$$

Also, the area occupied by carbonyl iron particles is given by:

$$A_{\text{CI}} = \frac{\pi}{8} D_{\text{CI}}^2 \quad (5.5)$$

Therefore, ratio of area in the unit triangle that is occupied by carbonyl iron particles, a_{CI} , is given by:

$$a_{\text{CI}} = \frac{A_{\text{CI}}}{A_{\text{unit}}} \quad (5.6)$$

$$a_{\text{CI}} = \frac{1}{\sqrt{3}} \pi \left(\frac{D_{\text{CI}}}{D_{\text{CI}} + D_{\text{abr}}} \right)^2, \quad \text{where } D_{\text{abr}} \geq (\sqrt{2} - 1) D_{\text{CI}}. \quad (5.7)$$

Based on this modified expression for a_{CI} , the numbers of active carbonyl iron particles and active abrasives are calculated in the next section.

5.2.2 Number of active particles

The methodology in deriving the expressions for number of active carbonyl iron particles, N_{CI} , and number of active abrasives, N_{abr} , is the same as that used for the base model. Firstly, the expression of N_{CI} can similarly be obtained by considering the following:

$$N_{\text{CI}} = \frac{(\text{contact area}) \times (\text{areal ratio of carbonyl iron particles})}{(\text{projected area of 1 carbonyl iron particle})} \quad (5.8)$$

$$N_{\text{CI}} = \frac{A_{\text{contact}} \times a_{\text{CI}}}{\frac{1}{4} \pi D_{\text{CI}}^2} \quad (5.9)$$

Substituting the expression for a_{Cl} obtained in Equation 5.7, the expression for N_{Cl} in the first extension is given by:

$$N_{\text{Cl}} = \frac{4}{\sqrt{3}} A_{\text{contact}} \cdot \frac{1}{(D_{\text{Cl}} + D_{\text{abr}})^2}, \quad \text{where } D_{\text{abr}} \geq (\sqrt{2} - 1) D_{\text{Cl}}. \quad (5.10)$$

Secondly, for the number of active abrasives, N_{abr} , the abrasive plane across the full area of contact between the finishing media and the workpiece surface is considered. The area already occupied by carbonyl iron particles is given by:

$$A_{\text{Cl, abr plane}} = N_{\text{Cl}} \cdot \pi a^2 \quad (5.11)$$

Therefore, the area available for abrasives on the abrasive plane, after applying the maximum ratio of $\frac{1}{2\sqrt{3}}\pi$ or 0.9069, is given by:

$$A_{\text{available, abr plane}} = \frac{1}{2\sqrt{3}} \pi \cdot (A_{\text{contact}} - N_{\text{Cl}} \cdot \pi a^2) \quad (5.12)$$

Using the geometrical relationship $a^2 = \frac{1}{4} D_{\text{abr}} (2D_{\text{Cl}} - D_{\text{abr}})$ and substituting the expression for N_{Cl} given in Equation 5.10, the equation above becomes:

$$A_{\text{available, abr plane}} = \frac{1}{2\sqrt{3}} \pi \cdot A_{\text{contact}} \cdot \left(1 - \frac{1}{2\sqrt{3}} \pi \cdot \frac{2D_{\text{abr}}}{D_{\text{Cl}} + D_{\text{abr}}} \cdot \frac{2D_{\text{Cl}} - D_{\text{abr}}}{D_{\text{Cl}} + D_{\text{abr}}} \right) \quad (5.13)$$

With the available area for abrasives known, the maximum number of active abrasives, $N_{abr, max}$, can be calculated in a similar method as done for the base model. $N_{abr, max}$ is given by:

$$N_{abr, max} = \frac{A_{available, abr\ plane}}{(\text{projected area of 1 abrasive particle})} \quad (5.14)$$

$$N_{abr, max} = \frac{2}{\sqrt{3}} \cdot A_{contact} \cdot \left(1 - \frac{1}{2\sqrt{3}} \pi \cdot \frac{2D_{abr}}{D_{CI} + D_{abr}} \cdot \frac{2D_{CI} - D_{abr}}{D_{CI}} \right) \cdot \frac{1}{D_{abr}^2} \quad (5.15)$$

Unlike the base model, the proportionality in Equation 4.24 cannot be used for this extension. When $v_{abr} < v_{abr, max}$, there are gaps between some CI particles, which results in floating CI particles if an expanded FCC configuration is considered. This is unrealistic is not justifiable. Therefore, the following expression is only valid when $v_{abr} = v_{abr, max}$. For the case where $v_{abr} > v_{abr, max}$, an alternate extension of the model is applicable (discussed in Section 5.3 later). No satisfactory model can be proposed currently for the case of $v_{abr} < v_{abr, max}$.

$$N_{abr} = \frac{2}{\sqrt{3}} \cdot A_{contact} \cdot \left(1 - \frac{1}{2\sqrt{3}} \pi \cdot \frac{2D_{abr}}{D_{CI} + D_{abr}} \cdot \frac{2D_{CI} - D_{abr}}{D_{CI} + D_{abr}} \right) \cdot \frac{1}{D_{abr}^2} \quad (5.16)$$

Equations 5.10 and 5.16 are the proposed expressions for the number of active carbonyl iron particles, N_{CI} , and the number of active abrasives, N_{abr} , to be used in the first proposed extension to the base model when the abrasive size exceeds the critical value given by the abrasive size criterion.

5.2.3 Force per particle

For the base model, the expressions for the force per carbonyl iron particle, F_{CI} , and force per abrasive particle, F_{abr} , were obtained by considering the product of two terms, namely the particle properties term and the neighbouring particles term. In the steps to derive the expressions, the bulk properties of the finishing media were used in a ratio form. As such, the actual arrangement of the particles in the finishing media does not directly affect the expressions.

Therefore, it is proposed that both the F_{CI} and F_{abr} for the first extension follow the same expressions used in the base model. They are reproduced below for reference:

$$F_{CI} = BD_{CI}^3 \cdot \left(k_{F,CI} \cdot BD_{CI}^3 \cdot \frac{N_{CI} \cdot D_{CI}^2}{N_{CI} \cdot D_{CI}^2 + N_{abr} \cdot D_{abr}^2} + k_{F,abr} \cdot \frac{N_{abr} \cdot D_{abr}^2}{N_{CI} \cdot D_{CI}^2 + N_{abr} \cdot D_{abr}^2} \right) \quad (4.30)$$

$$F_{abr} = D_{abr}^2 \cdot \left(k_{F,CI} \cdot BD_{CI}^3 \cdot \frac{N_{CI} \cdot D_{CI}^2}{N_{CI} \cdot D_{CI}^2 + N_{abr} \cdot D_{abr}^2} + k_{F,abr} \cdot \frac{N_{abr} \cdot D_{abr}^2}{N_{CI} \cdot D_{CI}^2 + N_{abr} \cdot D_{abr}^2} \right) \quad (4.31)$$

Equations 5.17 and 5.18 are the proposed expressions for force per carbonyl iron particle, F_{CI} , and force per abrasive particle, F_{abr} , to be used in the first proposed extension to the base model when the abrasive size exceeds the critical value given by the abrasive size criterion. Although the expressions are unchanged from the base model, note that both equations are functions of N_{CI} and N_{abr} , which have been modified in this first proposed extension. Therefore, both the values of F_{CI} and F_{abr} in this extension are affected indirectly.

5.3 MODEL EXTENSION FOR ABRASIVE VOLUME CRITERION

According to the abrasive volume criterion, the abrasive volume must not exceed a critical value whereby all the interstitial spaces are fully occupied by abrasives. The critical value, as a ratio to the volume of carbonyl iron particles, is given by Equation 4.12 in the previous chapter. This critical value can be interpreted as the saturation point for the abrasives in the finishing media. In a practical example, a finishing media composed of 100 g of carbonyl iron particles can accommodate a maximum of 13.5 g of Al_2O_3 abrasives.

When the abrasive volume exceeds this critical value, the FCC configuration of the carbonyl iron matrix is compromised to create additional room for the abrasives. The base model will then be rendered invalid. However, there is no physical limitation for preparing finishing media with abrasive volume exceeding this critical value. Therefore, a second extension to the base model is proposed in this section to consider conditions where the abrasive volume exceeds the critical value.

Similar to the first extension, an orderly and quantifiable change in the carbonyl iron matrix to create additional room for the abrasives is proposed. Based on this orderly change, expressions for N_{CI} , N_{abr} , F_{CI} , and F_{abr} , where necessary, are modified.

5.3.1 Proposed approach

Similar to the first extension to the base model, an orderly change in the carbonyl iron matrix is considered when abrasive volume exceeds the critical value. Specifically, the distance between carbonyl iron particles is increased to accommodate additional abrasives in the finishing media. To calculate how much the distance between carbonyl iron particles is increased, it is proposed that the abrasives in the finishing media are consolidated and redistributed evenly in the interstitial spaces as larger abrasives with an

equivalent diameter, $D_{abr, eqv}$. Figure 5.3 illustrates the general steps in the proposed approach.

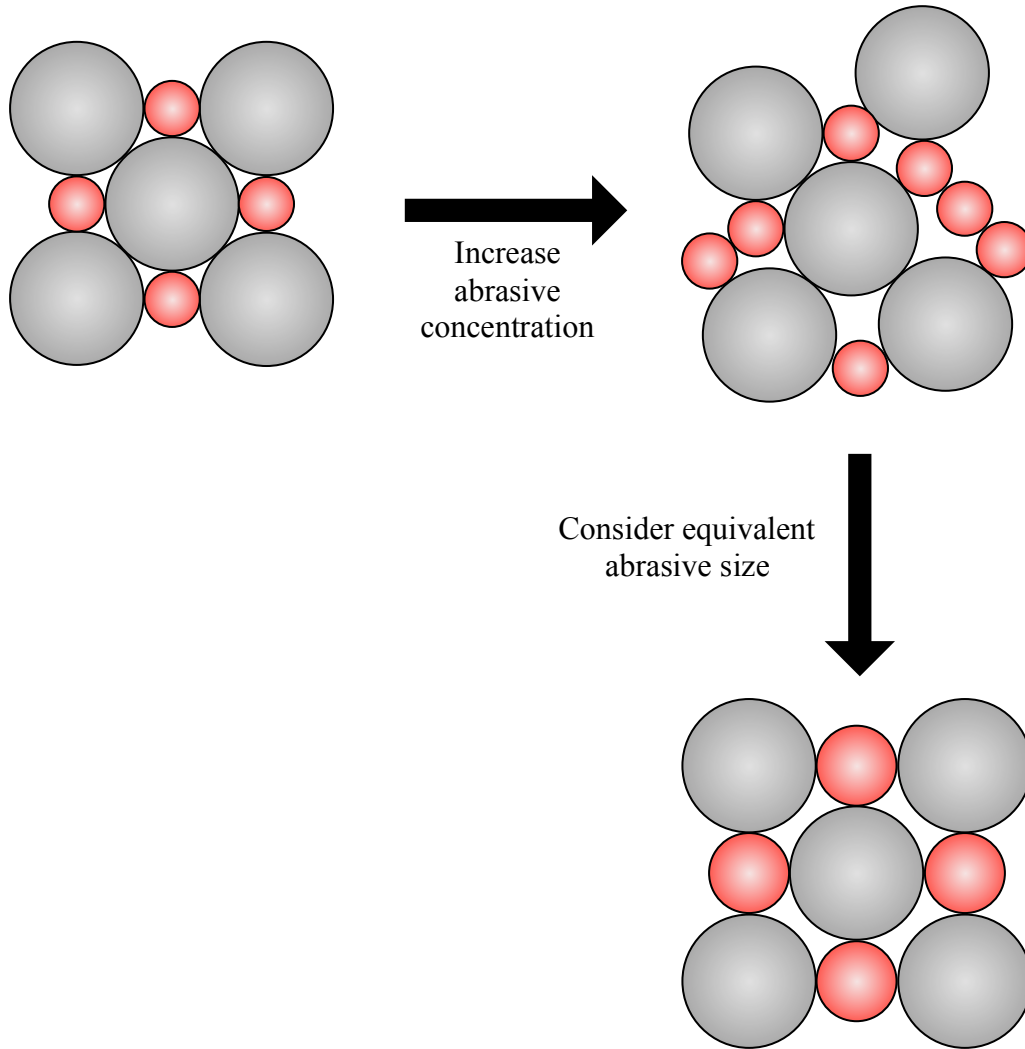


Figure 5.3: When abrasive volume exceeds critical value, an orderly arrangement of larger abrasives with equivalent abrasive size is considered.

The equivalent abrasive size, $D_{abr, eqv}$, is given by the relationship below:

$$\frac{\pi D_{\text{abr, eqv}}^2}{4} = \frac{\pi D_{\text{abr, max}}^2}{4} \cdot \frac{m_{\text{abr}}}{m_{\text{abr, max}}} \quad (5.17)$$

Substituting Equation 4.10 for $D_{\text{abr, max}}$ into Equation 5.17, the equivalent abrasive size becomes:

$$D_{\text{abr, eqv}} = (\sqrt{2} - 1) D_{\text{CI}} \cdot \left(\frac{m_{\text{abr}}}{m_{\text{abr, max}}} \right)^{\frac{1}{2}} \quad (5.18)$$

where m_{abr} and $m_{\text{abr, max}}$ are the mass of abrasives and maximum allowable mass of abrasives, and $D_{\text{abr, max}}$ is the critical abrasive size as given by the first criterion. Two points need to be highlighted. Firstly, projected area of abrasives is chosen as the basis of the ratio because the calculation of number of active abrasives is done on a two-dimensional abrasive plane. Secondly, the mass ratio of m_{abr} and $m_{\text{abr, max}}$ is chosen for convenience, and can be replaced by a volumetric ratio without affecting the result.

With the equivalent abrasive size, the second extension has effectively been reduced to the case of large abrasives, which is similar to the first extension. The ensuing calculations will therefore be modified from the work done for the first extension.

5.3.2 Number of active particles

As equivalent abrasive diameter is typically larger than the critical value given by the abrasive size criterion, the same steps used for the first extension are applicable here. The expression of number of active carbonyl iron particles, N_{CI} , is therefore given by:

$$N_{CI} = \frac{4}{\sqrt{3}} A_{\text{contact}} \cdot \frac{1}{(D_{CI} + D_{\text{abr, eqv}})^2} \quad (5.19)$$

where Equation 5.10 is adopted with the abrasive size term, D_{abr} , replaced by the equivalent abrasive diameter, $D_{\text{abr, eqv}}$.

To calculate the number of active abrasives, the area available for abrasives on the abrasive plane is considered. It is given by:

$$A_{\text{available, abr plane}} = \frac{1}{2\sqrt{3}} \pi \cdot (A_{\text{contact}} - N_{CI} \cdot \pi a^2) \quad (5.20)$$

Equation 5.19 and the geometrical relationship $a^2 = \frac{1}{4} D_{\text{abr}} (2D_{CI} - D_{\text{abr}})$ are substituted into Equation 5.20. Note that the geometrical relationship is based on the original abrasive size and not the equivalent abrasive size. $A_{\text{available, abr plane}}$ is then given by:

$$A_{\text{available, abr plane}} = \frac{1}{2\sqrt{3}} \pi \cdot \left(1 - \frac{1}{2\sqrt{3}} \pi \cdot \frac{2D_{\text{abr}}}{D_{CI} + D_{\text{abr, eqv}}} \cdot \frac{2D_{CI} - D_{\text{abr}}}{D_{CI} + D_{\text{abr, eqv}}} \right) \quad (5.21)$$

Then, with similar steps as seen in the first extension, the number of active abrasives, N_{abr} , is given by:

$$N_{\text{abr}} = \frac{2}{\sqrt{3}} \cdot A_{\text{contact}} \cdot \left(1 - \frac{1}{2\sqrt{3}} \pi \cdot \frac{2D_{\text{abr}}}{D_{CI} + D_{\text{abr, eqv}}} \cdot \frac{2D_{CI} - D_{\text{abr}}}{D_{CI} + D_{\text{abr, eqv}}} \right) \cdot \frac{1}{D_{\text{abr}}^2} \quad (5.22)$$

Note that term $v_{\text{abr}}/v_{\text{abr, max}}$, which is required when $v_{\text{abr}} < v_{\text{abr, max}}$, is not necessary because for this extension, $v_{\text{abr}} > v_{\text{abr, max}}$ is always true. Equations 5.19 and 5.22 are the

proposed expressions for the number of active carbonyl iron particles, N_{CI} , and the number of active abrasives, N_{abr} , to be used in the proposed extension to the base model when the abrasive volume exceeds the critical value given by the abrasive volume criterion.

5.3.3 Force per particle

Expressions for force per carbonyl iron particle, F_{CI} , and force per abrasive, F_{abr} , are similarly unchanged. The expressions derived for the base model remains valid. However, their values are indirectly affected by modifications made to N_{CI} and N_{abr} .

5.4 SUMMARY

In this chapter, two extensions have been proposed for the base model derived in the previous chapter. The first extension is applicable when the abrasive size exceeds the critical value given by the abrasive size criterion. The second extension is applicable when the abrasive volume exceeds the critical value given by the abrasive volume criterion. With the two extensions, the material removal rate model covers a more diverse range of conditions for the new MFAF process.

In the event where both the criteria are not fulfilled, an equivalent abrasive size, which was used in the second extension, may be similarly considered to reduce the condition to the case abrasive volume exceeding the critical value.

All the key equations for the base model and the two extensions are given below.

5.4.1 Material removal rate expression

The general material removal rate expression, which is applicable to the base model and both the extensions, is given by:

$$\text{MRR} = \underbrace{k_{\text{CI}} \cdot N_{\text{CI}} \cdot \left(\frac{3F_{\text{CI}}}{8E} \right) \cdot v}_{\text{MRR component for carbonyl iron particles}} + \underbrace{k_{\text{abr}} \cdot N_{\text{abr}} \cdot \left(\frac{3F_{\text{abr}}}{8E} \right) \cdot v}_{\text{MRR component for abrasives}} \quad (4.9)$$

5.4.2 Number of active particles

For the base model:

$$N_{\text{CI}} = \frac{2}{\sqrt{3}} A_{\text{contact}} \cdot \frac{1}{D_{\text{CI}}^2} \quad (4.18)$$

$$N_{\text{abr}} = \frac{2}{\sqrt{3}} \cdot A_{\text{contact}} \cdot \left(1 - \frac{1}{2\sqrt{3}} \pi \cdot \frac{D_{\text{abr}}}{D_{\text{CI}}} \cdot \frac{2D_{\text{CI}} - D_{\text{abr}}}{D_{\text{CI}}} \right) \cdot \frac{1}{D_{\text{abr}}^2} \cdot \frac{v_{\text{abr}}}{v_{\text{abr, max}}} \quad (4.25)$$

For first extension, where abrasive size exceeds the critical value given by the abrasive size criterion:

$$N_{\text{CI}} = \frac{4}{\sqrt{3}} A_{\text{contact}} \cdot \frac{1}{(D_{\text{CI}} + D_{\text{abr}})^2} \quad (5.10)$$

$$N_{\text{abr}} = \frac{2}{\sqrt{3}} \cdot A_{\text{contact}} \cdot \left(1 - \frac{1}{2\sqrt{3}} \pi \cdot \frac{2D_{\text{abr}}}{D_{\text{CI}} + D_{\text{abr}}} \cdot \frac{2D_{\text{CI}} - D_{\text{abr}}}{D_{\text{CI}} + D_{\text{abr}}} \right) \cdot \frac{1}{D_{\text{abr}}^2} \quad (5.14)$$

For second extension, where abrasive volume exceeds critical value given by the abrasive volume criterion:

$$N_{\text{Cl}} = \frac{4}{\sqrt{3}} A_{\text{contact}} \cdot \frac{1}{\left(D_{\text{Cl}} + D_{\text{abr, eqv}}\right)^2} \quad (5.19)$$

$$N_{\text{abr}} = \frac{2}{\sqrt{3}} \cdot A_{\text{contact}} \cdot \left(1 - \frac{1}{2\sqrt{3}} \pi \cdot \frac{2D_{\text{abr}}}{D_{\text{Cl}} + D_{\text{abr, eqv}}} \cdot \frac{2D_{\text{Cl}} - D_{\text{abr}}}{D_{\text{Cl}} + D_{\text{abr, eqv}}}\right) \cdot \frac{1}{D_{\text{abr}}^2} \quad (5.22)$$

The equivalent abrasive diameter, $D_{\text{abr, eqv}}$ is given by:

$$D_{\text{abr, eqv}} = \left(\sqrt{2} - 1\right) D_{\text{Cl}} \cdot \left(\frac{m_{\text{abr}}}{m_{\text{abr, max}}}\right)^{\frac{1}{2}} \quad (5.18)$$

5.4.3 Force per particle

For the base model and both extensions:

$$F_{\text{Cl}} = BD_{\text{Cl}}^3 \cdot \left(k_{\text{F, Cl}} \cdot BD_{\text{Cl}}^3 \cdot \frac{N_{\text{Cl}} \cdot D_{\text{Cl}}^2}{N_{\text{Cl}} \cdot D_{\text{Cl}}^2 + N_{\text{abr}} \cdot D_{\text{abr}}^2} + k_{\text{F, abr}} \cdot \frac{N_{\text{abr}} \cdot D_{\text{abr}}^2}{N_{\text{Cl}} \cdot D_{\text{Cl}}^2 + N_{\text{abr}} \cdot D_{\text{abr}}^2} \right) \quad (4.30)$$

$$F_{\text{abr}} = D_{\text{abr}}^2 \cdot \left(k_{\text{F, Cl}} \cdot BD_{\text{Cl}}^3 \cdot \frac{N_{\text{Cl}} \cdot D_{\text{Cl}}^2}{N_{\text{Cl}} \cdot D_{\text{Cl}}^2 + N_{\text{abr}} \cdot D_{\text{abr}}^2} + k_{\text{F, abr}} \cdot \frac{N_{\text{abr}} \cdot D_{\text{abr}}^2}{N_{\text{Cl}} \cdot D_{\text{Cl}}^2 + N_{\text{abr}} \cdot D_{\text{abr}}^2} \right) \quad (4.31)$$

Chapter 6

Experimental verification of material removal rate model

6.1 INTRODUCTION

In the previous chapters, a base removal rate model and two extensions were proposed for the new MFAF process. The proposed model and extensions established a relationship between the removal rate and process parameters such as the abrasive size, abrasive concentration, carbonyl iron particle size, and magnetic flux density at the polishing zone. However, the model and extensions are theoretical, and are based on several assumptions of ideal conditions. Therefore, there is a need to verify the model and extensions against experimental data.

In this chapter, experiments are designed to verify both the base model and the two extensions. Specifically, experiments are conducted by varying the abrasive size, abrasive concentration, carbonyl iron particle size and magnetic field strength to quantify their effects on the removal rate. Firstly, a partial set of the data points obtained is used to calculate the four constants in the model. Using the calculated constants, theoretical curves are generated from the base model and extensions. The remaining data points are then compared against the theoretical curves to validate the base model and extensions.

In addition, the base model and extensions are studied and analysed to understand the theoretical relationships between removal rate and the process parameters. Based on these theoretical relationships, a description for the material removal mechanism of the new MFAF process is constructed.

6.2 SETUP OF EXPERIMENT

6.2.1 Workpiece

The workpiece for the experiments were stainless steel (SUS316) blocks. SUS316 is austenitic and therefore non-magnetic. Workpieces of size 25 mm × 25 mm × 10 mm were cut to size from a stock square bar using the wire EDM process. Both the 25 mm × 25 mm faces were used for polishing during the experiments, while the 25 mm × 10 mm faces were used for clamping.

The surface produced by wire EDM was covered in an oxide layer. This oxide layer was removed by sandpapering, which was done manually on a sample grinder and polisher (Struers, TegraPol-25) with sandpapers of mesh size 320 rotating at 100 revolutions per minute. The resulting surface was planar with a surface texture of 0.2 Ra μm . Figure 6.1 is the photograph of a workpiece after wire EDM, and another workpiece after sandpapering.

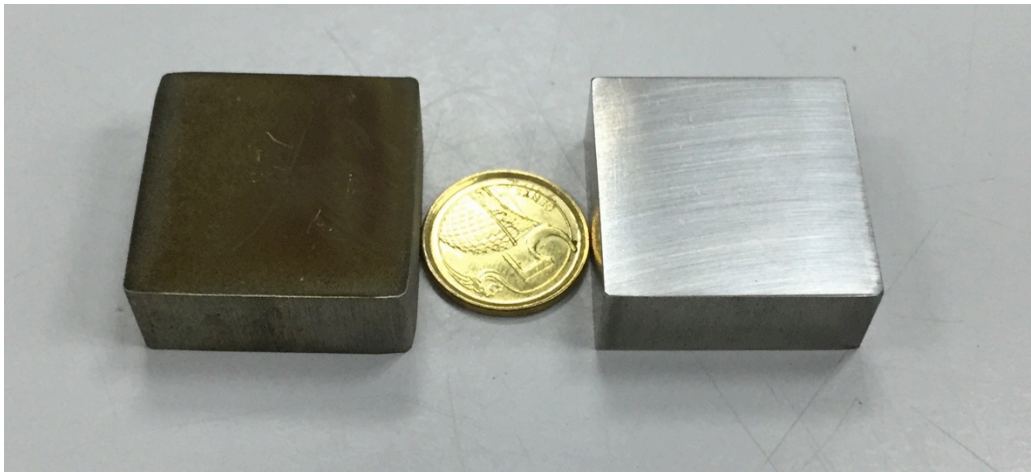


Figure 6.1: SUS316 workpieces after wire EDM (left) and after sandpapering to remove oxide layer (right).

6.2.2 Finishing media

The finishing media used consists of three components: magnetic carbonyl iron particles, non-magnetic abrasives, and carrier fluid. For carbonyl iron particles, commercially available products with different grades from BASF were used. They were CM grade (7.0 μm – 9.5 μm mean diameter), CS grade (6.0 μm – 7.0 μm mean diameter), and CC grade (3.8 μm – 5.3 μm mean diameter). For abrasives, commercially available alumina abrasives from Kemet and Universal Photonics were used, with mean diameter ranging from 0.6 μm to 15 μm . For carrier fluid, distilled water was used. No stabilizer or surfactant was added due to the short experiment runs (less than 10 minutes for each dose of finishing media).

To mix the finishing media, the required mass of each component was calculated and weighed. The components were then mixed and stirred manually until the finishing media was visually homogeneous. Since no stabilizer or surfactant was used, the finishing media was not stored for a long duration and was only prepared immediately before use. In addition, the finishing media was changed after every experimental run to eliminate variations arising from media conditions.

After the finishing media was supplied to the polishing tool, 5 ml of distilled water was manually supplied from a wash bottle every five minutes. This was to replenish the water scattered due to centrifugal forces while polishing.

6.2.3 Machine setup

The machine setup consists of the polishing unit prototype mounted on a desktop CNC milling machine (CNC Masters, CNC Baron). The position and feed rate of the polishing unit in the x -, y - and z -axis, and the spindle revolution speed are all numerically controlled. The prototype was designed in-house and custom-built. The setup was the

same as shown in an earlier chapter in Figure 3.15. A schematic diagram of the setup is shown in Figure 6.2.

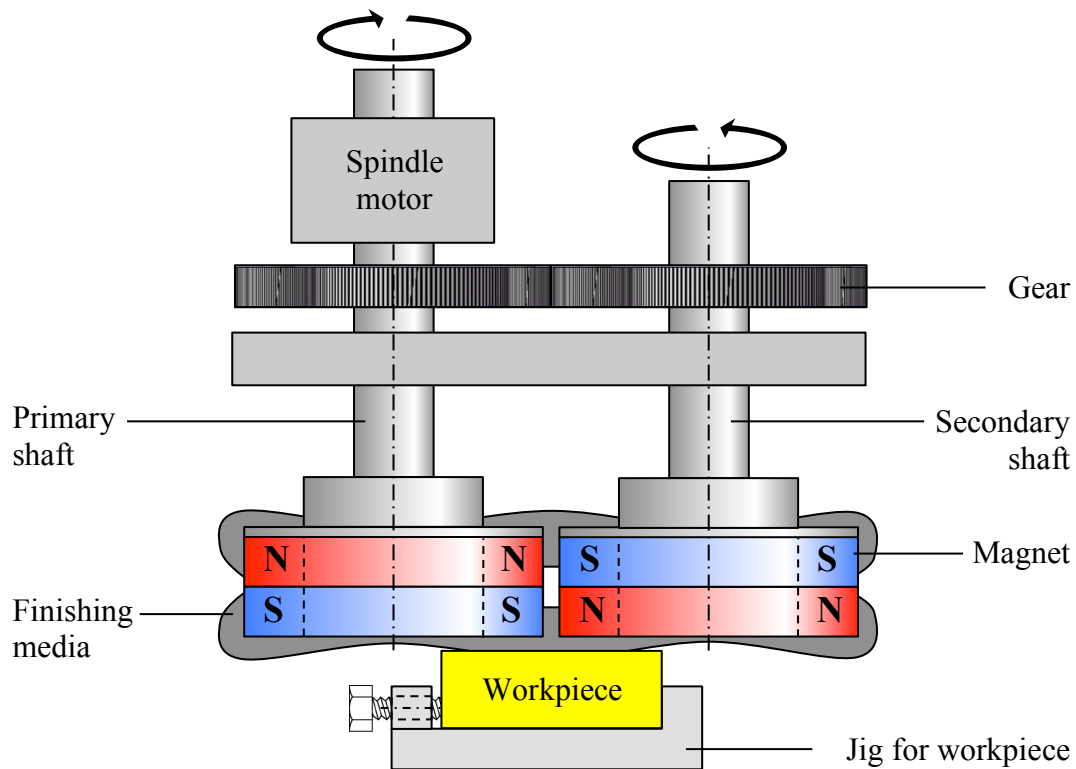


Figure 6.2: Schematic diagram of the polishing unit with a double-tool configuration.

The polishing unit consists of two parallel shafts made of aluminum alloy (6000 series), with a ring-shaped neodymium permanent magnet (grade N35, 30 mm outer diameter, 18 mm inner diameter, 12 mm thick, polarized along axis of symmetry) attached to the end of each shaft. The two magnets were arranged in opposite polarity, such that there is an attractive magnetic force between them. The axes of the two shafts were positioned 31 mm apart, meaning an air gap of 1 mm existed between the two

magnets. The spindle motor of the CNC machine drove one of the shafts, while the other was driven by a gear mechanism. As a result, the two shafts rotate in opposite directions.

The workpiece was clamped by a jig made of aluminum alloy (6000 series). Note that both the polishing unit and jig were made of aluminum alloy, and therefore they do not interfere with the magnetic field of the neodymium magnets.

6.2.4 Material removal rate measurement

To measure the removal rate, the workpiece surface was polished only at a selected area, instead of the whole surface. The height difference between the polished area and unpolished area is the material removal depth. Further, it was considered that the removal rate is linearly related to polishing time. Therefore, the removal rate can be calculated from the removal depth by dividing it with the polishing time. In this chapter, removal rate and removal depth are used interchangeably. The methodology and complete technical details of removal rate measurement are available in Appendix B.

6.2.5 Experimental conditions

Two sets of experiments were designed. The first set of experiments was designed to examine the effect of an increasing abrasive size on the removal rate. Abrasives used in the finishing media were varied between 0.6 μm and 15 μm . Also, experiments were conducted for two different amount of supply of abrasives, at 1.0 g and 2.7 g. The supplied amount of 2.7 g corresponds to the critical abrasive-to-carbonyl-iron volumetric ratio according to the abrasive volume criterion given earlier in Equation 4.12, while the supplied amount of 1.0 g was arbitrarily chosen for further comparisons. Table 6.1 shows the experimental conditions for this first set of experiments.

Table 6.1: Experimental conditions for first set of experiments, where abrasive size varies between 0.6 μm and 15 μm .

Machine	CNC Baron Milling Machine
Workpiece	Stainless steel <i>Dimension: 25 mm x 25 mm x 10 mm</i> <i>See Section 6.2.1 for details</i>
Polishing unit	
Magnet-to-magnet gap, w_{gap}	1 mm
Magnet-to-workpiece gap, z	1 mm
Spindle revolutions	300 /min
Finishing media	
Carbonyl iron particles	BASF, CM grade <i>Supplied mass: 20 g</i> <i>Mean particle size: 7.0 μm – 9.5 μm</i>
Abrasives	Alumina (Universal Photonics) <i>Supplied mass: 1.0 g, 2.7 g</i> <i>Mean particle size: 0.6 μm</i> Alumina (Kemet) <i>Supplied mass: 1.0 g, 2.7 g</i> <i>Mean particle size: 3 μm – 15 μm</i>
Carrier fluid	Distilled water <i>Supplied mass: 8 g</i> <i>Replenish 5 g every 5 minutes</i>
Polishing method	Dwell #1 <i>Duration: 15 s</i> <i>For polishing force measurement</i> Dwell #2 <i>Duration: 5 minutes</i> <i>For material removal depth measurement</i>

The second set of experiments was designed to examine the effect of a varying abrasive concentration on the removal rate. Abrasive concentration was varied by preparing finishing media with different abrasive-to-carbonyl-iron volumetric ratio, v_{abr} / v_{CI} . This was achieved by varying the abrasive mass between 0 g to 8 g. In effect, the ratio of v_{abr} / v_{CI} was between 0 and 0.768. Note that the abrasive saturation as given by the abrasive volume criterion in Equation 4.12 occurs when v_{abr} / v_{CI} is 0.259. In addition, two different sizes of alumina abrasives (0.6 μm and 15 μm) were used for the experiments for further comparisons. Table 6.2 shows the experimental conditions for this second set of experiments.

Table 6.2: Experimental conditions for second set of experiments.

Machine	CNC Baron Milling Machine
Workpiece	Stainless steel <i>Dimension: 25 mm \times 25 mm \times 10 mm</i> <i>See Section 6.2.1 for details</i>
Polishing unit	
Magnet-to-magnet gap, w_{gap}	1 mm
Magnet-to-workpiece gap, z	1 mm
Spindle revolutions	300 /min
Finishing media	
Carbonyl iron particles	BASF, CM grade <i>Supplied mass: 20 g</i> <i>Mean particle size: 7.0 μm – 9.5 μm</i>

Abrasive particles	Alumina (Universal Photonics)
	<i>Supplied mass: 2.7 g</i> <i>Mean particle size: 0.6 μm</i>
	Alumina (Kemet)
	<i>Supplied mass: 2.7 g</i> <i>Mean particle size: 15 μm</i>
Carrier fluid	Distilled water
	<i>Supplied mass: 8 g</i> <i>Replenish 5 g every 5 minutes</i>
Polishing method	Dwell #1
	<i>Duration: 15 s</i>
	<i>For polishing force measurement</i>
	Dwell #2
	<i>Duration: 5 minutes</i>
	<i>For material removal depth measurement</i>

6.3 EXPERIMENTAL RESULTS AND DISCUSSIONS

6.3.1 Abrasive size – Experimental results

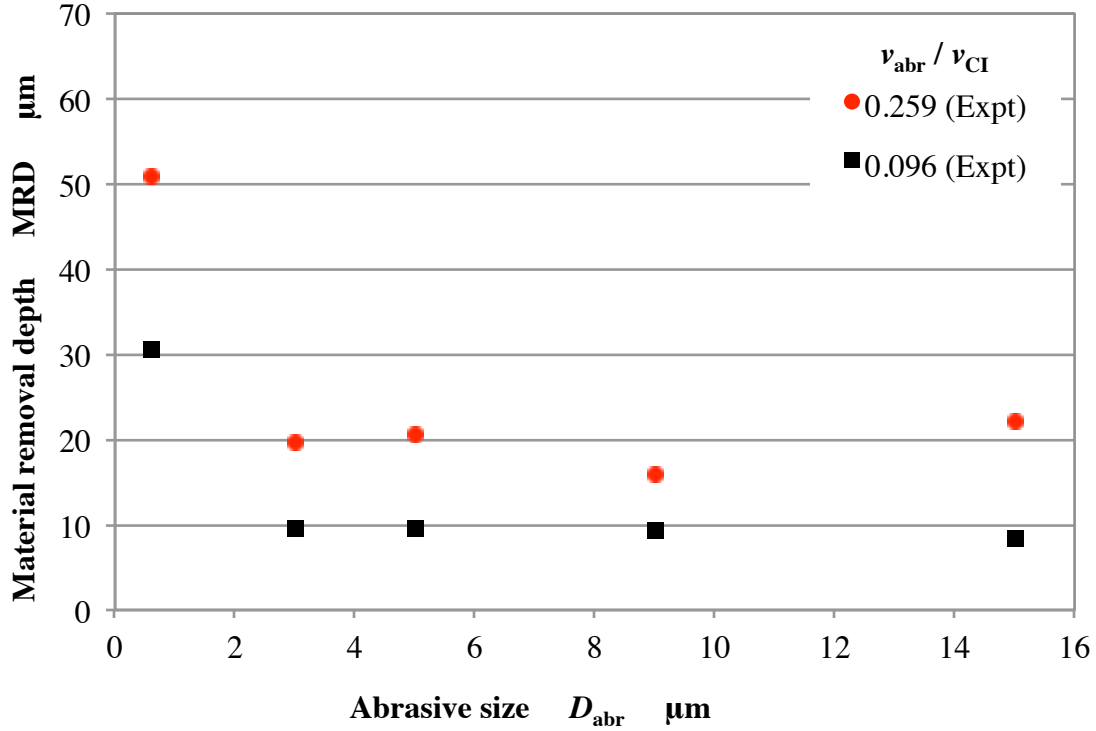


Figure 6.3: Experimental results of material removal depth against abrasive size.

Figure 6.3 shows the data points obtained from the first set of experiment where the abrasive size varies. No error bar is shown as the error range is very small. Firstly, it is found that the material removal depth decreases when the abrasive size is increased from 0.6 μm to 15 μm . This is true for both ratios of v_{abr} / v_{CI} (0.096 and 0.259), although higher removal rate is observed for when v_{abr} / v_{CI} is 0.259. This is expected, as a higher abrasive concentration translates to an increased number of active abrasives for material removal from the workpiece surface.

Note that caution was exercised by repeating this set of experiments several times to confirm the observed trend between the material removal depth and the abrasive size. There are two reasons why caution was warranted. Firstly, reported studies in the literature have not shown a universally agreed upon trend between removal rate and abrasive size. In fact, conflicting trends are sometimes reported even for the same process. An example is seen for the chemical-mechanical polishing (CMP) process, where Jeng and Huang [1] reported that the removal rate decreases with an increasing abrasive size, while Lee et al. [2] reported the opposite, where removal rate increases with an increasing abrasive size.

Secondly, caution was necessary because the new MFAF process is novel, and therefore cannot be compared *ceteris paribus* with other reported studies in the literature. Shinmura *et al.* [3] for example have reported for the magnetic abrasive finishing (MAF) process that an increasing particle size contributes to an increasing removal rate, which contradicts the experimental results reported above. However, the MAF process is substantially different to the new MFAF process even though both are magnetic field-assisted processes.

Thus, the repeatability of the results gives confidence to the observed trend between removal rate and abrasive size reported above.

6.3.2 Abrasive size – Theoretical model

In this section, theoretical curves were calculated and generated for the two sets of data points using the proposed model and extensions. To that end, suitable values for the four constants in the proposed model must be chosen. The four constants are the MRR factors k_{CI} and k_{abr} , and the force factors $k_{F, CI}$ and $k_{F, abr}$. The values of these constants were

selected iteratively by trial and error, based on the proposed guideline that $k_{\text{CI}} \ll k_{\text{abr}}$ (since abrasives remove material at a substantially higher rate than carbonyl iron particles) and $k_{F,\text{abr}} \ll k_{F,\text{CI}}$ (since neighbouring carbonyl iron particles provide much greater supporting contact force than neighbouring abrasives). The value of $k_{F,\text{CI}}$ was arbitrarily chosen as 1. In addition, the values of k_{CI} and $k_{F,\text{CI}}$ were scaled accordingly so that the absolute values of the removal rate given by the proposed model was comparable to the removal rate obtained experimentally. Table 6.3 shows the values that were selected for the constants.

Table 6.3: Values of constants for theoretical model.

	Values	Unit
MRR factors		
k_{CI}	1.5×10^4	Dimensionless
k_{abr}	1.5×10^6	Dimensionless
Force factors		
$k_{F,\text{CI}}$	1	$\text{N T}^{-2} \text{m}^{-6}$
$k_{F,\text{abr}}$	1×10^{-8}	$\text{N T}^{-1} \text{m}^{-3}$

The values of these constants were universal for all experimental conditions reported in this chapter. However, these values may not be applicable in a different set-up if there are changes in the polishing unit dimensional parameters (such as the magnet-to-magnet gap, w_{gap} , or the magnet-to-workpiece gap, z) or the material type of abrasives. In addition, some of these constants were related to each other in a multiplicative nature. Specifically, there are four multiplicative pairs in the proposed model: (1) $k_{\text{CI}} - k_{F,\text{CI}}$, (2)

$k_{\text{CI}} - k_{F, \text{abr}}$, (3) $k_{\text{abr}} - k_{F, \text{CI}}$, and (4) $k_{\text{abr}} - k_{F, \text{abr}}$. For each of these pairs, multiplying one member by k and dividing the other member by k resulted in no change on the removal rate given by the model. Hence, the relative values between the constants are of greater importance than their absolute values. Figure 6.4 illustrates the four multiplicative pairs between the constants for greater clarity.

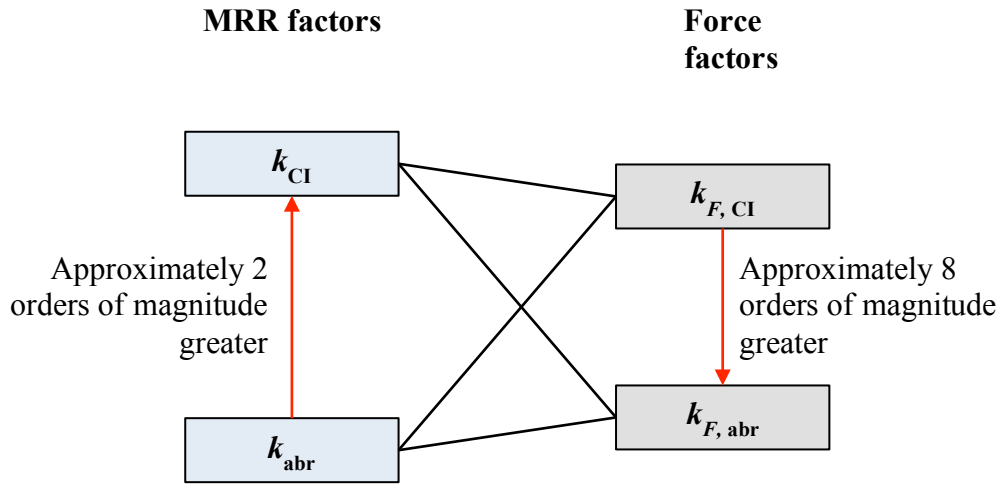


Figure 6.4: Multiplicative relationships (black lines) and relative relationships (red arrows) between the four constants in the proposed model and extensions.

Using the values of constants given in Table 6.3, theoretical curves were generated to fit the two sets of experimental data reported earlier. Figure 6.5 is a reproduction of the experimental data from Figure 6.3, with the theoretical curves now included.

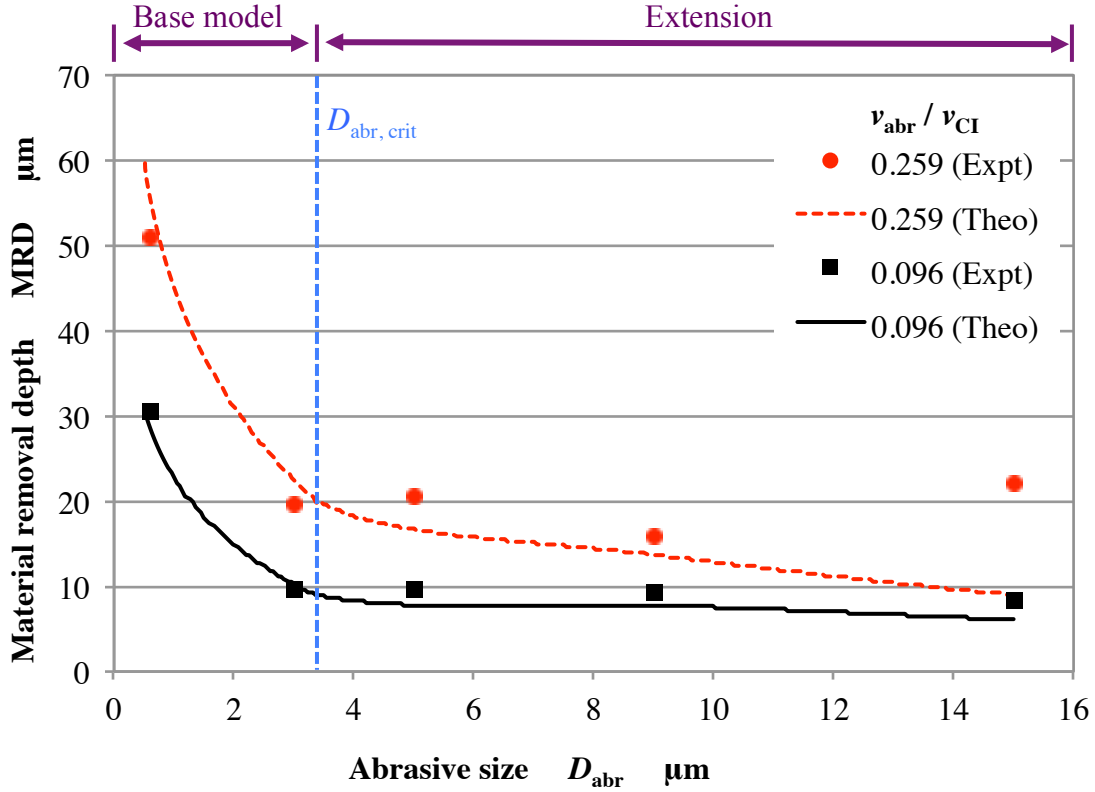


Figure 6.5: Experimental results and theoretical curves of material removal depth against abrasive size.

Both the theoretical curves appear as continuous curves in Figure 6.5, but each are in fact composed of the base model and the extension for abrasive size criterion given in Equation 4.11, which is reproduced below for reference.

$$D_{abr} \leq (\sqrt{2} - 1) D_{CI} \quad (4.11)$$

Substituting $D_{CI} = 8.25 \mu m$, the critical value of abrasive size, $D_{abr, crit}$, was calculated to be $3.4 \mu m$. This was the critical value for the abrasive size according to the proposed model and is demarcated in Figure 6.5 by the blue vertical line. In the zone to the left of the blue vertical line (when abrasive size is between $0.5 \mu m$ and $3.4 \mu m$), the

proposed base model is valid and is applied. In the zone to right of the blue vertical line (when abrasive size is between 3.4 μm and 15 μm), the abrasive size criterion is not obeyed. Hence, the extension for abrasive size criterion proposed in Section 5.2 was used instead. By design, both the base model and extension are equal to each other at the transition point of 3.4 μm .

Both the theoretical curves were a good fit to the experimental data. Therefore, for the range of parameters tested, the proposed base model and the extension for abrasive size criterion were validated for the new MFAF process. Applying the base model and extension for conditions not within the tested range of parameters may result in deviation with experimental data, as material removal mechanism may be substantially different for extreme cases, such as when the abrasive size is very small or very large.

6.3.3 Abrasive size – further discussion

In this section, the proposed model was further studied to establish a deeper understanding of the resulting theoretical trend between removal rate and the abrasive size. Specifically, the effects of an increasing abrasive size on the number of active carbonyl iron particles, number of active abrasives, force per carbonyl iron particle, force per abrasive particle, and ultimately the removal rate were analysed theoretically.

Firstly, the number of active carbonyl iron particles, N_{CI} , and the number of active abrasives, N_{abr} , were considered. In the following discussion, it is further considered that the abrasive concentration was at saturation level, which corresponded to a value of 0.259 for $v_{\text{abr}} / v_{\text{CI}}$. When the abrasive size does not exceed the critical value, N_{CI} is unchanged by an increasing abrasive size, since the carbonyl iron matrix is assumed to be in the ideal FCC configuration and is unperturbed. The value of N_{CI} is therefore constant, which can

be seen in the zone to the left of the blue vertical line in Figure 6.6(a), where the base model is applied.

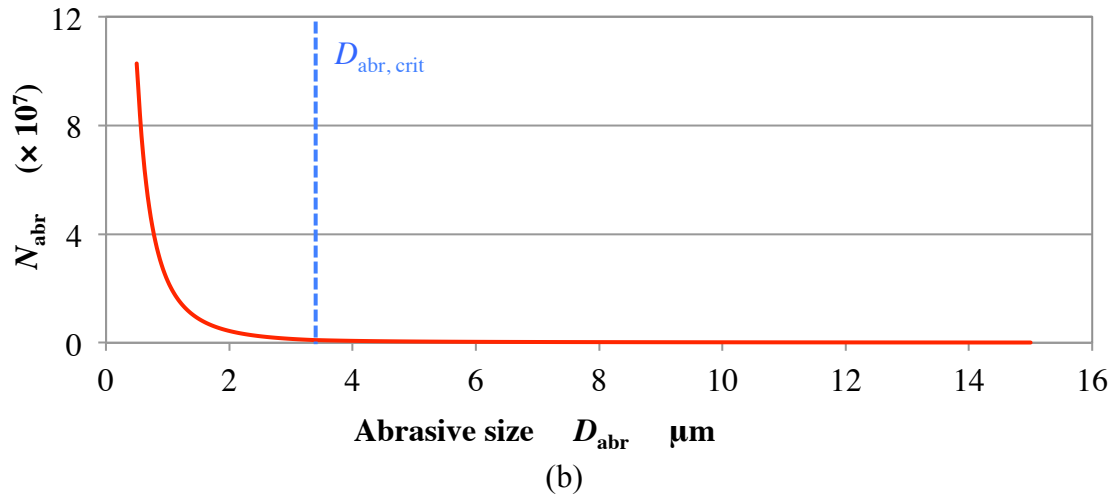
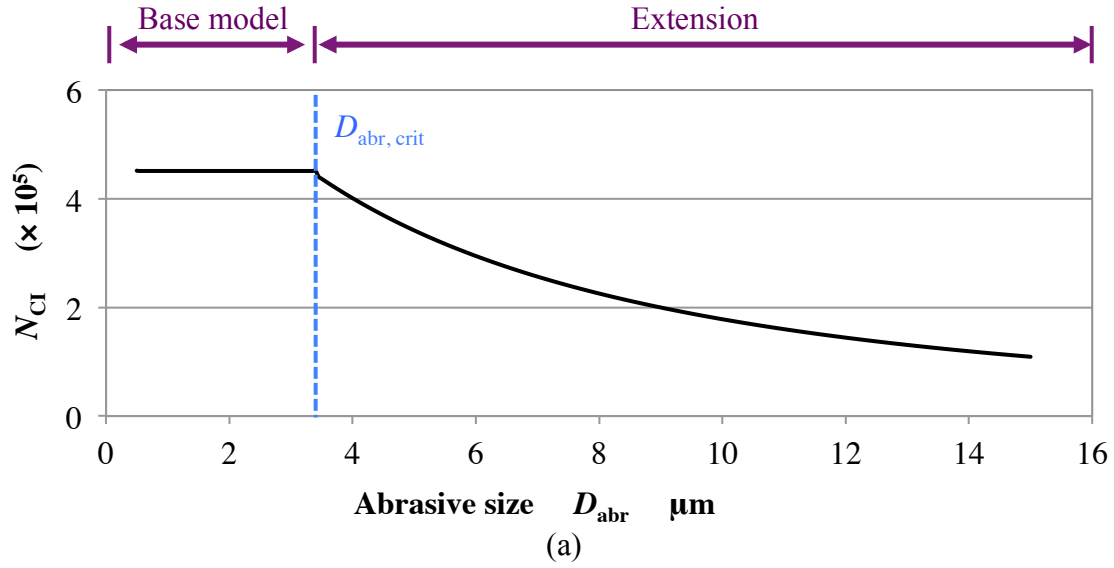


Figure 6.6: (a) Number of active carbonyl iron particles (black) and (b) number of active abrasives (red) against abrasive size, according to theoretical model.

On the other hand, N_{abr} decreases with an increasing abrasive size because the fixed interstitial spaces within the carbonyl iron matrix can only accommodate a smaller

number of the larger abrasives. In Figure 6.6(b), this can be seen in the zone to the left of the blue vertical line.

As the abrasive size increases beyond $D_{abr, crit}$, the carbonyl iron matrix is compromised to create additional space for the larger abrasives. In the proposed extension, additional space is created by considering an orderly increase in the distance between carbonyl iron particles in the matrix. As a result, the density of carbonyl iron particles per unit volume decreases, which means that N_{CI} also decreases. This is seen in the zone to the right of the blue vertical line in Figure 6.6(a), where the proposed extension for abrasive size criterion is applied. Despite the additional space created by the reduced density of carbonyl iron particles, N_{abr} continues to drop as the additional spaces required for larger abrasives dominates the additional space created. This is seen in the zone to the right of the blue vertical line in Figure 6.6(b).

Next, the force per carbonyl iron particle, F_{CI} , and force per abrasive particle, F_{abr} , was considered. Force per particle is dependent on the property of the particle itself, as well as the composition and properties of the neighbouring particles. Note that the values of force given in the following discussion are relative values instead of the true force per particle, as they were calculated based on arbitrarily valued constants. Hence, the absolute values carry no physical meaning, although the trends given by the model are still valid.

As abrasive size increases to $D_{abr, crit}$, F_{CI} increases slightly because the presence of larger abrasives as neighbours provides greater contact forces. F_{abr} also increases, with the main factor being the increase in the size of the abrasive particle itself, since force per abrasive particle is also related to its own projected area. These can be seen in the zone to the left of the blue vertical line in Figures 6.7(a) and (b) respectively, where the base model is applied.

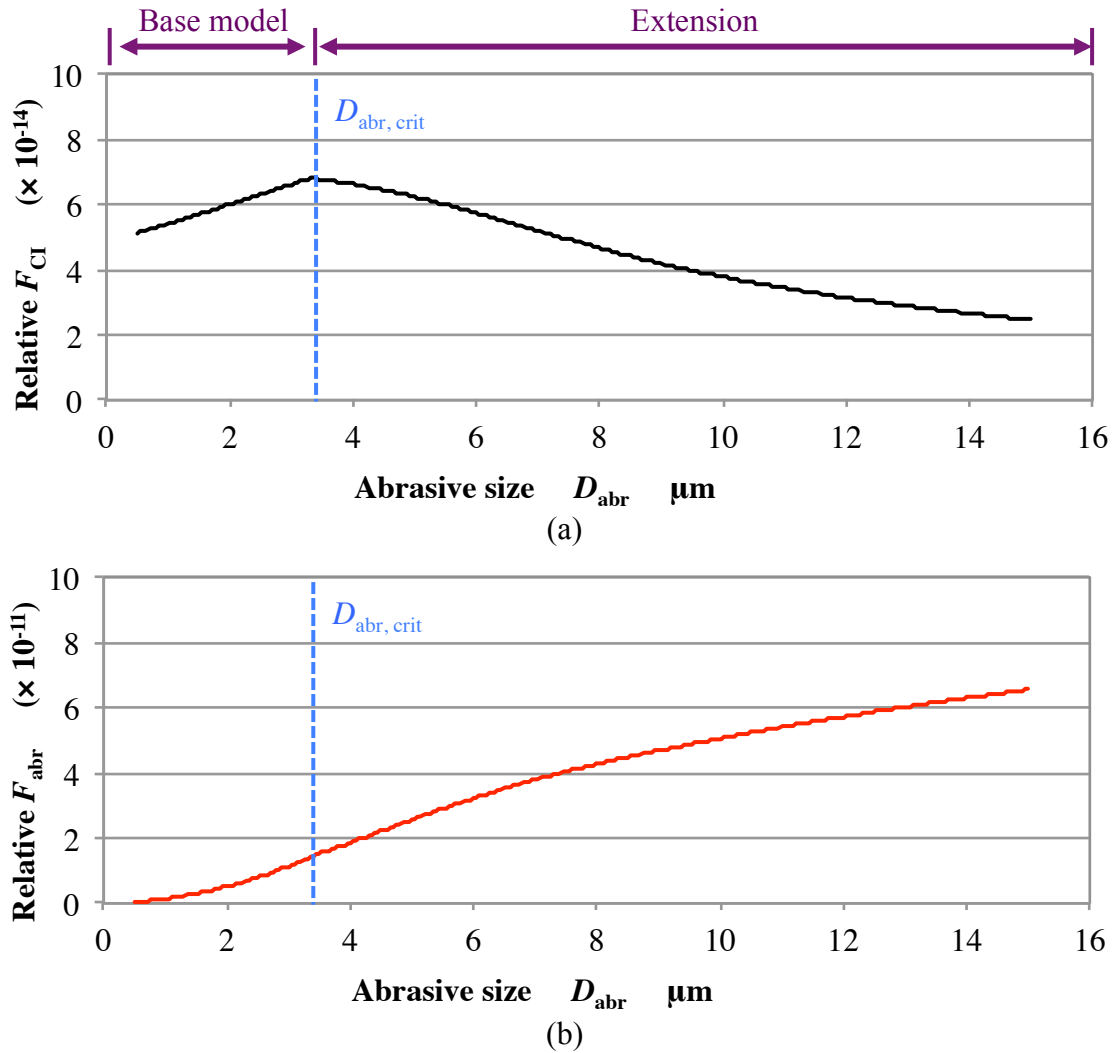


Figure 6.7: (a) Force per carbonyl iron particle (black) and (b) force per abrasive particle (red) against abrasive size, according to theoretical model.

When abrasive size increases beyond $D_{abr, crit}$, the value of F_{CI} declines, as seen in the zone to the right of the blue vertical line in Figure 6.7(a), where the extension for abrasive size criterion is applied. This is reasonable because earlier analysis established that the N_{abr} increases while the N_{CI} decreases. As a result, carbonyl iron particles constitute a lower proportion of the neighbouring particles, resulting in reduced

supporting contact forces. Ultimately, this translates into a decrease in F_{CI} . The same change in the composition of neighbouring particles also happens for abrasives, although the reduced supporting contact forces are mitigated by an increasing abrasive size. From the theoretical curve in Figure 6.7(b), it can be seen that the increase in abrasive size is the dominant factor, resulting in an overall increase of F_{abr} . The effect of decreasing supporting contact forces is manifested in the declining gradient of the theoretical curve.

In summary, an increasing abrasive size caused an increase in F_{abr} , which was favourable for increasing the removal rate, but also caused a significant decrease in N_{abr} , which was unfavourable for increasing removal rate. Between these two competing factors, the drop in N_{abr} dominated the increase in F_{abr} , ultimately resulting in a decreasing removal rate when the abrasive size was increased. This has been shown earlier in Figure 6.5. For the carbonyl iron particles, both the F_{CI} and N_{CI} decreased with an increasing abrasive size and the removal rate attributed to carbonyl iron particles was therefore comprehensively lower. However, the removal rate attributed to carbonyl iron particles was dwarfed by the removal rate attributed to abrasives. Therefore, the reduction in the removal rate component for carbonyl iron particles did not significantly change the overall removal rate.

6.3.4 Abrasive concentration – Experimental results

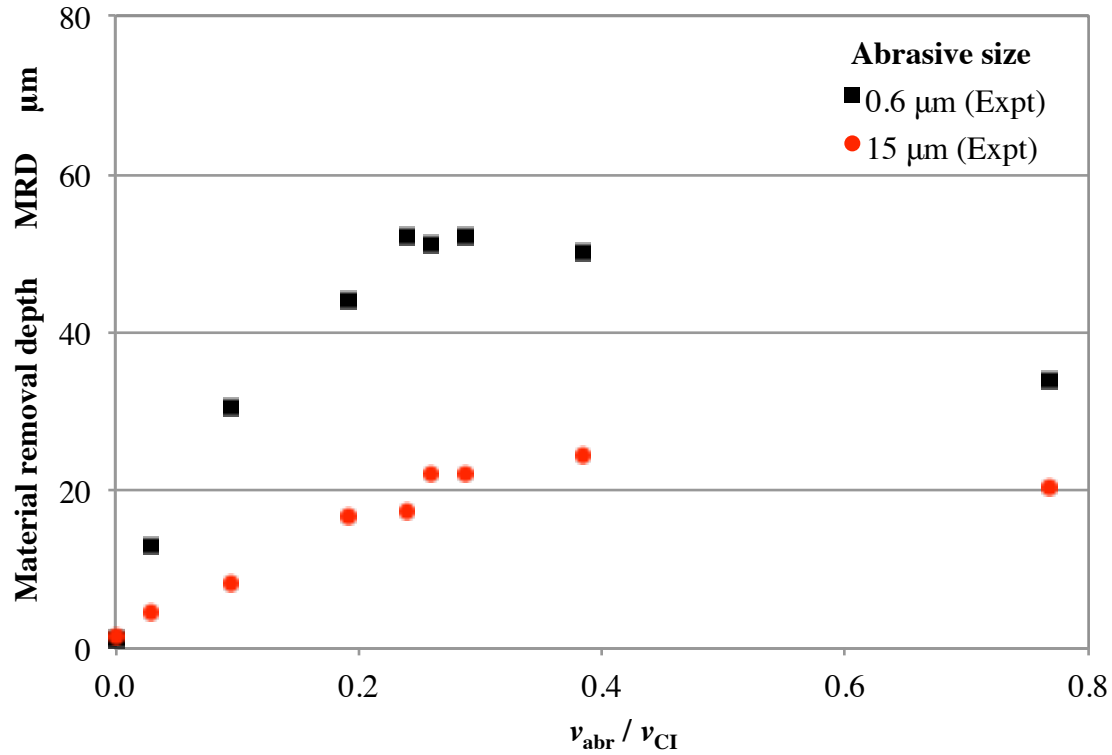


Figure 6.8: Experimental results of material removal depth against abrasive-to-carbonyl-iron volumetric ratio.

Figure 6.8 shows the data points from the second set of experiments, where the abrasive concentration in the finishing media was varied. The abrasive concentration was quantified by the abrasive-to-carbonyl-iron volumetric ratio, v_{abr} / v_{CI} . Initially, the removal depth increased with an increasing v_{abr} / v_{CI} . This initial trend was almost linear. When the ratio of v_{abr} / v_{CI} approached 0.3, an increase in the abrasive concentration no longer increased the material removal depth. On the contrary, the trend reversed and the removal depth decreased with any further increase of abrasive concentration, up to a value of 0.8 for v_{abr} / v_{CI} , which was the upper limit of the abrasive concentration in the experiments. This is true for both the abrasive sizes tested in the experiments.

The linear relationship between removal depth and abrasive concentration at low abrasive concentration was consistent with observations reported in other studies, such as Jeng and Huang [1], Jin and Zhang [4] (using experimental results from Forsberg) and Lee et al. [2]. The drop in removal depth past a certain value was less commonly reported in the literature, although Sidpara and Jain [5] had reported a similar trend for their MFAF process. In addition, many of the aforementioned studies reported that the removal rate increased with a downward concavity. Therefore, it is conceivable that the removal depth may decrease with an increasing abrasive concentration when the abrasive concentration is sufficiently high.

6.3.5 Abrasive concentration – Theoretical model

Theoretical curves were generated for the two sets of data points using the proposed model and extension. The four constants in the proposed model inherit the values previously calculated in Section 6.3.2 as there was no dimensional change in the polishing unit and experimental setup. The universality of the four constants across two sets of experiments was in fact a required condition for the proposed model to be valid. Figure 6.9 shows the experimental data from Figure 6.8 with the theoretical curves also included.

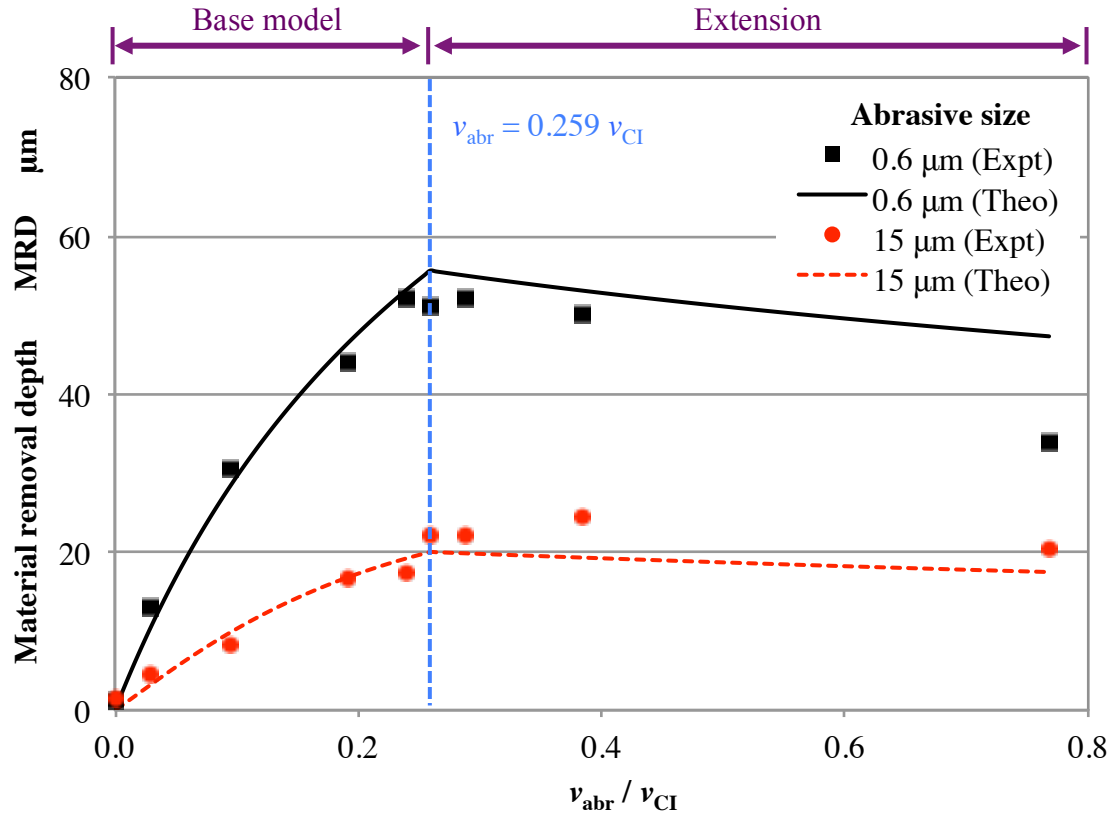


Figure 6.9: Experimental results and theoretical curves of material removal depth against abrasive-to-carbonyl-iron volumetric ratio.

The theoretical curves generated by the base model fit the data points reasonably for both the abrasive sizes of 0.6 μm and 15 μm. For the theoretical curves generated by the proposed extension for abrasive volume criterion as given by Equation 4.12, the deviation was more substantial. For both theoretical curves, there was a discontinuity when v_{abr} / v_{CI} is 0.259. This value corresponds to the transition between the base model and the proposed extension, and is demarcated by a blue vertical line in Figure 6.9. The reversal in the trend of removal depth occurred near the theoretical turning points for both sets of experimental data.

Note that the actual turning point for the removal rate may not coincide exactly with the theoretical value of 0.259 for v_{abr} / v_{CI} , as the proposed model was based on several assumptions of ideal conditions for the configuration of particles.

6.3.6 Abrasive concentration – further discussion

In this section, the proposed model was further analysed to establish a deeper understanding of the resulting theoretical trend between removal rate and the abrasive concentration. Specifically, the effects of an increasing abrasive concentration on the number of active carbonyl iron particles, number of active abrasives, force per carbonyl iron particle, force per abrasive particle, and ultimately the removal rate were analysed.

Firstly, the number of active carbonyl iron particles, N_{CI} , and the number of active abrasives, N_{abr} , were considered. For the base model, N_{CI} is a constant because the carbonyl iron matrix is unchanged even when the abrasive concentration was increased. This is shown in the zone to the left of the blue vertical line in Figure 6.10(a) where the base model is applied. N_{abr} on the other hand increases as it should with an increasing abrasive concentration. The increase of N_{abr} is almost linear because abrasives are assumed to be uniformly dispersed in the carbonyl iron matrix. This can be seen in the zone to the left of the blue vertical line in Figure 6.10(b).

In the zone to the right of the blue vertical line in Figure 6.10(a), N_{CI} decreases with an increasing abrasive concentration, as the distance between carbonyl iron particles is increased to create additional space for additional abrasives. Therefore, the density of carbonyl iron particles per unit volume is reduced and consequently less carbonyl iron particles are in contact with the workpiece surface. Likewise, more abrasives are now in contact with the workpiece surface, resulting in an increase of N_{abr} , albeit at a much

slower rate compared to the base model. This is shown in the zone to the right of the vertical blue line in Figure 6.10(b).

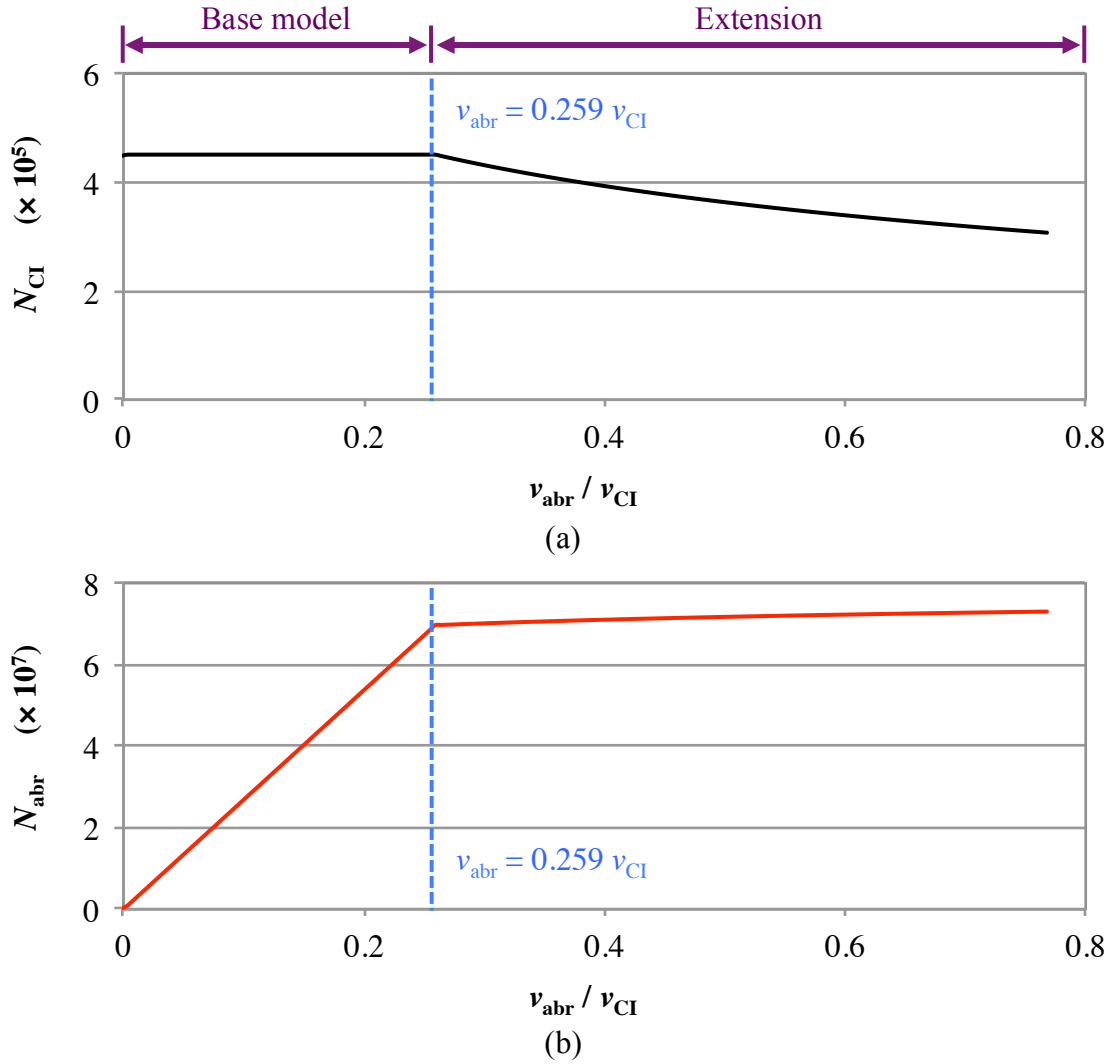


Figure 6.10: (a) Number of active carbonyl iron particles (black) and (b) number of active abrasives (red) against abrasive-to-carbonyl-iron volumetric ratio, according to theoretical model.

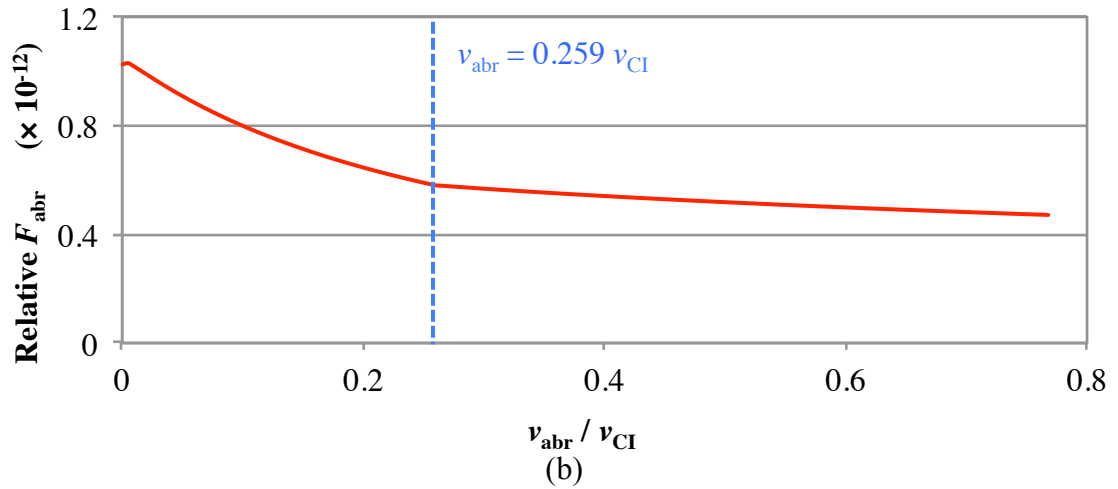
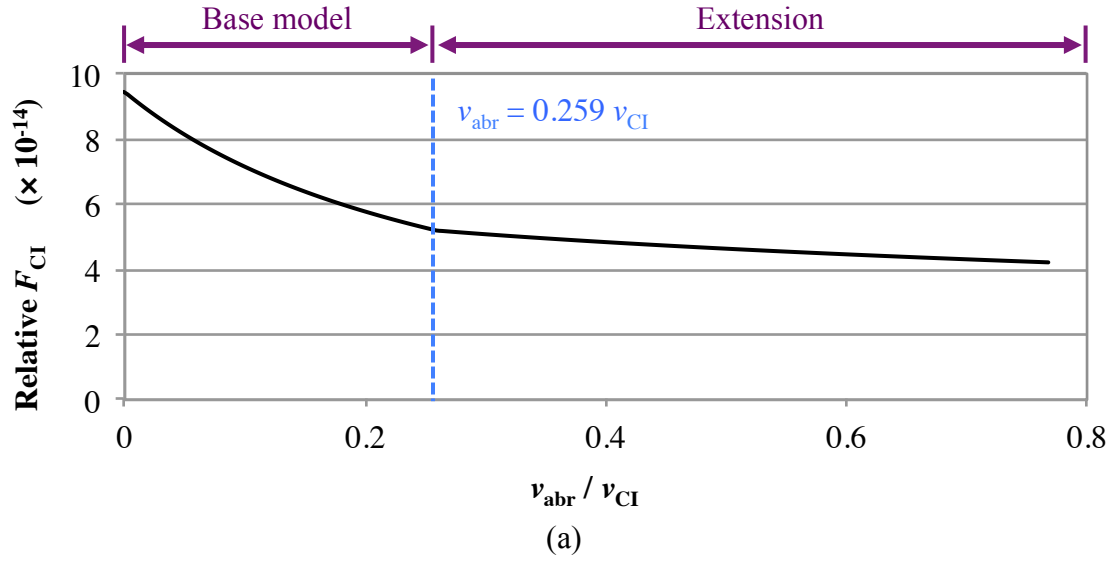


Figure 6.11: Force per carbonyl iron particle (solid line) and force per abrasive particle (dashed line), according to theoretical model.

Lastly, the force per carbonyl iron particle, F_{CI} , and the force per abrasive particle, F_{abr} was considered. As shown in Figures 6.11(a) and (b), the base model suggests that both F_{CI} and F_{abr} drop when abrasive concentration is increased. This is due to an increased proportion of neighbouring particles that are abrasives, which consequently decreases the supporting contact forces. Beyond the saturation point, two conflicting

events occur. On one hand, the decrease in N_{CI} further increases the proportion of neighbouring particles that are abrasives. On the other hand, the increase in N_{abr} greatly decelerates, which slows the change in the composition of the neighbouring particles. Combining both events, both F_{CI} and F_{abr} ultimately decrease with an increasing abrasive concentration, albeit at a slower rate compared to the base model. These can be seen in the zone to the right of the blue vertical line in Figures 6.11(a) and (b). Finally, the absolute values of F_{CI} and F_{abr} carry no physical meaning as they are calculated based on constants with arbitrarily chosen values.

Ultimately, the trend in the removal rate was a combination of the trends for N_{CI} , N_{abr} , F_{CI} and F_{abr} . The following discussion focused on N_{abr} and F_{abr} , since the material removal component attributed to abrasives dominated the component attributed to carbonyl iron particles. Prior to the saturation of abrasive concentration, the increase of N_{abr} trumps the effect of a decreasing F_{abr} , resulting in an overall almost-linear increase in the removal rate. While N_{abr} continues to increase beyond the saturation point, the drop in F_{abr} is more drastic, ultimately resulting in a decreasing removal rate when the abrasive concentration was increased. This results in the trend seen in the experimental data, where a turning point is seen.

Lastly, it is to be reiterated that the discontinuity in the theoretical curve when $v_{\text{abr}} / v_{\text{CI}}$ is 0.259 was only a theoretical turning point. Considering the assumptions of ideal conditions with the particle configuration for the base model and both extensions, the actual turning point was stochastic in nature. Therefore, the intention of the proposed model was to suggest that the turning point occurred near the theoretical value, instead of exactly at the theoretical value.

6.5 Comments on robustness of model

The nature of the model is such that the underlying concepts (such as particle packing, indentation of particles, force per particle) are generally applicable for different magnetic field-assisted processes that use polishing media of similar composition. However, the final model includes four constants that are dependent on the setup. While the agreement between theoretical and experimental data has been demonstrated on the setup reported in the present work, no conclusion can be drawn for a different setup or a similar but different process.

A recalculation of the constants is definitely required when there is a change in the tooling geometry, workpiece material, types of CI and abrasive particles, and type of carrier fluid. As for the robustness of the trends suggested by the model, no conclusion may be drawn until actual trials are conducted. Assessing the robustness of the model across different setups is an area that the candidate is keenly interested in, but not explored in the present work due to the exorbitant amount of resources required to undertake such a task.

Ultimately, magnetic field-assisted finishing process is a very complex system to be modeled successfully due to the many mechanical, fluidic, and chemical interactions of different components.

6.6 Comments on effect of workpiece material

Workpiece materials can affect the proposed model in two ways. Firstly, the model requires that the abrasive particles deform the workpiece material plastically. It has been established in literature [6] that plastic deformation for indentation of abrasive particles on most metallic workpiece. Only very ductile materials such as polyurethane

deform elastically. Therefore, very ductile workpiece will render the proposed model invalid.

Secondly, the workpiece material may affect the proposed model if it reacts chemically with the carrier fluid or the workpiece surface. There is a possibility that such chemical reaction introduces adhesion between particles and workpiece surface and thereby altering the mechanism of material removal. These interactions can be complex to describe or model and is beyond the scope of the current project.

6.7 Summary

In this chapter, experiments were conducted to verify the proposed base model and two extensions, which gave theoretical trends between removal rate and properties related to finishing media such as the abrasive size and abrasive concentration.

For variation in abrasive size, the experimental results showed that the removal rate was reduced when the abrasive size was increased, in line with the theoretical trend given by the proposed base model and the extension for abrasive size criterion. For variation in abrasive concentration, the experimental results showed that the removal rate initially increased when the abrasive concentration was increased, but eventually reached a maximum value before beginning to decrease with further increment in the abrasive concentration. This trend was also in line with the theoretical trend given by the proposed base model and the extension for abrasive volume criterion. In addition, the experimental turning points for the removal rate were close to the theoretical value of abrasive saturation as given by the model.

Finally, all the theoretical curves were generated using a universal set of values for the four constants in the proposed model. With that, the base model and both the

extensions have been successfully validated for abrasive size between 0.6 μm and 15 μm , and for abrasive-to-carbonyl-iron volumetric ratio between 0 and 0.8.

REFERENCES

- [1] Jeng YR and Huang PY, *A material removal rate model considering interfacial micro-contact wear behaviour for chemical mechanical polishing*. Journal of Tribology, Transactions of the ASME, 2005. **127**: p.190-197.
- [2] Lee HS, Jeong HD and Dornfeld DA, *Semi-empirical material removal rate distribution model for SiO₂ chemical mechanical polishing (CMP) processes*. Precision Engineering, 2013. **37**: p.483-490.
- [3] Shinmura T, Takazawa K, Hatano E, Matsunaga M and Matsuo T, *Study on magnetic abrasive finishing*. CIRP Annals-Manufacturing Technology, 1990. **39**(1): p. 325-328.
- [4] Jin XL and Zhang LC, *A statistical model for material removal prediction in polishing*. Wear, 2012. **274-275**: p.203-211.
- [5] Sidpara A and Jain VK, *Theoretical analysis of forces in magnetorheological fluid based finishing process*. International Journal of Mechanical Sciences, 2012. **56**(1): p.50-59.
- [6] Zhao Y and Chang L, *A micro-contact and wear model for chemical-mechanical polishing of silicon wafers*. Wear, 2002. **252**: p.220-226

Chapter 7

Summary

7.1 DEVELOPMENT OF NEW MFAF PROCESS

In this thesis, the developmental work of a new MFAF process has been presented. Firstly, the principles of the process have been described and theoretically understood. Secondly, the relationship between tool parameters and the process outcome has been established theoretically using magnetostatic analysis. Lastly, the capabilities of the process for surface texture reduction, achieving high removal rate and for surface finishing of structured surfaces have been demonstrated.

7.1.1 Principles and advantages of new MFAF process

The novelty of the process is mainly attributed to two key features that contribute to an increased material removal rate. The first key feature is the augmented magnetic flux density in the polishing zone, which is a result of the double-magnet configuration of the polishing tool. The double-magnet configuration is itself also a novel concept and has been patented by the author. Magnetostatic analysis has established and confirmed the benefits of the double-magnet configuration, with the magnetic flux density approximately doubled compared to that calculated for a single-magnet configuration. Measurements obtained using a magnetometer on physical setups showed the same improvement in magnetic flux density.

The second key feature is the *in situ* reformation of the finishing media during the process, which has the effect of maintaining the shape of the finishing media while it is in

contact with the workpiece. The benefits are two-pronged. Firstly, the change in tool geometry due to tool wear, which is a key weakness for traditional polishing tools, was eliminated. This is favourable for the process stability and also future applications in process automation. Secondly, maintaining the shape of the finishing media allowed for the exertion of a sustainable pressure on the workpiece surface. This is favourable for achieving a high removal rate.

The mechanism responsible for the *in situ* reformation of the finishing media has been analysed theoretically and described in this thesis. It was suggested that the *in situ* reformation is attributed to two mechanisms. The first is the dynamic magnetic field experienced by the finishing media, which exerts magnetic tension force on the carbonyl iron particles and result in rearrangements of the magnetic particles. The second mechanism is simply the physical interference of the finishing media on the two magnets, thus creating contact forces that also result in rearrangements of the magnetic particles.

The principles have been established by measuring the normal force and shear force during polishing. The polishing forces for the double-magnetic configuration were significantly higher than that for the single-magnet configuration. In addition, the *in situ* reformation of the finishing media has been confirmed by visual inspection of the contact between the finishing media and workpiece.

7.1.2 Magnetostatic analysis of tool parameters

Having established the principles and advantages of the double-magnet configuration, additional magnetostatic analyses have been conducted to understand the relationship between selected tool parameters and the magnetic flux density in the polishing zone. Specifically, the effect of magnet-to-magnet gap, w_{gap} , magnet-to-

workpiece gap, z , and the thickness of magnet, t_{magnet} , on the magnetic flux density were analysed. There were several findings.

Firstly, reducing w_{gap} was found to increase the magnetic flux density, which is favourable for high removal rate. However, a low w_{gap} also translates into a smaller polishing area. It was therefore suggested that an optimal w_{gap} exists for maximum volumetric removal rate. A value of 1 mm was arbitrarily selected for w_{gap} , as optimization is not in the scope of the thesis.

Secondly, reducing z was found to also increase the magnetic flux density. However, the distribution of magnetic flux density becomes less uniform when z is reduced. Values of z between 0.5 mm and 1.5 mm were found to be of good balance between high magnetic flux density and distribution uniformity.

Lastly, magnetic flux density was found to increase with t_{magnet} albeit at a diminishing rate. Considering the availability of stock magnet, a value of 12 mm was chosen for t_{magnet} because it is able to achieve more than 80 % of the asymptotic magnetic flux density. The suggested values of w_{gap} , z and t_{magnet} were used in the design and fabrication of prototype of the polishing unit.

In addition to the three tool parameters above, the merit of including magnetic caps to reduce flux leakage has also been assessed. It was found that the magnetic flux density in the configuration with magnetic cap is 5 % higher, and that increasing the thickness of the magnetic caps resulted in diminishingly higher magnetic flux density. Since the advantage is marginal and predictable, magnetic caps were not included in the first prototype.

7.1.3 Capabilities of new MFAF process

Using the prototype of the polishing unit, the capabilities of the new MFAF process were demonstrated. Firstly, the capability of the new MFAF process in achieving mirror finish on workpiece surface was established. A 25 mm² area on a stainless steel (SUS316) workpiece was polished from an initial surface texture 0.431 $\mu\text{m Ra}$ to 0.016 $\mu\text{m Ra}$ in 30 minutes. A similar workpiece made of titanium alloy (Ti-6Al-4V) was polished from an initial roughness of 0.480 $\mu\text{m Ra}$ to 0.073 $\mu\text{m Ra}$.

Secondly, the ability of the new MFAF process to achieve high removal rate was validated by comparing against results reported in the literature for other processes. The results have been shown in Figure 3.19, where the removal rate of the new MFAF process at 11.8 $\mu\text{m}/\text{min}$ was among the highest. Caution however must be advised as the reported values may not be optimized for removal rate and may vary substantially depending on the process conditions and workpiece material.

Lastly, the feasibility of the new MFAF process for polishing of structured surfaces has been assessed. Specifically, 2.5-D V-shaped channels with width of 0.2 mm and depth of 0.1 mm were polished. The surface texture of the channels was reduced, although micrographs suggested that the removal rate at the peaks and valleys of the channels were different. In addition, the peak-to-valley height of the channels was reduced from an initial value of 100 μm to 14 μm after polishing. Hence, the new MFAF process in its current form is unable to achieve uniform removal rate for structured surfaces. Despite its limitation, the new MFAF process has potential for finishing of structured surfaces, as traditional polishing tools will completely destroy the structures on the surface.

7.2 MATERIAL REMOVAL RATE MODEL

A material removal rate model based on contact mechanics has been proposed for the new MFAF process. This new model aims to better represent the relationship between the removal rate and the media properties, given that the finishing media in the new MFAF process is complex as it is composed of two types of particles with different properties. In the proposed model, the removal rate is related to the number of active carbonyl iron particles, N_{CI} , number of active abrasives, N_{abr} , force per carbonyl iron particle, F_{CI} , and force per abrasive particle, F_{abr} . Expressions were then derived to relate these terms to the media properties, which include the abrasive size, abrasive concentration and carbonyl iron particle size. To obtain the aforementioned expressions, it was assumed that the particles were spherical with uniform size distribution. It was further assumed that the carbonyl iron matrix is a perfect FCC configuration. Also, the derivations of expressions for F_{CI} and F_{abr} were based on a new proposed framework that considered the effects of contact forces attributed to neighbouring particles. This approach is novel and has not been previously considered in other models. The complete derivation and the final form of the proposed model have been shown in Chapter 4.

In Chapter 5, the proposed model is extended to two conditions when assumptions made in the base model do not hold. The first condition was when the abrasive size exceeds the critical size of interstitial spaces in the carbonyl iron matrix. An orderly increase in the distance between carbonyl iron particles was considered and the expressions derived for the base model were then modified accordingly. The second condition was when the abrasive concentration exceeds the saturation level, which occurs when all the interstitial spaces have been fully occupied. The approach considered was to calculate an equivalent abrasive size, which allowed the problem to be reduced to that

encountered for the first condition. The complete derivation and the final form of the two proposed extensions have been shown in Chapter 5.

The proposed model and extensions were compared against experimental data for verification. A partial set of the experimental data was used to calculate the four constants in the proposed model. Using these constants, theoretical curves of removal rate against abrasive size, and removal rate against abrasive concentration, were generated. The theoretical curves were in good agreement with the trend exhibited by experimental data.

For removal rate against abrasive size, the removal rate was found to decrease with an increasing abrasive size. This is true for the range of abrasive size experimented on, which was between 0.6 μm and 15 μm . The mechanism contributing to the advantage of small abrasives was studied by analyzing the number of active particles and force per particles in the proposed model. It was found that larger abrasives had greater force per particle, but the number of active abrasives is significantly decreased. The overall effect was therefore an increasing removal rate when abrasive size is decreased.

For removal rate against abrasive concentration, it was found that the removal rate initially increased when abrasive concentration is increased, but the trend eventually reversed. This is true for the range of abrasive concentration experimented on, where the abrasive-to-carbonyl-iron volumetric ratio was between 0 (no abrasive) and 0.8. The turning point of removal rate occurred near the theoretical abrasive saturation level, where the abrasive-to-carbonyl-iron volumetric ratio is 0.259. Similarly, the mechanism contributing to the observed maximum point has been proposed and described in this thesis.

In conclusion, the proposed model and two extensions have been successfully validated by experimental data.

Chapter 8

Future work

8.1 GOALS OF SURFACE FINISHING DEVELOPMENT

Presently, there are two key areas of interest in the development of surface finishing. The first pertains to development of new processes for increasingly challenging requirements – freeform, structured surface, and internal channels. Internal channel especially is a key area, driven by the rise of additive manufacturing, which allows designers to now create many components with very complex internal surface. Additively manufactured parts however have poor surface texture, which require post-processing.

A second area of interest relates to process automation, which is advantageous for quality control and reduced reliance on skilled labor. A key component of process automation is translating process monitoring into process control, and one way to achieve that is by developing a process model to understand the relationship between process variables and process outcome.

8.2 PROCESS DEVELOPMENT

A new MFAF process has been developed in this thesis. Novel process principles leading a high removal rate have been established, and the capability of the process for surface texture reduction has been demonstrated. The work presented may be expanded upon in several different directions.

The first potential direction is the design improvement of the polishing unit. The current prototype is based on neodymium magnets. The use of electromagnet may be

more advantageous, as it allows the magnetic flux density to be configurable. The ability to configure allows the effect of magnetic flux density on the polishing outcome to be studied and better understood. In addition, the magnetic field may be switched off, allowing the finishing media to be easily removed and replaced. However, the design of the double-magnet configuration with an electromagnet provides technical challenges, given that the magnetic poles are required to rotate in opposite directions. Such a design is theoretical implementable but not trivial.

The second potential direction also pertains to the design of polishing unit. In the current embodiment of the polishing unit, the bottom surface of the polishing tool is planar. As a result, the polishing unit has difficulty assessing selected geometry of the target surface, such as concave surfaces, due to geometrical interference. One potential solution is to consider a tilted tool design, which has been outlined in the patent awarded for the double-magnet configuration. In the tilted tool design, which is shown in Figure 8.1, the magnets are curved in shape and the axis are at angled from each other. With the tilted design, the contact surface is now convex instead of planar, which consequently eliminates interference for many different shapes of target geometry.

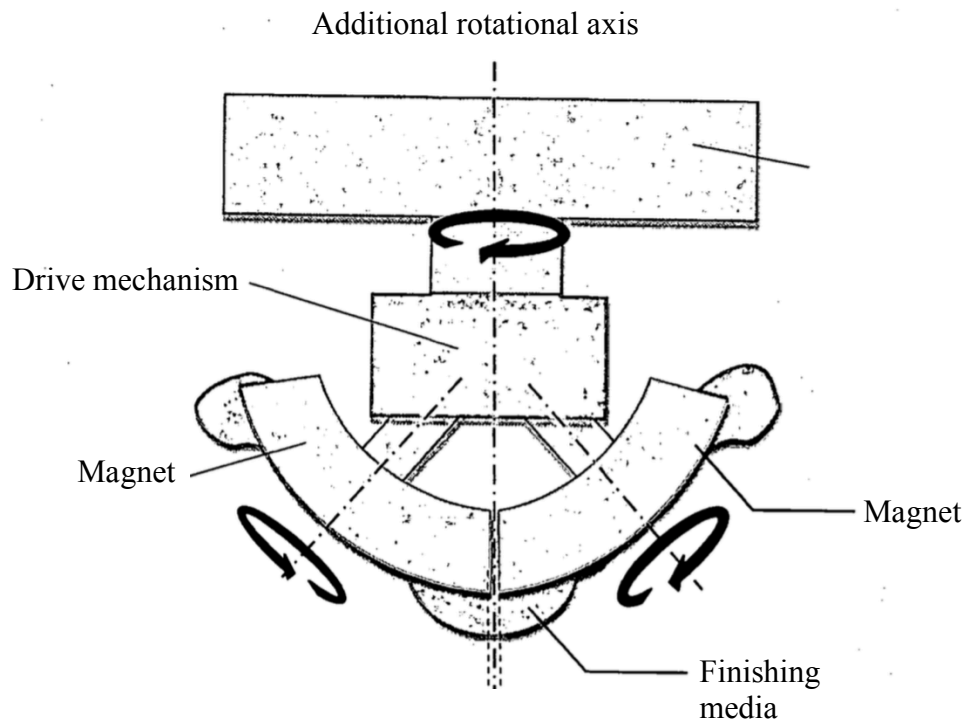


Figure 8.1: Tilted polishing unit as described in patent awarded for the new MFAF process.

In addition to the convex contact surface, another potential benefit of the tilted polishing tool is the angle of attack of the finishing media. The angle of attack is the angle between the velocity vector of the particle and the surface at the instant when the particle impacts the workpiece surface. In the design described in the thesis, the velocity vector is parallel to the surface, resulting in a zero angle of attack. However, in the tilted design, a nonzero angle of attack exists. It is speculated that this angle of attack may be advantageous for the material removal mechanism.

The design of such a tilted polishing unit presents significant technical challenges. Firstly, the drive mechanism required to rotate the two magnets in opposite directions is not trivial and will likely require proprietary mechanism. Secondly, the shape of the magnets is complex, and may again require proprietary process to fabricate. The use of

electromagnets bestows the benefits mentioned previously, but will further complicate the design of the polishing unit.

A third potential extension of the work done in this thesis is to further explore the composition of the finishing media used in the new MFAF process. In this thesis, the finishing media comprises magnetic carbonyl iron particles and non-magnetic alumina abrasives suspended in distilled water. The presented studies mainly considered the effects of changing the abrasive size and abrasive concentration. Future work may wish to consider other factors such as the type of abrasive, shape of abrasives, type of carrier fluid, or type of magnetic particles. Other innovations, such as coating magnetic particles with abrasives can also be considered. It will be of academic interests to establish the relationships between these factors to the surface texture, material removal rate, and media life. The ultimate goal is to understand the complex mechanism of how the finishing media affects the process outcome in MFAF processes.

Lastly, the surface finishing of structured surfaces using the new MFAF process may be further explored. In this thesis, it has been shown that the new MFAF process is a promising method for 2.5D structured surfaces, although the current embodiment of the process is unable to achieve uniform removal rate for the structures. The non-uniform removal rate may be due to the use of rotation to actuate the abrasives. The use of other modes of actuation, such as a linear vibration may be beneficial as it allows the velocity vector to be better controlled. For 2.5D structures, aligning the velocity vector to the direction parallel to the structures may improve the uniformity of removal rate.

8.3 MATERIAL REMOVAL RATE MODEL

Material removal rate model is integral for process control. Presently, it is possible to monitor process variables closely with various sensors, as well as to control them by feedback loops. However, without a material removal rate model, they cannot be translated into monitoring or controlling the process outcome.

In this thesis, a material removal rate model based on contact mechanics has been proposed and verified experimentally. The motivation for the proposed model is to better represent the relationship between removal rate and the properties of the finishing media, which consists of two types of particle with different properties. In the work presented in this thesis, the main focus is the effect of abrasive size and abrasive concentration. Many aspects of the proposed model may be modified, improved and expanded upon.

Firstly, the model proposed a new framework to consider how the composition of neighbouring particles affects the forces per particle for both carbonyl iron particles and abrasives. The current expression of forces per particle proposed in the thesis is based on the ratio of projected area of the two types of active particles. The resulting theoretical trend agreed reasonably with experimental data, but newer models may also consider the effect of neighbouring particles from different perspectives that may better represent the interactions of the neighbouring particles.

Secondly, the model considered only the magnetic carbonyl iron particles and non-magnetic abrasives, and opted to not consider the presence of carrier fluid in the finishing media. How the presence of carrier fluid affects the model is complex, and requires sophisticated treatment. Both fluid mechanics and chemistry may have to be considered to arrive at a satisfactory representation of the removal mechanism.

Lastly, several other factors can be considered to obtain a better representation of the removal mechanism in MFAF processes. These include considering a non-uniform

distribution for the particles, or how a change in the target material affects the finishing mechanism (may involve material science and chemistry). These factors are not currently well understood in MFAF process and may introduce significant complexity to the process model. Proposing a verifiable process model that considers these factors will be a significant academic achievement, and a true hallmark of erudition.

Appendix A

Magnetostatic analysis with ANSYS

A.1 INTRODUCTION

In this thesis, magnetostatic analysis is used to visualize the magnetic flux lines of the polishing tool, and also to calculate the magnetic flux density at points of interest, which are typically points in the polishing zone. Magnetostatic analysis presented in this thesis is conducted with the magnetostatic module in the ANSYS software package, which is capable for two-dimensional model.

A.2 THEORY

Magnetostatic analysis is based on the finite element modeling of static magnetic fields. Fundamentally, the magnetostatic equations are the Gauss's law for magnetism and Ampere's law, given in their partial differential forms by Equation A.1 and A.2 respectively.

$$\nabla \cdot \mathbf{B} = 0 \quad (\text{A.1})$$

$$\nabla \times \mathbf{H} = \mathbf{J} \quad (\text{A.2})$$

where ∇ denotes divergence, \mathbf{B} is the magnetic flux density, \mathbf{J} is the current density and \mathbf{H} is the magnetic field intensity.

For the analyses, permanent magnets may also be used. The magnetization of a permanent magnet is given by:

$$\mathbf{B} = \mu_0 (\mathbf{M} + \mathbf{H}) \quad (\text{A.3})$$

where μ_0 is the permeability of free space and \mathbf{M} is the magnetization field of the permanent magnet. A complete treatment of magnetostatic equations is available elsewhere [1].

A.3 PREPROCESSING

A.3.1 Model generation

The polishing unit is three dimensional, but the magnetostatic analysis is limited on a two-dimensional plane. Therefore, the plane containing the diameters of both the magnets on the polishing tool is selected. Figure A.1 is an image capture in the ANSYS environment of the selected plane.

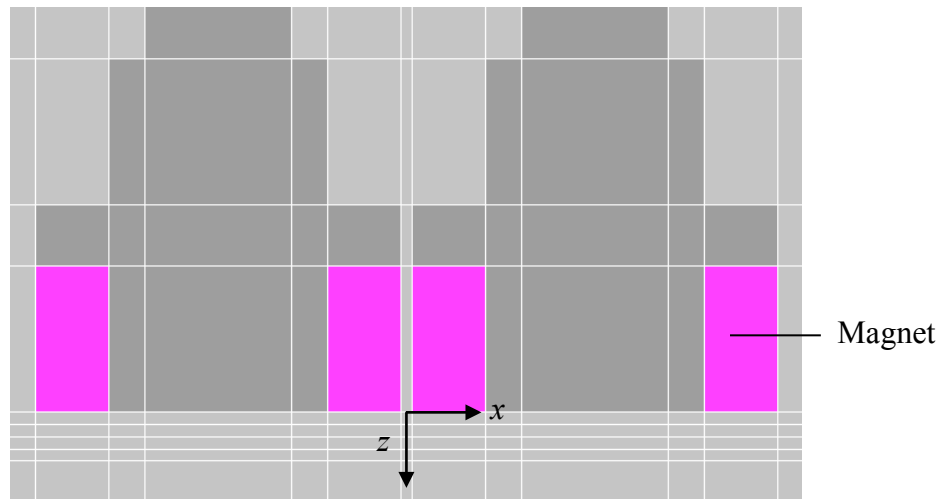
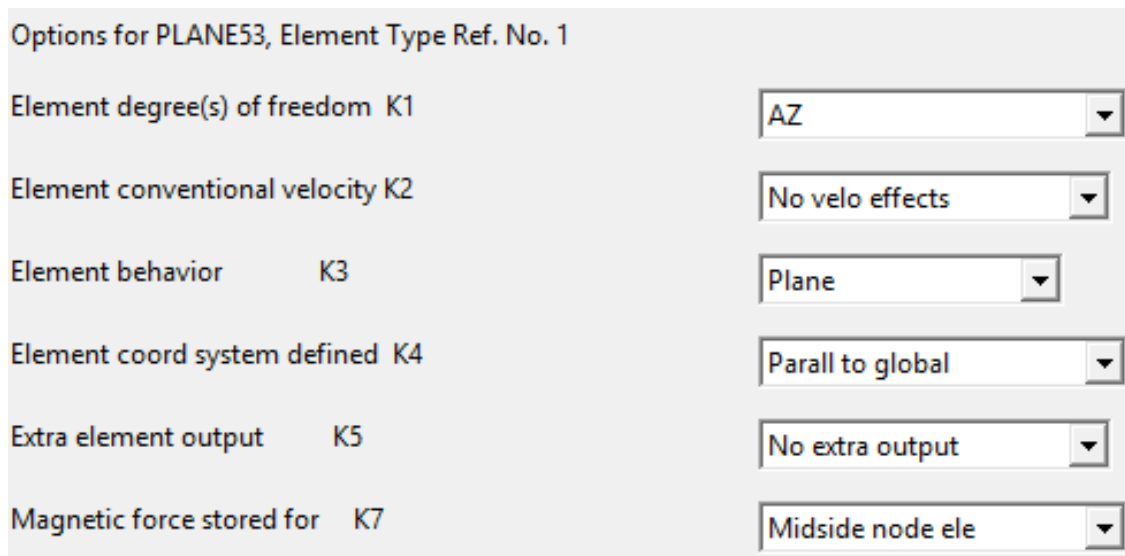


Figure A.1: An image capture in the ANSYS environment of the plane selected for magnetostatic analysis.

A.3.2 Element properties

The PLANE53 element is used in the magnetostatic analysis. It is a two-dimensional magnetic solid that is defined by up to eight nodes and up to four degrees of freedom per node. The PLANE53 element has non-linear magnetic capability for modeling B-H curves or permanent magnet demagnetization curves and is therefore suitable for the analysis required in this thesis. The full description of the element is available online [2].

The selected options for the PLANE53 elements are as given in the screen capture below.



Options for PLANE53, Element Type Ref. No. 1

Element degree(s) of freedom K1	AZ
Element conventional velocity K2	No velo effects
Element behavior K3	Plane
Element coord system defined K4	Parall to global
Extra element output K5	No extra output
Magnetic force stored for K7	Midside node ele

Figure A.2: Selected element type options for PLANE53.

A.3.3 Material properties

For the magnetostatic analyses presented in this thesis, a total of five material types were defined. They are the neodymium magnets (two material types for different

polarity), SUS430 (magnetic), SUS316 (non-magnetic) and air. SUS316 and air are in fact indistinguishable and are defined separately for the purpose of clarity only. Table A.1 shows the material properties of the five materials.

Table A.1: Material properties for the five material types.

No.	Material	Coercivity (A/m)	B-H curve	Relative permeability
1	Neodymium permanent magnet (Grade N35)	9.39×10^5	See Table A.2	-
2	Neodymium permanent magnet (Grade N35)	-9.39×10^5	See Table A.2	-
3	SUS430 (magnetic)	-	See Table A.3	-
4	SUS316 (non-magnetic)	-	-	1
5	Air	-	-	1

For neodymium permanent magnet, the required data input are the coercivity and the B-H curve. The input for the B-H curve is in fact the demagnetization curve of the magnet. Both can be obtained from accompanying data sheet typically supplied by the magnet maker. Figure A.3 shows the B-H and demagnetization curves for Grade N35 neodymium permanent magnet from HKCM Engineering [3]. Note that the properties of permanent magnets supplied by different vendors may vary slightly.

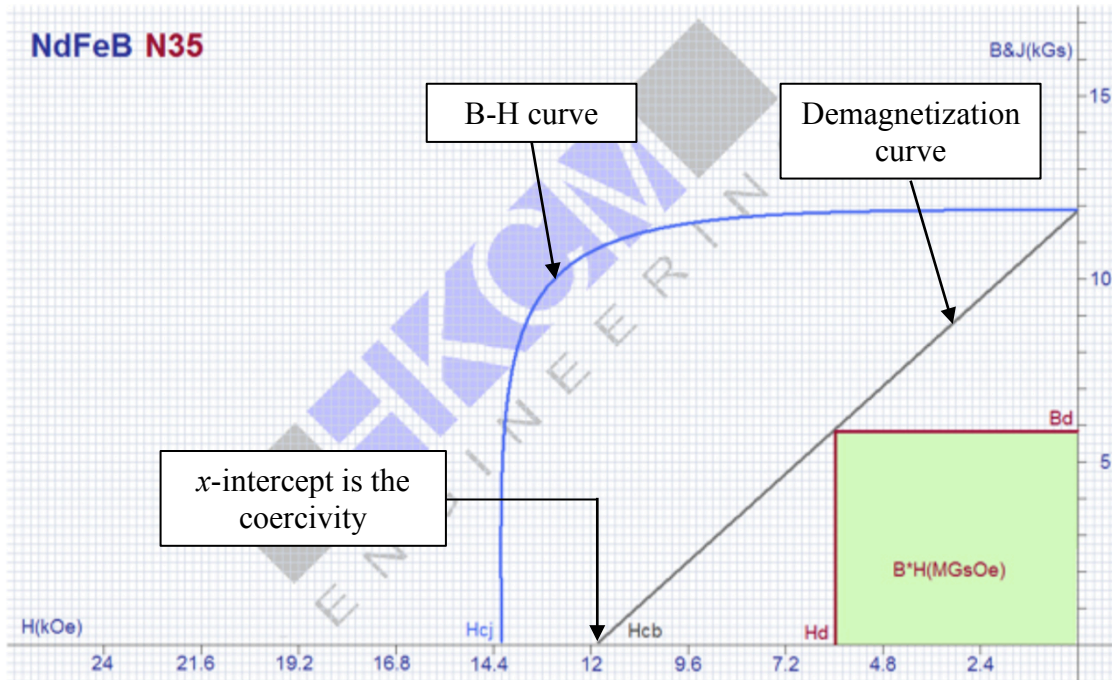


Figure A.3: B-H and demagnetization curves for Grade N35 neodymium permanent magnet supplied by HKCM Engineering [3].

The coercivity is read from the x -intercept of the demagnetization curve. Note that the required unit conversion from Oe to A/m is given by:

$$1 \text{ Oe} = \frac{1000}{4\pi} \text{ A/m} \quad (\text{A.4})$$

To input the demagnetization curve as a B-H curve, the demagnetization curve is translated to the right into the first quadrant, with the x -intercept at the origin. Two points that define the translated line are then input into ANSYS in a table form, as given below (the origin may not be used because of a software bug):

Table A.2: Data input for B-H curve of Grade N35 neodymium permanent magnet.

Point	H		B	
	Oe	A/m*	Gauss	T*
1	5800	4.62×10^5	5800	0.58
2	11800	9.39×10^5	11800	1.18

**Required unit for data input*

For SUS430, which is magnetic, the B-H curve is not typically included in the data sheet but may be available upon request. The B-H curve used [4] for magnetostatic analyses in this thesis is given below. The corresponding curve is illustrated in Figure A.4. Note that the magnetic properties of SUS430 are dependent on material processing. Therefore, materials supplied by different vendor may have varying magnetic properties.

Table A.3: Data input for B-H curve of Grade N35 neodymium permanent magnet [4].

Point	H		B	
	Oe	A/m*	Gauss	T*
1	0	0.00	0	0
2	1.71	136.08	850	0.085
3	2.50	198.94	2466	0.247
4	3.16	251.46	4763	0.476
5	3.68	292.85	7144	0.714
6	4.74	377.20	9356	0.936
7	6.18	491.79	11261	1.126

8	10.26	816.46	12503	1.250
9	16.32	1298.70	13183	1.318
10	23.95	1905.88	13608	1.361
11	28.82	2293.42	13790	1.379
12	46.05	3664.54	14055	1.406
13	97.37	7748.46	15015	1.502
14	157.9	12565.28	15714	1.571
15	227.63	18114.22	16150	1.615
16	300.00	23873.24	16412	1.641

**Required unit for data input*

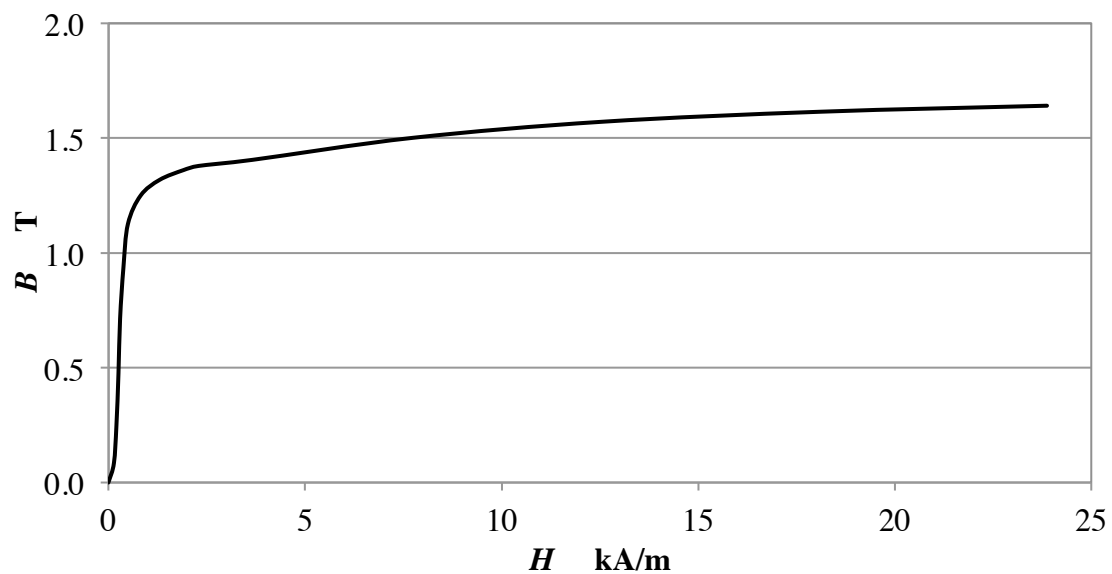


Figure A.4: B-H curve for SUS430 by Carpenter [4]. Annealed (75.5 HRB), 788 °C H_2 dried for 2 hours.

A.4 SOLVING AND POSTPROCESSING

The model generated is then meshed in a two-step process. First, the model is meshed with quad elements of 1 mm edge length. The elements are mapped and are therefore arranged orderly in a rectangular grid. Secondly, the meshed model is refined at critical areas near the magnets and in the polishing zone. The element edge length is 0.1 mm in these refined areas.

After meshing, the model is then solved with the default frontal solver available in the ANSYS software package. Default options and values are used, as shown in the screen capture below. Additional boundary conditions are not necessary because the default far-field conditions are suitable for the analyses required.

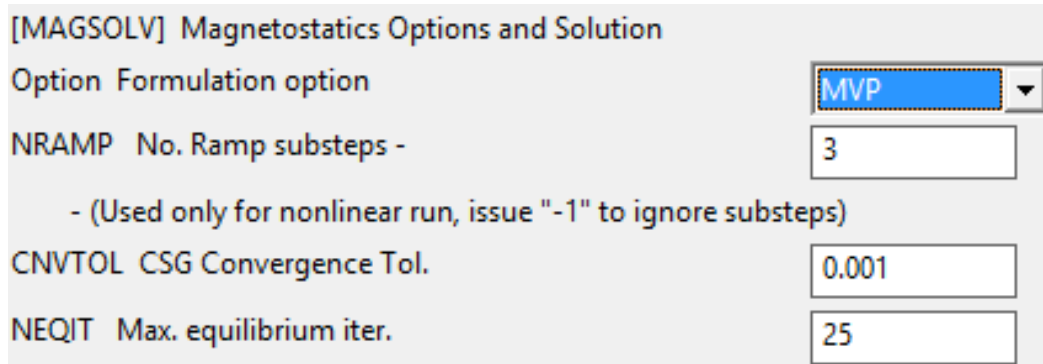


Figure A.5: Selected options for magnetostatics solver.

After the solutions have been obtained, post-processing is done to visualize the magnetic flux lines and to read the magnetic flux density at selected nodes. These are illustrated in Figure A.6 and Figure A.7.

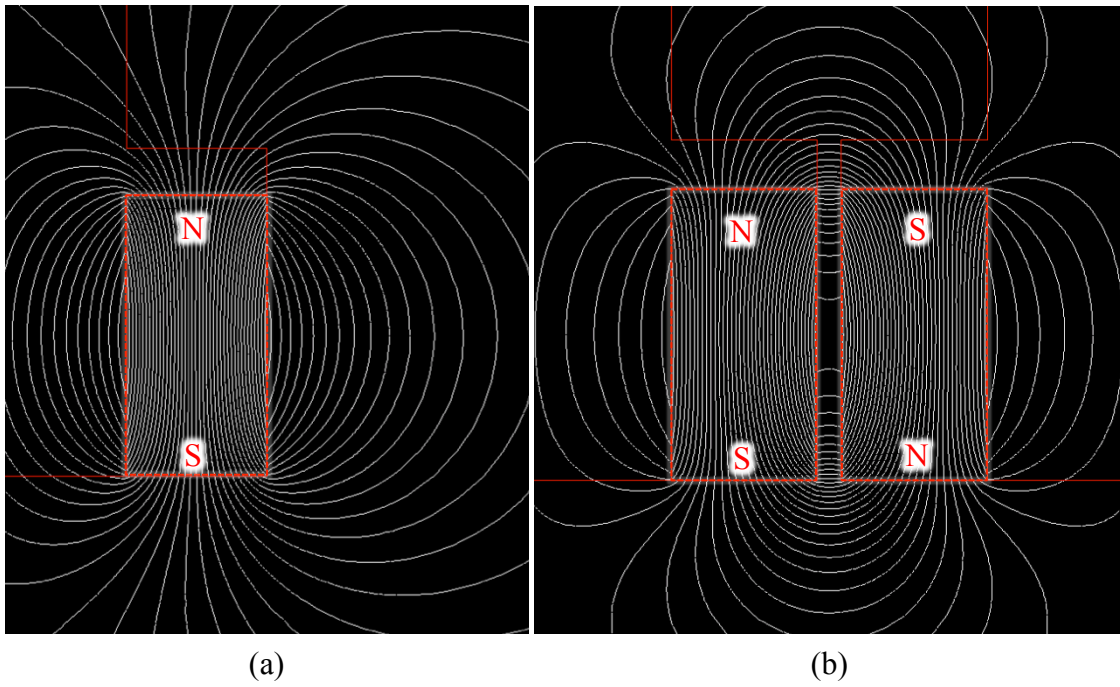


Figure A.6: Magnetic flux lines for (a) single-magnet configuration, and (b) double-magnet configuration. Magnets are highlighted for clarity.

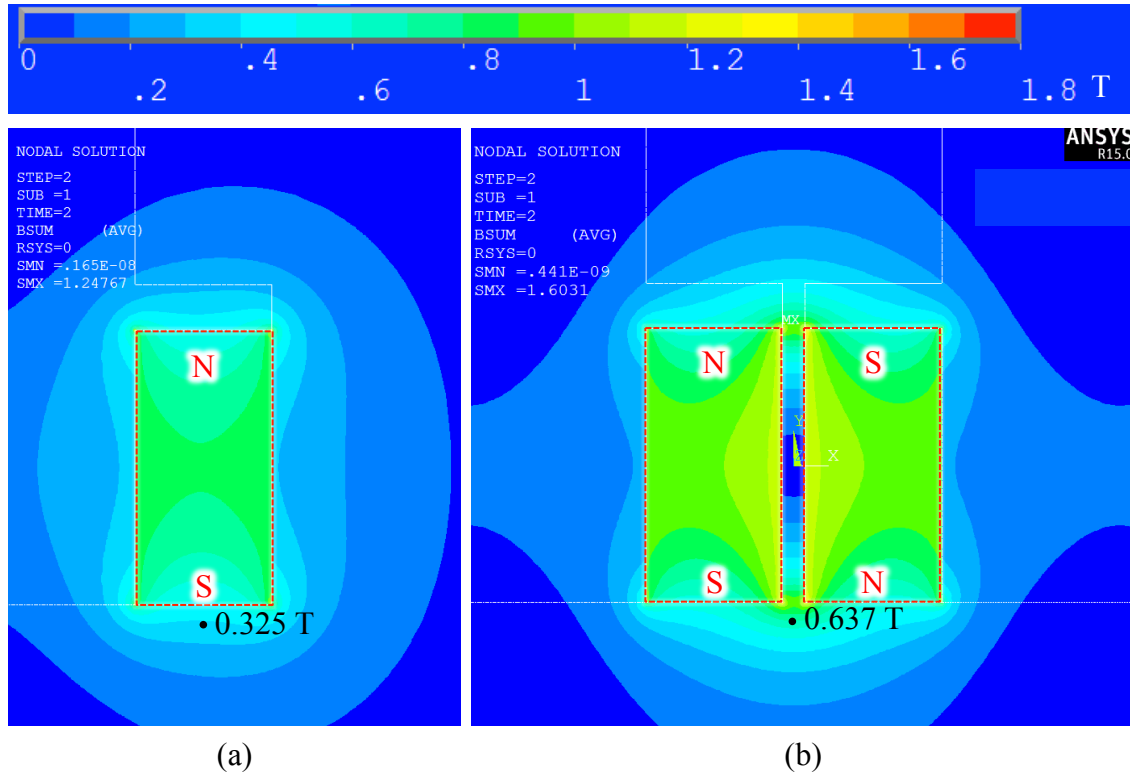


Figure A.7: Contour plots of magnetic flux density for (a) single-magnet configuration, and (b) double-magnet configuration. Magnets are highlighted for clarity.

A.5 VALIDATION OF MAGNETOSTATIC ANALYSIS

The theory and fundamentals of magnetostatic analysis have been proven in the literature and are well established. Therefore, the reliability of the results rests on the correct use of the finite element method and the correct input of data. To validate the procedure outlined in this Appendix, the calculated results from magnetostatic analysis were compared against readings from a vector magnetometer (Hirst Magnetic Instruments, Gaussmeter model GM07). Note that the Hall probe on the vector magnetometer can only measure the magnetic flux density component along one

direction at any given time. Post-processing for the magnetostatic analysis was therefore modified to give the magnetic flux density components, instead of the vector sum.

Validations were done for two different setups.

A.5.1 Validation for single-magnet configuration

The first was a simple one-point validation for a single ring magnet. Specifically, the magnetic flux density on the magnet surface calculated by magnetostatic analysis was compared against a physical Grade N35 neodymium permanent magnet.

In the direction normal to the magnet surface, the value given by the magnetostatic analysis was 0.47 T, while the value measured by the magnetometer was 0.48 T (average of 3 readings). Therefore, the value given by magnetostatic analysis was validated.

A.5.2 Validation for double-magnet configuration

The second validation was a more elaborate process done for the double-magnet configuration. The x and z components of the magnetic flux density were measured at multiple points with the magnetometer (see Figure A.1 for orientation of the axes). Specifically, the measured points were between $x = 0$ mm and $x = 1.9$ mm, with a uniform spacing of 0.1 mm between the points. The z -coordinates were 1 mm and 2 mm for the z component, and 2 mm for the x component ($z = 1$ mm was not measured due to geometrical constraint of the magnetometer). For positioning, the magnetometer was mounted on a precision 2-axis positioning stage. Schematic diagrams of the setup are given in Figure A.8.

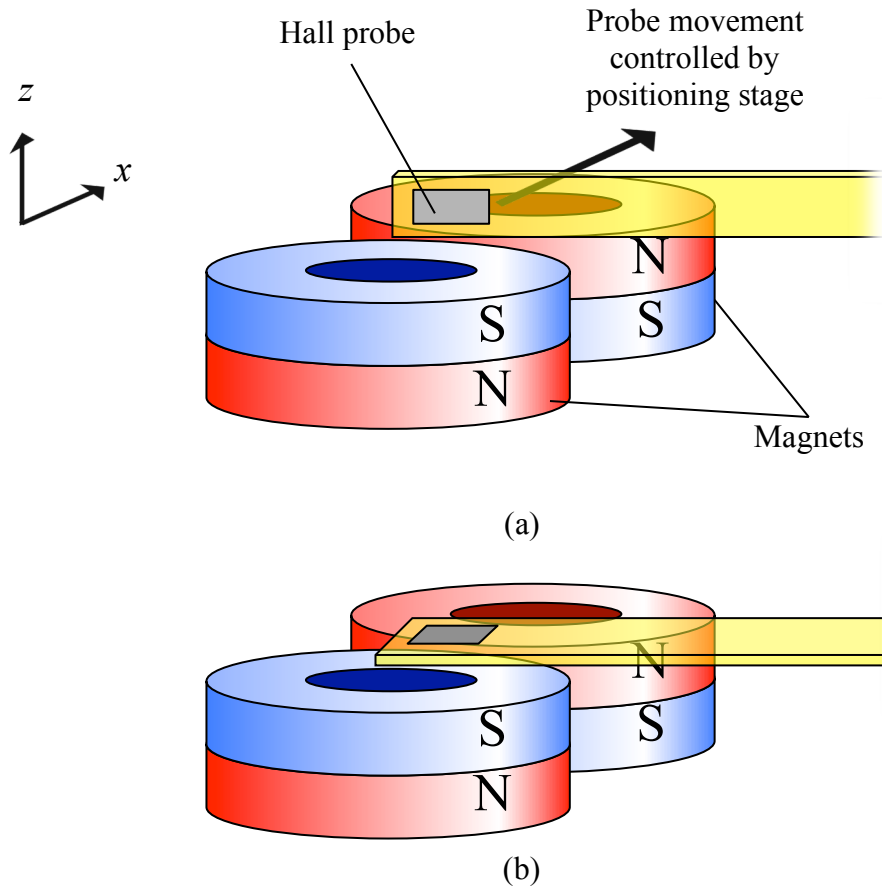


Figure A.8: Measurement of magnetic flux density components in the (a) x direction and (b) z direction, using a vector magnetometer.

The measured values were then compared with values at the same points as given by magnetostatic analysis. The plots comparing the measured values with the calculated values are shown in Figure A.9.

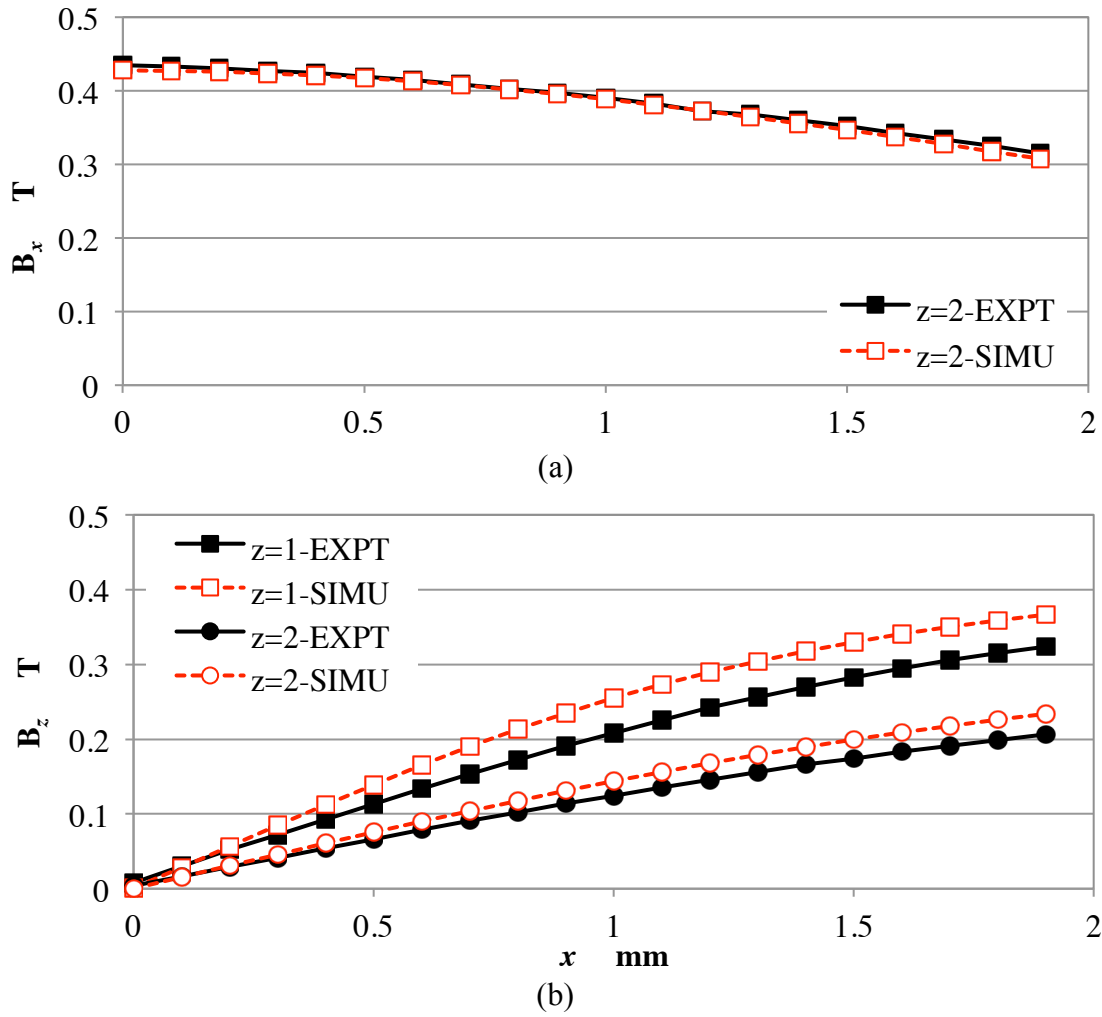


Figure A.9: Comparison between calculated and measured values of magnetic flux density, for (a) x component, and (b) z component.

Values for the x component were in good agreement, while the measured values for the z component were lower than the calculated values obtain from magnetostatic analysis. The trend however was in good agreement. The lower values obtained by measurement may be due to standard errors with the z -coordinate during the setup attributed to the probe thickness.

From the comparisons above, the magnetostatic analysis for the double-magnet configuration has therefore also been validated.

REFERENCES

- [1] Donohoe JP, *Magnetostatic fields*. Retrieved on 4 November 2015 from <http://my.ece.msstate.edu/faculty/donohoe/ece3313magnetostatics.pdf>.
- [2] *PLANE53 2-D 8-node magnetic solid*. ANSYS documentation. Retrieved on 4 November 2015 from http://mostreal.sk/html/elem_55/chapter4/ES4-53.htm.
- [3] *BH Diagram. Material, grade: NdFeB, N34 /ICE 260/95*. HKCM Engineering. Retrieved on 4 November 2015 from http://www.hkcm.de/archive/HKCM_Magnet-Cube%20W08Au-N35.pdf.
- [4] *B-H curves*. Retrieved on 4 November 2015 from <http://www.eng-tips.com/viewthread.cfm?qid=118215>

Appendix B

Measurement of material removal rate

In this thesis, the measured and reported values of material removal rate are the peak material removal rate, which is defined as the greatest depth of the polished spot or the polished area per unit time. The reported values are given in $\mu\text{m}/\text{min}$. The volumetric material removal rate is not used because peak removal rate allows comparison of the polishing performance at one single point, which is advantageous in comparing the magnetic flux density.

To measure the peak removal rate, the workpiece is selectively polished to create polished area and keep unpolished area on the same surface. The difference in profile heights of the two areas allows calculation of the material removal. To obtain the profile heights, two-dimensional scans are made with a stylus profilometer (Taylor Hobson, Form Talysurf 2, 10 nm vertical resolution). Reported values are averaged from three measurements. Figure B.1 is a schematic diagram of the two-dimensional scans on a flat workpiece after polishing and an example of the profile obtained. From the profile obtained, the peak material removal is measured. Peak material is defined as the maximum difference in the vertical direction between the before and after profiles when they are superimposed on each other, and is measured visually. Dividing the peak material removal by the polishing time results in the peak material removal rate. The material removal rate is therefore assumed to be uniform over the duration of the polishing time. This assumption is reasonable because of the short polishing time (5 minutes). Over this duration, the process is stable.

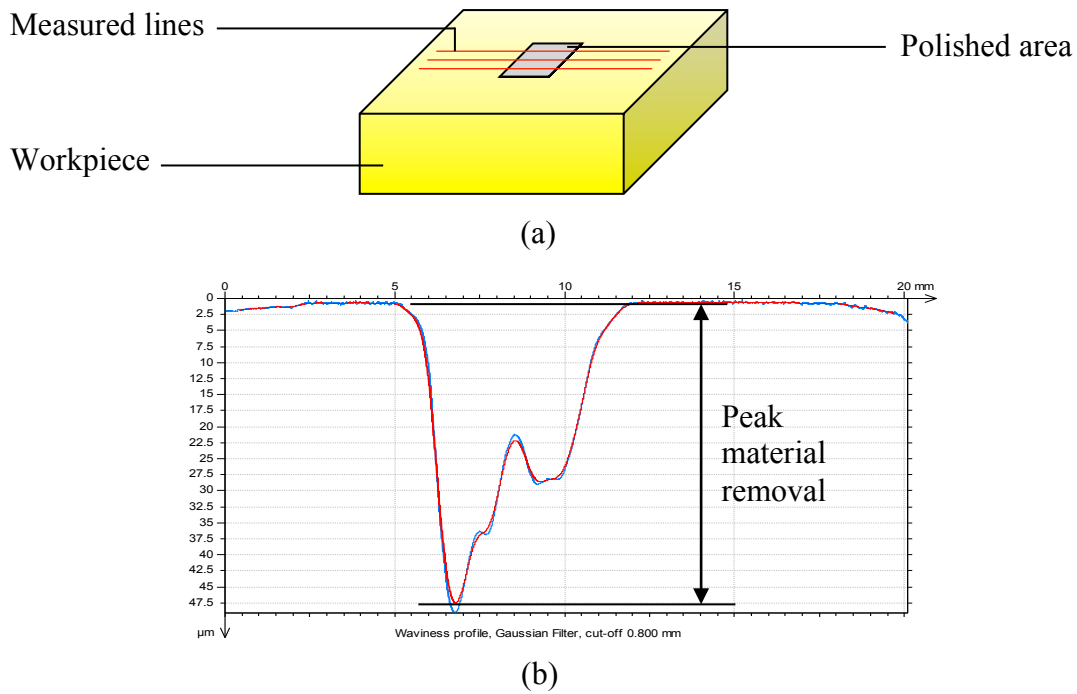


Figure B.1: (a) Schematic diagram of the two-dimensional line scans on a flat workpiece, and (b) an example of the profile obtained.

Note that the material removal profile is not symmetrical. This is due to standard errors related to dimensional accuracy of the polishing unit prototype. Specifically, the co-planarity of the bottom faces of the two magnets is important in achieving a symmetrical material removal profile. In the current prototype, the bottom faces of the two magnets are offset by approximately 100 μm , resulting in asymmetrical removal profile. However, the errors are repeatable and therefore do not affect the trends observed and reported.